

**A MULTI-LEVEL TRADE-OFF METHODOLOGY FOR ANALYZING
COLLABORATIVE SYSTEM-OF-SYSTEM ALTERNATIVES**

A Thesis
Presented to
The Academic Faculty

by

Nicholas Anthony Molino

In Partial Fulfillment
of the Requirements for the Degree
Doctor of Philosophy in the
School of Aerospace Engineering

Georgia Institute of Technology
May 2015

Copyright © 2015 by Nicholas Anthony Molino

**A MULTI-LEVEL TRADE-OFF METHODOLOGY FOR ANALYZING
COLLABORATIVE SYSTEM-OF-SYSTEM ALTERNATIVES**

Approved by:

Professor Dimitri N. Mavris, Advisor
School of Aerospace Engineering
Georgia Institute of Technology

Dr. Jean Charles Domercant
School of Aerospace Engineering
Georgia Institute of Technology

Dr. James S. Taylor
Naval Sea Systems Command (NAVSEA)
*Naval Surface Warfare Center, Panama
City Division*

Professor Daniel P. Schrage
School of Aerospace Engineering
Georgia Institute of Technology

Professor Eric Feron
School of Aerospace Engineering
Georgia Institute of Technology

Date Approved: April 6, 2015

ACKNOWLEDGEMENTS

*Plans fail for lack of counsel,
but with many advisers they succeed.
Proverbs 15:22*

I am extremely grateful for the opportunity afforded to me by Professor Dimitri Mavris to pursue a Doctor of Philosophy at Georgia Tech. He has been an incredible teacher, advisor, confidant, and friend. He works extremely hard to give students a chance to strive for a new mindset and academic excellence that can set us apart. His efforts have built a framework for the rest of my career to build upon.

Thank you to my committee members who each contributed so much time and thought into my work. Dr. Jean Charles Domercant has been more invested than I could have ever hoped for. Hours upon hours have been spent bouncing ideas off of him, and his constructive criticism and insights have been indispensable. Dr. Sam Taylor from the Naval Surface Warfare Center in Panama City has supported my work since the day I first presented to NAVSEA. His feedback as a voice-of-the-customer has shaped so much of my work. Words cannot accurately express how much I appreciate the time he has taken out of his busy schedule to meet with me in person, on the phone, and over email throughout the years. Professor Daniel Schrage has been a source of imperative insights related to systems and concurrent engineering. I have been exceedingly impressed by the ideas he provided to make my work transparent and valuable for the engineering community. Finally, Professor Eric Feron played a significant role in helping me solve multiple technical problems that I was having trouble overcoming. His suggestions for technical solutions in collaborative control and linear programming provided a level of depth to my work that I am very grateful for.

On a personal note: I am eternally grateful to my wife, teammate, and best friend Carolyn Elizabeth (Upton) Molino. Her support, excitement and empathy over the years

has been amazing. She has continually sacrificed of herself so that I could pursue this endeavor. I am inspired by the woman she is and for her partnership in our faith in Christ. She is truly a Proverbs 31 woman:

*A wife of noble character who can find? She is far more precious than jewels.
The heart of her husband trusts in her, and he will have no lack of gain. She
brings him good, not harm, all the days of her life...Many women do noble things,
but you surpass them all.*

I have to attribute a great deal of my efforts to my mom who always encouraged me to pursue engineering. She was the first person to teach me to be a diligent problem solver, and she has always inspired me to strive for greatness through hard work.

There are many more loved ones who have supported me over the years, though I will not name them all. However, I am exceedingly grateful for all of the family, friends, mentors, and lab-mates that have poured into me.

TABLE OF CONTENTS

| | |
|--|-------------|
| ACKNOWLEDGEMENTS | iii |
| LIST OF TABLES | viii |
| LIST OF FIGURES | ix |
| LIST OF SYMBOLS OR ABBREVIATIONS | xvi |
| SUMMARY | xix |
| I INTRODUCTION | 1 |
| 1.1 The Advantages of Collaboration | 2 |
| 1.2 Applications for Collaboration | 7 |
| 1.3 Representative Scope for this Work | 8 |
| II MOTIVATION AND BACKGROUND | 10 |
| 2.1 Robotic and Unmanned Systems in the Department of Defense | 10 |
| 2.2 The DoD Process for Determining, Developing and Implementing Solutions | 14 |
| 2.3 Unmanned System Solutions Available Within the DoD | 21 |
| 2.4 Systems Engineering as an Enabler | 24 |
| 2.5 The Wide Scope of Systems Engineering Teams | 25 |
| III THE ANALYSIS AND DESIGN OF SYSTEMS-OF-SYSTEMS | 28 |
| 3.1 What is Design? | 28 |
| 3.2 A Foundation: Systems Engineering and System-of-Systems Engineering | 31 |
| 3.3 A Framework: SoSE Core Elements | 36 |
| 3.4 Examples of SoSE Analysis and Design | 43 |
| 3.5 Global-Metric Reviews | 68 |
| 3.6 Next Steps | 80 |
| IV RECAPITULATION AND PROPOSED EXPERIMENTS | 81 |
| 4.1 Experimental Approach | 84 |
| 4.2 Next Steps | 87 |
| V REPRESENTATIVE TEST PROBLEM | 89 |
| 5.1 Establishing the Need and Defining the Problem | 90 |

| | |
|---|------------|
| VI EXPERIMENT SET A: SUBSYSTEM (SENSOR) LEVEL | 107 |
| 6.1 Modeling and Analyzing Sensors: A Review | 107 |
| 6.2 A New Formulation | 114 |
| 6.3 Virtual Experimentation Environment and Geometric Orientations | 141 |
| 6.4 Experimental Approach and Results | 145 |
| 6.5 Recapitulation: A New Sensor Experimentation Method | 153 |
| 6.6 Motivation for Experiment Set B | 155 |
| VII EXPERIMENT SET B: SYSTEM (VEHICLE) LEVEL | 157 |
| 7.1 Sizing and Synthesis Methods | 157 |
| 7.2 Filling the Gaps | 159 |
| 7.3 Applied Formulation | 160 |
| 7.4 Experimental Approach and Results | 176 |
| 7.5 A Foundation for SoS Analysis and Design | 183 |
| VIII EXPERIMENT SET C: SYSTEM-OF-SYSTEMS LEVEL | 184 |
| 8.1 Optimal Control for Area Coverage | 187 |
| 8.2 Experimental Approach | 191 |
| 8.3 Experiment 6: SoS Modeling of Point-Masses and Simplified Sensors | 192 |
| 8.4 The Full Method | 220 |
| 8.5 Experiment 7: Application of the Full Method | 221 |
| 8.6 Experiment Set C Conclusions | 226 |
| IX SUMMARY AND CONCLUSIONS | 227 |
| 9.1 Experimental Overview | 229 |
| 9.2 Making a Decision | 233 |
| 9.3 Lessons Learned | 235 |
| 9.4 Where to go Next | 236 |
| APPENDIX A — THE DEFENSE ACQUISITION SYSTEM | 238 |
| APPENDIX B — SE AND SOSE CHARACTERISTICS | 243 |
| APPENDIX C — SENSOR ORIENTATION | 251 |
| APPENDIX D — LATERAL RANGE CURVES FROM VXE | 260 |

| | | |
|------------|---|-----|
| APPENDIX E | — SIZING AND SYNTHESIS REVIEW | 283 |
| APPENDIX F | — HYDRODYNAMIC ANALYSIS | 288 |
| REFERENCES | | 313 |

LIST OF TABLES

| | | |
|----|---|-----|
| 1 | Levels of Autonomy Defined by the DoD [163] | 12 |
| 2 | RMS and REMUS 100 Comparison Chart | 99 |
| 3 | MCM MOE Subset for this Research | 105 |
| 4 | Constants and Variable Ranges for the Parametric Sonar Experimental Setup | 139 |
| 5 | Single- and Dual-Vehicle Simulation Data | 204 |
| 6 | SoSE Artifact Characteristics [38] | 250 |
| 7 | FLS Parameter Setup Used for VXE Results in Figure 139 | 261 |
| 8 | FLS Parameter Setup Used for VXE Results in Figure 140 | 262 |
| 9 | FLS Parameter Setup Used for VXE Results in Figure 141 | 263 |
| 10 | FLS Parameter Setup Used for VXE Results in Figure 142 | 264 |
| 11 | FLS Parameter Setup Used for VXE Results in Figure 143 | 265 |
| 12 | FLS Parameter Setup Used for VXE Results in Figure 144 | 266 |
| 13 | FLS Parameter Setup Used for VXE Results in Figure 145 | 267 |
| 14 | FLS Parameter Setup Used for VXE Results in Figure 146 | 268 |
| 15 | FLS Parameter Setup Used for VXE Results in Figure 147 | 269 |
| 16 | SSS Parameter Setup Used for VXE Results in Figures 148–150 | 270 |
| 17 | SSS Parameter Setup Used for VXE Results in Figures 151–153 | 272 |
| 18 | SSS Parameter Setup Used for VXE Results in Figures 154–156 | 274 |
| 19 | SSS Parameter Setup Used for VXE Results in Figures 157–159 | 276 |
| 20 | SSS Parameter Setup Used for VXE Results in Figures 160–162 | 278 |
| 21 | SSS Parameter Setup Used for VXE Results in Figures 163–165 | 280 |

LIST OF FIGURES

| | | |
|----|--|----|
| 1 | Unmanned System References in Various DoD Strategy Documents [90] . . . | 10 |
| 2 | An Overview of the Capabilities-Based Approach [156] | 17 |
| 3 | Identification of Capability Gaps and Resulting JCIDS Action, adapted from [31] | 18 |
| 4 | DoD Present and Future Unmanned Systems with Associated Roles [33] . . | 22 |
| 5 | DoD Unmanned Aircraft Systems [163] | 23 |
| 6 | DoD Unmanned Ground Systems [163] | 23 |
| 7 | DoD Unmanned Maritime Systems [163] | 24 |
| 8 | Core SoSE Elements and Their Relationships [43] | 37 |
| 9 | Core SoSE Elements and Their Associated Artifacts [37] | 38 |
| 10 | Unwrapping the Trapeze Model to Create an SoSE Wave Model [38] | 39 |
| 11 | Top Down Decision Support Process [131] | 40 |
| 12 | Georgia Tech’s Concurrent Engineering Methodology [132] | 40 |
| 13 | Comparison of Two Accepted Frameworks [132, 38] | 41 |
| 14 | A Generic SoSE Process to be Built Upon | 42 |
| 15 | Hierarchical Unified Tradeoff Environment for Systems-of-Systems Analysis [21] | 48 |
| 16 | Ender’s Inverse and Forward Design Multivariate Plot [21] | 49 |
| 17 | Poole’s Methodology Matrix of Alternatives [120] | 53 |
| 18 | Poole’s Applied Method [120] | 54 |
| 19 | Talley’s SoS Design Process [145] | 57 |
| 20 | Talley’s Process for Design at Each SoS Level [145] | 57 |
| 21 | Domercant’s Complexity Metric for Two SoS Architectures [44] | 61 |
| 22 | Inputs and Outputs for Each Step of the ARCHITECT Methodology [66] . | 63 |
| 23 | An SoS ROSETTA Decomposition [66] | 64 |
| 24 | A Generic SoSE Process with Potential Activities to be Integrated | 65 |
| 25 | A Generic SoSE Process with the Surrogate Modeling Approach Applied . . | 67 |
| 26 | Shannon’s entropy function in the case of two possibilities with probabilities p and $1 - p$ [137] | 70 |
| 27 | Example of Wang’s Progression of Domain Awareness Over Time [169] . . . | 71 |

| | | |
|----|--|-----|
| 28 | The theoretical speed for minimum rate of exergy destruction for insects, birds, and airplanes [14] | 74 |
| 29 | Hierarchical Breakdown of an F-5E Fighter Jet for Exergy Analysis [125] | 75 |
| 30 | Global Control Volume/Stream-Tube for Overall Vehicle Exergy Analysis [124] | 76 |
| 31 | Specific Exergy for Various Energy Flows [134] | 76 |
| 32 | The proposed energy-based approach will be applied to the AoA | 82 |
| 33 | Subsystem Level Experimental Setup | 85 |
| 34 | System Level Experimental Setup | 86 |
| 35 | SoS Level Experimental Setup | 87 |
| 36 | Decomposed Level-by-Level Experimental Approach | 88 |
| 37 | Mine Warfare Regions [17] | 93 |
| 38 | MIW Mission Area [Google Maps Satellite Imagery] | 96 |
| 39 | REMUS 100 UUV [99] | 98 |
| 40 | Remote Minehunting System (RMS) [96] | 98 |
| 41 | REMUS 100 UUV Components View [99] | 99 |
| 42 | RMMV Components View [149] | 100 |
| 43 | RMS AQS-20 Components View [2] | 100 |
| 44 | Existing P_D Generation Process | 110 |
| 45 | (1a) Definition of lateral range. (1b) Fictitious lateral range curve. (1c) Definite range law (“cookie cutter”). (1d) Imperfect Sensor. Adapted from Gage [57]. | 112 |
| 46 | Inverse cube law approximations for the lateral range of a sensor [89, 155]. | 112 |
| 47 | Existing P_D Generation Process Alongside Virtual Experimentation Augmentations. | 114 |
| 48 | “An illustration of how echo level, reverberation and ambient noise behave as a function of range.” [39] | 117 |
| 49 | SL_{omni} as a function of Electrical Power, P_E | 120 |
| 50 | Required beam width Plots for a Circular Piston Array | 124 |
| 51 | Required beam width Plots for a Linear Array | 124 |
| 52 | Directivity Index as a Function of Array Size | 125 |
| 53 | Source Level as a Function of Directivity and Electrical Power ($\eta_{ac} = 0.5$) | 125 |
| 54 | Initial Deterministic Sensor Design of Experiments | 127 |
| 55 | Initial Deterministic Sensor Design of Experiments | 128 |

| | | |
|----|--|-----|
| 56 | Active Sonar ROC Curves with Rician <i>Signal + Noise</i> pdf Statistics and Exponential <i>Noise</i> pdf Statistics [39]. (dB values on the curves are $10 \log(d)$) | 132 |
| 57 | Thermal (Molecular) Noise and Knudsen Curves Adapted from Urick [154]. | 133 |
| 58 | Three Computer Generated Views of the Manta Mine. | 134 |
| 59 | Attenuation and Total Transmission Loss as functions of operating frequency and range over which the signal spreads. The environmental properties are: $\{z = 10m, T = 20^\circ C, S = 34.7g/kg, pH = 8\}$ | 138 |
| 60 | FLS Deterministic Results | 140 |
| 61 | SSS Deterministic Results | 140 |
| 62 | Existing P_D Generation Process Alongside Virtual Experimentation Augmentations | 141 |
| 63 | Lateral Range Curve Experimental Setup | 142 |
| 64 | One set of FLS lateral range curve experimental results at discrete velocities | 143 |
| 65 | Subset of FLS Lateral Range Curves | 144 |
| 66 | Subset of SSS Lateral Range Curves | 145 |
| 67 | Subsystem Level Experimental Setup | 146 |
| 68 | FLS R_{max} from the sonar equation and <i>ESW</i> experimental results | 147 |
| 69 | SSS R_{max} from the sonar equation and <i>ESW</i> experimental results | 147 |
| 70 | Sonar Equation predicted maximum range versus VXE Maximum Range | 148 |
| 71 | FLS predicted maximum range versus actual maximum range | 150 |
| 72 | SSS predicted maximum range versus actual maximum range | 150 |
| 73 | Operations Analysis vs. VXE Generated Detection Curves | 151 |
| 74 | Number of Passes Required for $P_D = 98\%$ | 152 |
| 75 | Number of Passes Required for $P_D = 98\%$: Uniform Sensor and all 90 VXE Sensor Designs at Varying Velocities ($V_\infty = \{2, 5, 8\} m/s$) | 153 |
| 76 | A New Sensor Experimentation Method - The VXE Approach | 154 |
| 77 | Varying Fidelity Sizing and Synthesis Approach [103] | 158 |
| 78 | Allmendinger's Submersible Design Process with Mission Systems Considered [5] | 159 |
| 79 | System (Vehicle) Level Considerations for the SoS Design Process | 161 |
| 80 | Implemented Sizing and Synthesis Process | 161 |
| 81 | REMUS and RMMV Sized Vehicle Examples, produced by Missile DATCOM. | 164 |
| 82 | Steady Level Search Free-Body Diagram, $TW = L, D = T$ with $\sin(\alpha) \approx 0$ | 165 |

| | | |
|-----|---|-----|
| 83 | Required and Available Power and Thrust Examples | 167 |
| 84 | Implemented Sizing and Synthesis Process | 168 |
| 85 | Vehicle Sizing Iterations with an FLS, $P_{ac} = 0.1W$ | 169 |
| 86 | Vehicle Sizing Iterations with an SSS, $P_{ac} = 0.1W$ | 169 |
| 87 | Sizing results for one sensor type per vehicle | 170 |
| 88 | Endurance and power required for REMUS style vehicles with installed sensors | 172 |
| 89 | Endurance and power required for RMMV style vehicles with installed sensors | 172 |
| 90 | Coverage Factor Scatter Plots for REMUS Style Vehicles | 173 |
| 91 | Coverage Factor Scatter Plots for RMMV Style Vehicles | 174 |
| 92 | Coverage Factor over time for REMUS Style Vehicles w/ FLS | 175 |
| 93 | Coverage Factor over time for REMUS Style Vehicles w/ SSS | 175 |
| 94 | Coverage Factor over time for RMMV Style Vehicles w/ FLS | 176 |
| 95 | Coverage Factor over time for RMMV Style Vehicles w/ SSS | 176 |
| 96 | System Level Experimental Setup | 177 |
| 97 | Experiment 3: Coverage Factor Comparisons for Point Mass Vehicles | 178 |
| 98 | The Sonar Equation and Operations Analysis over-predicts coverage due to a lack of information linking sensor performance to vehicle operations. . . . | 178 |
| 99 | Experiment 4: Coverage Factor Comparisons for Sized Vehicles | 179 |
| 100 | Coverage Factor comparisons for sized-REMUS style vehicles with sensors modeled through the old approach versus the new approach | 180 |
| 101 | Coverage Factor comparisons for sized-RMMV style vehicles with sensors modeled through the old approach versus the new approach | 180 |
| 102 | Experiment 5: Coverage Factor Comparisons for Competing Vehicle Analyses with VXE Sensors | 181 |
| 103 | Coverage Factor comparisons for REMUS style vehicles modeled as point masses versus sizing and synthesis | 182 |
| 104 | Coverage Factor comparisons for RMMV style vehicles modeled as point masses versus sizing and synthesis | 182 |
| 105 | Decomposed Level-by-Level Experimental Approach | 192 |
| 106 | One Vehicle, $V_{\infty} = 3 m/s$, $\sigma = 5 m$, $t_f = 0.2 hr$, $P_s = 2 W$, $E_f = 8.3 kJ$. . . | 194 |
| 107 | Two Vehicles, $V_{\infty, \forall i} = 3 m/s$, $\sigma = (5, 10) m$, $t_f = (0.2, 0.1) hr$, $P_s = (2, 4) W$, $E_f = (8.3 + 5.2) = 13.5 kJ$. No way-point collaboration; No vehicle avoidance. | 195 |
| 108 | Two Vehicles, $V_{\infty, \forall i} = 3 m/s$, $\sigma = (5, 10) m$, $t_{f, \forall i} = 0.16 hr$, $P_s = (2, 4) W$, $E_f = (6.7+7.8) = 14.5 kJ$. With way-point collaboration; No vehicle avoidance. | 196 |

| | | |
|-----|--|-----|
| 109 | Two Vehicles, $V_{\infty, \forall i} = 3 m/s$, $\sigma = (5, 10) m$, $t_f = (0.2, 0.12) hr$, $P_s = (2, 4) W$, $E_f = (8.6 + 5.8) = 14.4 kJ$. No way-point collaboration; With vehicle avoidance. | 198 |
| 110 | Two Vehicles, $V_{\infty, \forall i} = 3 m/s$, $\sigma = (5, 10) m$, $t_{f, \forall i} = 0.16 hr$, $P_s = (2, 4) W$, $E_f = (6.8 + 8.0) = 14.8 kJ$. With way-point collaboration; With vehicle avoidance. | 199 |
| 111 | Two Vehicles, $V_{\infty, \forall i} = 3 m/s$, $\sigma = (5, 10) m$, $t_f = (0.2, 0.12) hr$, $P_s = (2, 4) W$, $E_f = (8.6 + 5.9) = 14.5 kJ$. No way-point collaboration; With new vehicle avoidance. Position and energy plots are associated with plot (a). | 200 |
| 112 | Two Vehicles, $V_{\infty, \forall i} = 3 m/s$, $\sigma = (5, 10) m$, $t_{f, \forall i} = 0.18 hr$, $P_s = (2, 4) W$, $E_f = (7.6 + 8.9) = 16.5 kJ$. With way-point collaboration; With new vehicle avoidance. Position and energy plots are associated with plot (a). | 202 |
| 113 | Two Vehicles, $V_{\infty, \forall i} = 5 m/s$, $\sigma = (5, 10) m$, $t_f = 0.1 hr$, $P_s = (2, 4) W$, $E_f = (15.7 + 16.5) = 32.2 kJ$. With way-point collaboration; With vehicle avoidance. | 203 |
| 114 | Four Vehicles, $V_{\infty, \forall i} = 3 m/s$, $\sigma_{\forall i} = 25 m$, $t_f = 1.48 hrs$, $P_{s, \forall i} = 10 W$, $E_f = (105 + 105 + 105 + 105) = 420 kJ$. With way-point collaboration; With vehicle avoidance. | 206 |
| 115 | Four Vehicles, $V_{\infty, \forall i} = 3 m/s$, $\sigma = (20, 20, 30, 30) m$, $t_f = 2.6 hrs$, $P_s = (8, 8, 12, 12) W$, $E_f = (184 + 184 + 182 + 183) = 733 kJ$. With way-point collaboration; With vehicle avoidance. | 207 |
| 116 | Maximum Coverage Effort Results for Ten Vehicles | 213 |
| 117 | Representative RMMV Style Design | 214 |
| 118 | Maximum Specific Coverage Results for Ten Vehicles | 215 |
| 119 | Shortest Tours for Determining Minimum Number of Robots [110] | 216 |
| 120 | Initial Required Distance for Heuristic Coverage Algorithm | 218 |
| 121 | Iterative Required Distance After the Initial Distance | 219 |
| 122 | Full Developed Method with Comments | 220 |
| 123 | Full Developed Generalized Method with Comments | 221 |
| 124 | Defining the Problem | 222 |
| 125 | Decomposing the Problem | 222 |
| 126 | Coverage Algorithm Example Progression for $f = V_{\infty, i} S_i \tau_{i, k} / P_{i, total}$ | 223 |
| 127 | System Parameters for Coverage Algorithm with $f = V_{\infty, i} S_i \tau_{i, k} / P_{i, total}$ | 224 |
| 128 | Vehicle Tracks and Target Locations for Virtual Experimentation | 224 |
| 129 | Coverage Algorithm Example Progression for $f = V_{\infty, i} S_i \tau_{i, k}$ | 225 |
| 130 | System Parameters for Coverage Algorithm with $f = V_{\infty, i} S_i \tau_{i, k}$ | 225 |

| | | |
|-----|---|-----|
| 131 | Vehicle Tracks and Target Locations for Virtual Experimentation | 225 |
| 132 | Final Multi-Level Trade-off Methodology Alongside the Top-Down Decision Support Process | 227 |
| 133 | Decomposed Level-by-Level Experimental Approach | 229 |
| 134 | The Applied Method Leads to a Portfolio of Non-Dominated Results for a Decision Maker to Choose Between | 233 |
| 135 | DoD Needs Identification and Solution Process [83] | 238 |
| 136 | Interaction of the DoD Decision Support Systems [44, 9] | 242 |
| 137 | 2D Coordinate Transformation | 253 |
| 138 | Example of Axis Rotations with $\Theta = \alpha$ | 256 |
| 139 | FLS VXE Results for Parameterization in Table 7 | 261 |
| 140 | FLS VXE Results for Parameterization in Table 8 | 262 |
| 141 | FLS VXE Results for Parameterization in Table 9 | 263 |
| 142 | FLS VXE Results for Parameterization in Table 10 | 264 |
| 143 | FLS VXE Results for Parameterization in Table 11 | 265 |
| 144 | FLS VXE Results for Parameterization in Table 12 | 266 |
| 145 | FLS VXE Results for Parameterization in Table 13 | 267 |
| 146 | FLS VXE Results for Parameterization in Table 14 | 268 |
| 147 | FLS VXE Results for Parameterization in Table 15 | 269 |
| 148 | SSS VXE Results for Parameterization in Table 16 with $freq = 400kHz$. . | 270 |
| 149 | SSS VXE Results for Parameterization in Table 16 with $freq = 1000kHz$. | 271 |
| 150 | SSS VXE Results for Parameterization in Table 16 with $freq = 1600kHz$. | 271 |
| 151 | SSS VXE Results for Parameterization in Table 17 with $freq = 400kHz$. . | 272 |
| 152 | SSS VXE Results for Parameterization in Table 17 with $freq = 1000kHz$. | 273 |
| 153 | SSS VXE Results for Parameterization in Table 17 with $freq = 1600kHz$. | 273 |
| 154 | SSS VXE Results for Parameterization in Table 18 with $freq = 400kHz$. . | 274 |
| 155 | SSS VXE Results for Parameterization in Table 18 with $freq = 1000kHz$. | 275 |
| 156 | SSS VXE Results for Parameterization in Table 18 with $freq = 1600kHz$. | 275 |
| 157 | SSS VXE Results for Parameterization in Table 19 with $freq = 400kHz$. . | 276 |
| 158 | SSS VXE Results for Parameterization in Table 19 with $freq = 1000kHz$. | 277 |
| 159 | SSS VXE Results for Parameterization in Table 19 with $freq = 1600kHz$. | 277 |
| 160 | SSS VXE Results for Parameterization in Table 20 with $freq = 400kHz$. . | 278 |

| | | |
|-----|---|-----|
| 161 | SSS VXE Results for Parameterization in Table 20 with $freq = 1000kHz$ | 279 |
| 162 | SSS VXE Results for Parameterization in Table 20 with $freq = 1600kHz$ | 279 |
| 163 | SSS VXE Results for Parameterization in Table 21 with $freq = 400kHz$ | 280 |
| 164 | SSS VXE Results for Parameterization in Table 21 with $freq = 1000kHz$ | 281 |
| 165 | SSS VXE Results for Parameterization in Table 21 with $freq = 1600kHz$ | 281 |
| 166 | Mattingly's Aircraft Sizing Process, Adapted by Nam [102, 113] | 283 |
| 167 | Nam's Comprehensive, Generalized Sizing Process [113] | 284 |
| 168 | Evan's Design Spiral, Adapted by Lamb [49, 92] | 285 |
| 169 | Lamb's Ship Design and Feasibility Process [92] | 286 |
| 170 | Reynolds Number at a depth of 10 meters, $Re = V_\infty l / \nu_\infty$ | 295 |
| 171 | Coefficient of Friction – Prandtl–vonKármán Theoretical Turbulent Solutions | 296 |
| 172 | Coefficient of Friction – Including the Schoenherr Line | 297 |
| 173 | Coefficient of Friction – Schoenherr Line and Hama's Approximation | 298 |
| 174 | Coefficient of Friction – Schoenherr Line and Schultz-Grunow's Approximation | 299 |
| 175 | Coefficient of Friction – Schoenherr Line and Hoerner's Interpolation | 300 |
| 176 | Coefficient of Friction – Hama Turbulence Approximation and the Transitional Estimate | 301 |
| 177 | Hoerner Skin Friction Drag Coefficient Plot | 301 |
| 178 | Zero-Lift Drag Coefficient for Elliptical Sections, $c/t = \{2,4,6,8,10\}$ | 302 |
| 179 | Streamlined Vehicle Body Example | 304 |
| 180 | Streamline Body Shape Corrections, $l/d = \{2,4,6,8,10\}$ | 305 |
| 181 | Cylindrical Vehicle Body Example | 307 |
| 182 | Cylindrical Shape Corrections, $l/d = \{2,4,6,8,10\}$ | 307 |
| 183 | Coefficient of Drag for a Sphere from Hoerner[70] | 310 |
| 184 | Total Wetted Drag Coefficient, Streamlined Body Shape, $l/d = \{2,4,6,8,10\}$ | 311 |
| 185 | Total Drag Coefficient, Streamlined Body Shape, $l/d = \{2,4,6,8,10\}$ | 312 |

LIST OF SYMBOLS OR ABBREVIATIONS

| | |
|------------------|---|
| ANN | Artificial Neural Nets. |
| AoA | Analysis of Alternatives. |
| AUV | Autonomous Underwater Vehicle. |
| CBA | Capabilities-Based Assessment. |
| CDF | Cumulative Density Function. |
| CE | Concurrent Engineering. |
| CONOPS | Concepts of Operations. |
| COTS | Commercial Off The Shelf. |
| DDD | Dull, Dirty and Dangerous. |
| DoD | Department of Defense. |
| DoDAF | Department of Defense Architecture Framework. |
| DoE | Design of Experiments. |
| DOTmLPP-P | Doctrine, Organization, Training, materiel, Leadership and education, Personnel and Facilities, and Policy. |
| EGM | Entropy Generation Minimization. |
| EOD | Explosive Ordnance Disposal. |
| FLS | Forward-Looking Sonar. |
| ICDs | Initial Capabilities Documents. |
| IEC | International Electrotechnical Commission. |
| IEEE | Institute of Electrical and Electronics Engineers. |
| INCOSE | International Council on Systems Engineering. |
| ISO | International Organization for Standardization. |
| JCIDS | Joint Capabilities Integration Development System. |
| KPP | Key Performance Parameters. |
| MCM | Mine Counter-Measures. |
| MIW | Mine Warfare. |
| MOE | Measure of Effectiveness. |
| MOP | Measure of Performance. |

| | |
|--------------------|---|
| M&S | Modeling and Simulation. |
| NAVSEA | Naval Sea Systems Command. |
| QFD | Quality Function Deployment. |
| REMUS | Remote Environmental Monitoring Unit. |
| RMMV | Remote Multi-Mission Vehicle. |
| RMS | Remote Mine-hunting System. |
| RVM | Relevance Vector Machines. |
| SE | Systems Engineering. |
| SME | Subject Matter Expert. |
| SoS | System-of-Systems. |
| SoSE | System-of-Systems Engineering. |
| S&T | Science and Technology. |
| SVM | Support Vector Machines. |
| TTCP | The Technical Cooperation Program. |
| TTPs | Tactics, Techniques and Procedures. |
| UAS | Unmanned Aircraft System. |
| UAT | Universal Approximation Theorem. |
| UCAV | Unmanned Combat Aerial Vehicle. |
| UGS | Unmanned Ground System. |
| UMS | Unmanned Maritime System. |
| USV | Unmanned Surface Vehicle. |
| UUV | Unmanned Underwater Vehicle. |
| UWIED | Underwater Improvised Explosive Device. |
| γ | Coverage Rate. |
| λ_I | Ideal Coverage Ratio. |
| λ_R | Random Coverage Ratio. |
| $\bar{\mathbf{d}}$ | Vehicle design vector. |
| $\bar{\mathbf{G}}$ | Vector of constraints. |
| $\bar{\mathbf{p}}$ | System state vector. |

| | |
|------------|---------------------------------|
| \bar{s} | Subsystem design vector. |
| \bar{u} | System control vector. |
| \bar{X} | Vector of specified systems. |
| \bar{F} | Vector of performance measures. |
| A | Search Area. |
| A_S | Total Search Area. |
| ce | Coverage Effort. |
| t | Search Time. |
| V_∞ | Vehicle Velocity. |
| ESW | Effective Sweep Width. |
| S | Sweep Width. |

SUMMARY

As unmanned vehicle capabilities have matured, the design and development of autonomous collaborative systems-of-systems (SoS) has gained increased attention. This has been motivated by the indication that significant improvements in overall effectiveness may be possible by employing many systems in cooperation with one another. In addition, these large-scale groupings of systems are often meant to operate in diverse and widely distributed environments. However, as the potential combinations of vehicles, subsystems, and operational concepts becomes increasingly large, a systematic approach is needed for designing and analyzing alternatives. Furthermore, the discrete nature of the problem can cause variations in effectiveness that are counter-intuitive, such as a point of diminishing returns as the number of systems grows.

Systems-of-systems are hierarchical in nature, consisting of top-level mission requirements that are decomposed into system- and subsystem-level performance measures. The overarching research objectives of this dissertation are to show that the analysis of alternatives for collaborative systems-of-systems should be performed at varying levels of the system-of-system hierarchy and to provide novel means for performing those analyses. In particular, it has been postulated that an energy-based approach to analyzing system-of-system (SoS) components across multiple levels of the SoS hierarchy will enable more accurate and transparent trade-offs for SoS analysis of alternatives. Various steps of the design process are established and argued for or against, and significant focus is placed on the analysis of alternatives.

This dissertation begins by demonstrating that collaborative behavior can be a beneficial and impressive trait of a species. However, there seem to be some species that have what it takes to cooperate effectively while others do not. Similarly, methodical processes are needed to design groupings of systems that are to work together as effectively as possible. In fact, varying design considerations can prove to be either beneficial or detrimental to

the cooperative operations of a grouping of unmanned systems. Therefore, delineation of the vehicle capabilities at the subsystem, system and SoS levels are imperative steps in determining overall effectiveness, which is systematically presented in this dissertation.

Next, the dissertation is scoped based on stakeholder requirements. This is necessary since there are almost enumerable applications for collaborative unmanned systems. However, the concepts brought forward in this dissertation are made more concrete and clear if they are placed in reference to a specific application. The application chosen is to utilize a group of unmanned underwater vehicles (UUVs) which are to operate in a collaborative fashion in order to search for underwater objects. The example scenario provides an application for illustrating the phenomenon discussed in regards to the analysis of alternatives of collaborative SoS. This problem is representative in that it provides the opportunity to consider multiple levels of the system-of-system hierarchy. The significance of providing more or less analytic detail is traced and the effect on mission requirements is quantified. The formal problem definition is formulated through generic SoS engineering processes by characterizing the objectives, design variables, and constraints.

The method developed as an approach to substantiating the overarching hypothesis of this dissertation is built from the ground up. The foundation is laid on structured SoS engineering principles and terminology and the framework comes together through investigating existing SoS engineering methods. The full substance of the method comes together after reviewing the analytical content of the various SoS engineering methods. Subsequently, unique aspects for the new method developed within this dissertation are delineated. Finally, an experimental approach is presented which tests and substantiates the overarching hypothesis of this dissertation.

A new virtual experimentation approach is presented for creating sensor performance representations that are functions of vehicle operations. The sonar equation is used as a baseline sensor model for comparison against the new virtual experimentation method. Dozens of forward-looking and side-scan sonar experiments are designed, and data is provided to show the extent to which typical sensor modeling over-predicts performance without

vehicle operations considered. In addition, comparisons are made between possible representations of vehicle performance. An underwater vehicle sizing and synthesis process is developed to enable comparisons between system-level component modeling approaches. The experiments attest to significant gaps in accuracy when performing sensor and operational trade-offs without energy-based modeling of the collaborative vehicles. Finally, a heuristic path-planning algorithm is formulated, and mixed-integer linear programming is used to choose between alternative SoS designs.

The deliberate and transparent analysis of alternative systems-of-systems is a rich area for research. While there are multiple disciplinary challenges that must be overcome in creating groupings of systems that work together efficiently, there is also a need for the large-scale perspectives provided through systems engineering and concurrent engineering. However, as this dissertation shows, the large-scale focus of the problem should be accompanied by detailed physics-based analyses. In particular, in this dissertation, the need for physics-based analyses is substantiated through the comparison of energy-based approaches against some common methods found in the literature.

CHAPTER I

INTRODUCTION

The relevance of autonomous systems and vehicles in everyday life has dramatically increased as technology and computing capabilities have flourished over the last few decades. Robotic systems are no longer constrained to assembly line manufacturing roles. Instead, they are becoming the cars that egress our roads, the aircraft that transverse the skies, and the underwater systems that explore the oceans. These systems are not entering a world of isolation. Rather, they must operate within groupings of systems, otherwise known as *systems-of-systems* (SoS).

From an engineering perspective, it is important to analyze and design groupings of systems that function in the most efficient manner possible while maintaining situational awareness with the world in which they operate. This emphasizes the idea of analyzing a full SoS across independent systems and their individual parts. At the highest level of consideration is the collective behavior of all the independent systems and how they work together. The next level down in aggregation takes into account the individual systems: how they are designed, whether they are homogeneous or heterogeneous, etc. Further decomposing the SoS then allows an engineer to consider the subsystems: the low-level components such as vehicle sensors, communications and localization capabilities, and potential payloads which allow the systems to work together and sense their domain.

This dissertation has worked to develop a methodological structure for analyzing and designing groupings of systems by considering the multiple levels of the SoS hierarchy introduced above. Instead of focusing on a single discipline, this research presents a systematic, energy-based approach for integrating various disciplines in order to perform trade-offs and converge on well substantiated solutions in a transparent and repeatable way.

1.1 *The Advantages of Collaboration*

Cooperation and collaboration are fundamental driving forces of the world around us. They can be observed in nature from the perspectives of the macroscopic down to the microscopic; from herds of animals to the cells within organisms. Yet, ever since Charles Darwin proposed the theory of evolution by natural selection [114], the force of *competition* has received much more attention than that of cooperation. A recent article in Scientific American by Martin Novak, director of the Program for Evolutionary Dynamics at Harvard University, provides an elegant description of the dilemma behind competition over cooperation [116]:

For decades biologists have fretted over cooperation, scrambling to make sense of it in light of the dominant view of evolution. Charles Darwin, in making his case for evolution by natural selection – wherein individuals with desirable traits reproduce more often than their peers and thus contribute more to the next generation – called this competition the ‘struggle for life most severe’. Taken to its logical extreme, the argument quickly leads to the conclusion that one should never ever help a rival and that an individual might in fact do well to lie and cheat to get ahead. Why, then, is selfless behavior such a pervasive phenomenon?

In response, Novak has shown through his research over the last two decades “that instead of opposing competition, cooperation¹ has operated alongside it from the get-go to shape the evolution of life on earth, from the first cells to *Homo sapiens*” [116]. Therefore, an implication of Novak’s research is that clear benefits and advantages must be available when groups act in a collaborative fashion.

Furthermore, it is reasonable to surmise that the presence of *competition* in the evolutionary process has even contributed to the *necessity* of collaboration. Many predators, for example, hunt in packs partly to increase their odds of successfully acquiring prey. Similarly, a herd of gazelle stand a much better chance of survival against their predators than an individual will [177]. Kennedy, in his book entitled *Swarm Intelligence*, describes the

¹Cooperation is well defined as the act of collaborating with others towards a common goal [106].

phenomenon as follows [86]:

Fish school, birds flock, bugs swarm – not just so they can mate, but for reasons extending above and beyond that. For instance, schools of fish have an advantage in escaping predators, as each individual fish can be a kind of lookout for the whole group. It is like having a thousand eyes. Herding animals also have an advantage in finding food: if one animal finds something to eat, the others will watch and follow. Social behavior helps individual species members adapt to their environment, especially by providing individuals with more information than their own senses can gather.

The benefits of collaboration are not only intuitively obvious but are well supported by research. However, it is axiomatic that ineffective cooperation abounds. People often seem incompetent when working in a cooperative fashion (whether in business, politics, athletics, etc.) which has led to entire industries focused on developing more effective collaborative teams. Even ant colonies, which are often seen as ubiquitous examples of team work, struggle in cooperating. As McCreery conveyed in the journal *Insectes Sociaux* [105]:

Cooperative transport, or the movement of an object by two or more individuals, is a particularly impressive example of collaboration among workers. Many ant species perform this behavior, but there is extreme interspecific variation in efficiency. Why are some ant species so efficient at cooperative transport, while others are so inefficient?

During collaborative transport, some ants have been observed to lack coordination, pulling an item in various directions for long periods of time resulting in little to no progress while others are able to quickly and efficiently manage movement in a straight line [179, 36, 18]. It turns out that the efficiency of the cooperative transport process is highly dependent on a number of disparate factors such as the number of ants, even within a particular species. Intuitively, increasing the number of carriers should, and sometimes does, have a positive effect. However, there is a point of diminishing returns where workers may cause impeded paths or wasted effort if more ants are present than are needed. Another

factor is the direction of travel wherein the members of the group may all face forward, some may walk backwards, or two ants will pull in opposing directions counteracting each other. Information transfer is another observed phenomenon. Without communication the transport tends to be highly inefficient and often fails completely. Alternatively, with information transfer present, the ants tend to establish distinct roles within the group, move more quickly, and attain a higher probability of success.

As was observed by McCreery, collaborative behavior can be a beneficial and impressive trait of a species. However, there seem to be some species that have what it takes to cooperate effectively while others do not. If engineers were to design a group of collaborative ants, there would be a plethora of design options to experiment with. Which species of ant should be used? How many ants? Can ants from two or more species work together? How should they share information? Should new capabilities be added through genetic advances? What measures of effectiveness should be used to determine the best solutions?

Additionally, the issue of effectiveness implies the consideration of energy transfer of the constituent components throughout the cooperative task and the subsequent overall efficiency. After all, “energy is an additive property, that is, the energy of a composite system is the sum of the energies of the subsystems” [16]. This leads to the first two observations of this dissertation:

Observation 1 *The efficiency, and therefore the effective energy usage, of a cooperative process is dependent on an array of factors including the number of agents, the operational scheme, information transfer, and unique characteristics of the individuals.*

Observation 2 *The total energy transfer that takes place during a collaborative process is a function of the energy transfer amongst all constituent components according to the First Law of Thermodynamics.*

The questions posed above along with the stated observations provide the basis for this dissertation. In particular, this research asks questions (and offers methodical solutions) about designing systems and groupings of systems that are to work together as effectively as

possible. A foundation is built on defining high level mission requirements and subsequently decomposing the problem across multiple levels of the SoS hierarchy. Design options at each level of the hierarchy including individual systems, subsystems, and groupings of systems are considered and trade-offs are presented. What it means to obtain an *effective* grouping of systems for a well defined *cost* is examined. Various steps of the design process are established and argued for or against, and significant focus is placed on the analysis of alternatives.

The situation can be modeled mathematically, which is nontrivial in solution. The desire is to minimize a set of performance measures, $\bar{\mathcal{F}}$, which are functions of the system designs, subsystem designs, the number of systems, the discretized states of the systems during a mission, and the operational control of the systems. Therefore,

$$\bar{\mathbf{X}} = [X_1(\bar{d}_1, \bar{s}_1), X_2(\bar{d}_2, \bar{s}_2), \dots, X_n(\bar{d}_n, \bar{s}_n)]$$

is a set of n specified systems, X_1, \dots, X_n , which are each a function of the system design variables, \bar{d}_n , and the subsystem design parameters, \bar{s}_n . Similarly,

$$\bar{\mathbf{p}} = [\bar{p}_1(t), \bar{p}_2(t), \dots, \bar{p}_n(t)]$$

is a set of n state vectors for each of the n systems as they progress throughout the mission (or process) time, t . The states of each system can also be specified relative to their position within an m -dimensional space, \mathbb{R}^m , where $\bar{p}_n(t) = f(p_{n,1}, p_{n,2}, \dots, p_{n,m})$. The operational control of each system throughout the mission is defined by the set

$$\bar{\mathbf{u}} = [\bar{u}_1(t), \bar{u}_2(t), \dots, \bar{u}_n(t)]$$

which are the control vectors for each of the n systems. The specified systems vector, $\bar{\mathbf{X}}$, along with the permissible excitation inputs of the systems, $\bar{\mathbf{u}}(t)$, are fundamental in describing the dynamics of the systems in order to calculate the states over time, $\bar{\mathbf{p}}(t)$. A state-based approach allows the system designs and behaviors to be mapped to the mission processes through differential equations [52].

The set of performance measures to be minimized are functions of the variable sets specified above, subject to functional constraints, $\bar{\mathbf{G}}$. Side constraints can also be included.

$$\begin{aligned} \min \quad & \bar{\mathcal{F}} = f(\bar{\mathbf{X}}, \bar{\mathbf{p}}, \bar{\mathbf{u}}) \\ \text{subject to} \quad & \bar{\mathbf{G}} = g(\bar{\mathbf{X}}, \bar{\mathbf{p}}, \bar{\mathbf{u}}) \leq 0 \end{aligned} \tag{1}$$

The set of performance measures $\bar{\mathcal{F}}$ may result in a single- or multi-objective optimization scenario. The performance measures may include effectiveness metrics such as area coverage rate, fuel efficiency, minimum energy expenditure, and maximum situational awareness among others. Most practical engineering problems, especially on the scale of a collaborative grouping of systems, are multi-objective in nature. Therefore, there is likely not a single *best* solution, but rather a set of potential solutions that must be analyzed and decided between. Since the performance is also a function of time, the problem can be restated as an attempt to minimize the integral of the performance over the mission, task or process. The final time, t_f , may or may not be constrained.

$$\min \quad \bar{\mathcal{F}} = \int_0^{t_f} f(\bar{\mathbf{X}}, \bar{\mathbf{p}}, \bar{\mathbf{u}}) dt \tag{2}$$

Furthermore, the allowable variations of the system, subsystem, and operational control parameters ($\bar{\mathbf{X}}(\bar{\mathbf{d}}, \bar{\mathbf{s}}), \bar{\mathbf{u}}(t)$), have no guarantee of continuity. Similarly, the number of systems, n , utilized in the collaborative grouping is inherently discrete. Therefore, it cannot be automatically assumed that any of the performance measures in the performance vector $\bar{\mathcal{F}}$ are smooth. An overarching question from a mathematical perspective is then: *how should changes be made to $\bar{\mathbf{X}}(\bar{\mathbf{d}}, \bar{\mathbf{s}})$, $\bar{\mathbf{p}}(t)$, and $\bar{\mathbf{u}}(t)$ in order to obtain minimized solutions for $\bar{\mathcal{F}}$?*

It should be noted that the goal of this dissertation work is not to specifically solve Equation 1. In fact, solutions to Equation 1 for a given application can be non-unique, riddled with local-minima, and/or have no closed-form solution. Instead, this work strives to develop a methodical structure for determining the sets of variables and transfer functions that will allow designers and engineers to analyze and perform trade-offs between alternative multi-system solutions in a transparent and repeatable way. Furthermore, the consideration of energy usage at all levels of the cooperative hierarchy is of prime importance in accordance with Observation 2. This leads to the overarching hypothesis of this dissertation:

Hypothesis 1 *An energy-based approach to analyzing system-of-system (SoS) components across multiple levels of the SoS hierarchy will enable more accurate and transparent trade-offs for SoS analysis of alternatives.*

Hypothesis 1 conveys the fact that the research objective of this dissertation is not to focus on a single discipline, but to integrate multiple disciplines in order to analyze and trade-off SoS alternatives. Beyond the integration of multiple disciplines, the method developed in this work also spans across the SoS hierarchy rather than being restricted to the analysis of a single level, such as the subsystem level. Also, the use of the words “more accurate” in Hypothesis 1 implies that the method will not only be developed, but will be compared against existing analysis methods.

1.2 Applications for Collaboration

As is often the case, when scientists and engineers observe a highly effective attribute of nature they will try to emulate it in technology. Over the last few decades, this has surely been the case for the field of cooperative robotics. Robotic and unmanned systems provide both economic and practical benefits. From the economic perspective there are typically lower costs and risks of liability associated with the use of a robotic system over the use of a human. From a practical perspective, robotic and unmanned systems can be highly effective in accomplishing hazardous and/or mundane tasks. Furthermore, it is often presumed that if a single system is advantageous, than a cooperative collection of robotic systems should provide even greater benefits (just as nature shows is possible for the group behavior of a species). As was stated earlier, however, the analysis of alternative systems and collaborative capabilities will be crucial in acquiring the benefits provided by collaboration.

A survey written in 1997 of cooperative robotic literature pointed out that between the years of 1987–1995 alone, “well over 200 papers have been published in this field of cooperative (mobile) robotics, encompassing theories from such diverse disciplines as artificial intelligence, game theory/economics, theoretical biology, distributed computing/control, animal ethology and artificial life” [27]. Since 1997, the field has continued to flourish. In

2008, editors of the IEEE (Institute of Electrical and Electronics Engineers) Robotics and Automation Magazine stated that “The field of multiagent robotics has recently reached a level of maturity in that systems are beginning to transition from proof-of-concept laboratory environments to deployed real-world systems” [87].

Robotic and unmanned systems are great candidates for the application of cooperative behaviors for several reasons, including:

- Certain tasks may be too complex for a single robot to perform [27].
- Performance benefits may be gained through a multi-robotic system in terms of time savings and/or area coverage [27].
- Simpler distributed robotic systems “promise a significant cost reduction in their design, manufacturing, and operation” [108] relative to a more complex, single system solution.
- Distributed collaborative systems “lead to higher degrees of scalability and adaptability in response to changes in mission goals and system capabilities” [108].
- Multi-robot systems offer “redundancy, increased spatial coverage and throughput, flexible reconfigurability, spatially diverse functionality, and the fusing of physically distributed sensors and actuators” [87].

The benefits of collaborative robotics can surely be embraced by many parties throughout industry and the military. Various entities already have a long history of using cooperative robots in production facilities, manufacturing plants, and assembly lines (although these implementations typically, if not always, involve statically mounted systems). Visions for the future include dynamic collaborative robots that assist in agricultural efforts, monitor areas with surveillance equipment, transport cargo alongside civilian vehicles on interstates, and more.

1.3 Representative Scope for this Work

As has been shown, there are almost enumerable applications for collaborative unmanned systems and the number of possibilities seem to have no limit in the future. However,

the concepts brought forward in this dissertation will be more concrete and clear if they are placed in reference to a specific application. The application chosen in this work is to utilize a group of unmanned underwater vehicles (UUVs) which are to operate in a collaborative fashion in order to search for underwater objects. This is an application which has found increased relevance over the years. Example scenarios include the search for underwater debris in a large area (*e.g.*, the search for Malaysian Airlines Flight 370 [144]) and underwater mine warfare [117]. This application provides a clear reference point for demonstrating design considerations such as potential combinations of vehicles, sensors and control scheme characteristics that will prove to be either beneficial or detrimental to the cooperative operations. The application scenario also provides a case study for testing the developed method which is built upon systematic decomposition of the required mission, first-principles physics-based analyses of vehicles, sensors, and operating environments, and agent-based simulation as a virtual experimentation apparatus.

Stakeholder relevance is another consideration in scoping this work. Government entities are often ubiquitous in revolutionary technology development and implementation. The case of collaborative robotic systems has been no different. The United States government, and particularly the Department of Defense (DoD), has invested a considerable amount of resources into the development of unmanned robotic systems and has accordingly advocated the advancement of collaborative capabilities [163]. For that reason, investigation into the DoD's motivation for these types of systems and an understanding of the DoD's system development and acquisition process is relevant and germane for this research. Therefore, further motivation for this dissertation and background on the stated aspects of the DoD as a major stakeholder in collaborative system utilization will be detailed in the next chapter. Then, multiple processes which consider systems-of-systems from a System Engineer's perspective will be presented, especially those relevant to the DoD.

CHAPTER II

MOTIVATION AND BACKGROUND

2.1 Robotic and Unmanned Systems in the Department of Defense

As the field of collaborative robotic systems has matured over the last three decades, the United States Department of Defense (DoD) has increasingly embraced the use of unmanned systems to assist in the projection of power and to keep the warfighter out of harm's way. Incorporation of unmanned systems into the military force structure can have a significant impact on tactics, techniques, and procedures (TTPs) and concepts of operations (CONOPS). Accordingly, over the last ten years a great deal of attention has been conferred to unmanned systems as shown in Figure 1, which displays the frequency of unmanned system references throughout seven of the recent DoD key strategy documents [90, 33].

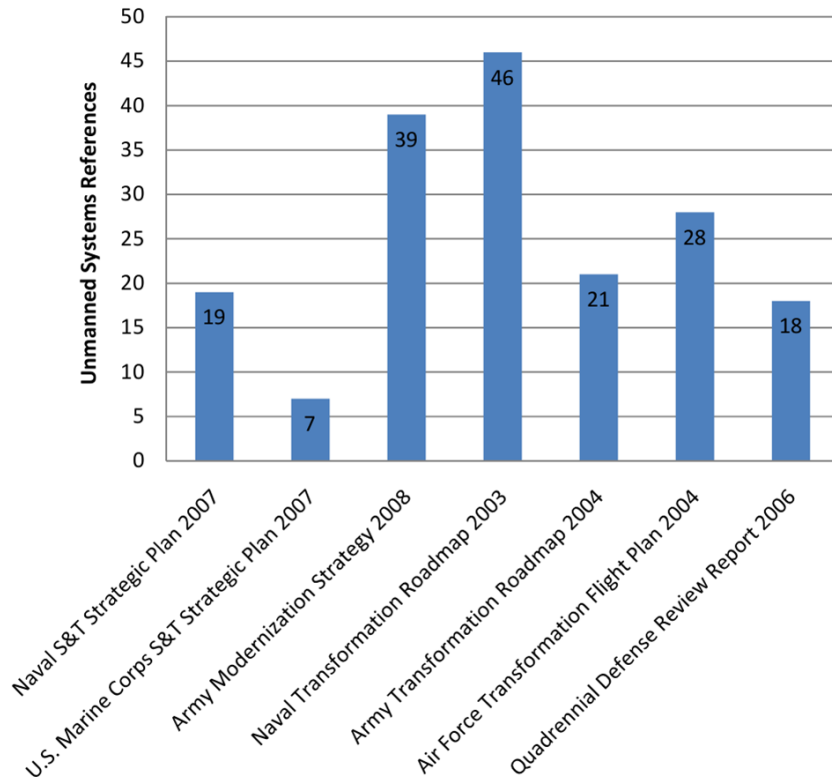


Figure 1: Unmanned System References in Various DoD Strategy Documents [90]

Other seminal publications released by the DoD in reference to unmanned systems include: *Unmanned Systems Integrated Roadmap FY2011–2036 (and FY2013–2038)* [163, 164], *Unmanned Systems Roadmap 2007–2032* [33], *Unmanned Aircraft Systems Roadmap 2005–2030* [173], *The Navy Unmanned Undersea Vehicle Master Plan* [157], *The Navy Unmanned Surface Vehicle Master Plan* [159], *Naval Expeditionary Warfare Vision 2010* [153], *U.S. Army Unmanned Aircraft Systems Roadmap 2010–2035* [161], *The U.S. Air Force Remotely Piloted Aircraft and Unmanned Aerial Vehicle Strategic Vision* [158], *Technology Horizons—A Vision for Air Force Science and Technology During 2010–2030* [151], and the *Unmanned Ground Systems Roadmap 2011* [162].

As the most recent Unmanned Systems Integrated Roadmap (FY2013) states, “there are no requirements for unmanned systems within the Joint force, but some capabilities are better filled by unmanned systems” [164]. In particular, unmanned systems are preferred for missions characterized as dull, dirty, or dangerous. These missions may consist of long-duration and mundane tasks (dull), hazardous conditions (dirty), and/or be inherently life-threatening (dangerous). In these situations, unmanned systems can better fill the capability gap through persistence, versatility, survivability, and reduced risk to human life.

2.1.1 Collaboration Enabled by Autonomy

Operational capabilities of robotic and unmanned systems range from remotely piloted control to completely autonomous functionality. The current levels of technology available to the DoD (along with ethical concerns) have resulted in robotic and unmanned systems that are mostly remotely piloted. However, the DoD does desire greater levels of autonomy [163], which is an important factor in the development of operational concepts for collaborative unmanned systems. Consequently, the DoD has developed a scale of autonomy with four levels of distinction. In order of increasing autonomy the scale is comprised of complete human operation, human delegated operation, human supervised operation and fully autonomous operation. The scale, along with the definition of each level of autonomy, is shown in Table 1.

Table 1: Levels of Autonomy Defined by the DoD [163]

| Level | Name | Description |
|-------|------------------|---|
| 1 | Human Operated | A human operator makes all decisions. The system has no autonomous control of its environment although it may have information-only responses to sensed data. |
| 2 | Human Delegated | The vehicle can perform many functions independently of human control when delegated to do so. This level encompasses automatic controls, engine controls, and other low-level automation that must be activated or deactivated by human input and must act in mutual exclusion of human operation. |
| 3 | Human Supervised | The system can perform a wide variety of activities when given top-level permissions or direction by a human. Both the human and the system can initiate behaviors based on sensed data, but the system can do so only if within the scope of its currently directed tasks. |
| 4 | Fully Autonomous | The system receives goals from humans and translates them into tasks to be performed without human interaction. A human could still enter the loop in an emergency or change the goals, although in practice there may be significant time delays before human intervention occurs. |

The Air Force has echoed this desire for increased autonomy in a recent study called *Technology Horizons* [151]:

The single greatest theme to emerge from ‘Technology Horizons’ is the need, opportunity, and potential to dramatically advance technologies that can allow the Air Force to gain the capability increases, manpower efficiencies, and cost reductions available through far greater use of autonomous systems in essentially all aspects of Air Force operations.

The report goes on to say that “growth in military use of remotely piloted vehicles has been rapid...they will have increasingly autonomous capabilities...some systems may operate collaboratively in multiple-craft missions to increase survivability and deliver effects that could not be achieved individually” [151]. Similarly, other branches of the military have conveyed the desire for autonomy-enabled collaborative multi-agent systems [162, 161, 117]. Ultimately, as the *DoD Unmanned Systems Integrated Roadmap* states, collaborative autonomous systems are not just desired, but required [163]:

*In addition to understanding the environment, unmanned systems **must** also possess the ability to collaborate through the sharing of information and deconfliction of tasking. Collaborative autonomy is an extension of autonomy that enables a team of unmanned systems to achieve common goals without human oversight.*

2.1.2 Recapitulation

A brief summary of the salient details presented up to this point is given below followed by **Observation 3** and **Research Question 1**.

- Collaboration is a fundamental and highly effective attribute of nature.
- Multiagent roboticists have increasingly applied the biological concept of cooperation to gain capabilities not possible through single agent systems.
- The field of collaborative robotics has matured and flourished over the last few decades.
- The DoD has increasingly embraced the use of robotic and unmanned systems within the military force structure and is a major stakeholder in the research and development of these systems.
- The DoD has identified that there is a need and opportunity to gain significant capability increases through the greater use of autonomous technologies.
- The DoD has also determined that unmanned systems utilized within the force structure must possess the ability to operate in a collaborative fashion.
- Cooperation in and of itself does not guarantee greater effectiveness.
- Cooperative SoS should be deliberately designed to meet specific requirements.
- There is an implied necessity for methods that can effectively analyze cooperative SoS architecture alternatives.

Observation 3 *The United States Department of Defense desires greater development and application of autonomous collaborative systems in order to gain increased capabilities across a variety of operations.*

Since the DoD is a major stakeholder in the development and utilization of these types of systems, it is prudent to investigate the procedures used by the DoD to develop and implement such systems. This leads to the following research question:

Research Question 1 *What are the current procedures used by the DoD for the development and implementation of systems and force elements (such as a group of unmanned systems operating in a collaborative manner)?*

2.2 The DoD Process for Determining, Developing and Implementing Solutions

As a consequence of **Observation 3**, the research presented in this dissertation is concerned with the analysis and design of groups of autonomous, unmanned, collaborative systems. Through the investigation of **Research Question 1** (which is detailed in this section), it has become clear that the current procedures utilized by the DoD for the implementation and development of systems and force elements begins with the determination of a *capability*¹ *gap*, as opposed to the identification of a system or force element itself [83]. After a capability gap has been identified, the determination of potential solutions to fill the gap begins. This is a top-down approach, which means that the process begins with high-level goals and then asks “What solutions will meet our needs?”, as opposed to a bottom-up approach which begins with a specific system and asks “What can we do with this technology?”. As will be discussed, Systems Engineering (SE) processes provide valuable tools for managing the analysis and integration of multiple solutions that can fill capability gaps in the manner the DoD desires.

Formally, the starting point of identifying a need within the DoD and recommending a solution is called a Capabilities-Based Assessment (CBA). According to the *Joint Defense Capabilities Study Final Report* [156]:

...a capabilities-based approach elevates the discussion of joint needs to a more strategic level, centering on desired effects rather than specific weapon systems and platforms...strategic objectives would frame the desired effects, which in turn would define the needed capabilities, and ultimately the platforms and weapon systems to be acquired.

¹The DoD defines a “capability” as the ability to execute a specified course of action; the ability to achieve an objective in a military operation [30][83].

The report goes on to say that “this approach would reverse our current practices of packaging weapon systems and platforms into capabilities, assessing what effects we can achieve on the battlefield, and planning operations based on those achievable effects.” In order to meet strategic goals, the objective is to identify potential materiel² and non-materiel solutions, considering solutions based on changes to anything within the full range of doctrine, organization, training, materiel, leadership and education, personnel and facilities (DOTMLPF)³ [40].

Multiple DoD recognized capability gaps were already established in **Section 2.1**. It was also shown that there is a wealth of evidence in the DoD literature suggesting unmanned collaborative systems as solutions to the stated capability gaps. **Therefore, unmanned collaborative systems are analyzed in this work through a top-down capabilities-based perspective.** This is an important point because this research is not suggesting a technology (collaborative systems) and then trying to find an application for them (which would be a bottom-up approach). The capabilities described that are desired by the DoD include:

- Keeping the warfighter out of harm’s way whenever possible.
- Increasing the efficiency of manpower.
- Reducing development and operational costs of systems and assets.
- Increasing the survivability of systems.
- Gaining greater situational awareness.

The capabilities listed above are all strategic level goals that are stated in terms of desired effects, not specific systems (in accordance with a top-down approach). It was pointed out in **Section 2.1** that the DoD has spent considerable effort studying and developing unmanned systems as solutions to fill the capability gaps described above (along with more

²Materiel is defined as *the equipment, apparatus, and supplies used by an organization or institution* [107].

³DOTMLPF is often augmented with ‘Policy’ and subsequently conveyed as DOTmLPP-P. The small ‘m’ is meant to convey that materiel solutions are not preferred if there is another solution available.

gaps not delineated here). Some of the reasons why unmanned collaborative systems are appropriate candidates for filling these needs are as follows:

- Keeping the warfighter out of harm's way whenever possible *through the use of unmanned systems in performing dull, dirty and dangerous (DDD) missions.*
- Increasing the efficiency of manpower *through the assistance of unmanned systems.*
- Reducing development and operational costs of systems and assets since *unmanned systems are typically less expensive to acquire and operate than manned systems.*
- Increasing the survivability of systems *through collaborative operations.*
- Gaining greater situational awareness *through the use of collaborative, geographically dispersed sensing units.*

Furthermore, a capabilities-based approach is not just about filling needs. It is also about mitigating uncertainty: “The United States cannot definitively predict who its next adversary will be or where the next conflict will occur. A capabilities-based approach would help mitigate this uncertainty by emphasizing the nation’s ability to shape the battlefield, regardless of whom we fight or where we fight” [156]. This makes it clear that the development and utilization of unmanned collaborative systems should be organic and applicable to varying missions, not just a single concept of operations. An overview of the capabilities-based approach is shown in Figure 2.

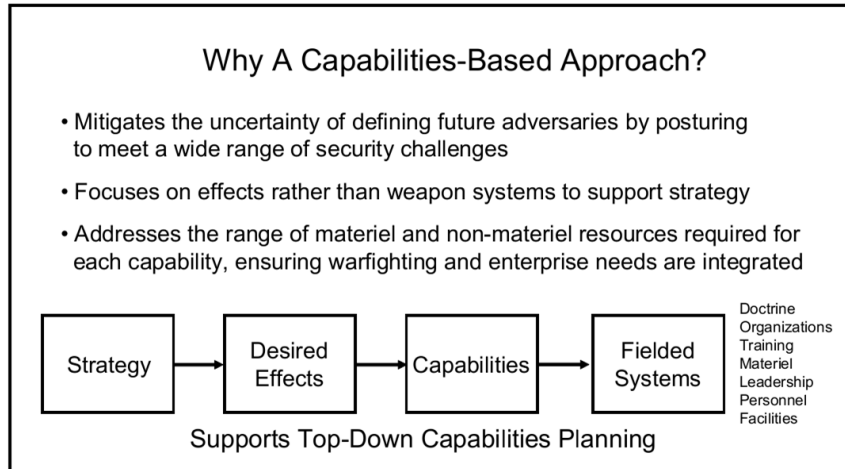


Figure 2: An Overview of the Capabilities-Based Approach [156]

2.2.1 The Joint Capabilities Integration Development System (JCIDS)

A Capabilities-Based Assessment (CBA) is part of the DoD’s process for developing or acquiring a capability such as that provided by groups of unmanned collaborative systems. Specifically, the CBA is the precursor, or formal starting point, of a DoD process called the Joint Capabilities Integration Development System (JCIDS). “The CBA is an analytic basis to identify capability requirements and associated capability gaps...results of a CBA or other study provide the source material for one or more Initial Capabilities Documents (ICDs), or other JCIDS documents” [31]. The JCIDS process attempts to identify and acquire a solution, whether it is materiel or non-materiel.

A simplified view of the process is shown Figure 3. The “Capability Requirements” portion on the left is a product of the CBA. The JCIDS actions on the right of the figure are dependent on the existence of gaps and whether or not the gap can be filled through some means available throughout the Joint forces (through a DOTMLPF change). A more detailed explanation and view of the process is available in Appendix A.

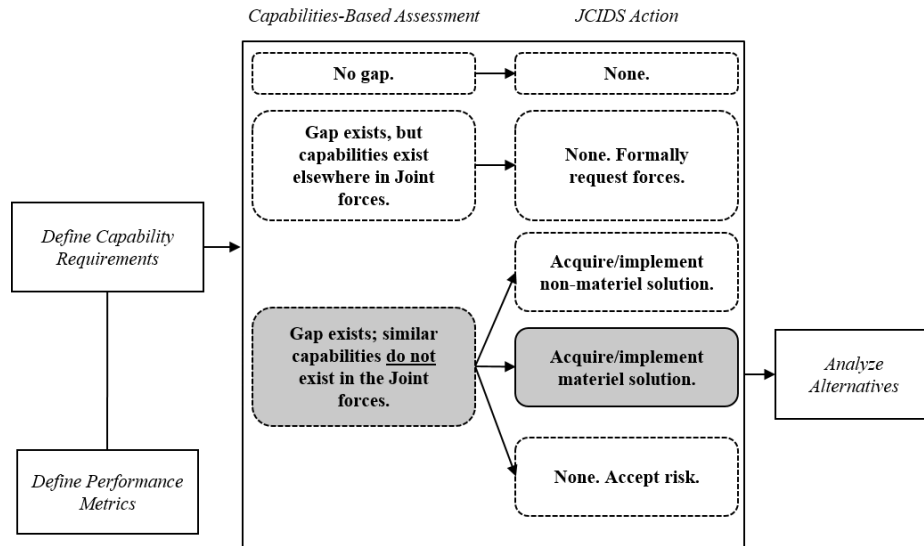


Figure 3: Identification of Capability Gaps and Resulting JCIDS Action, adapted from [31]

The situation which exists in relation to unmanned collaborative systems is similar to that described in the third decision node in Figure 3, which is highlighted in gray. Namely, there is a gap in capabilities, no similar capabilities currently exist in the Joint forces to fill that capability, and it has been proposed that the best solution for filling the gap is through the development of collaborative unmanned systems that utilize high levels of autonomy. This does not mean that new unmanned systems necessarily need to be developed since many already exist within the DoD. However, the proposed solution is to increase the autonomy of these systems, implement new and revolutionary subsystems when necessary (sensors, communication devices and schemes, etc.), apply appropriate control algorithms for collaboration and cooperative CONOPS, and develop new transformational unmanned systems to further fill gaps only if necessary.

Other aspects of the CBA and JCIDS process which are relevant, but tangential, to this research can be found in Appendix A. A brief history of the JCIDS process and its role in the overall Defense Acquisition System can be found there as well.

2.2.2 Recapitulation

This section has presented a rather simplified explanation of the CBA, the JCIDS, and the associated acquisition processes. However, the goal was not to get overly detailed, but to

convey some of the important aspects of the system acquisition and development process in order to set a frame of reference for the research in this dissertation. The main point to take away from this discussion is that *“the key for JCIDS [including the initial CBA] is to establish the high level operational capabilities which are required, place them in the context of overall strategic and operational goals, and be able to compare them to legacy solutions, if any, in order to evaluate the most appropriate path forward to satisfy the capability requirements and reduce or eliminate any associated capability gaps”* [31]. An important detail is that development and acquisition within the DoD requires a thorough investigation of capability gaps and solutions to those gaps. Analysis is therefore an important element in determining one solution over another.

It should be noted that there is no intent within this dissertation to produce any CBA, JCIDS, or DoD Decision Support System documentation. Rather, the purpose of the previous discussion and investigation was to answer **Research Question 1** and motivate the type of process that is crucial in acquiring and developing solutions within the DoD context. Specifically, since the DoD is a major player in the research and development of collaborative unmanned systems, it is important to understand the DoD perspective in this research and development. Furthermore, a key observation is that the DoD utilizes a top-down hierarchical process in determining appropriate materiel acquisitions and developments. The process begins with the identification of a need due to a capability gap and then proposes solutions that can fill the gap. The array of options to fill such a gap may be enormous, since options range from utilizing available systems with various possible CONOPS, developing new systems for use within current CONOPS, augmenting current systems with new systems, and developing new systems along with new CONOPS.

As the next few sections will point out, the number of possible solution alternatives for using unmanned collaborative systems within the DoD are expansive. Therefore, analysis techniques with adequate level of detail will need to be investigated and appropriate design management processes will need to be implemented. It will be shown that Systems Engineering (SE) techniques are appropriate for managing the multitude of requirement sets, disciplinary analyses, and decision making nodes inherent in the design and analysis of

collaborative unmanned systems. Not only so, but many researchers have already applied SE techniques to other development and acquisition programs within the DoD context and will provide a substantial structure for this research to build upon. In addition, quantitative analysis will be given much attention, since “*According to the Joint Chiefs of Staff, technology evaluation for large-scale heterogeneous system architectures is confounded by two opposing constraints: the need for highly detailed analysis and the desire to maintain the large-scale focus of the problem*” [20, 135]. Various means of analysis are investigated relevant to each level of the system design hierarchy and models are developed in representing the physics of the problem, including sensor modeling, vehicle sizing and synthesis, operational planning, system dynamics, and optimal control.

Response to Research Question 1: *The current procedures used by the DoD for the development and implementation of systems and force elements includes a top-down hierarchical capabilities-based approach to defining needs, capability gaps, requirements and performance metrics, determining the appropriate solutions (possibly including systems and force elements) to fill the gaps, and proceeding with the acquisition of solutions if necessary.*

Observation 4 *The DoD has stated specific capability gaps for which no similar capabilities currently exist within the Joint forces to fill that capability, and it has been proposed that the best solution for filling the gap is through the development and implementation of collaborative unmanned systems.*

Observation 5 *Changes and modifications to the operations and capabilities of existing systems should be attempted before designing and acquiring new systems.*

Observation 6 *Due to the large number of solution alternatives possible for designing a group of unmanned collaborative systems, low-level quantitative analysis must be used alongside high-level engineering management strategies.*

2.3 Unmanned System Solutions Available Within the DoD

In order to move forward with unmanned collaborative systems as a solution, questions should be asked as to what steps must be taken in order to implement such a solution. Do materiel solutions (systems and subsystems) currently exist within the DoD that can be utilized to fill the gaps? Can operational concepts be created, implemented, or changed in order to fill the gaps with existing systems? Do new systems need to be developed? How does the development of new systems affect the operational concepts? How can decisions be made regarding alternative systems, groupings of systems, and operational concepts?

Currently, many unmanned systems are in service within various branches of the DoD that can potentially be integrated into collaborative architectures⁴. Figure 4 illustrates the various types of unmanned systems already available to the Air Force, the Army, and the Navy along with the capabilities (or roles) of the systems. The chart also shows the types of systems that are in acquisition (as of 2007) as well as systems envisioned to be incorporated in the future. In addition, Figures 5–7 display specific unmanned aerial, unmanned ground, and unmanned maritime systems available as of 2011.

Multiple areas of research contribute to the ability to employ these systems within a collaborative architecture. These areas can be delineated across several fields of science and engineering:

- **System Design:** Vehicle design considerations including material science and structures, aerodynamics/hydrodynamics, propulsion and power system design, thermodynamics and heat transfer, stability and control, subsystem integration (sensors, communications and localization subsystems), vehicle performance, etc.
- **Electrical Engineering/Computer Science/Robotics:** Artificial intelligence, game theory, graph theory, behavioral control, distributed computing/control, interrobot communications, motion coordination, task allocation, distributed sensing and actuation, network theory, man-machine interfacing, architectural reconfigurability, localization

⁴An **architecture** is the structure of components, their relationships, and the principles and guidelines governing their design evolution over time [IEEE Std 610.12 and DoDAF].

and mapping, collision avoidance, health diagnosis and prognosis, target identification and discrimination, etc. [87, 108, 101]

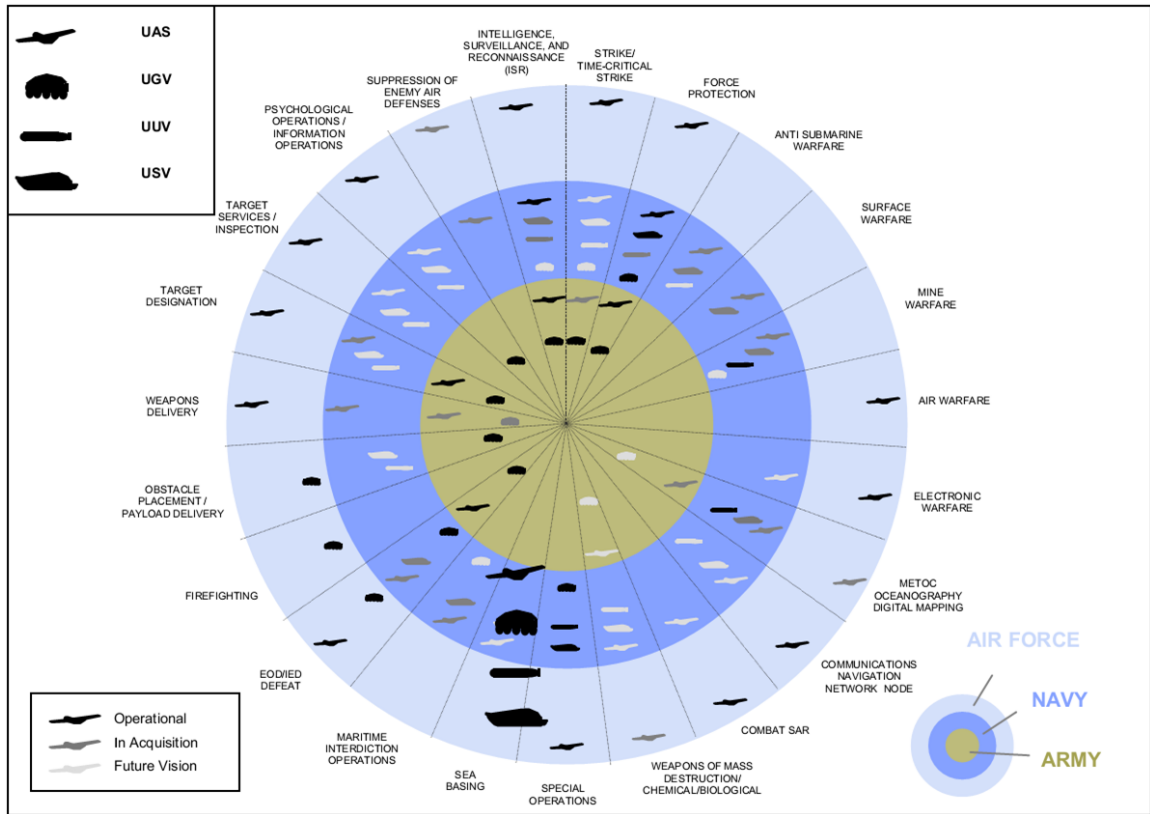


Figure 4: DoD Present and Future Unmanned Systems with Associated Roles [33]

An examination of the multiple disciplines and fields described above makes it clear that many engineering and manufacturing specialties must cooperate on the research and development of a group of unmanned collaborative systems. However, the various disciplines and specialties “often use different names, notations, and views of information even when describing the same concept...yet, the products of the many disciplines must work together to meet the needs of users...they must perform as desired when all the components are integrated and operated” [118].

It is apparent that the design of any single unmanned autonomous system is a truly interdisciplinary exercise. Moreover, the integration of multiple unmanned autonomous systems into a collaborative architecture is an even greater multidisciplinary task. On top of this, a

capabilities-based approach is essential. Since the research presented in this dissertation is concerned with the analysis and design of groups of autonomous, unmanned, collaborative systems (as a consequence of **Observation 3**), it is important that an approach is utilized which can manage the requirement sets, disciplinary analyses, and decision making nodes that will be encountered.




| DoD Unmanned Aircraft Systems <small>(As of 1 JULY 2011)</small> | | | | | |
|--|---|--|--------------------------------|--|---|
| General Groupings | Depiction | Name | (Vehicles/GCS) | Capability/Mission | Command Level |
| Group 5 • > 1320 lbs • > FL180 |  | •USAF/USN RQ-4A Global Hawk/BAMS-D Block 10 •USAF RQ-4B Global Hawk Block 20/30 •USAF RQ-4B Global Hawk Block 40 | •3/3 •20/6 •5/2 | •ISR/MDA (USN) •ISR •ISR/BMC | •JFACC/AOC-Theater •JFACC/AOC-Theater •JFACC/AOC-Theater |
| |  | •USAF MQ-9 Reaper | •73/85* *MQ-1/MQ-9 some OCS | •ISR/RSTA/EW/ STRIKE/FP | •JFACC/AOC- support corps, Div, Brig, SOF |
| Group 4 • > 1320 lbs • < FL180 |  | •USAF MQ-1B Predator | •165/85* | •ISR/RSTA/STRIKE/FP | •JFACC/AOC-Support Corps, Div, Brig |
| |  | •USA MQ-1 Warrior/MQ-1C Gray Eagle | •31/11 •2/0 | •(MQ-1C Only-CS/LG) •Demonstration Only | •NA •NA |
| |  | •USN MQ-8B Fire Scout VTUAV | •14/8 | •ISR/RSTA/ASW/ ASUW/TMW/DMCM/ EOD/FP | •ISR/RSTA/ASW/ ASUW/TMW/DMCM/ EOD/FP •Demonstration Only |
| Group 3 • < 1320 lbs • < FL180 • < 250 knots |  | •USA MQ-5 Hunter | •45/21 | •ISR/RSTA/BDA | •Corps, Div, Brig |
| |  | •USA/USMC/SOCOM RQ-7 Shadow | •368/265 | •ISR/RSTA/BDA | •Brigade Combat Team •Small Unit |
| Group 2 • 21-55 lbs • < 3500 AGL • < 250 knots |  | •USN/SOCOM/USMC RQ-21A ScanEagle | •122/13 | •ISR/RSTA/FORCE PROT | •Small Unit/Ship |
| |  | •USA / USN / USMC / SOCOM RQ-11 Raven | •5628/3752 | •ISR/RSTA | •Small Unit |
| Group 1 • 0-20 lbs • < 1200 AGL • < 100 knots |  | •USMC/SOCOM Wasp | •540/270 | •ISR/RSTA | •Small Unit |
| |  | •SOCOM SUAS AECV Puma | •372/124 | •ISR/RSTA | •Small Unit |
| |  | •USA gMAV / USN T-Hawk | •270/135 | •ISR/RSTA/EOD | •Small Unit |

Figure 5: DoD Unmanned Aircraft Systems [163]




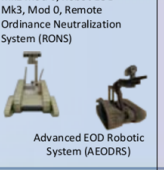

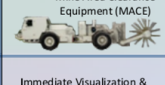


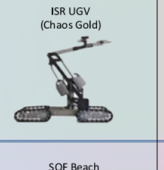





| Unmanned Ground Systems | | | | |
|---|--|---|--|--|
| Mission Areas | Air Force | Army | Navy | Other |
| Maneuver <u>Neutralize the enemy:</u> • IED Defeat Systems • Disarm / Disrupt • Reconnaissance • Investigation • Explosive Sniffer | All-Purpose Remote Transport Sys (ARTS)  F6A-ANDROS / HD-1  | MARCbot IV-N Throwbot xBOT / PackBot FIDO  | Mk1 Mod 0 Robot EOD Mk2 Mod 0, Robot EOD Mk3, Mod 0, Remote Ordinance Neutralization System (RONS)  Advanced EOD Robotic System (AEODRS) | |
| Maneuver Support <u>Mitigate obstacles and hazards:</u> • Area/Route Clearance • Mine Neutralization • Counter IED • CBRNE | Defender  Mine Area Clearance Equipment (MACE)  | MV-4B  Panther II  | ISR UGV (Chaos Gold)  | Local Area Network Droids (LANdroids)  |
| Sustainment <u>Maintain and support:</u> • Common Robotic Kit • EOD • Convey • Log/Resupply | Immediate Visualization & Neutralization (IVAN)  | RC50/60 Mini-EOD R-Gator Andros HD-1 TALON IIB TALON IV TALON/PackBot EOD  | SOF Beach Reconnaissance UGV  | DARPA - Legged Squad Support System  SOCOM - Autonomous Expeditionary Support Platform (AESP) |

Figure 6: DoD Unmanned Ground Systems [163]

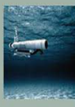

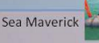

| Unmanned Maritime Systems | | |
|--|---|---|
| Mission Areas | Unmanned Surface Vehicles (USV) | Unmanned Underwater Vehicles (UUV) |
| Mine Counter-Measures (MCM) | Mine Countermeasure (MCM) USV  Remote Mine-hunting System (RMS) AN/WLD-1  | Surface Mine Countermeasure (SMCM) User Operational Evaluation -System Increment 1 -System Increment 2  Battlespace Prep Autonomous Undersea Vehicle (BPAUV)  Surface Mine Countermeasure (SMCM) UUV  |
| Anti-Submarine Warfare (ASW) | ASW USV  |  Sea Stalker  Sea Maverick Semi-Autonomous Hydrographic Recon Vehicle  |
| Maritime Security <ul style="list-style-type: none"> • ISR • Port Surveillance • Special Operations Forces (SOF) Support • Electronic Warfare | SeaFox  Modular Unmanned Scouting Craft Littoral (MUSCL) Use Operational Evaluation  | Mk18 Mod1 Swordfish UUV Sys Mk 18 Mod 2 Kingfish UUV Sys Hull Underwater Vehicle / Hull Underwater Localization Sys (HULS)   Littoral Battlespace Sensing AUV Littoral Battlespace Sensing Glider  ECHO Ranger  |

Figure 7: DoD Unmanned Maritime Systems [163]

2.4 Systems Engineering as an Enabler

As was stated in the previous section, it is important that this research utilizes an approach to analyze and design groups of autonomous, unmanned, collaborative systems which can manage the requirement sets, disciplinary analyses, and decision making nodes that will be encountered. Fortunately, Systems Engineering (SE) tools and processes provide such a desired approach. The International Council on Systems Engineering (INCOSE) defines Systems Engineering as presented below [77]:

Systems Engineering is an interdisciplinary approach and means to enable the realization of successful systems. It focuses on defining customer needs and required functionality early in the development cycle, documenting requirements, and then proceeding with design synthesis and system validation while considering the complete problem: operations, cost and schedule, performance, training and support, test, manufacturing, and disposal. SE considers both the business and the technical needs of all customers with the goal of providing a quality product that meets the user needs.

In accordance with the above definition, SE provides the desired approach. Also, it is clear that an SE approach will not only provide a top-down hierarchical perspective (*i.e.*, a capabilities-based approach), but will be capable of considering the effects of individual system and even subsystem analysis and design in relation to the overall cooperative architecture. As such, attention can be focused towards varying levels of aggregation (*i.e.*, the subsystem, the system, or the overall SoS level) as necessary.

2.5 The Wide Scope of Systems Engineering Teams

Systems Engineering is often implemented within the context of large-scale concurrent engineering (CE) design activities in government and industry. “Concurrent engineering used together with systems engineering provides the necessary framework for not only product innovation but also for process and organization innovation” [97]. In other words, CE along with SE provides a process through which multiple disciplinary teams come together to converge on a total system solution. **Therefore, the synthesis of analyses from various disciplines is imperative in developing a method for a Systems Engineering approach (as this dissertation has set out to accomplish).** However, within CE, multiple subject matter experts, if not teams of subject matter experts, often collaborate towards a solution with a systems engineer or program manager leading the effort. Consequently, it is a tall order to pursue a dissertation in which multiple disciplines must be handled by a single author. Although it is not possible for the author to become an expert in all of the areas that will be covered in this work, there is significant rigor to allow an approach to be tested and analyzed. An example of the wide scope necessary for performing quantitative analyses of a large-scale Operations Analysis design effort is offered by the Naval Academy [152]:

While mathematics provides the basic framework and tools for a quantitative approach, it is by no means a sufficient prerequisite for the solution of operational problems. In problems involving the detection of underwater targets, for example, a knowledge of the physics of underwater sound propagation is essential...In all problems, knowledge of related fields is essential to an understanding of the

problem itself. Thus the analysis of an important problem may properly involve mathematicians, physicists, economists, psychologists, engineers, etc.—a mixed-team approach.

This is similar to the obstacle faced by a control systems engineer who must understand the physical principles that characterize multiple subsystems even though the theories and laws for each discipline can vary greatly. Therefore, the control systems engineer, much like the systems engineer, must have a working knowledge of the necessary disciplines, but cannot possibly be an expert in all that is required. In fact, a major attraction of the systems and controls engineering disciplines is the interdisciplinary nature of the work. The goal is to manage the high level scope of the project while synthesizing the physics of the problem [53]:

The control system engineer sees the “big picture” in the challenge to harmonize the operation of a number of interconnected subsystems, each which operates under a different set of laws. But at the same time the control system engineer is almost totally dependent on the other disciplines. It is simply impossible to gain a sufficient understanding of the details of each of the subsystems in a typical process without the assistance of individuals having an intimate understanding of these subsystems...The analyst needs mathematical models of the processes in the system under study: equations and formulas that predict how the various devices will behave in response to the inputs to these devices.

A seminal example of a CE team managed by SE is NASA JPL’s Advanced Projects Design Team (or Team X). One account of Team X working on a system solution involving 16 engineers stated that “The 16 Team X engineers provide expertise in the various specialized subsystems needed for space mission design, including power, thermal, and telecommunications. The team leader is also a systems engineer” [100]. The interdependencies between disciplines becomes increasingly relevant in this type of environment, and it is crucial for the systems engineer at the center of the project to manage the information flow and design trades. Another author points out about Team X that [61]:

This is a group of spacecraft subsystem experts and system engineers, who together with mission leaders and scientists, use models to quantitatively explore and thereby create conceptual designs for spacecraft. A typical Team X exercise tries to obtain a feasible solution for a desired mission by adjusting the design of each subsystem.

Other successful examples include work at Ford Motor Company [178], John Deere & Company, and the Cadillac Motor Division of General Motors (who received a Malcolm Baldrige National Quality Award in 1990 for their quality improvement efforts brought about by CE) [6].

In the next chapter, multiple concepts which are important for implementing an SE approach will be elaborated upon, including the constructs of design, analysis, and synthesis. Important terms will be defined, Systems-of-Systems Engineering will be explained, and multiple Systems Engineering and Systems-of-Systems Engineering methods will be presented as state-of-the-art approaches.

CHAPTER III

THE ANALYSIS AND DESIGN OF SYSTEMS-OF-SYSTEMS

3.1 What is Design?

For this research it was important to clearly understand the factors, processes and principles that go into designing a product. In general, a product to be designed can take the form of any *thing* desired whether it is a technology, a process, a team, a corporation, a system, a group of systems, etc. In an article from the journal *Science* in 1970 entitled *Design*, Josef Blumrich stated that “design establishes and defines solutions to and pertinent structures for problems not solved before, or new solutions to problems which have been previously solved in a different way” [23]. Blumrich’s definition of design provides a concise statement of the nature of design in an engineering sense, which in essence is to provide a solution to a problem of interest. This is the perspective that will be taken throughout this dissertation, but it is not the only perspective available.

Whether design is applied to an engineering product or not, design is inherently a creative process. Creativity, however, does not mean a lack of thoroughness. Rather, all design should include rigor (even analytical rigor) in order to transform an abstract idea into a practical, feasible and viable reality. As the aircraft designer Daniel Raymer states, “Design is not just the actual layout [of an aircraft], but also the analytical processes used to determine what should be designed and how the design should be modified to better meet the requirements” [122]. George Dieter provides a simple way to think about the balance of ingenuity and analytical rigor in the design process through the four *C*’s of design [42]:

- Creativity: Requires creation of something that has not existed before or not existed in the designer’s mind before.
- Complexity: Requires decisions on many variables and parameters.
- Choice: Requires making choices between many possible solutions at all levels, from

basic concepts to smallest detail of shape.

- **Compromise:** Requires balancing multiple and sometimes conflicting requirements.

Design can be broken into various subcategories depending on the maturity of a product. Sometimes these subcategories are demarcated with terms such as conceptual design, preliminary design, and detailed design.

Continuing with the theme of analytical rigor in engineering design, it is well stated that “Good design requires both analysis and synthesis” [42]. The etymology of the word *analysis* can be traced back to Greek roots for the process of breaking something apart, loosening, or releasing. In contrast, synthesis bears its origins in the composing of elements or the merging of various things (ideas, objects, etc.). In the field of engineering, many designers view analysis as more than just the decomposition of a thing. Rather, analysis consists of the application of appropriate scientific disciplines and computational tools to assist in understanding the performance and behavior of the manageable parts of a decomposed product [42].

Synthesis, on the other hand, consists of the recombination of elements into an overall working system. However, what does it mean to design a “working” system? Or a “good” system? Or an “effective” system? These questions lead to the idea of being able to measure the “goodness” or “effectiveness” of a product. Ultimately, being able to provide a measure of goodness is exactly what the design process aims to produce, since without such an abstraction decision makers and stakeholders will have nothing concrete to help them decide whether or not they desire the product that has been designed. Similarly, during the design process, the designer needs measures of goodness available in order to make trades on specific aspects of the product and determine the combination of parameters that result in the “best” possible design. Therefore, during the design process (*i.e.*, before a product or process actually exists), the ability to measure the effectiveness of the system is completely dependent on the modeling and analysis performed. If the modeling and analysis efforts are far from the true physics of the problem, then the resultant effectiveness measures will be worth very little. Unfortunately, stakeholders will not realize this until the product is

produced and turns out to be much less effective than the engineers had promised. However, if analytical rigor is utilized in the modeling process and the true physics of the problem is incorporated as much as possible, than the effectiveness measures can provide a good feel of what to expect in the real-world. At the least, relative trends between changes in design variables and the effectiveness measures can be quantified. If historical data for similar products is available, than comparisons can be made and corrections can even be implemented in the analyses.

Effectiveness measures go by different names depending on the community involved or the level of system hierarchy being considered (*e.g.*, measures of performance, measures of effectiveness, measures of merit, key performance parameters, etc.). No matter what title is used, these measures are extremely important in being able to assess the value of a design. For example, effectiveness measures drive the analysis of alternatives process, their partial derivatives are often calculated to enable sensitivity analyses, and they are used as the desired objectives in optimization processes. Ultimately, they convey the information desired by decision makers in order to ascertain whether or not customer requirements and desirements are being achieved.

These concepts are important since the research presented in this dissertation is concerned with the *analysis* and *design* of groups of autonomous, unmanned, collaborative systems. As this section points out, design requires both *analysis* and *synthesis*, and alternative designs must produce some type of inherent “goodness” or “effectiveness” that can be measured as functions of design variables and operational uses.

The next few sections will further develop the terminology used throughout this work and explore the principles of analysis and design from the viewpoint of Systems Engineering (SE) and Systems-of-Systems Engineering (SoSE). Then, the method developed as an approach to substantiating the overarching hypothesis of this dissertation will be built from the ground up. The foundation is laid on structured SoSE principles and terminology. The framework will come together through investigating existing, and accepted, SoSE frameworks and generic engineering processes. However, framing the method is just a step in

constructing the whole. Much like when building a home: “Framing, or ‘rough carpentry’, is the basic building skill of new construction and almost every remodeling addition project” [82]. Following the building of the framework, the full substance of the method will come together after reviewing the analytical content of various existing SoSE methods. Subsequently, unique aspects for the new method developed within this dissertation will be delineated. Finally, an experimental approach will be presented which will test the overarching hypothesis of this dissertation.

3.1.1 Further Research Questions

Research Question 2 *What are the core principles that drive the design of a system-of-systems?*

Research Question 3 *What are the existing SoSE frameworks that are accepted by the SoSE community and the DoD?*

Research Question 4 *What insights can be gleaned from existing analytic and quantitative SoSE approaches?*

3.2 A Foundation: Systems Engineering and System-of-Systems Engineering

Before discussing some of the core analysis and design principles related to Systems and System-of-Systems Engineering, accepted standard definitions for both a *system* and a *system-of-systems* (SoS) are presented.

ISO (the International Organization for Standardization), IEC (the International Electrotechnical Commission), and IEEE (the Institute of Electrical and Electronics Engineers) have participated in the development of international standards for various engineering terms. The ISO/IEC/IEEE Standard 24765 for systems and software engineering vocabulary uses various statements for the definition of a system including a “combination of interacting elements organized to achieve one or more stated purposes; a collection of interacting components organized to accomplish a specific function or set of functions within

a specific environment; an interacting combination of elements to accomplish a defined objective” [78]. Another highly regarded organization, the International Council on Systems Engineering (INCOSE), conveys a similar definition for a system which is almost exactly equivalent with the ISO/IEC/IEEE standard. In regards to an SoS, the ISO/IEC/IEEE Standard 24765 definition states that an SoS is “a large system that delivers unique capabilities, formed by integrating independently useful systems”. INCOSE, on the other hand, defines an SoS with a bit more detail stating that an SoS is “a system-of-interest¹ whose system elements are themselves systems; typically these entail large inter-disciplinary problems with multiple, heterogeneous, distributed systems” [77].

At first glance, the definition given above for a *system* seems very similar to that of the definitions for an SoS. In particular, the *system* definition states that a system is a combination of interacting elements organized for a purpose, a collection of interacting components for a specific function within a given environment, which sounds similar to the definition of an SoS. However, a few major differences can be seen in the definitions: 1) an SoS contains elements which are *independent* of one another, while the system definition makes no such requirement for its contained elements; 2) the definition for a system refers to the functionality of the elements within a “specific environment”, whereas the SoS definition makes no such constraint and actually conveys the idea that the elements of an SoS can be widely distributed, whether geographically or otherwise; 3) the SoS definition conveys the idea that an SoS provides a unique capability not achievable by any of the individual components in and of themselves.

The definitions presented above are helpful in making it clear what types of technological groupings are addressed by a specific effort. However, much greater detail to defining the specific differences between systems and systems-of-systems can be pursued. For a more in depth discussion about those defined differences, refer to Appendix B. In addition, novel ways for classifying systems-of-systems are provided in Appendix B as well.

¹A system-of-interest is defined as a system whose life cycle is under consideration.

3.2.1 Critical Terminology

A key element to constructing a methodical approach for this work is understanding how Systems Engineering (SE) and Systems-of-Systems Engineering (SoSE) can be applied to the analysis and design of groups of autonomous, unmanned, collaborative systems. In light of this, various terms associated with the analysis, measurement, and comparison of products and processes are presented here. This will establish a frame of reference for important terminology used throughout the rest of this work. Additional terminology which is relevant but somewhat tangential to the current discussion is provided in Appendix B.

- Performance Requirement: The measurable criteria that identifies a quality attribute of a function or how well a functional requirement must be accomplished [76].
- Measure of Performance (MOP): An engineering performance measure that provides design requirements that are necessary to satisfy a Measure of Effectiveness (MOE; see definition below). There are generally several MOPs for each MOE [76]. Furthermore, MOPs are “Related to inherent parameters (physical and structural) but measure attributes of system behavior” [65].
- Measure of Effectiveness (MOE): The metrics by which an acquirer will measure satisfaction with products by the technical effort [76]. “The criterion by which solutions will be judged - proposed solutions, solutions under test, or solutions in being” [65]. Further, a “measure of how a system performs its functions within its environment. An MOE is generally an aggregation of MOPs” [64]. “A quantifiable value that expresses the effectiveness of the system, system of system, or process under test” [120].
- Trade-off Analysis: An analytical evaluation of design options/alternatives against performance, design-to-cost objectives, and life cycle quality factors [76].
- Analysis of Alternatives: “The evaluation of the performance, operational effectiveness, operational suitability and estimated costs of alternative systems to meet a mission capability...including the sensitivity of each alternative to possible changes in key assumptions or variables” [120].

3.2.2 Design Insights from Systems and Systems-of-Systems Engineering

In **Section 2.4**, it was pointed out that Systems Engineering (SE) can provide an appropriate approach for the analysis and design of groups of autonomous, unmanned, collaborative systems. In addition, it was stated that an SE approach can provide a top-down hierarchical perspective (*i.e.*, a capabilities-based approach), and will also be able to consider the effects of individual system and subsystem analysis and design in relation to the overall cooperative SoS. As such, attention can be focused towards varying levels of aggregation (*i.e.*, the subsystem, the system, or the SoS level) as necessary.

Systems Engineering is more than applicable to the design of an SoS from a system engineer's perspective. "Techniques for treating large and complex systems by isolating the critical components and modeling them are at the heart of the growing discipline called systems engineering" [42]. In many ways, System-of-Systems Engineering (SoSE) is really just a form of SE. It is obvious that the development of a collaborative SoS is a highly interdisciplinary endeavor which incorporates many difficult decisions, analyses and trade-offs which would benefit from specialized SE processes and tools. Similarly, the DoD has recognized that specialized SE techniques are imperative in managing the SoS problem. Consequently, they decided to "develop a guide for systems engineering of systems of systems (SoS), recognizing the value of systems engineering as a key enabler of successful systems acquisition and the growing importance of systems interdependencies in the achievement of war fighter capability" [43]. In reference to SoSE, the DoD has stated that "SoS systems engineering deals with planning, analyzing, organizing, and integrating the capabilities of a mix of existing and new systems into an SoS capability greater than the sum of the capabilities of the constituent parts [40]...the SoS may deliver capabilities by combining multiple collaborative and autonomous-yet-interacting systems. The mix of systems may include existing, partially developed, and yet-to-be-designed independent systems" [43].

The DoD's *Systems Engineering Guide for Systems of Systems* describes major differences between the design and implementation of systems and systems-of-systems. The areas in which comparisons are presented include operational environments, management and oversight, implementation, and engineering and design considerations. Relevant insights

for this research include the operational environments and the engineering and design considerations. Systems are typically designed with specific operational objectives in mind, whereas SoS components may be called upon to perform a set of operational objectives that they were not individually designed for. Therefore, performance of the system from an engineering design perspective may not consider the overall performance within an SoS architecture. Ideally, in designing an SoS and its associated components, high level mission effectiveness of the SoS will be satisfied while balancing the performance capabilities of the individual systems.

From an SoSE perspective, an important consideration is whether the systems that will be integrated into the SoS architecture already exist, if some will be completely new designs, if all will be completely new designs, and if any technologies will be infused. On one extreme of this consideration is that all of the systems and subsystems to be used exist and are subsequently being integrated into the SoS architecture, whereas the opposite extreme is that every system and subsystem must be completely developed and designed. The middle ground, and what is most relevant to the DoD, is the situation where some systems exist, but there is still a gap in capabilities in which new system developments/acquisitions and appropriate technology infusion may be able to close the gap. These are important design considerations due to “the fact that different systems within the SoS will most likely be in different stages of their respective life cycles” [44].

This discussion on the similarities and differences between SE and SoSE leads to the conclusion that SoSE is a specialized form of SE. SoSE attempts to manage many more levels of detail than SE in general. As such, attention can be focused towards varying levels of aggregation. This includes individual system and subsystem design or a much broader perspective of SoS design. The perspective of SoS design takes into consideration how all the elements of the collaborative architecture should be designed and operated in order to meet a set of required *capabilities*. Such an endeavor requires novel design approaches for the development and evaluation of these collaborative systems-of-systems.

As was stated earlier, the research presented in this dissertation is concerned with the analysis and design of groups of autonomous, unmanned, collaborative systems, where the

design goal is to fill a capability gap required by a stakeholder. **Although the discussion up to this point has centered on filling a gap within the DoD, the approach developed within this work for analysis and design is able to handle any generic required capability.** However, every problem requires specialized analyses and assumptions that must be brought to light by the designer or system engineer.

3.3 A Framework: SoSE Core Elements

Figure 8 below demonstrates the core elements of the SoSE process as suggested by the DoD. The figure, which is referred to as a trapeze model, is attempting to demonstrate the differences and relationships between various points of the SoS life-cycle, including development and operations. The development of a *new* SoS is specified to consist of: 1) Translating SoS capability objectives into high-level SoS requirements; 2) Understanding the constituent systems and their relationships; and 3) Monitoring and assessing potential impacts of changes on SoS performance. Although each of the areas outlined for the development of an SoS are initiated for a new SoS, iteration will occur over time assuming that desired capabilities and requirements will change. The desired changes over time are communicated through the persistent SoS overlay framework, SoS upgrade processes, and external influences. In particular, the dark gray box is specified as part of the persistent framework. Its extended title is: Developing, Evolving and Maintaining an Architecture for the SoS. Three boxes are shown to be part of the SoS upgrade process, including *assessing the extent to which SoS performance meets capability objectives over time, orchestrating upgrades to the SoS*, and *addressing SoS requirements and solution options*.

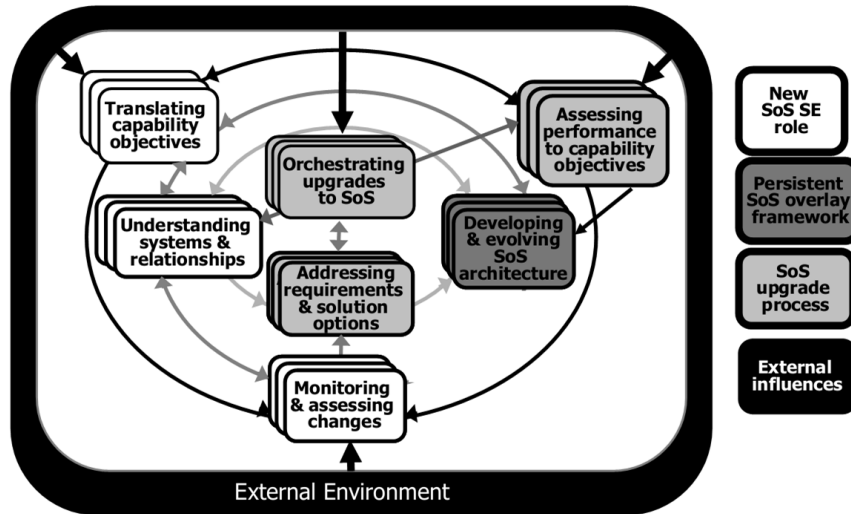


Figure 8: Core SoSE Elements and Their Relationships [43]

The SoSE core elements described above provide context for appropriate SE processes, but they are not usable tools in and of themselves. In order to implement the SoSE approach, the identification of key engineering artifacts² is necessary. These artifacts should convey information about the progress of the SoS design and be implemented into an accepted process or methodology. An effort to establish SE artifacts within an SoSE context was initiated through a cooperative international effort in 2007: *“The U.S. is working with the Australia Defense Materiel Organization on an initiative to develop a shared view of SoS SE and the critical supporting artifacts. This work is an ongoing activity under The Technical Cooperation Program (TTCP) Technical Panel 4: Systems Engineering and Modernization”* [37, 172]. The artifacts developed through this effort have been superimposed over the DoD SoSE elements trapeze model and is shown in Figure 9. Table 6 in Appendix B provides the particular characteristics of each artifact.

²SoSE artifacts are work products developed/composed from various sources by the SoSE team which are managed at the SoS level. They are used by system engineers at both the SoS and single system level in the process of developing, maintaining, enhancing, deploying, and assessing SoS capabilities [94].

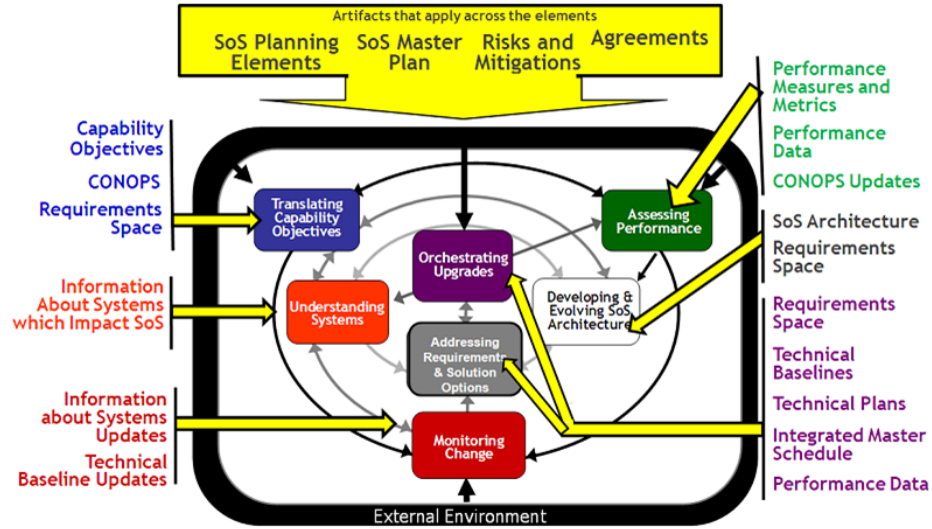


Figure 9: Core SoSE Elements and Their Associated Artifacts [37]

Although the trapeze model of SoSE elements and artifacts presents an insightful view of the salient features of SoSE, it does not provide much help in actually implementing an SoSE process. Due to this shortcoming, a wave model implementation has been suggested: “A wave model of SoS SE unwinds the trapeze model and then maps the core elements to a more familiar view of SoS SE as a series of six time-sequenced major steps in implementing an SoS SE process” [38]. The wave model is shown below in Figure 10. The arrows represent the process flow of the model and the circles embedded within arrows represent potentially iterative steps.

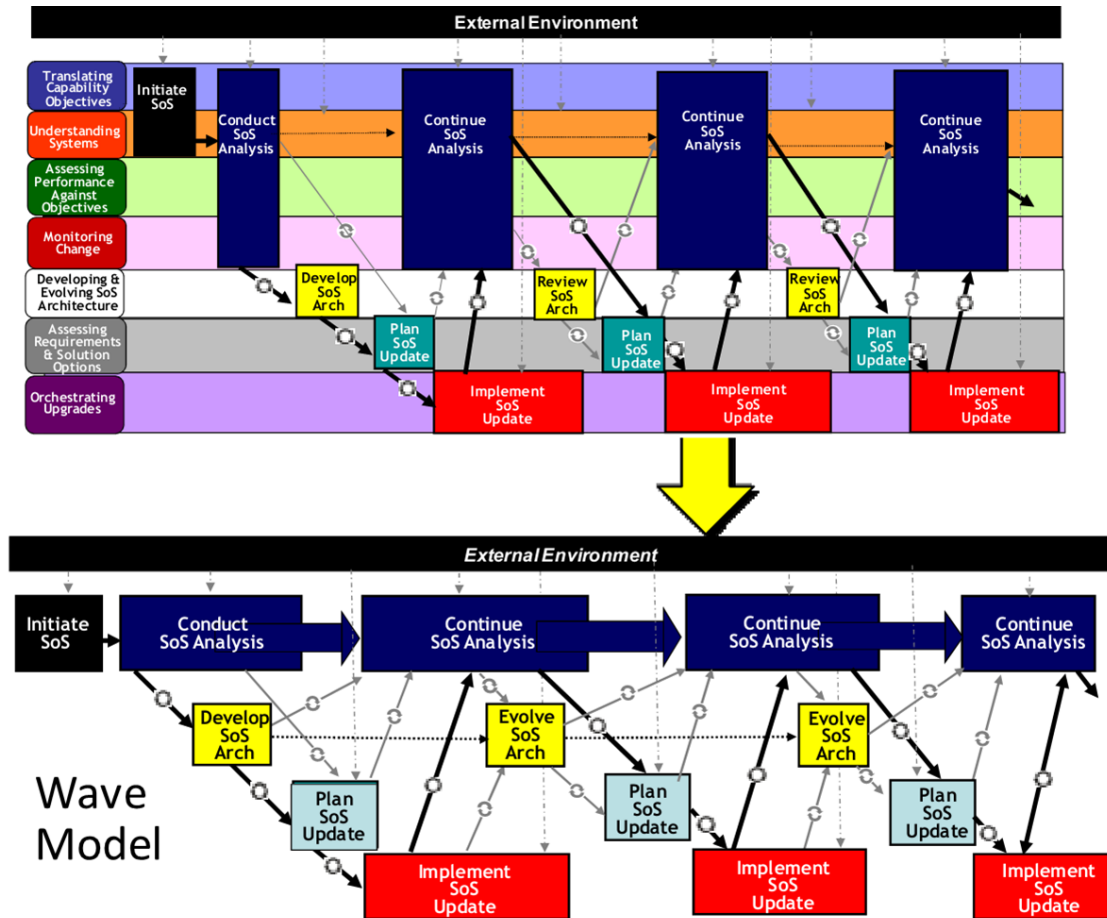


Figure 10: Unwrapping the Trapeze Model to Create an SoSE Wave Model [38]

The wave model is a helpful representation of an accepted SoSE process, although specific activities to be performed are not delineated. It is a framework meant to be built around. A few aspects of the wave model are relevant for framing the method desired in this research. The most relevant piece is to *Conduct SoS Analysis*, since this work is specifically focused on the analysis and design of an unmanned collaborative SoS. In order to conduct an SoS analysis, a desired SoS must be defined based on capability requirements, which is the purpose of the *Initiate SoS* artifact. In fact, multiple alternative SoS solutions should be generated. This includes varying operational concepts and potential systems and subsystems to be used within the SoS [94]. Each alternative baseline will depend on the selection of systems, the numbers of systems, and the various possible CONOPS. Further

descriptions of the specific elements of the wave model are given in Appendix B.

The wave model above has some similarities with another accepted engineering process: the Top Down Design Decision Support Process which is at the heart of Georgia Tech's (GT) Concurrent Engineering Methodology developed by Schrage and Mavris [131]. The decision support process is given in Figure 11.

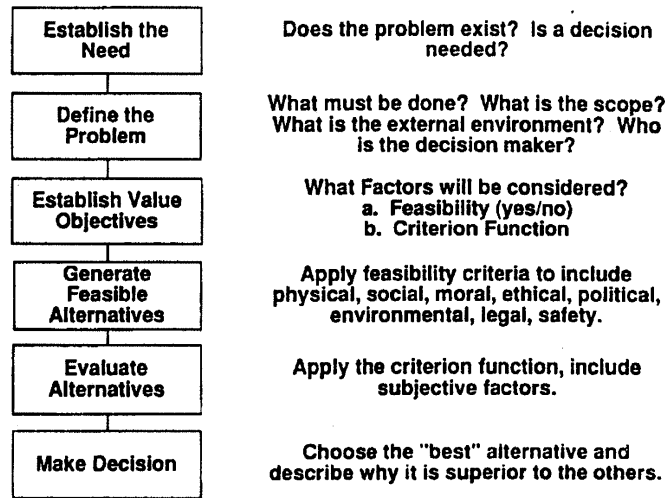


Figure 11: Top Down Decision Support Process [131]

The Top Down Decision Support Process was used as a foundation to build upon, resulting in the Georgia Tech Concurrent Engineering Methodology framework as shown in Figure 12.

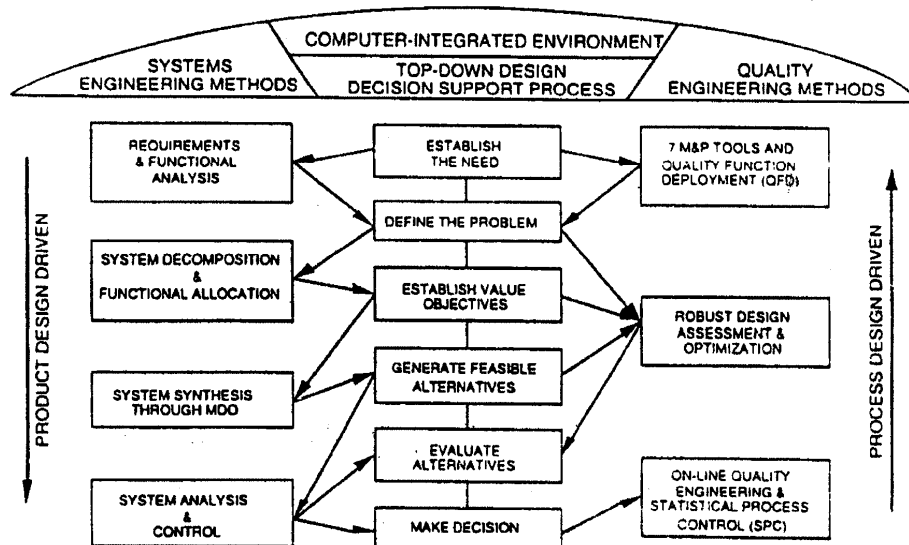


Figure 12: Georgia Tech's Concurrent Engineering Methodology [132]

In particular, the product design driven systems engineering methods are relevant to this research. In fact, many similarities are seen between frameworks when part of the GT method is placed alongside the SoS initiation and analysis artifacts of the SoSE wave model. This is shown in Figure 13.

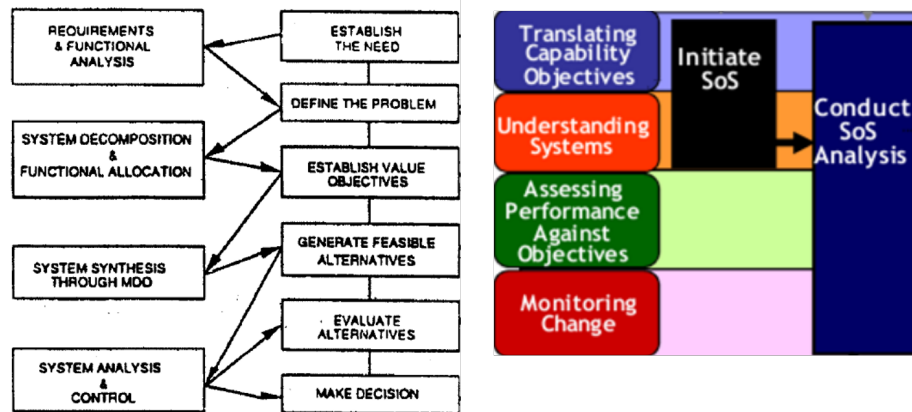


Figure 13: Comparison of Two Accepted Frameworks [132, 38]

A take-away from the review of the frameworks presented above is the fact that a new method can, and often should, be built upon respected and accepted work that has blazed a trail. By taking that perspective, new developments can be made in specific areas in order to provide new and useful approaches along with revealing new and compelling observations not previously available. Since this work is focused on the analysis of alternatives (AoA), a majority of the work spent substantiating the approach is focused on the AoA. However, the AoA has to exist within an appropriate framework. Therefore, a generic framework is adapted from the models presented above. Accordingly, there will be many specific ways to accomplish each step through the generic process, but the majority of the focus will be on substantiating an energy-based analysis of alternatives approach for collaborative systems-of-systems. The adapted generic framework is shown in Figure 14.

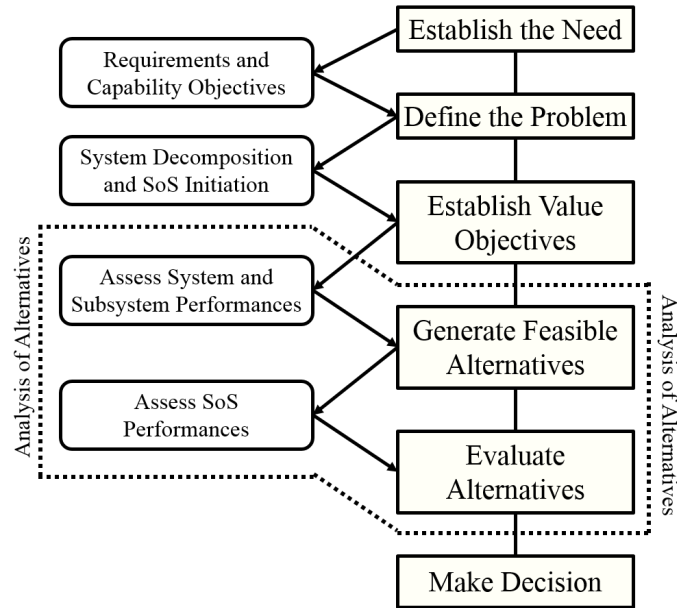


Figure 14: A Generic SoSE Process to be Built Upon

The generic framework presented above can now be built around in order to produce a method for performing the analysis of alternative systems-of-systems. The main contributions from this research are in the analysis of alternatives, which are highlighted in the generic process of Figure 14. However, the process is simply generic and has no substance at this point. Therefore, actual tools for providing substance to each step must be provided. In order to provide substance to the process, actual implementations of SoSE processes will now be investigated. Multiple authors in the field of SE have researched SoSE processes over the last few years with the goal of implementing analytical rigor into the process. Therefore, a few examples of these proposed SoS design methodologies are presented. Each process investigated will have similarities to the generic processes presented so far, but none will fit perfectly. A couple of important points will resurface as these methods are investigated: 1) All of the methods that are presented utilize modeling and simulation (M&S) techniques in order to infuse analytical and quantitative rigor; 2) Special attention will be paid to the ways in which these methods handle the analysis of alternatives for the systems-of-systems.

This section has responded to Research Questions 2 and 3, which asked:

- *“What are the core principles that drive the design of a system-of-systems?”*

- “What are the existing SoSE frameworks that are accepted by the SoSE community and the DoD?”

The next section will address Research Question 4: “What insights can be gleaned from existing analytic and quantitative SoSE approaches”?

3.4 Examples of SoSE Analysis and Design

3.4.1 The PrObabilistic System of System Effectiveness Methodology (POSSEM)

Soban developed the Probabilistic System of System Effectiveness Methodology (POSSEM) in response to the need for a way to assess military system effectiveness at the campaign level, which can be seen as the system-of-systems level. The method was designed to intelligently link changes at the engineering level of systems to clearly defined campaign level (*i.e.*, SoS level) measures of effectiveness. The importance of such a method is that “...decision makers need a way to quantify system effectiveness for three primary purposes: resource allocation, requirements definition, and trade studies between system components” [140]. There are five main steps to Soban’s method:

1. Create Conceptual Model: The creation of the conceptual model in the POSSEM approach is highly related to using Systems Engineering techniques in order to carefully plan a way forward for a particular design problem. The conceptual model in POSSEM is used to answer three important questions:
 - What problem are we trying to solve?
 - What level of detail do we need?
 - What tools are needed and what tools are available?

In answering the first question, “What problem are we trying to solve?”, the designer must consider customer requirements, applicable constraints, potential trade-offs and the overarching goals of any analyses that will be performed. By answering this question the designer can then identify the necessary Measures of Effectiveness (MOEs) which will convey the appropriate information to decision makers and stakeholders.

The second question, regarding level of detail, is important because the ability to measure certain elements of the analysis is highly dependent on the level of fidelity available in the analysis tools and the mathematical rigor that has been utilized. The third question about available and needed tools will answer the question of whether or not the actual level of fidelity desired can be achieved. In POSSEM, these questions are answered through an iterative process since the answer to one question may change depending on the answer to another (*e.g.*, the level of detail possible may change if only a certain level of fidelity can be achieved with the available analysis tools). After answering these questions, the designer will be ready to define appropriate scenarios and missions, establish baseline vehicles and technologies, and determine specific inputs and outputs for the analysis.

2. Identify Key Decision Nodes: In this step the designer(s) constructs tree diagrams related to the desired mission scenarios in order to identify key points at which a human will make decisions concerning the campaign. Probability distributions are then assigned to the paths in order to represent uncertainty in the human decision making process from an operational point of view. “The goal is to retain the flexibility and uncertainty of having a human involved in the decision and assumption making process, yet create an environment in which the computer codes may be run quickly and efficiently.”
3. Create Linked Analysis Environment: This step includes the integration of various analysis models in order to create an environment suitable for investigating the SoS at the campaign level. This environment should be able to answer questions posed in the development of the conceptual model. This step is an exercise in computational synthesis.
4. Create Full Probabilistic Environment: In this step, probabilistic methods are applied to the linked analysis environment of step 3. To do this, ranges are placed on selected input variables of the analysis environment and a Design of Experiments (DoE) is setup in order to run design cases in a systematic fashion that will provide the most

valuable information for a regression analysis. Partial derivatives are then determined, providing insight into the amount of variability each input variable contributes to the outputs. These outputs are tracked for each level of the analysis, from the system component levels all the way up to the campaign level MOEs. Probability distributions are applied to the input variables, and a Monte Carlo simulation is conducted to determine the probability of success in the response space.

5. Analysis: The final step of POSSEM creates links from the outputs of each level of analysis to the next level of analysis (*i.e.*, from the component level of subsystems up to the campaign level of the entire system-of-systems). “In this way, there is a traceable computational path that links the final Measures of Effectiveness down through the engineering level inputs.” The analysis should be able to aid the designer(s) in decision making for resource allocation, trade studies between components, and refining/defining requirements.

Observations from Soban’s POSSEM formulation include:

- High level MOEs are extremely important in order to perform trade-offs, determine resource allocation, and verify the ability to meet necessary requirements.
- Defining the appropriate measures of goodness at all levels of the SoS hierarchy should be done in a traceable manner. SoSE techniques and systematic methods such as POSSEM can assist the designer(s) in establishing the appropriate metrics to track.
- The analysis of components in isolation of the SoS is not sufficient for assessing the overall performance of the SoS. Instead, analysis should be performed with components linked together in the form of integrated analysis environments.
- The benefits of linked analyses of an SoS is reflective of Maier’s explanation (see Appendix B.2) that the design of collaborative systems-of-systems is dependent on the designer exerting control at the interfaces of the components.

A final comment about Soban’s formulation regarding measures of goodness is appropriate. At each level of the SoS hierarchy, as Soban pointed out, there will be various inputs

and outputs (or measures) of analysis. It is clearly difficult, if not impossible, to generalize a set of goodness measures that will be appropriate for any and all SoS designs at any level of the SoS hierarchy. Therefore, a systematic way to determine appropriate measures for a given SoS would be beneficial, but this is not explicitly given in Soban’s formulation. However, it becomes increasingly clear that measures of goodness at the system level (*e.g.*, aircraft, ships, etc.) and even the subsystem level (*e.g.*, jet engines, radar equipment, etc.) are typically related to physics-based measures such as speed, power consumption, etc. However, there are some measures at the system level that are more abstract, such as the survivability of an aircraft (an argument can be made that a measure such as survivability is really an SoS level measure since it is a function of the characteristics of the other systems that are interacting with it in addition to its own characteristics). Nonetheless, Soban gives examples of abstract measures reformulated as functions of physics-based parameters, where the functions are defined as appropriate variable mappings. Furthermore, at the SoS level, measures of goodness are typically framed in terms of probabilities of success of some mission. The distinction between physics-based assessment and more abstract measures will be important throughout this work. The influence of system level performance on SoS level effectiveness will also be paramount.

3.4.2 A Top-Down, Hierarchical, System-of-Systems Approach

Ender and Biltgen formulated and tested a “top-down, capabilities-focused design methodology” which allows decision makers and designers to perform simultaneous bottom-up and top-down design of an SoS [47, 21]. According to Ender, SoS design space manipulation is typically performed using a top-down requirements flow approach in which high-level requirements are decomposed and then flow down a hierarchy of decision making levels. This top-down hierarchical approach parallels the capability-based approach desired by the DoD and referenced by this research. However, Ender found a crucial shortcoming: “This top-down requirements flow approach therefore requires an iterative process between adjacent levels [of the SoS hierarchy] to verify that the design solution satisfies the requirements, with no direct flow between nonadjacent hierarchy levels” [47]. In other words, Ender observed

that the effect of changes to one level of the SoS hierarchy on another level of the hierarchy could not be assessed unless the levels were adjacent (subsystem to system levels, system to SoS levels, etc.). In response to these shortcomings, Ender developed a methodology that “enables decision makers anywhere across a system-of-systems hierarchy to rapidly and simultaneously manipulate the design space, however complex...this takes the notion of top-down requirements flow one step further to allow for simultaneous bottom-up and top-down design, enabled by the use of neural network surrogate models to represent the complex design space.”

In addition, the method presented by Ender is *quantitative* in nature, not qualitative as many SE approaches tend to be. This is enabled by the use of physics-based modeling and simulation (M&S) environments which are stitched together and integrated into an SoS hierarchy. Furthermore, the integrated M&S environment is executed at numerous design points after which the results are used to create parametric representations of the design space that can be rapidly calculated.

The benefits of Ender’s method are numerous, but a major benefit is the notion of instantaneous *bottom-up* design (or forward design), which allows the SoS designers to quickly measure the impact of changes on low-level component design decisions on the overall SoS MOEs and requirements. Similarly, Ender’s rapid, quantitative, *top-down* design approach (or inverse design) allows the designers to place limits or constraints on the high-level MOEs (or requirements) to drive the low-level system and subsystem performance attributes. This enables the notion of top-down *design*, as opposed to the traditional process of top-down *requirements flow*. Finally, Ender points out that the quantitative modeling and simulation of SoS architectures typically results in a design space with “multiple discontinuous behaviors” and highly non-linear, multi-modal topologies. In order to perform the rapid top-down and bottom-up design of an SoS, Ender utilized neural network regressions to represent the design space, enable rapid parametric calculations, and facilitate probabilistic analyses.

Figure 15 below presents an example of the hierarchical sensitivity space produced through this method. The plots shown are filled by taking a slice of the design space at the current settings of requirements, design variables and technologies at each level of

the hierarchy (on the x-axes) and plotting them against the MOPs and MOEs at each level of the hierarchy (on the y-axes). Since the design space is represented by the parametric neural net equations, this sensitivity space is interactive, allowing designers to make changes to requirements, design variables, and technologies and instantaneously see the effect on the MOPs and MOEs. This type of environment, known as the Unified Tradeoff Environment, was adapted by Ender but formalized by Baker [11].

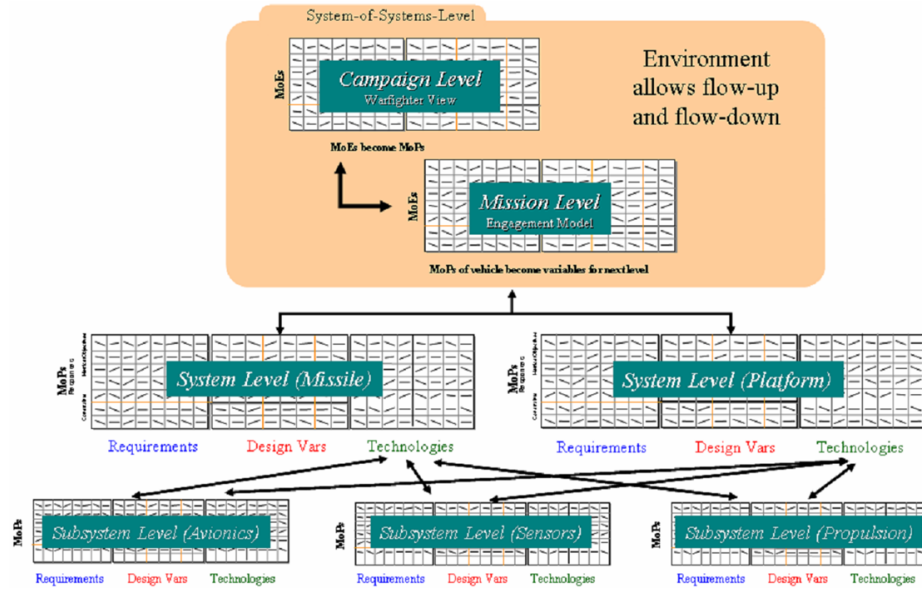


Figure 15: Hierarchical Unified Tradeoff Environment for Systems-of-Systems Analysis [21]

A multivariate plot showing the relationship of forward design versus inverse design that results from Ender’s design process is shown in Figure 16 below. The plot is filled with design points generated by a Monte Carlo simulation executed on the neural net regressions. Viewing the design space in this manner as opposed to only using the partial derivative sensitivity space shown above is a major contribution of Ender’s work. As he states, “*Viewing a hierarchical system-of-systems design space populated using a Monte Carlo simulation brings in the notion of total versus partial derivatives...In the field of mathematics, the partial derivative of a function of several variables is the derivative of that function with respect to only one of those variables, with all other variables held constant. Generally speaking, a curve on a two-dimensional plot is a partial derivative, because it shows how a function varies with respect to one variable. If any of the other variables that*

define that function change, the shape of that curve will change. A total derivative, however, is the derivative of that function when all of the variables are allowed to vary” [47]. Using this type of analysis, Ender observed “interesting phenomena that might not have been possible otherwise. This was due to the fact that the data representing the design space was presented in bulk, rather than just static curves showing a response as a function of one variable, with all other variables (and assumptions) held constant.”

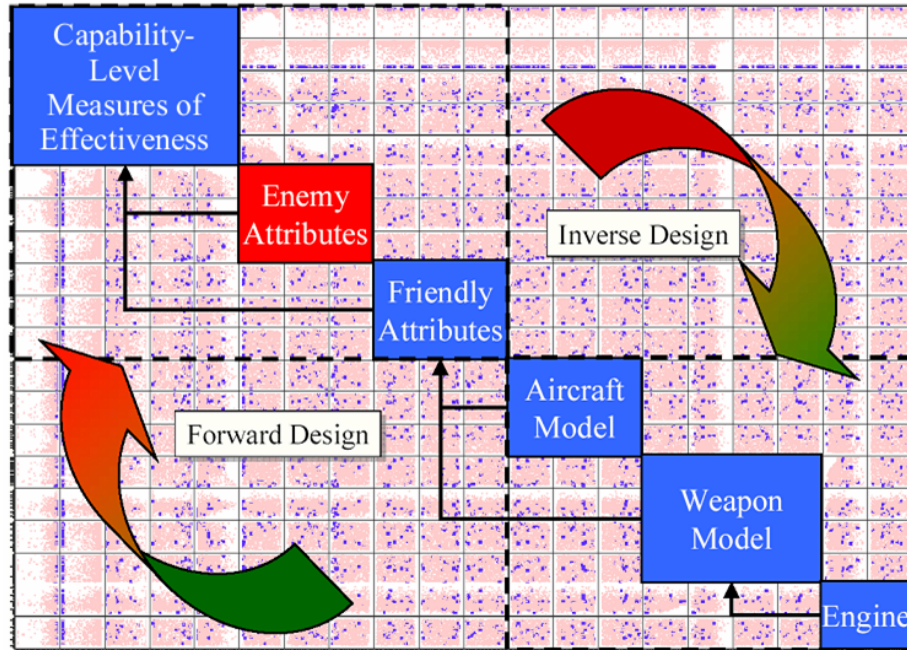


Figure 16: Ender’s Inverse and Forward Design Multivariate Plot [21]

Ender does not provide specific insight for developing measures of goodness in his methodology. They appear to be developed in an ad-hoc fashion depending on the design problem at hand. Accordingly, Ender specifies measures for his test problem based on accepted measures of effectiveness of a gun launched guided projectile meant to intercept a small, indirect fire mortar target, from the literature.

Finally, a last note on Ender’s work. The simultaneous top-down and bottom-up approach of Ender’s method is built upon the ability to create neural network regressions of the design space. However, this is not a trivial task. In fact, because of the highly discontinuous nature of SoS design problems, creating regressions of the design space can require analysis execution efforts which approach computational limits in time. This concern is

outlined further in the next section.

3.4.3 Regressing SoS Architectures

Surrogate modeling techniques can be extremely useful in representing complex, highly computational analyses, with simple to calculate regressions [143]. However, the simplicity of a quick-to-execute regression comes at the cost of high computational effort in creating the regression from the complex analyses in the first place. In particular, at least some of the design variables for an SoS problem are discrete, discontinuous, and large in terms of variable range. A regression technique which uses broad sampling of designed experiments such as a Central Composite Design or a Box-Behnken [111] will likely under sample the design space [75]. Furthermore, SoS performance measures are often calculated based on numerous complex modeling efforts which, when synthesized, can produce multiple discontinuities, non-linear behavior, and multi-modal topologies [47]. Therefore, capturing the nonlinear and discontinuous characteristics of an SoS design space through regression analyses can be computationally expensive and mathematically difficult (if even possible).

Second-order regressions, even with large sample sets of data (*e.g.*, a space-filling DoE) cannot capture the discontinuities often associated with SoS design topologies. Even if multiple second-order response surface equations are used in a piece-wise fashion, they may still suffer the “curse of dimensionality”³ inherent of SoS design problems [143]. Alternative options with promise include the *adaptive methods* such as Support Vector Machines (SVM), Relevance Vector Machines (RVM) and Artificial Neural Nets (ANN). The adaptive methods primarily depend on training data regardless of the number of input variable dimensions, therefore they can overcome the curse of dimensionality. Kernel-based methods (*e.g.*, SVM and RVM) store training data to be used during prediction of the responses. Unfortunately, this causes them to be slow in prediction despite their relatively quick speed of training. ANNs on the other hand require a computationally expensive training process, but they are rapid in prediction [143]. Furthermore, ANN’s are known to be superior in modeling nonlinear data sets [174].

³R. Bellman. Dynamic Programming. Princeton Univ. Press, 1957

The superiority of ANN’s in modeling nonlinear data stems from Kolmogorov’s Universal Approximation Theorem (UAT). The UAT states that [79]:

Any continuous function defined on a compact subset of \mathbb{R}^r can be uniformly approximated (in an appropriate metric) by a function of the form [of a single layer perceptron neural network].

This can be stated mathematically as given by Xu [181]:

Let φ be a continuous activation function. Given any continuous real valued function f on the interval $[0, 1]^{\mathbb{R}}$ and $\varepsilon > 0$, then there exists a matrix $W = [w_1, w_2, \dots]$, vectors α and β , and a parameterized function $Y(\varphi, W) : [0, 1] \rightarrow \mathbb{R}$ such that:

$$|Y(\varphi, W) - f(x)| < \varepsilon \quad \forall x \in [0, 1]^n$$

$$\text{where } Y = \sum \alpha \varphi(Wx + \beta)$$

In other words, the UAT guarantees that an ANN can produce a regression of any continuous function within a specified error, ε . Unfortunately, the training time and data set size required to obtain less than ε error for a highly nonlinear function is unbounded, and the ability to capture discontinuities is still not guaranteed.

Despite these limitations, ANNs and other regression techniques can be powerful tools in representing complex analyses and providing closed-form solutions. With enough computational effort and analysis data, these regressions may be able to even capture discontinuities within acceptable error bounds. This was the approach taken by both Ender [47] and Biltgen [20].

3.4.4 A Methodology for the Robustness-Based Evaluation of Systems-of-Systems Alternatives Using Regret Analysis

The intent of Poole’s work was to “improve the current state-of-the-art in early defense acquisition processes through increasing the engineer’s and decision maker’s ability to compare the robustness of competing alternatives” [120]. Poole developed a methodology that “coupled regret analysis and massive scenario generation with surrogate modeling techniques in a parametric environment.”

Poole's definition of *robustness* is the ability of a system to perform well over a wide range of conditions. This type of formulation is advantageous for its handling of uncertainty, especially in considering changes to operating environments and mission requirements. Another important piece of Poole's method is the integration of regret analysis which is "a way of measuring the merit of a particular system solution for a set of operating conditions." According to Poole, "regret is the difference between a system's evaluation metric(s) and the best system's evaluation metric(s) for a scenario." It is a measure of the degree to which a system falls short of the optimum for a particular solution.

Ultimately, in formulating the methodology, Poole points out that although the steps used in a methodology architecture must be settled upon, there are many different architectures that can actually be utilized. This is because there are multiple tasks possible for each step of the method. Figure 17 below displays a matrix of alternatives provided by Poole for fulfilling each task of the method. The matrix is only a subset of possible tools available in the literature, but even with the subset shown there are 338,688 possible methodologies that could be constructed if each step of the method was assigned only a single tool from the matrix. Obviously, the number of combinations grows if multiple tools are allowed to be used in any of the steps shown.

| Task | Alternative 1 | Alternative 2 | Alternative 3 | Alternative 4 | Alternative 5 | Alternative 6 | Alternative 7 |
|----------------------------|--------------------------|-------------------------------|-------------------------------------|--------------------------|---------------------------|----------------------------|--------------------------|
| 1. Establish the need | User Query | Technologist Query | Gap Analysis | | | | |
| 2. Define the problem | Utility Curves | Functional Flow Block Diagram | Scenario and Environment Definition | Requirements Tracing | Kano Method | Interrelationship Diagraph | Cause and Effect Diagram |
| 3. Establish MoPs and MoEs | Tree Diagram | GOTChA | Affinity Diagram | Pugh Diagram | Prioritization Metrics | QFD | |
| 4. Generate architectures | DoDAF | FEAF | Gartner | MoDAF | TOGAF | Zachman | |
| 5. Generate alternatives | Swarming | Morphology | Brainstorming | BOGSAT | | | |
| 6. Analyze alternatives | Expert Query | Structure Simulation | Continuous Simulation | Discrete Time Simulation | Discrete Event Simulation | Build & Test | Surrogate Models |
| 7. Compare results | AHP | OEC | TOPSIS | Pareto Frontiers | | | |
| 8. Make a decision | Electronic Design Review | BOGSAT | Single Point Decision | Report - based | | | |

Figure 17: Poole’s Methodology Matrix of Alternatives [120]

Poole goes on to conclude that the tools selected for each engineering task of a methodology must be chosen based on their appropriateness relative to the particular application. Therefore, the options chosen from the matrix of alternatives above (or one like it) will vary depending on the problem at hand. Poole applies his work to a specific SoS example of a U.S. Air Force Persistent Precision Strike mission involving multiple Unmanned Combat Aerial Vehicles (UCAVs). The method settled upon for Poole’s application is shown in Figure 18 below. However, Poole does not provide any direction on how to down select alternative pieces of the methodology other than utilizing subject matter expert (SME) opinions.

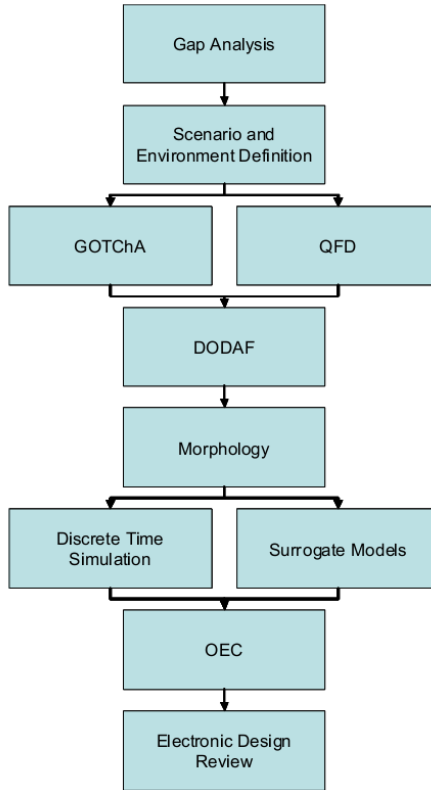


Figure 18: Poole's Applied Method [120]

As was shown in the matrix of alternatives, Poole does present a number of options for establishing measures of goodness (MOEs and MOPs). These options include using a tree diagram, the GOTChA⁴ method, an affinity diagram, a Pugh diagram, prioritization metrics, or a Quality Function Deployment (QFD). Each of these methods are based on decomposing a problem and qualitatively determining the measures of merit desired. Poole does not outline the process which was used in his research to perform the GOTChA and QFD methods, even though those were the processes used to choose the MOPs and MOEs in the Persistent Strike test problem. Instead, similar to Ender, Poole states metrics in a rather ad-hoc fashion. The MOPs selected for the individual aircraft were *fuel capacity* and *weapons capacity*. The MOEs were delineated as:

1. The percentage of available targets located and killed by the SoS
2. Time for the available targets to be found and killed

⁴The GOTChA process is a method of brainstorming approaches to solve the requirements [13]

3. The number of times the aircraft had to resupply during the mission
4. The cost of operating the systems

Again, similar to Ender, these metrics seem to have been established by reviewing the pertinent literature related to Poole's test problem.

3.4.5 The CONceptual Design of Opportunistic and Robust System-of-Systems (CONDOR-SS) Method

The CONDOR-SS method was developed due to the observation of several gaps in existing SoS design methods. These gaps were delineated by Talley as follows [145]:

- Existing SoS design methods are incapable of modeling all of the different types of relevant uncertainty.
- Existing SoS design methods do not specifically address the fact that there can be propitious effects from uncertainty as well as pernicious.
- Existing SoS design methods focus on identifying the most effective design alternative with respect to the relevant uncertainty. However, no method focuses on determining if the uncertainty should be reduced before making the final design decision.

Clearly, these observed gaps were characterizations of the way uncertainty is handled in SoS design. As Talley states, *“the design of the SoS, especially in the conceptual design phase, is generally characterized by significant uncertainty...it is possible for all three types of uncertainty (aleatory, epistemic, and error) and the associated factors of uncertainty (randomness, sampling, confusion, conflict, inaccuracy, ambiguity, vagueness, coarseness, and simplification) to affect the design process.”* Aleatory uncertainty is due to natural, unpredictable variations in system performance, whereas epistemic uncertainty arises from a lack of knowledge about the behavior of the system [72]. Aleatory uncertainty is often referred to as irreducible uncertainty. Epistemic, however, can be reduced or eliminated in principle. Error can be considered a type of uncertainty since the true value is unknown. However, error is not due to a lack of knowledge, but is a deviation from correctness or

accuracy. Talley presumes that error is typically insignificant compared to aleatory and epistemic uncertainty. Therefore, error is not considered in the CONDOR-SS formulation.

The overall SoS design methodology presented through CONDOR-SS utilizes a top-down design approach. In the formulation, the design process begins at the highest level of the SoS and then moves down to the next level of abstraction. Once the design process is initiated at the second level, information may be fed back up to the level above it (a feedback loop of sorts) to determine if objectives and constraints are being met. The purpose of these feedback loops is to reduce uncertainty throughout the process. This process continues down all the levels of the SoS being considered. Each level of the SoS hierarchy follows the same specific steps delineated by Talley. These steps include:

1. Define the problem
2. Define systems, the system architectures, and scenarios
3. Identify system and scenario uncertainties
4. Create or select a Modeling and Simulation (M&S) environment
5. Identify critical uncertainty and design variables
6. Create surrogate models
7. Identify new alternatives
8. Evaluate alternatives for the SoS level
9. Quantify the value of reducing uncertainty
10. Gain more information
11. Select a concept or group of concepts for the SoS design level

Figure 19 below displays the overall design process including feedback loops at each level of the SoS. Figure 20 zooms in to present the steps performed within each level of the SoS design process facilitated by CONDOR-SS.

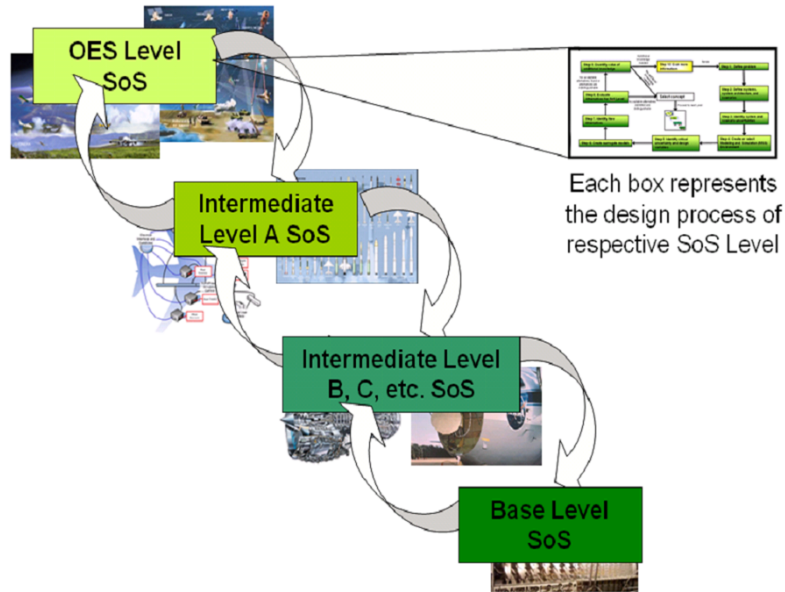


Figure 19: Talley's SoS Design Process [145]

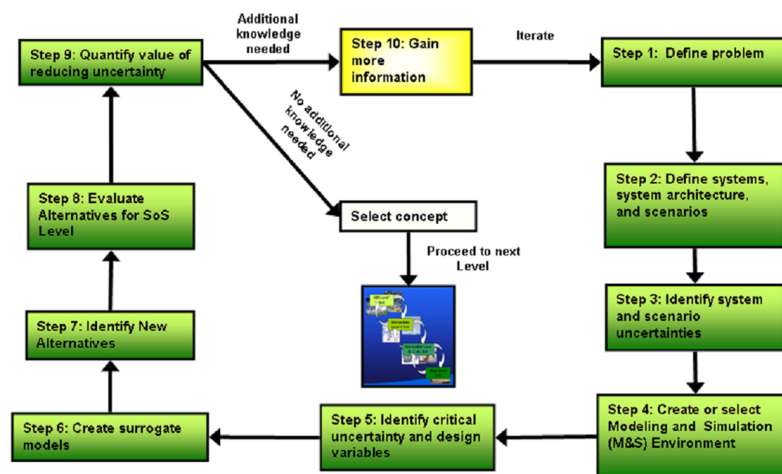


Figure 20: Talley's Process for Design at Each SoS Level [145]

In the CONDOR-SS method, defining the MOEs and MOPs occurs during the first step (Define the Problem) of each design level. Once again, definition of the MOEs and MOPs in the method are assessed through consideration of the design problem at hand. There is no formal approach presented by Talley.

While the CONDOR-SS method has a great deal of potential in the design of systems-of-systems, as Talley points out the method is very “computationally expensive...and if large numbers of uncertain variables are considered, this technique would be impractical

to implement, even with the use of techniques like surrogate models to reduce the analysis time.”

3.4.6 Digraph Modeling for Architectures (DiMA)

As has been discussed in this work, the analysis of systems-of-systems is a highly combinatorial, difficult to manage problem. In order to implement analytical rigor in the design of an SoS, modeling and simulation (M&S) environments are often utilized. This provides the benefit of quantitative analysis and infuses information above that available through qualitative Systems Engineering techniques. All of the methods presented so far have advocated the use of physics-based M&S along with various types of regression analyses for representing the M&S environments through parametric equations. However, these campaign-level SoS M&S environments, often referred to as *constructive simulations*, are generally expensive to create and utilize. In addition, they are difficult to verify and validate. Balestrini developed the Digraph Modeling for Architectures (DiMA) process in response to these shortcomings. In developing DiMA, the objective was to enable the quantitative comparison of architectures in terms of their ability to satisfy a capability without resorting to constructive simulations in a rapid, affordable and defensible manner [12].

In the DiMA formulation, instead of specifically attempting to measure performance and effectiveness of the individual systems, the goal is to measure a series of network metrics to assess the overall behavior of the SoS. The network metrics measure the cyclicity of the networked systems in the SoS through the use of Graph Theory and Network Theory. The required SoS capabilities are described as a cycle of functions. Therefore, calculating the network metrics conveys the ability of the architecture to perform a capability.

The steps of the DiMA process are as follows:

1. **Identify Functions** Determine which functions are required to achieve the capability or capabilities of interest (these functions are not yet linked to any particular systems).
2. **Identify Systems** Determine the types of systems to be included in the architecture (at this point systems are identified that can perform the functions required by Step 1).

3. **Identify Requirements for Functional Interaction** Determine which interactions or relations must exist between systems for a functional relation to be possible.
4. **Determine Probability of Occurrence** Determine probability of occurrence of interactions between the system types (Balestrini recommends that the values given in this step be defined through SME opinion).
5. **Create the In-degree Constraint Matrix and Out-degree Constraint Matrix** Specify the maximum number of inputs and outputs each system type can have for each function. These matrices tend to be sparse.
6. **Define Force Structure** Specify the numbers for each type of system.
7. **Simulate Stochastic Engagements** This step consists of creating a representative Engagement Matrix from the Engagement Generation Matrix.
8. **Compute Network Metrics** In this step the stochastic engagements can be analyzed to compute metrics from the networks (or graphs) for each of the different repetitions.
9. **Perform Statistical Analysis** The repetitions executed of the two previous steps must be analyzed to obtain statistics of the performance of the architecture.

DiMA is novel in that it does not attempt to directly calculate typical MOEs and MOPs. Instead, the network metrics are used to describe the SoS behavior in a way that allows the relative comparison of architectures in a rapid fashion without detailed analyses. A major benefit of this is that architectures can be compared from a global perspective. The network metrics implemented by Balestrini are attempting to convey information that is characteristic of any SoS. In addition, the consequence of adding or removing an element from the architecture can be quickly assessed. However, DiMA does not provide much information on the low-level performance of individual systems, which consequently means it cannot provide insight into the sensitivity of low-level design changes against the overall SoS capabilities.

3.4.7 The Architecture Real Options Complexity-Based Valuation Methodology (ARC-VM)

The Architecture Real Options Complexity-Based Valuation Methodology (ARC-VM) was developed by Domercant as a way to assist in “acquisition-level decision making, where there is a stated desire for more informed trade-offs between cost, schedule, and performance during the early phases of design” [44]. In developing the methodology, Domercant first introduces a framework for measuring architectural complexity of an SoS. Then, a valuation strategy based on Real Options is established.

A major component of Domercant’s methodology relevant to this work is the development of a measure of complexity as an *objective measure* which provides the ability to perform “more informed tradeoffs when determining the number, types, and relative complexity of constituent systems under consideration, the degree of overlapping/redundant functionality present, and also the patterns and levels of collaboration that provide the greatest benefits” [44]. Similar to Balestrini’s network metrics in DiMA, Domercant’s complexity measure provides a metric with a global perspective of the SoS architecture. Whereas most of the SoS design techniques presented so far utilized metrics that were determined in an ad-hoc fashion depending on the problem at hand, Domercant’s complexity measure is *objective* and should be able to apply to any architecture of multiple interacting elements. Furthermore, the complexity of an SoS should have a definable relationship to important design consequences such as “the cost, schedule, and performance of acquisition programs.”

Figure 21 below shows two different SoS architectures and their calculated complexity values as formulated by Domercant. The complexity values are defined as a utility function of the elements of complexity shown. The elements of the complexity function include the *Functional Distribution Complexity* (FDC), the *Functional Processing Complexity* (FPC), the *Resource State Complexity* (RSC), and the *Resource Processing Complexity* (RPC).

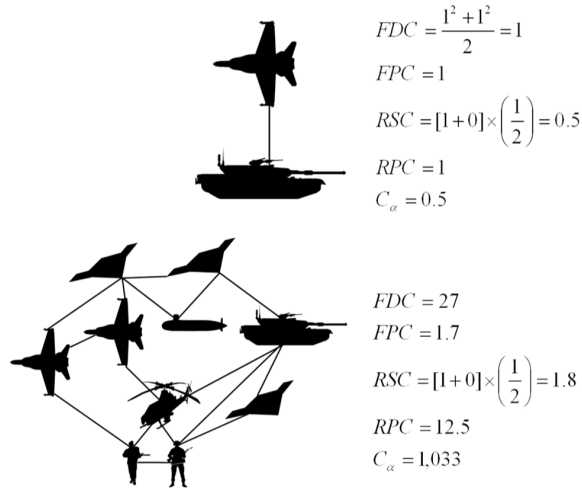


Figure 21: Domercant's Complexity Metric for Two SoS Architectures [44]

3.4.8 Rapid Architecture Alternative Modeling (RAAM)

The goal of developing the RAAM method was to: “Develop a new methodology for compactly describing and evaluating architecture alternatives. This will improve capability based analysis by reducing runtime and model creation complexity as compared to existing executable architecture models with limited to no fidelity loss” [75]. The methodology is initiated with a set of stakeholder required capabilities which are inputs to the method. The method consists of six main steps and results in a recommended portfolio of systems to be procured that can address the required capabilities. The steps of the RAAM method are as follows:

1. Determine Required Derived Capabilities
2. Create Capability Hierarchy
3. Define Candidate Systems
4. Define System of Systems Computer Models
5. Analyze Potential System of Systems Architectures
6. Determine Optimum Portfolio

As has been stated in this work, Iacobucci points out that “the system of systems architecture alternative space is discrete and the computational models are often non-linear...surrogate models are difficult to fit across such a large design space with discrete elements [and] broad sampling [such as Monte Carlo simulation] may miss important non-linear interactions” [75]. Iacobucci claims that RAAM can overcome these issues by rapidly exploring the entire design space and the fidelity of the included models are only limited by the effort of the analyst. Ultimately, however, it is a 1st-order, low fidelity analysis technique [66].

3.4.9 The Architecture-Based Technology Evaluation and Capability Tradeoff Method (ARCHITECT)

The Architecture-Based Technology Evaluation and Capability Tradeoff Method (ARCHITECT) was developed to be a capability-based SE method for improving agility in defense acquisition by (1) streamlining the development of key elements of JCIDS and DoDAF⁵, (2) moving the creation of DoDAF products forward in the defense acquisition process, and (3) using DoDAF products for more than documentation by integrating them into the problem definition and analysis of alternatives phases [66]. The formalized steps of the ARCHITECT method consist of problem formulation, metrics derivation, gap analysis, alternative identification and generation, alternative analysis, and decision-support. Figure 22 below shows the inputs and outputs required by each step of the ARCHITECT process. It is noticeably built around the framework provided by the Georgia Tech Top Down Decision Support Process.

⁵DoDAF is the *Department of Defense Architecture Framework* which was created to aid in design and decision-making for large and complex systems and SoS in a capability-based context [66].

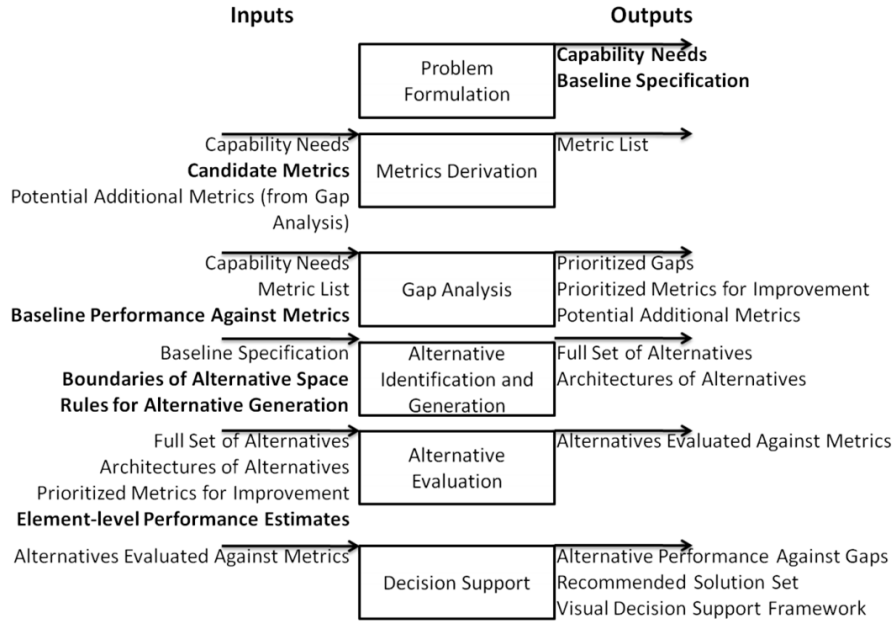


Figure 22: Inputs and Outputs for Each Step of the ARCHITECT Methodology [66]

For the metrics derivation portion of the ARCHITECT process, Griendling utilized the Relational-Oriented Systems Engineering Technology Tradeoff Analysis (ROSETTA) construct. ROSETTA was developed to provide “a structured means for fusing qualitative and quantitative data in engineering analyses” [66]. It can assist in the derivation of metrics since it provides a formal way to decompose and map the information needed at the capability level down to the measurable values that will be used to compare alternatives. Not only does ROSETTA provide a structure to perform the decomposition and mapping, but it tracks *how well* the candidate metrics map back up to the capabilities level. It also accounts for the impact of metric dependencies, which can allow the designer to reduce the total metric set by removing redundancies. “By understanding how the metrics are correlated, it is possible to identify cases where improvements in one area will lead to improvements in another, and therefore track only the less expensive of the two metrics.” The SoS breakdown of the ROSETTA framework as applied to the ARCHITECT method is shown in Figure 23 below. It starts by assigning mappings from the desired mission to the capabilities required for that mission. The designer can then map capabilities down to MOEs, MOEs to MOPs (even several levels of MOPs), and finally map MOPs down to the

independent design variables (IVs).

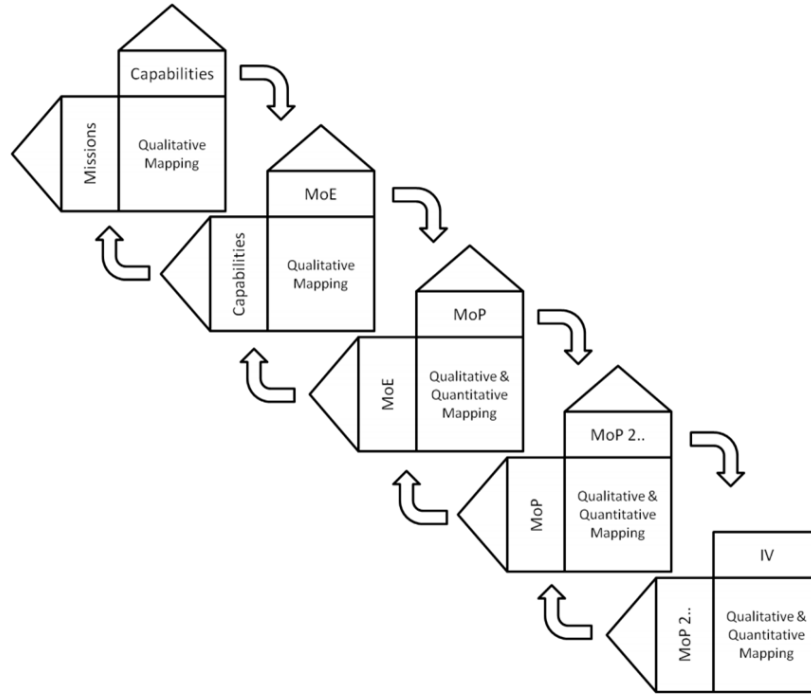


Figure 23: An SoS ROSETTA Decomposition [66]

3.4.10 Further Observations

From the methods surveyed and presented, multiple activities have been established as possible pieces to be integrated into a generic SoSE process for the analysis and design of unmanned, collaborative, systems-of-systems. To portray this, the various techniques along with their authors have been placed alongside the generic process presented earlier (see Figure 24 below). As is shown, options are available to assist in *Defining the Problem* (conceptual model creation, formal problem formulation techniques, uncertainty considerations), *System Decomposition and SoS Initiation* (integrating available models, generating alternatives, deriving metrics), and *Analyzing SoS Alternatives* (design of experiment techniques to cut down the design space, regression analyses, multivariate plots, uncertainty analysis, network analysis, complexity analysis, regret analysis, and the integration of executable architectures).

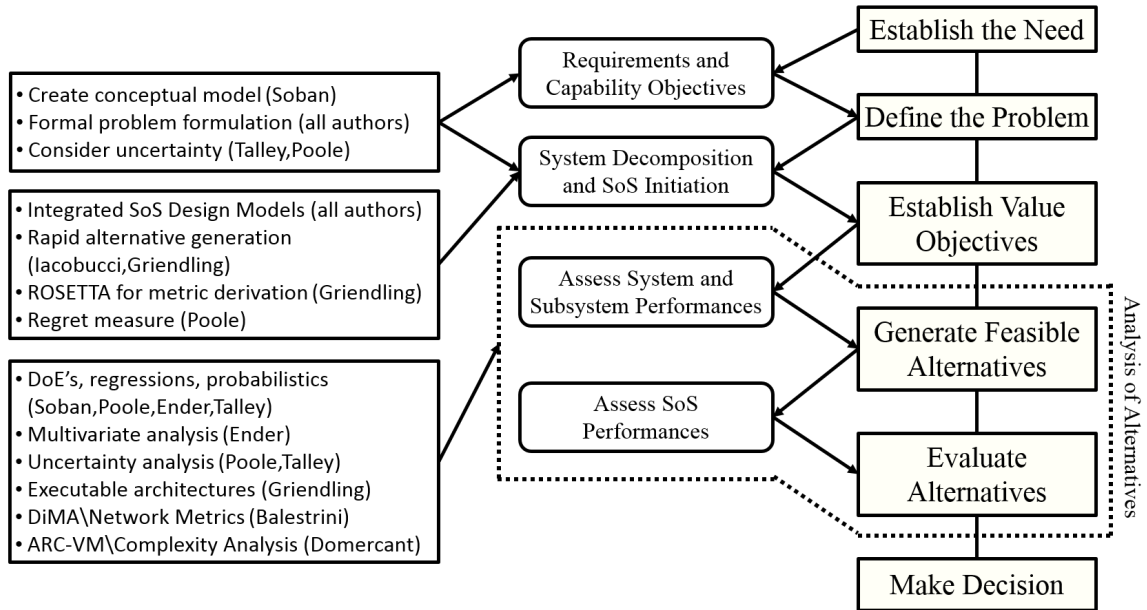


Figure 24: A Generic SoSE Process with Potential Activities to be Integrated

The review of the SoSE methods presented in the previous section has provided a response to Research Question 4: *What insights can be gleaned from existing analytic and quantitative SoSE approaches?*

Various observations are gleaned from the methods presented and surveyed above. First, each method contains multiple engineering activities that can be used as tools (or approaches) within a generic SoSE process. As was stated in **Section 3.2.2**, the wave model mostly provides structure for performing SoSE activities. It does not suggest specific tools to be implemented, and so it lacks substance. The reason for this is that every SoS problem will have unique characteristics and considerations, so the engineering activities justifiably should be tailored to the specific problem.

Observation 7 *The unique engineering characteristics and requirements for each specific SoS design problem lead to tailored engineering activities and metric formulations that provide substance to generic SoSE frameworks.*

In other words, each method tends to follow a generic decision/engineering process such as given by Schrage and Mavris [132], but then tailors the analyses and metrics for the

specific problem characteristics. The way in which each author chose the MOPs and MOEs was highlighted multiple times throughout the review process. It is clear that an appropriate approach is to decompose each individual SoSE problem from definitive requirements definitions and then determine the appropriate sets of performance measures, engineering metrics, and independent design variables that will map back up to the mission level.

Subsequent observations unfold into at least three parallel paths possible for analyzing alternative SoS designs based on the literature review presented here. One path will be called the brute force approach. The brute force approach is one in which a full analysis is performed for every possible SoS alternative for a specific set of requirements. Depending on the depth of reality modeled by the engineers and scientists along with the number of alternatives to be analyzed, the brute force approach may be computationally infeasible. However, if the analyses can be computed within a feasible time, then the brute force approach can provide a rich amount of information for analyzing SoS alternatives.

The second path will be called the surrogate approach. In the surrogate approach, a subset of design analyses are actually executed based on a design of experiments. The number of initial analyses is therefore significantly less than the brute force approach, and the associated computational effort follows the same trend. A regression, or surrogate model, is then created based on the subset of analyses. If the regression is found to have acceptable accuracy relative to the truth set, then the regression can presumably be used to interpolate new data. In this way, the surrogate approach theoretically allows even more analysis capabilities than the brute force approach because full and partial derivatives of the design space can potentially be calculated. However, if an acceptable error bounds is not achieved, then the surrogate approach is not very useful. The process can be expanded based on surrogate modeling tools that are common to many of the techniques presented. The expansion is shown below in Figure 25.

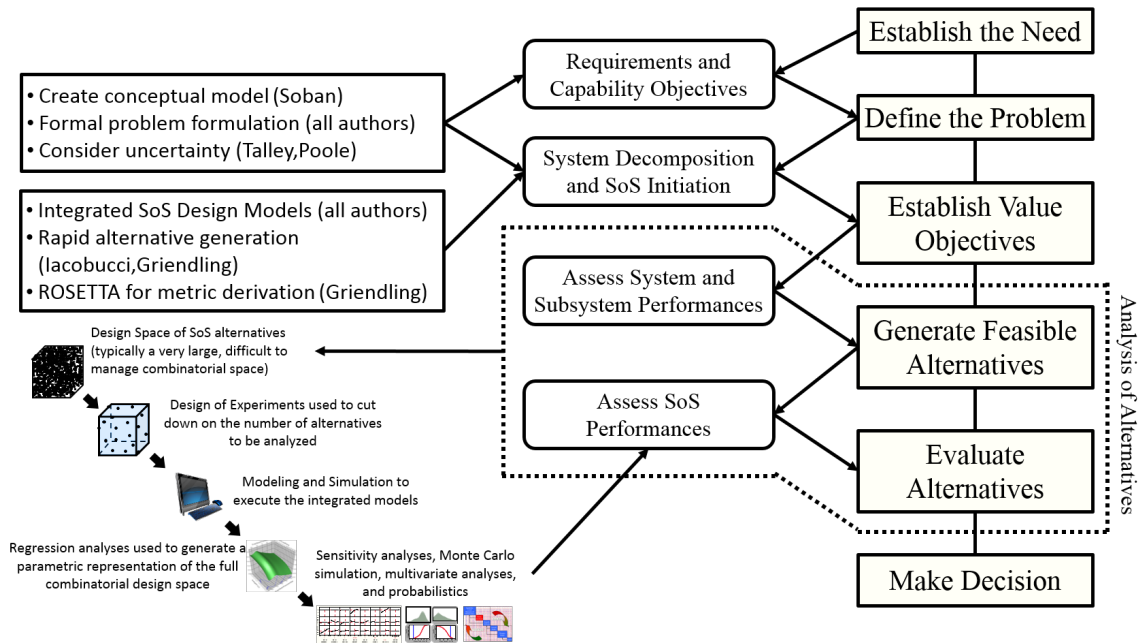


Figure 25: A Generic SoSE Process with the Surrogate Modeling Approach Applied

The third path will be referred to as the *proxy* approach. This is the technique which utilizes an overarching metric to represent the SoS alternatives, such as network metrics or complexity. In the proxy approach, the complete physics of the problem is not calculated, but instead a representation is calculated based on the overarching metric. This was the approach taken by both Balestrini [12] and Domercant [44]. They each provided generic metrics that attempt to quantify properties of an overall SoS without having to track every MOP and design variable. This isn't to say that the authors have ignored a full fledged SoS analysis. In fact, there is no reason that the metrics they presented shouldn't be used alongside a full analysis. However, what they have shown is that it is possible to glean some useful insights about SoS alternatives without measuring every performance effect.

These three approaches do not have to be completely independent paths. Crossover is possible and can be beneficial. However, delineating them in this way helps to provide a concise classification of possibilities.

Observation 8 *The brute force and surrogate approaches try to model most aspects of an SoS design problem (or at least the most impactful variables), but*

can be untraceable and often based on formulations that do not take the physics of the problem into account.

Observation 8 will be substantiated further during the subsystem analysis chapter.

Observation 9 *The proxy approach attempts to reveal underlying characteristics of an SoS, but in general does not consider performance effects across all levels of the SoS hierarchy (i.e., the subsystem, system and SoS levels).*

An interesting result of this review is the idea of the proxy approach. The idea of quantifying an entire SoS with a global metric is attractive. The reason is that there can tend to be so many dimensions to an SoS, that it is sometimes difficult to assess the overall differences in performance, and to convey that to a decision maker in a concise way. As it turns out, there are additional metrics that have been found in the literature that can provide insight. A few salient examples will be reviewed next.

3.5 Global-Metric Reviews

At this point, it is helpful to restate the overarching hypothesis of this dissertation:

Hypothesis 1: *An energy-based approach to analyzing system-of-system (SoS) components across multiple levels of the SoS hierarchy will enable more accurate and transparent trade-offs for SoS analysis of alternatives.*

What is meant by *accurate* and *transparent*? Accuracy in this context means not only that the trade-offs are physics-based, but that the developed method will be quantitatively compared against existing methods. Inherently, an energy-based approach would take the physics of the problem into consideration. Transparency in this context means that the trade-offs are clearly measurable in a mathematical sense. In other words, with an energy-based approach, the change in a parameter at one level of the SoS hierarchy will have a clear differentiable effect on another level of the hierarchy. This is shown in Equation 3, where y is a performance or effectiveness measure of level k , k is the SoS level index where $k = \{1, 2, 3\}$ for the subsystem, system and SoS levels respectively, and $f(E)$ is an energy-based functional for level k . Alternatively, Equation 4 conveys that the change in y as a

function of a non-energy-based functional x may or may not be zero. The hypothesis is that Equation 3 is measurable and guaranteed, while Equation 4 may be measurable, but is not guaranteed.

$$\frac{dy_{\forall k}}{df(E_{\forall k})} \neq 0 \quad (3)$$

$$\frac{dy_{\forall k}}{df(x_{\forall k})} \stackrel{?}{=} 0 \quad (4)$$

3.5.1 Information Entropy

Wang and Hussein [168] [170] have implemented the idea of using an information-based approach to develop target search strategies in the presence of uncertainty. They utilize the information entropy function in order to accomplish this. One of the attractive aspects of the information entropy approach applied by Wang and Hussein is that they used it for search missions, which is the type of SoS problem that this dissertation is scoped to.

Information entropy is one of Shannon's four measures of information: entropy, conditional entropy, mutual information, and conditional mutual information [183]. Shannon developed the concept of information entropy while at Bell Laboratories in 1948 [137]. The information entropy function, H , developed by Shannon is rooted in the measure of entropy ubiquitous in thermodynamics and statistical mechanics. Shannon stated that the information entropy function can...

...play a central role in information theory as measures of information, choice and uncertainty. The form of H will be recognized as that of entropy as defined in certain formulations of statistical mechanics... We shall call $H = -\sum p_i \log p_i$ the entropy of the set of probabilities p_1, \dots, p_n . The entropy in the case of two possibilities with probabilities p and $q = 1 - p$, namely $H = -(p \log p + q \log q)$ is plotted [below]:

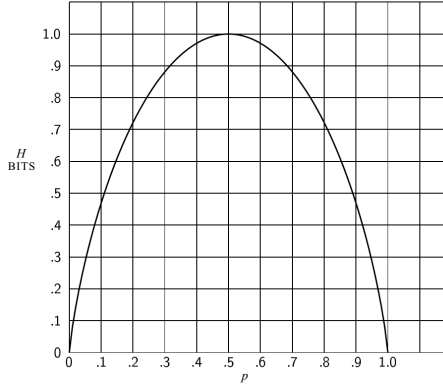


Figure 26: Shannon's entropy function in the case of two possibilities with probabilities p and $1 - p$ [137]

The information entropy function produces a quantity that describes the amount of uncertainty attributed to a process or task. In Figure 26 above, for a set of possibilities under given probability distributions, if the entropy function is zero, then there is either complete uncertainty or complete knowledge. When the probability p is 0.5, there is actually a maximum amount of uncertainty in this example. This is similar to flipping a coin. If the coin is a fair-coin and this is known, then a person flipping the coin would have a maximum uncertainty of the pending outcome. However, if the coin is weighted to one side, and the person flipping the coin knows this, then the uncertainty about the pending outcome is much less.

The usefulness of an uncertainty metric such as information entropy in an SoS search mission is that a designer would care about the SoS alternative that produces the greatest situational awareness. Therefore, if various SoS alternatives could be quantified in terms of the information entropy, then a designer could choose the set of SoS designs that produce the minimum uncertainty. Wang's [169] approach was to use uncertainty maps throughout the execution of a mission so that over time the agents would move in such a way as to minimize the uncertainty over the entire area. An example is shown in Figure 27.

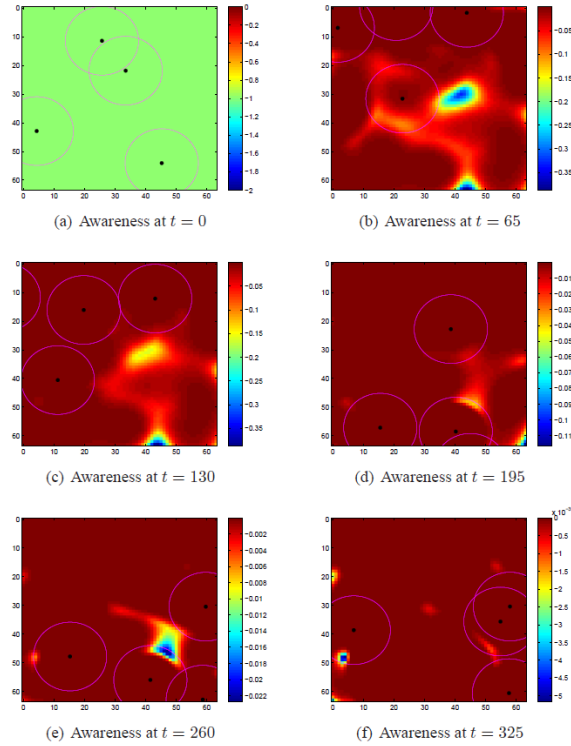


Figure 27: Example of Wang’s Progression of Domain Awareness Over Time [169]

Although information entropy seems like a promising global metric, it is only calculated over time through simulation. Therefore, analyses of each SoS alternative would have to be performed just to acquire the information entropy value. Furthermore, information entropy is a probabilistic function without an underlying energy-based functional.

3.5.2 Exergy Analysis

“Every system...can be described by the thermodynamic concept of exergy, which articulates what a working system *consumes*, as opposed to the energy of the system which is *conserved*” [138].

The statement above is promising. It conveys that exergy is a measure that can describe *every system*. Therefore, according to the statement above, exergy may be the type of measure that could be used to compare systems-of-systems based on a common metric at all levels of the SoS hierarchy. But what exactly is exergy?

Exergy analysis is a concept also derived from thermodynamics. The energy crisis of the 1970s caused engineers to consider new ways of emphasizing efficiency in system design

and ultimately led to a completely new analysis and design concept. The resulting design methodology is called *exergy analysis* and the thermodynamic optimization component is referred to as *entropy generation minimization* (EGM). Conventional thermodynamic design methods had been centered around application of the First Law of Thermodynamics (conservation of energy). However, exergy analysis and EGM introduced the simultaneous application of the first and second law [15].

It is useful to create a distinction between energy and exergy in order to understand exergy better. Energy flows into and out of a control volume along paths of mass flow, heat transfer, and work. As stated by the first law of thermodynamics, energy is conserved, not destroyed. Exergy, however, is an entirely different concept. Exergy represents the energy that is *useful*. In other words, it represents the ability of the energy stream (mass flow, heat transfer, and work) to do work. As Bejan states [15]:

The first attribute of the property ‘exergy’ is that it makes it possible to compare on a common basis different interactions (inputs, outputs, work, heat). Another benefit is that by accounting for all the exergy streams of the system it is possible to determine the extent to which the system destroys exergy. The destroyed exergy is proportional to the generated entropy. Exergy is always destroyed, partially or totally: this is the statement made by the second law of thermodynamics...By performing exergy accounting in smaller and smaller subsystems, we are able to draw a map of how the destruction of exergy is distributed over the engineering system of interest. In this way we are able to pinpoint the components and mechanisms (processes) that destroy exergy the most. This is a real advantage in the search for improving efficiency (always by finite means), because it tells us from the start how to allocate engineering effort and resources.

Multiple observations can be gleaned from the statement above: 1) Exergy enables the comparison of different types of interactions⁶ (inputs, outputs, work, heat); 2) Exergy

⁶Interactions due to flow into and out of a system do not need to imply that exergy is only calculable for static systems. The flow can be into and out of a control volume, where the control volume is relative to the body-axis reference frame of the vehicle. Therefore, flow into and out of the control volume is affected by the vehicle body in the flow stream which is one type of exergy interaction.

analysis can be applied to varying levels of system aggregation (systems, subsystems, smaller and smaller subsystems); 3) Exergy destruction can be mapped out over a system of interest, pointing out the areas where effort and resources should be spent.

There are many design problems in which exergy analysis has been successfully employed [134]:

- Power generation systems including steam cycle power plants, gas turbine cycles, combined cycle power plants, nuclear power plants and geothermal energy conversion processes. In addition, solar technology and fuel cell technologies have benefited from the application of exergy analysis.
- Other applications include heat exchangers, reciprocating engines, jet engines, aircraft, chemical processes, etc.

In fact, since exergy can be used to describe *any system* (as was pointed out earlier), it has been demonstrated across a wide spectrum of applications from biological organisms to man-made machines. This is shown in Figure 28 below.

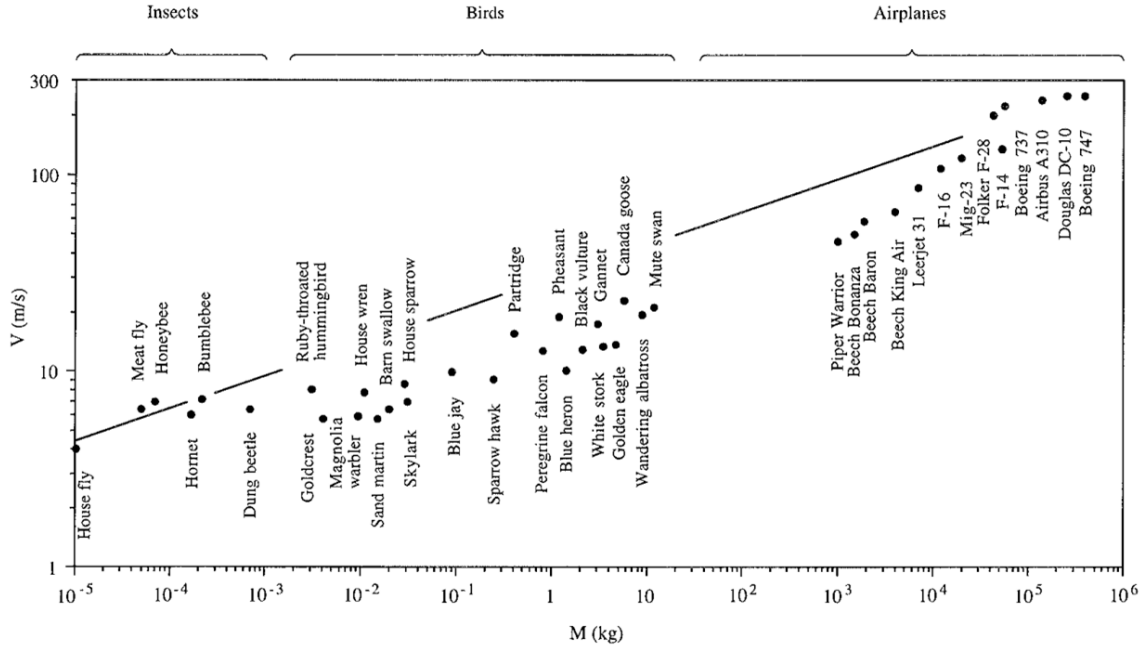


Figure 28: The theoretical speed for minimum rate of exergy destruction for insects, birds, and airplanes [14]

The basic exergy balance equation for a control volume is shown below.

$$\Delta X_{CV} = \sum_k (1 - \frac{T_0}{T_k})(Q_k) - W - P_0(\Delta V) - T_0(S_{gen}) + \sum_{out} m_j \gamma_j - \sum_{in} m_i \gamma_i \quad (5)$$

One of the shortcomings of being able to apply exergy analysis to an SoS problem is that “the rates of exergy destruction should be used very cautiously to characterize the performance of system components because, in general, a part of the exergy destruction occurring in a component is caused by the inefficiencies of the remaining system components...In complex thermal systems it is very difficult and costly to separate these two parts of the exergy destruction within a system component” [16]. The implication is that the exergy analysis of *thermal* systems is highly dependent on the operational interactions between the components in terms of thermal inefficiencies. However, the components of an SoS are not thermally connected.

Application of the exergy analysis to individual systems and subsystems can be formulated in a few ways. Roth [125] applied the exergy equations directly to the individual

components of an aircraft. “This enabled the comparison of component effects at all levels of the system hierarchy, e.g. skin-friction drag can be compared to compressor efficiency on an ‘apples-to-apples’ basis.” In order to carry out this analysis, Roth performed a hierarchical breakdown of components and calculated the exergy destruction at each level of aggregation. The hierarchical breakdown is shown in Figure 29 below.

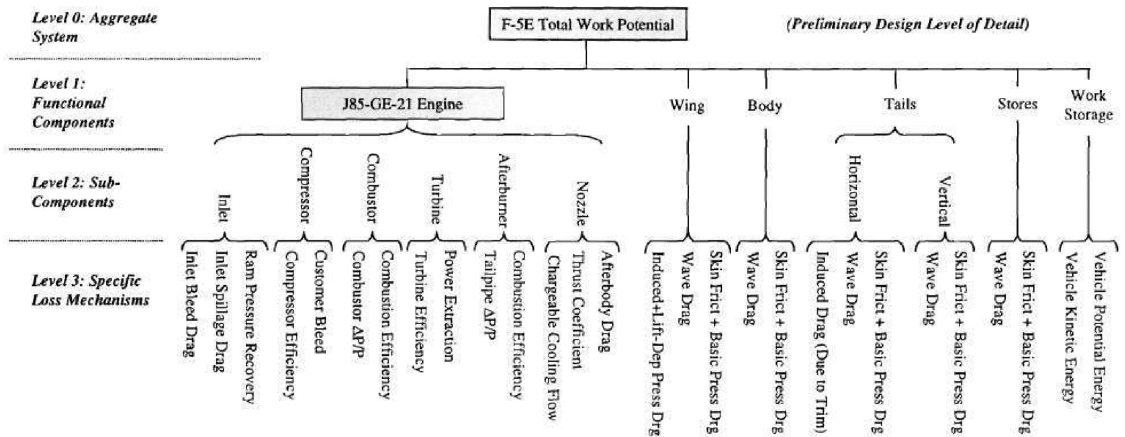


Figure 29: Hierarchical Breakdown of an F-5E Fighter Jet for Exergy Analysis [125]

The approach used by Roth is the type of analysis commonly used in the analysis of power generation systems.

Another approach that has been used specifically for vehicles in motion was implemented by Riggins [123]. In this implementation, a vehicle is placed in a control volume called a *global stream-tube*. An example of a vehicle within this global stream-tube control volume is shown in Figure 30 below:

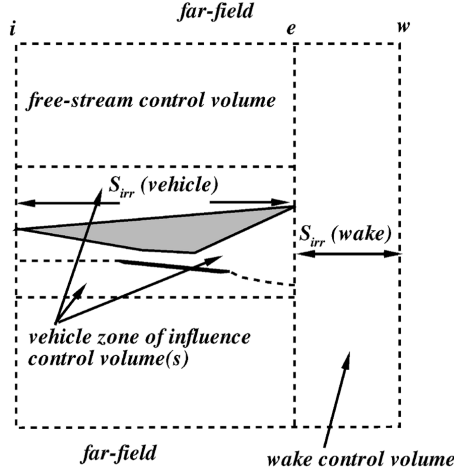


Figure 30: Global Control Volume/Stream-Tube for Overall Vehicle Exergy Analysis [124]

Using the global stream-tube construct, the total rate of exergy destruction is defined as follows:

$$\dot{S}_{total} = \dot{S}_{vehicle} + \dot{S}_{wake} = \dot{S}_{irr(vehicle)} + \dot{S}_{rev(vehicle)} + \dot{S}_{wake} \quad (6)$$

A shortcoming of the stream-tube approach is that calculation of the dynamics of the wake behind a vehicle is imperative, and that depth of information is usually not available with reasonable accuracies in the early design stages.

Finally, Sciubba [134] provides a summary of the specific exergy for different energy flows:

| Type of energy flow | Specific energy | Specific exergy | Source | Notes |
|--------------------------|-----------------|---|-------------|---|
| Kinetic | $0.5V^2$ | $0.5V^2$ | / | J/kg; follows from definition |
| Potential | $g\Delta z$ | $g\Delta z$ | / | J/kg; follows from definition |
| Heat | q | $q \left(1 - \frac{T_0}{T_q} \right)$ | / | J/kg; follows from definition |
| Mechanical | w | w | / | J/kg; follows from definition |
| Electrical ² | $It\Delta V$ | $It\Delta V$ | / | J; follows from definition |
| Chemical, pure substance | Δg_G | $\mu - \mu_0 + RT_0 \ln \left(\frac{c}{c_0} \right)$ | Wall 1977 | $\mu - \mu_0 = \Delta g_G = g_G - g_{G,0}$ |
| Radiation ² | I | $\sigma \left(T^4 - \frac{4T^3T_0}{3} + \frac{T_0^4}{3} \right)$ | Petela 1964 | W/m ² ; for black body radiation |

Figure 31: Specific Exergy for Various Energy Flows [134]

The implication is that without the ability to calculate heat transfer, the exergy balance of the components of an SoS is simply a function of the specific kinetic, potential,

mechanical, and electrical energies. Therefore, a complete exergy analysis is not reasonable for an entire SoS during conceptual design, however, exergy-analysis boils down to an energy analysis when heat transfer is not available between components. This is further motivation that an energy-based approach can provide accurate and transparent trade-offs between disparate components of an SoS.

3.5.3 The Coverage Factor and Coverage Ratio

The final metric to be reviewed is especially relevant to this dissertation due to its relationship to search missions. In particular, quantifying the effect of various search strategies along with the capabilities of particular search systems requires the application of the science of detection. In a general sense, the following paragraph provides a physical basis from which to begin quantification of any detection capability [152]:

If one is to acquire information concerning the absence or presence of an object, enemy or otherwise, a transfer of energy must take place from the object being searched for to the searcher. There is simply no means in nature, other than energy transfer, by which information may be acquired across a distance. It is for this reason that any discussion of detection, be it by radar, sonar, or visual means, must involve a consideration of energy transfer.

The excerpt above conveys the idea that energy transfer is relevant in performing a search mission. The energy required to operate a sensor is consequently germane. However, the energy required for vehicle motion is pertinent as well. Therefore, a formulation is desired that combines the energy of the sensor and the energy of motion. The area searched by a given vehicle with an associated sensor during some time period t can be specified as:

$$A(t) = V_{\infty}St \tag{7}$$

where S is the width of a sensor (twice the radius) and V_{∞} is the velocity of the vehicle. Equation 7 is called the *search effort*. Next, if A_S is defined as the total area for the desired search then the ideal *coverage ratio* is defined as:

$$\lambda_I(t) = \frac{A(t)}{A_S} = \frac{V_{\infty}St}{A_S} = \gamma t \tag{8}$$

where γ is defined as the coverage rate (1/time). So, depending on the velocity of the sensor vehicle and the sweep width of the sensor, the total area can be covered in some time $T = A_S/V_\infty S$ if there is no overlap of search paths. If there are multiple vehicles searching an area with no overlap, then the total ideal coverage ratio can be redefined as:

$$\lambda_I(t) = \frac{\sum_{i=1}^n V_{\infty,i} S_i t_i}{A_S} = \sum_{i=1}^n \gamma_i t_i \quad (9)$$

Ideal coverage is not practical since search patterns can often overlap and gaps in coverage are very likely. However, it does provide an upper bound on what is possible. Non-ideal coverage can be estimated by calculating the probability of covering slices of the area during a slice of time (dA and dt). This is called the random coverage ratio approximation, λ_R , which shows a limiting effect (*i.e.*, a lower bound). Without going into the derivation here, the probability of covering any slice of the area at a slice of time by randomly moving through the region is $1 - e^{-V_\infty S dt/dA_S}$. Since the area coverage rate was defined as $\gamma \triangleq V_\infty S/A_S$, the coverage factor for random coverage of a single vehicle is:

$$\lambda_R(t) = 1 - e^{-\frac{V_\infty S t}{A_S}} = 1 - e^{-\gamma t} \quad (10)$$

and for multiple vehicles operating in non-overlapping regions of the search area, the random coverage factor is:

$$\begin{aligned} \lambda_R(t) &= \sum_{i=1}^n \left(1 - e^{-\frac{V_{\infty,i} S_i t_i}{A_S}} \right) = \sum_{i=1}^n (1 - e^{-\gamma_i t_i}) \\ &= n - \sum_{i=1}^n (e^{-\gamma_i t_i}) \end{aligned} \quad (11)$$

If the vehicles all have homogeneous coverage efforts, $ce = V_{\infty,i} S_i t_i$, then the number of vehicles required to cover an area A_S up to a desired coverage, λ_R , can be calculated:

$$n = \frac{\lambda_R}{1 - (e^{-ce/A_S})} \quad (12)$$

If the vehicle coverage efforts are non-homogeneous, then the number of vehicles would be:

$$n = \lambda_R + \sum_{i=1}^n e^{-ce_i/A_S} \quad (13)$$

Note that both the ideal and random coverage factors assume constant velocity, search width, and search area over the mission time. Therefore, the coverage rate, γ_i , is constant over time.

The sensor sweep width, S , can be defined as a function of the *probability of detection* of a sensor at discrete ranges. In a sense, the coverage factor, λ , describes the effect of the probabilistic sweep width over time as the mission progresses. In fact, the development of the coverage factor was partly to “establish a search measure of effectiveness with units of time which is well-defined even when detection is not a certain event” [46]. Consequently, the coverage factor, λ , is defined as the cumulative density function (CDF) for the probability of detecting an object at time t . If a total mission time is specified along with a sweep width and velocity, then the coverage factor in that amount of time is known.

A benefit of the coverage factor is that it mostly combines energy-based parameters from each level of the SoS hierarchy. Specifically, the velocity (which is a function of vehicle energy) and the total coverage of multiple vehicles at the SoS level can be expressed as energy-functionals. Unfortunately, a link between sensor width, S , and the energy of the vehicle has not been formally established in the literature to the knowledge of the author. In fact, Chapter 6 will go into vigorous detail about how the sweep width is currently calculated. It will be shown that sweep widths are either generated from real-world experimental data (which is extremely hard and costly to acquire) or they are assumed to be functions of simplified probabilities of detection and theoretical sensor range.

If experimental data is available then a link between the sensor performance, the vehicle motion, and the effective sweep width can be established. However, as was stated, experimental data is very hard to come by, especially for the large number of sensor alternatives that are considered in this work early in conceptual design. On the other hand, theoretical ranges of the sensors can be calculated, but in the current literature there is no link established between the motion of the carrier vehicle and changes in the probabilities of detection. In other words, sensor ranges and therefore sweep widths are kept constant at all vehicle velocities in the existing approaches. **Consequently, one of the major contributions of this dissertation will be a formalized link between sensor sweep**

width and vehicle performance based on the use of a virtual experimentation environment.

Observation 10 *The coverage factor metric has the potential to combine energy-based parameters from each level of the SoS hierarchy. However, there is currently a missing link between the sweep width parameter at the subsystem level and the other levels of the hierarchy (system and SoS). In addition, the coverage factor has not previously been applied to an SoS problem and it has not taken into consideration energy-limited performance relationships between search systems and their subsystems.*

3.6 Next Steps

In order to move forward with this research, the remainder of this document will be structured as follows:

- The salient observations from the literature review will be reiterated.
- The overarching hypothesis of this dissertation will be restated along with proposed experiments.
- A representative example problem will be presented. The representative example problem is motivated by mine warfare in the U.S. Navy in which there is a capability-gap. The suggested solution to this capability-gap is the use of unmanned, collaborative, systems-of-systems. Therefore, potential SoS solutions must be analyzed and designed.
- Each level of the SoS hierarchy will be decomposed based on subsystem level analysis and design, system level analysis and design, and SoS level analysis and design.
- The effect of energy-based parameters on each level of the SoS hierarchy will be measured through the coverage factor formulation.
- Substantiation of the hypotheses will be reviewed in the Summary and Conclusions.

CHAPTER IV

RECAPITULATION AND PROPOSED EXPERIMENTS

The goal of this chapter is to restate the main hypothesis of this work in light of the observations gleaned so far and to propose a series of experiments for substantiating the hypothesis. The overarching hypothesis of this work was built upon Observations 1 and 2:

Observation 1 *The efficiency, and therefore the effective energy usage, of a cooperative process is dependent on an array of factors including the number of agents, the operational scheme, information transfer, and unique characteristics of the individuals.*

Observation 2 *The total energy transfer that takes place during a collaborative process is a function of the energy transfer amongst all constituent components according to the First Law of Thermodynamics.*

These observations led to the overarching hypothesis of this dissertation:

Hypothesis 1 *An energy-based approach to analyzing system-of-system (SoS) components across multiple levels of the SoS hierarchy will enable more accurate and transparent trade-offs for SoS analysis of alternatives.*

Up to this point, support for **Hypothesis 1** has been provided by answering various research questions through the literature review which has led to additional observations, which are repeated below. However, *substantiation* of Hypothesis 1 will be provided through the experimental approach to-be-outlined.

Observation 6 showed that *due to the large number of solution alternatives possible for designing a group of unmanned collaborative systems, low-level quantitative analysis must be used alongside high-level engineering management strategies.* This observation led to the specification of a generic SoSE framework as was shown in Figure 14.

Observation 7 concluded that *the unique engineering characteristics and requirements for each specific SoS design problem lead to tailored engineering activities and metric formulations that provide substance to generic SoSE frameworks*. Various engineering activities were delineated as a result of the literature review of specific SoSE analytic approaches. It also became clear that the main hypothesis of this dissertation is to provide an energy-based approach to the analysis of alternatives, as shown in Figure 32. Note that the *requirements definition* and *system decomposition* steps are not the focus of this work.

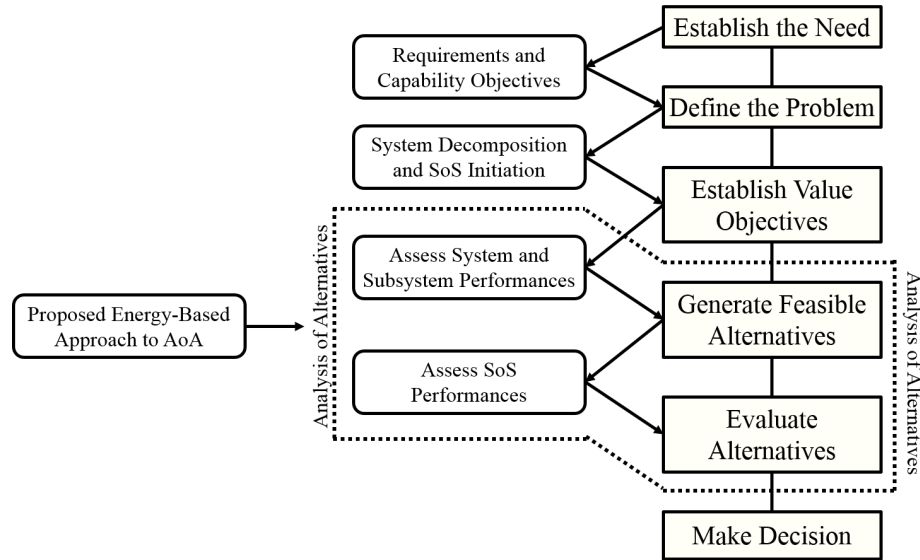


Figure 32: The proposed energy-based approach will be applied to the AoA

Observations 8 and **9** provided insight into analytic SoSE processes currently used: the brute force approach, the surrogate approach, and the proxy approach. Two competing benefits are identified in the approaches delineated. The surrogate approach often provides an avenue to make trades across various levels of the SoS hierarchy, however, there is little direction in being able to perform “apples-to-apples” comparisons between disparate components of the SoS. Furthermore, different levels of the hierarchy are often analyzed based on subsystem or system specific assumptions that do not provide physics-based changes across the varying levels of the hierarchy. In terms of the proxy approach, a common metric for SoS characterization is well formulated. However, the present metrics do not consider varying levels of the SoS hierarchy. Therefore, there is no route provided for making subsystem and system level trades based on the disparate performance capabilities.

Investigating other potential metrics to use in an SoS analysis led to the discovery that exergy analysis can describe the work potential of any system. However, it was pointed out that for the SoS problem, exergy analysis simplifies down to a conservation of energy analysis. Therefore, additional substantiation was provided for an energy-based approach to SoS analysis of alternatives. Additionally, the coverage factor metric was described, which is especially relevant to this dissertation work since it has been scoped down to the analysis of collaborative systems performing a search mission. In particular, **Observation 10** stated that *the coverage factor metric has the potential to combine energy-based parameters from each level of the SoS hierarchy. However, there is currently a missing link between the sweep width parameter at the subsystem level and the other levels of the hierarchy (system and SoS). In addition, the coverage factor has not previously been applied to an SoS problem and it has not taken into consideration energy-limited performance relationships between search systems and their subsystems.*

Accordingly, the coverage factor can appropriately play two roles in this dissertation: (1) it can be used as a metric of effectiveness for the overall search mission *if a link is established between the sweep width parameter at the subsystem level and the other levels of the hierarchy (system and SoS)*, and (2) it can be used to test the overarching hypothesis of this work. The reason is that the coverage factor is often calculated based on simple sensor and vehicle models that are not energy-based. Therefore, the experimentation in this work will lean on comparisons between the coverage factor calculations when energy-based formulations are used across the levels of the SoS hierarchy versus when energy-limited formulations are not used. This leads to another hypothesis:

Hypothesis 2 *If the performance parameters of the coverage factor metric are defined as energy-based functionals that link the various levels of the SoS hierarchy, then the coverage factor can be used to provide more accurate and transparent analysis of alternatives between disparate SoS subsystem and system components.*

Hypothesis 2 is then dependent on the following two hypotheses:

Hypothesis 3 *If a relationship is formed between sensor energy, sensor detection capability, and sensor velocity, then an energy-based link will be established between the effective sweep width parameter at the subsystem level and the vehicle performance at the system level.*

Hypothesis 4 *If the coverage effort is defined as a function of linked energy-based parameters from the subsystem level up through the SoS level, then the coverage effort can be formulated as a cost function within a mixed-integer linear programming optimization for the selection of alternative SoS designs.*

If Hypotheses 3 and 4 are substantiated through experimentation, then Hypothesis 2 will be proven true as well. Finally, if Hypothesis 2 is shown to be true, then the overarching hypothesis of this dissertation, Hypothesis 1, will be substantiated as well.

Hypothesis 1 *An energy-based approach to analyzing system-of-system (SoS) components across multiple levels of the SoS hierarchy will enable more accurate and transparent trade-offs for SoS analysis of alternatives.*

Through the testing of the above hypotheses, a full analysis of alternatives approach will be developed which meets the requirements of all the stated hypotheses.

4.1 Experimental Approach

Experimental Apparatus: Hypotheses 2, 3 and 4 will be tested through the application of the coverage factor against a representative SoS example problem, to-be-delineated in the next chapter. At each level of the SoS hierarchy, current approaches which do not link the levels of the hierarchy through an energy-limited approach will be presented. Then comparisons will be made between analyses and trade-offs formulated through both the new energy-based approach and the current approach. The experimental approach is dependent on data acquisition and analysis of various paths to the SoS design problem at each level of the SoS hierarchy.

4.1.1 Experiment Set A: Subsystem Level Comparisons

Subsystem Level Analysis

Purpose: Test whether or not current subsystem (specifically sensor) level analyses provide energy-limited functionals that can be linked to the system and SoS levels of the hierarchy.

In developing Experiment Set A, it will be shown that there is a disconnect between current sensor level formulations in terms of static sensor performance and dynamic sensor operations. In other words, there are two general trends in modeling sensors: analysis without implementation and implementation without analysis. Sensor performance modeling often focuses deeply on the analysis of sensors based on the physics of the problem, including acoustic interactions with the environment. Alternatively, Operations Analysis and robotics literature places significant focus on implementing sensors for specific applications, but tend to make generalized assumptions about the physics of the sensors due to a lack of empirical data and/or modeling capability. There is accordingly a gap in capability since without implementing the physics of the sensors into the operational analyses, energy conservation between the sensors and the operations cannot be mapped.

Experiment Set A will be demonstrated through filling the above stated gap and then providing data delineating the benefits of the new approach. It builds a bridge between the detailed physics-based modeling of sensors and the required operational mission planning through virtual experimentation. Specifically, data is acquired to compare the three different approaches through three different analyses. Each path will be clearly delineated in Chapter 6. However, the experimental setup for Experiment Set A is shown in Figure 33. A clear overview of the approach taken for both Experiments 1 and 2 will be presented in the associated chapter.

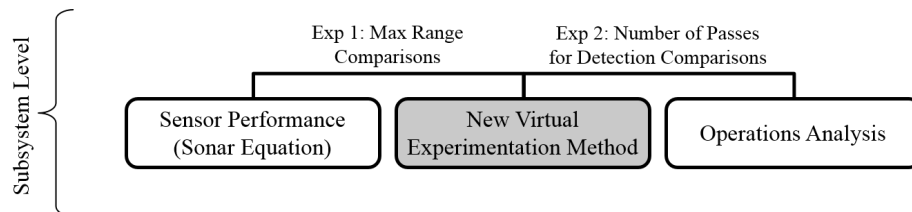


Figure 33: Subsystem Level Experimental Setup

4.1.2 Experiment Set B: System Level Comparisons

System Level Analysis

Purpose: Test whether or not current system (specifically vehicle) level analyses provide energy-limited functionals that can be linked to the subsystem and SoS levels of the hierarchy.

In developing Experiment Set B, a multi-level design method is produced for generating alternative sensor and vehicle designs that are to be utilized within a collaborative system-of-system mission. The vehicle and sensor performance is calculated through energy-limited functionals which link the subsystem and system levels of the SoS hierarchy. It is shown that varying design considerations can prove to be either beneficial or detrimental to the cooperative operations of a grouping of unmanned systems based on the coverage factor metric. Therefore, delineation of the single vehicle capabilities in terms of energy-based performance at both the subsystem and system level is an imperative step in determining overall effectiveness. Three experiments make up Experiment Set B: Experiments 3, 4 and 5. The experimental setup for Experiment Set B is shown in Figure 34. The arrows leading into Experiment Set B represent data and analysis flows from the subsystem level experiments. A clear overview of the approach taken for each experiment at the system level will be presented in Chapter 7.

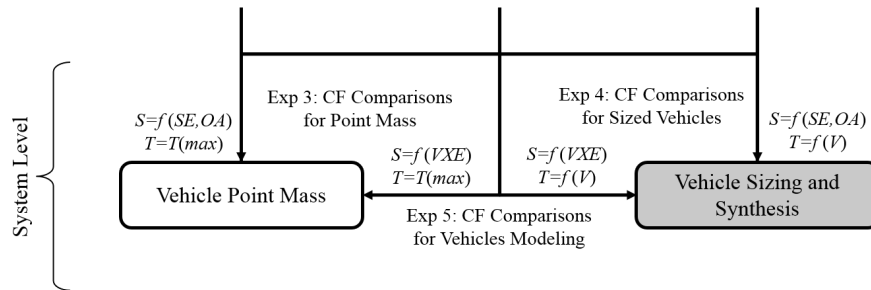


Figure 34: System Level Experimental Setup

4.1.3 Experiment Set C: SoS Level Comparisons

System-of-System Level Analysis

Purpose: Test whether or not current SoS (specifically mission) level analyses provide energy-limited functionals that can be linked to the subsystem and system levels of the hierarchy.

In developing Experiment C, there are two current approaches that are outlined, which can come off as qualitative versus quantitative. The systems engineering approach can be extremely detailed in defining and decomposing the problem and offering architectural solutions that should be analyzed. On the other hand, the field of collaborative control can be very quantitative in analyzing particulars of control theory. However the full system integration is often lacking, with various simplifying performance assumptions made at the subsystem and system levels. The two experimental paths for Experiments 6 and 7 which make up Experiment Set C are shown in Figure 35. The arrows leading into each experiment represent the information and data flow from Experiments 1-5.

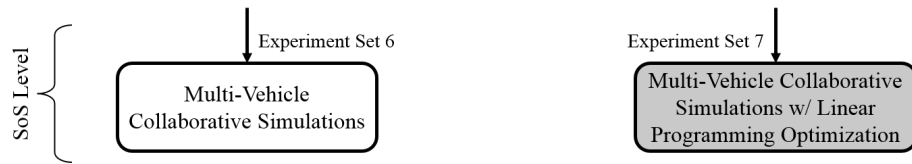


Figure 35: SoS Level Experimental Setup

Experiment Set C utilizes the results of Experiment Sets A and B to reinforce the importance of an energy-based approach to analyzing and designing the collaborative system-of-systems. First, area coverage utilizing single- and multi-vehicle search schemes is shown through simulation without subsystem and system effects considered very deeply. Then, the experiments from the subsystem and system chapters are brought back into the fold for new collaborative vehicle experiments. Various linear programming optimization goals are delineated which leads to the realization that a new, heuristic area coverage algorithm is needed in order to define SoS alternatives. Finally, the overarching hypothesis of this dissertation is substantiated through the SoS level experimental results.

4.2 Next Steps

The goal of this chapter was to reinforce the main hypothesis of this work and to propose a series of experiments for substantiating the hypothesis. The coverage factor metric has been chosen as a measuring stick for comparing the results of the multiple experiments proposed. This can appropriately be accomplished *if a link is first established between the*

sweep width parameter at the subsystem level and the other levels of the hierarchy (system and SoS). The linkage will be provided in Chapter 6.

Part of the experimental plan is based on the use of a representative example problem. Therefore, in the next chapter the representative example problem will be presented. The representative example problem is motivated by mine warfare in the U.S. Navy in which there is a capability-gap. The suggested solution to this capability-gap is the use of unmanned, collaborative, systems-of-systems. Therefore, potential SoS solutions must be analyzed and designed.

The overall experimental approach described above that will be utilized is shown in Figure 36. The gray boxes represent methods which link the levels of the SoS through energy-based functionals. The white boxes are other approaches typically utilized for analyzing SoS performance and effectiveness at varying levels of the system-of-system hierarchy.

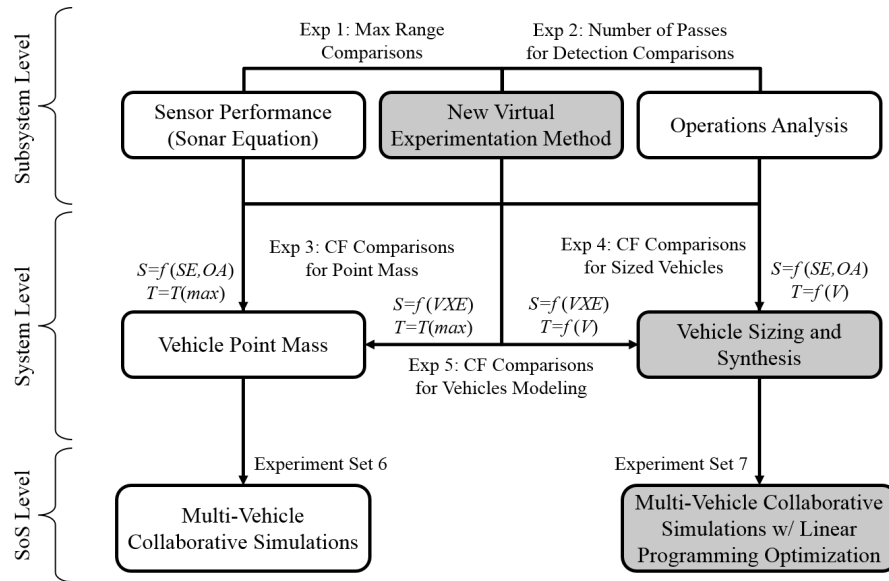


Figure 36: Decomposed Level-by-Level Experimental Approach

CHAPTER V

REPRESENTATIVE TEST PROBLEM

As was stated by **Observation 3**, the DoD desires greater development and application of autonomous collaborative systems in order to gain increased capabilities across a variety of operations. Consequently, the research presented in this dissertation is concerned with the analysis and design of groups of autonomous, unmanned, collaborative systems. Also, in reference to the JCIDS and CBA processes, it was mentioned in **Section 2.2.2** that development and acquisition programs within the DoD require thorough investigations of capability gaps and solutions to those gaps. Therefore, the analysis of existing and potential alternatives through a system-of-systems engineering (SoSE) framework is of high priority.

The overarching research objectives of this dissertation are to show that the analysis of alternatives for collaborative systems-of-systems should be performed at varying levels of the system-of-system hierarchy and to provide novel means for performing those analyses. In particular, it has been postulated that a formulation built on an energy-based approach to multi-level analysis of SoS components will enable more accurate and transparent subsystem and system trade-offs for SoS analysis of alternatives. Characterization of the design space will be demonstrated in this chapter through the application of the generic SoSE process to a *Representative Example Problem*.

In **Section 3.3**, a generic SoSE process was provided as a framework for defining and analyzing an SoS design problem. It is therefore the basis of delineating the experimental testbed utilized for the application of the experimental approach provided in the previous chapter. Specific implementations of the requirements and system decomposition portions of the SoSE process are setup and demonstrated throughout the remaining sections of this chapter. The analysis of alternatives portion is left for the following three experimental approach chapters.

The Representative Example Problem The purpose of the *Representative Example Problem* is to illustrate the phenomenon discussed in regards to the analysis of alternatives of collaborative systems-of-systems. In particular, the example problem that has been chosen is based on utilizing groups of unmanned autonomous vehicles to perform a subset of tasks within a Navy Mine Countermeasures (MCM) mission. This problem is representative in that it provides the opportunity to consider multiple levels of the system-of-system hierarchy. Therefore, the effects of providing more or less analytic detail to the experimental setup can be traced and the sensitivity of these effects on resulting mission requirements can be quantified. In addition, stochasticity will be present in the analysis due to probabilistic sensor models and collaborative control decision-making of the systems. However, uncertainty due to “noise” factors will be restrained (these controlled noise factors will be pointed out through the setup details below). A formal problem definition for the *Representative Example Problem* to be solved for through the SoSE process above should constitute a set of n objectives ($\mathbf{F} = f_1, f_2, \dots, f_n$) which are functions of n design variable sets ($\mathbf{X} = \mathbf{X}_1, \mathbf{X}_2, \dots, \mathbf{X}_n$) and are subject to n sets of constraints ($\mathbf{G} = \mathbf{g}_1, \mathbf{g}_2, \dots, \mathbf{g}_m$). The formal problem definition must be formulated through the SoSE process by characterizing the objectives, design variables, and constraints. Application of the generic SoSE process to this representative example problem will ultimately allow the investigation of novel analysis techniques through detailed experimentation.

5.1 Establishing the Need and Defining the Problem

The overarching goal of defining the problem is to enumerate the desired SoS mission(s), highlight capability gaps that must be overcome, define requirements, list potential systems and determine varying CONOPS to be used within the SoS.

In the POSSEM method (which was reviewed in Section 3.4.1), Soban provides guidance for defining the SoS program through the creation of a conceptual model [140]. The creation of the conceptual model in the POSSEM approach is designed to carefully plan a way forward for a particular design problem by answering various questions, although all of the questions are not applicable to this work. The first relevant question at this stage of the SoS

development program suggested by Soban is: “What problem are we trying to solve?”. This question is abstract and open ended and Soban states that the purpose of this first question is to aid the analyst in identifying the basic goals of the analyses that will be performed. However, more tangible questions can be inferred, such as: What scenarios/missions should be considered?; Are there any baseline vehicles and technologies that should be utilized and analyzed?; What are the customer requirements, applicable constraints, potential trade-offs and overarching goals of any analyses that will be performed?

Soban’s next Conceptual Model question is: “What level of detail is needed?”. In this dissertation, the answer to this question as applied to a collaborative system-of-systems is actually trying to be solved for. Soban points out that analysts often allow the current capabilities of their tools to drive the level of detail in their analysis rather than the other way around. This was corroborated through the literature review of SoS analysis methods in **Chapter 3** of this work. Many of the SoS analysis methods mentioned give a great deal of attention to the SoS mission level and may be very low fidelity at the system and subsystem technical levels. However, disregarding detail at the lowest levels of analysis may cause the overall SoS results to be misleading. Therefore, the experiments performed through this testbed will attempt to substantiate what is appropriate for a collaborative SoS. Nonetheless, after the appropriate level of detail is confirmed, the designer should then be able to more appropriately identify the specific analysis input variables, the necessary Key Performance Parameters (KPP), Measures of Performance (MOPs), Measures of Effectiveness (MOEs), and any potential sources of uncertainty and stochasticity. Ultimately these are the concrete means by which trade-offs can be made, optimizations can be performed, insights can be gleaned, and information can be conveyed to decision makers and stakeholders.

The final question in developing the conceptual model as posed by Soban is: “What tools are needed and available?”. In answering this question a survey of appropriate tools and models should be conducted. If an available tool has shortcomings in the level of desired detail, the designer should at least provide explanations about the assumptions and recognized limitations. Often the designer will likely need to build at least some of their

own tools in order to capture the levels of detail and nuances desired for a specific problem.

5.1.1 Naval Mine Warfare and the use of Unmanned Systems

This section will address the first question outlined above: “What problem are we trying to solve?”. It will include the mission definition, recognition of capability gaps, identification of potential systems and CONOPS to be utilized, and the specification of any applicable requirements, constraints, overarching goals and potential trade-offs.

Mission Definition and Identified Capability Gaps Naval mines are a significant threat to both military and civilian maritime operations. As adversaries have gained access to inexpensive underwater improvised explosive devices (UWIEDs) and to more sophisticated mine technologies, the U.S. Navy has placed a great deal of emphasis on the mine warfare problem. The Navy is particularly interested in maintaining the capability to achieve forcible entry onto defended shores by means of amphibious assault as well as keeping commercial shipping lanes threat free. In addition, mines and UWIEDs pose a threat to the homeland security of the U.S. since “terrorists can use or threaten to use mines and UWIEDs for a variety of political, economic, or military ends...” [148].

Modern naval mines and UWIEDs have varying characteristics and capabilities depending on their sophistication, design and environmental placement (including position within the water column and the water conditions, e.g., turbidity, sea state, bottom type, etc.). The types of mines that can be placed in different regions of the water environment are shown in Figure 37. Mines and UWIEDs may utilize various sensors for target discrimination including magnetic, acoustic, electrical, and pressure sensors [17]. Just one mine/UWIED can be acquired for little expense and yet produce millions of dollars worth of damage to a ship, not to mention the economic tolls to follow. For example, on April 14, 1987, an Iranian contact mine was struck by the USS Samuel B. Roberts frigate. The mine was based on a 1908 Russian design estimated to cost only \$1500, and yet the damage sustained by the USS S.B. Roberts was on the order of \$96 million [17]. Accordingly, the Navy has placed a great amount of emphasis over the last few decades on expanding and improving the mine warfare (MIW) capabilities of the fleet.

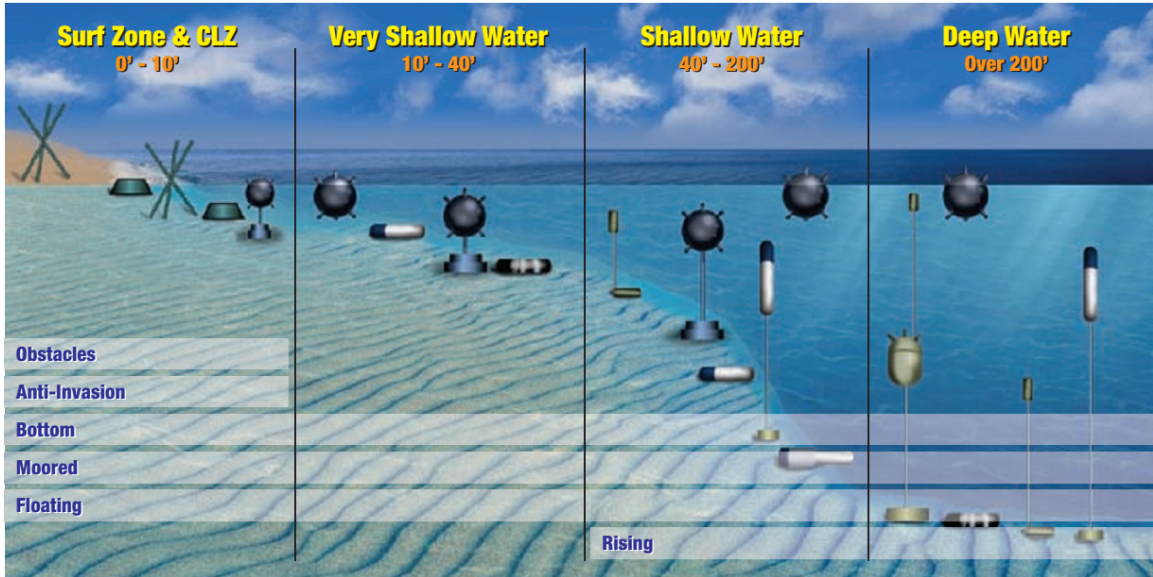


Figure 37: Mine Warfare Regions [17]

The Navy utilizes multiple approaches for engaging in Mine Countermeasures (MCM) operations. Most modern MCM operations include Avenger class MCM-dedicated ships, MH-53 Sea Dragon helicopters, explosive ordnance disposal (EOD) divers, and marine mammal systems. Three key strategies are typically utilized for MCM operations. These include mine sweeping (the trailing of chains or the generation of acoustic, magnetic, or electric signatures for detonating mines), mine hunting (which entails seeking out and destroying individual mines), and mine breaking (transiting a vessel through a minefield to clear a path for other ships to follow) [17, 74]. The U.S. preferred strategy is mine hunting since it can provide a “high degree of certainty that an area of concern is mine-free or the risk of a mine strike has been minimized”, and as the Navy saying goes, “Hunt if you can...Sweep if you must” [17].

High level goals for the advancement of MCM operations include discontinuing the use of humans and mammals, significantly decreasing the expected operations time, and increasing the overall confidence in neutralizing a mine field. In addition, the Navy’s recent focus on network-centric distributed systems has led to system architectures which often-times include disparate technologies and capabilities (*e.g.*, architectures composed of various

aerial, surface and underwater unmanned and manned systems). Consequently, it becomes increasingly difficult to compare and gauge the performance contribution that each system will have on the overall network-centric architecture. The Navy has proposed the need for innovative means to evaluate assimilation, modeling, and simulation methods as applied to the development and use of distributed and autonomous ocean systems, as outlined in the Naval S&T Strategic Plan [117]. Therefore, there is a need for developing novel methods to analyze and design unmanned, collaborative, systems-of-systems capable of performing in the mine warfare battlespace.

Various facets regarding the development of the unmanned MCM SoS should also be addressed by the desired design analyses. Considerations include: determining the appropriate combinations of unmanned vehicle systems that should be employed (including the number of each particular system), the types of sensors and communications packages that should be utilized, whether or not any existing vehicles can carry the necessary sensors and communications packages, the CONOPS that should be considered, and the appropriate amount of collaboration between the systems. Subsequently, the design of a group of unmanned collaborative systems to perform an MCM mission is a large combinatorial problem in which all levels of the SoS hierarchy should be considered. In speaking of utilizing underwater vehicles, Gooding writes [62]:

“To reap the full potential of these technologies, AUVs [autonomous underwater vehicles] must be capable of working together in a cooperative manner...Such systems may be composed from a vast range of vehicle types and sizes, sensors, navigation suites, communication packages, etc., resulting in a nearly limitless set of alternative configurations. For this reason, the design and employment of a cost-effective multiple AUV system requires an understanding of the system’s dynamics and, in particular, the relationships between system configuration and performance characteristics...ultimately, though, it is the overall system effectiveness – the degree to which the system serves its intended purpose – that must be assessed in order to make appropriate decisions.”

Consequently, the identified capability gaps for the MCM perspective of this Representative Example Problem are as follows:

- Provide a means to analyze the overall performance of multiple SoS architectures performing mine-hunting missions while gauging and comparing the performance contributions of each individual system.
- Implement SoS designs which consist of unmanned collaborative systems such that humans and mammals will not be present in the mine field.
- Major considerations for comparing SoS architectures should include minimization of operations time and maximization of confidence of neutralizing the mine field.
- Inclusion of system dynamics and subsystem performance should be included in the analysis of alternatives even though this considerably increases the number of alternatives to be analyzed and the fidelity required.

The considerations outlined above for the use of unmanned systems in mine warfare provide a basis to work upon for partially answering the question, “What problem are we trying to solve?”. In accordance with developing a conceptual model via the POSSEM approach, the high-level mission was defined and capability gaps were identified for both the real-world application of MIW systems and the ability to effectively analyze the SoS. Setting up a specific scenario will be outlined in the next few paragraphs, followed by the recognition of baseline vehicles and technologies to be utilized and analyzed. Then, the final piece of developing the conceptual model will encompass the identification of customer requirements, applicable constraints, potential trade-offs and overarching goals of any analyses to be performed.

Specific Scenario Definition The scenario considered for this example problem is based on the detection and classification of underwater mines in a full $10 \times 10 \text{ km}^2$ area. By the technical definition, the detection and classification tasks make up the first half of the mine hunting mission of MCM. Also, it is widely considered in current operations that detection and classification occur simultaneously. The mission area is shown in Figure 38 in which

the satellite image was acquired from a Google Maps snapshot off of Virginia Beach. Only the detection and classification phases of the MCM mission will be considered in order to bound the problem. Identification and Mine neutralization are other tasks under the MCM umbrella and will not be considered within this work.

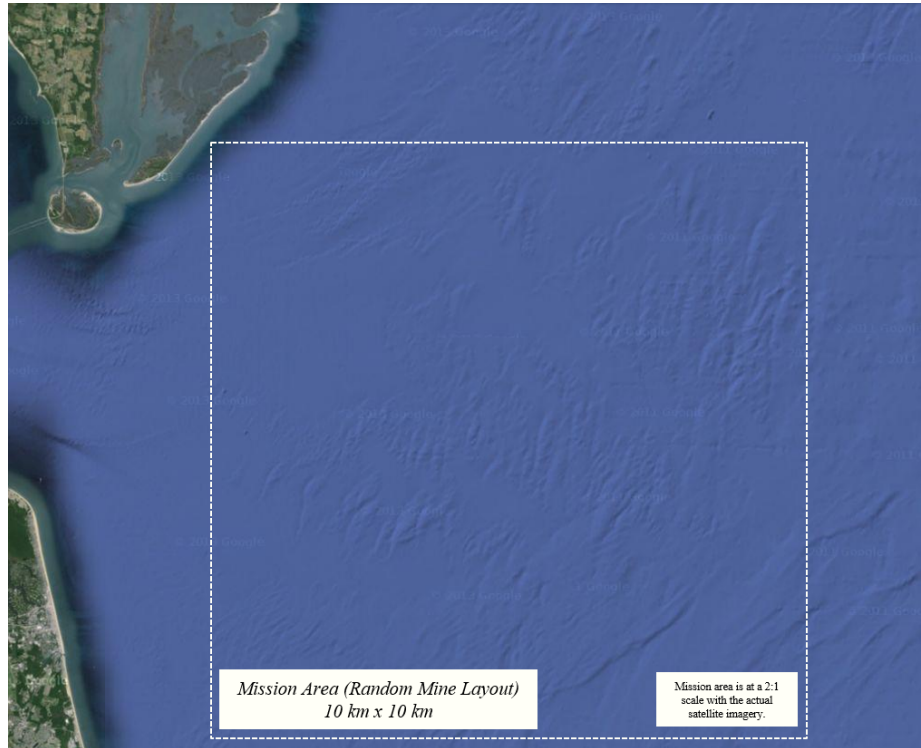


Figure 38: MIW Mission Area [Google Maps Satellite Imagery]

The mines are to be laid down randomly within the full area so that the mission commander has no prior knowledge as to exactly where each mine is located. Also, it is assumed that there are no major obstacles in the area that must be avoided.

Baseline Vehicles and Technologies Unmanned underwater vehicles (UUVs) are usually designed based on mission and task requirements by commercial companies and are then purchased by the military as commercial off the shelf (COTS) products. However, in order to define the requirements that the COTS systems must meet as well as perform analysis of alternatives, design and mission analyses must be initiated. There are many types of missions and tasks that may be performed such as underwater reconnaissance, bathymetry mapping, communications relaying, maintenance inspection, ship hull cleaning, underwater

mine hunting, etc. The Representative Example Problem used throughout this research, however, is underwater mine hunting (in particular the detection and classification phases of mine hunting). Therefore, certain assumptions can be made about the baseline vehicles and technologies that will be utilized within the SoS architectures. Furthermore, manipulations of the baseline designs must be possible in order to determine if new or alternative designs will best meet the mission requirements.

The main objectives of the mine hunting task within this research are to maximize the ability to positively detect and classify mines within the specified mission area while minimizing the operational time-line. Therefore, two major considerations for the baseline vehicle designs include the ability to perform the mission at a high rate of motion while being able to carry and utilize the appropriate sensors for accomplishing the task at hand.

The requirement of performing the mission at a high rate of motion leads to the insight that the vehicles should likely be shaped in such a way that will minimize drag while in forward movement. Therefore, the vehicle hull should be torpedo-shaped in order to achieve minimum drag at high speeds. As is stated by Evans and Nahon [50]: “In recent years, autonomous underwater vehicles have had an increasingly pervasive role in underwater research and exploration. These vehicles generally have a streamlined, torpedo-shaped body, and are intended for long-distance missions where their low drag enables high speeds and coverage of a large distance.” Therefore, the shape of the hull will be important in defining the baseline vehicles and any variations in the baseline vehicle designs. The Navy has planned to implement various systems for the future of MCM operations. Two vehicles in particular that meet the desired torpedo-shape characteristics are the Hydroid REMUS 100 (Remote Environmental Monitoring Unit) UUV shown in Figure 39 and the Lockheed Martin Remote Minehunting System (RMS) shown in Figure 40. These two systems have been chosen as baseline vehicles for this example problem since they are already desired by the Navy and are torpedo-shaped vehicles capable of rapid operations. Another factor considered for choosing these two vehicles is the fact that they are very different in design. The radical differences will allow design space trade-offs to be made between extremely disparate systems and capabilities. The RMS is a semi-submersible

vehicle with a towed sonar array (RMS is the name for the combination of a suite of 5 major subsystems including the Remote Multi-Mission Vehicle and the variable depth AQS-20A sonar along with support equipment). The RMS utilizes diesel fuel for power, has a snorkel for air-intake, and is overall much larger than the REMUS UUV. The snorkel also has a radio frequency (RF) communications antenna included which can be utilized during operations. The REMUS on the other hand is much smaller, is battery powered, and cannot communicate via radio communications during operations since it is completely submerged (although it does include an RF antenna that can be utilized to a degree when the vehicle surfaces). Table 2 provides a comparison of some of the salient differences between the RMS and the REMUS vehicles.



Figure 39: REMUS 100 UUV [99]

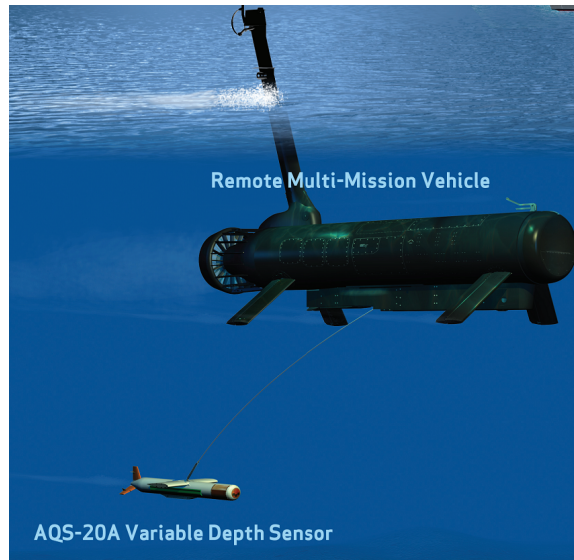


Figure 40: Remote Minehunting System (RMS) [96]

The next requirement mentioned is being able to carry and utilize the appropriate payload for accomplishing the detection, classification, reacquisition and identification tasks while communicating and collaborating. The payload packages will necessarily include sensors (acoustic and electro-optic sensors), localization devices such as inertial measurement

Table 2: RMS and REMUS 100 Comparison Chart

| | REMUS 100 | RMS |
|---------------------------|------------------|-------------|
| Diameter (m) | 0.19 | 1.22 |
| Power Source | Li-Ion Batteries | Diesel Fuel |
| Specific Energy (kW·h/kg) | 0.14 | 11.88 |
| Req. Sensor Power (kW) | 0.2 | 2 |
| Expected Endurance (h) | 20 | 24 |

units (IMUs) and underwater acoustic positioning system hardware for LBL (long baseline) and SBL (short baseline) transducers, communications hardware, on-board computing systems, propulsion system hardware, and power sources (batteries and/or fuel). All of these subsystems will have weight and volume requirements depending on the available technology and desired fidelity. For example, a high powered sonar will likely be larger and heavier than a less powerful and lesser performing system. Also, additional volume will be required for ballast tanks or buoyancy sections and associated hardware. The REMUS 100 can be refitted to carry a number of various subsystems. A physical decomposition of some baseline systems fitted to the REMUS vehicle are shown in Figure 41. Similarly, a decomposition of the RMMV is shown in Figure 42 and alternative subsystem and physical component options for the RMS AQS-20 variable depth sonar array are shown in Figure 43. The RMMV shown in Figure 42 is representative of the first version of the RMMV, and the components are not modular in practice. However, for the purposes of this research variations around the baseline will be allowed.

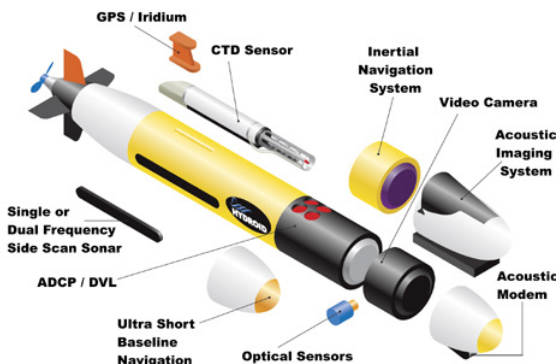


Figure 41: REMUS 100 UUV Components View [99]

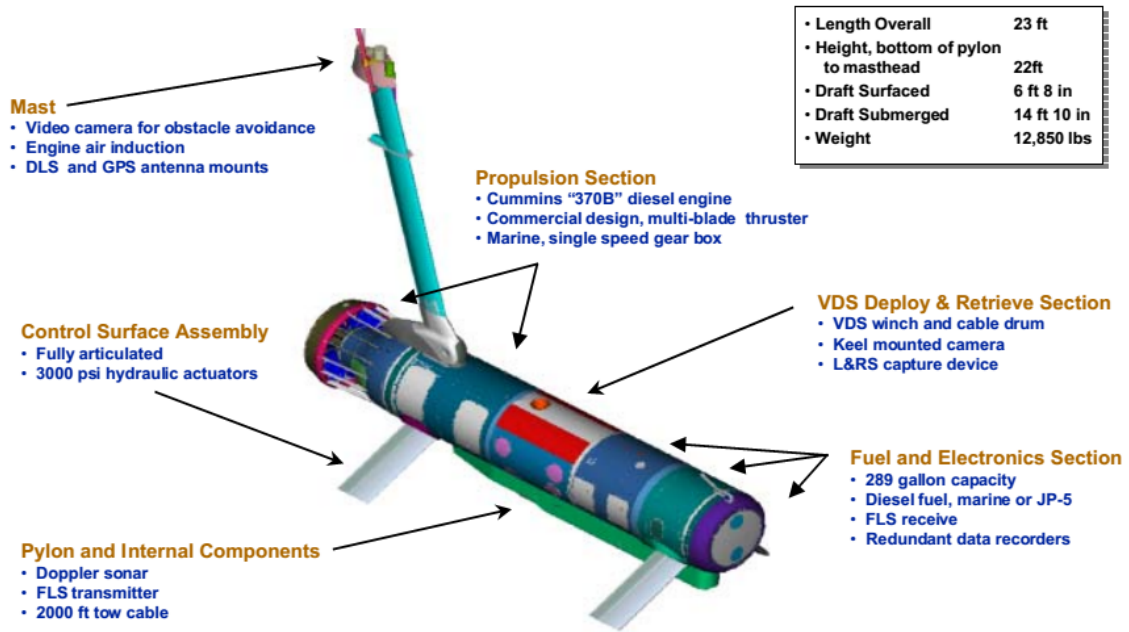


Figure 42: RMMV Components View [149]

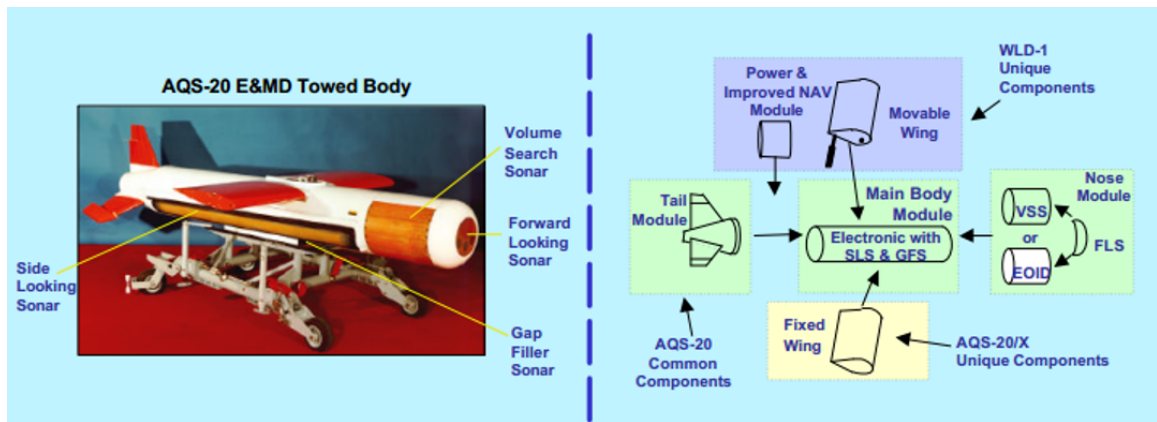


Figure 43: RMS AQS-20 Components View [2]

More specifically, subsystems that most affect the capabilities desired for this mission should be addressed as baseline technologies. For detection and classification of mines, high frequency sonar systems will be required. These include forward looking sonar (FLS), side scan sonar (SSS), synthetic aperture sonar (SAS), gap filler sonar (GFS), and volume search sonar (VSS). The operating frequency, beam width, and resolution of each type of sonar will

vary depending on the specific sonar category and the desired task. If the purpose of the sonar is detection/classification than a high frequency sonar will be required as compared to the operating frequency of a acoustic communication system. However, if the purpose of the sonar is identification, than the operating frequency will be even higher along with a high resolution and small beam width. However, the range of an identification sonar will be significantly depressed compared to other sonar systems. Other options for identification include optical cameras and laser ranging systems. These systems are categorized as electro-optic identification (EOID) systems. In order to provide communications capabilities, acoustic communications (ACOMMS) modems/transmitters and radio frequency (RF) modems/transmitters will be required. Localization of the vehicles and subsystems in the underwater environment is an enormous research task in and of itself. For that reason localization subsystems in this research are modeled as providing perfect navigation capabilities.

In summary, the REMUS 100 and the RMS will serve as the baseline systems to be considered in this testbed. Initial perturbations around these vehicles will be based on varying the subsystems of each vehicle. Then larger perturbations will be introduced by geometrically resizing the vehicles in order to create new designs. This will require sizing and synthesis methods in the analysis step which will begin by defining a desired payload, determining expected ranges based on operational concepts, and defining desired sensor capabilities. Then the sizing and synthesis will iteratively determine the size of the vehicle, the appropriate fuel or battery volume, and the consequent propulsion system design until convergence is achieved. This sizing and synthesis analysis will provide a large number of alternative vehicle designs with various subsystem sets for performing the mine hunting mission as part of varying SoS architectures.

Customer Requirements, Applicable Constraints, Potential Trade-offs and Over-arching Goals Up to this point a mission has been defined with specific scenarios, identified capability gaps, and baseline systems and technologies. The final piece of developing

the conceptual model can be addressed by identifying the customer requirements, applicable constraints, potential trade-offs and overarching goals for the analyses that are to be performed.

The Universal Naval Task List (UNTL) is a Department of Defense document meant to “provide joint force, naval, and ground commanders with an interoperability tool for use in articulating their mission requirements” [165]. The UNTL uses a hierarchical structure to index different tasks within levels of war. The highest level is *Strategic level national military tasks*, then *Strategic level theater tasks*, *operational level tasks*, and at the lowest level *tactical tasks*. Navy tactical tasks (NTA) refer to tactical level tasks to be operated by Naval forces. Mission requirements set forward for the mine warfare tasks relevant to this research from the UNTL include the following:

- NTA 1.3.1 - Perform Mine Countermeasures - To detect, identify, classify, mark, avoid, neutralize, and disable (or verify destruction of) and exploit mines using a variety of methods including air, surface, and subsurface assets: (Measure 1) - Percent residual risk to friendly forces; (Measure 2) - Hours to complete clearing of mines; (Measure 3) Cleared operations area in nm^2 .
- NTA 1.3.1.1 - Conduct Mine Hunting - To detect, locate, and mark mines that present a hazard to force mobility in an overt, covert, and/or clandestine manner. The employment of sensor systems (including air, surface, and subsurface assets) to locate and dispose of individual mines. Mine hunting is conducted to determine the presence or absence of mines in a given area: (Measure 1) - Area searched in nm^2 ; (Measure 2) - Hours to complete marking of minefield; (Measure 3) - Number of mine-like objects found.
- NTA 1.3.1.1.1 - Reacquire Minelike Contacts (MILC) - To reacquire a MILC using one or more of several search techniques, to include all surface, air and underwater techniques: (Measure 1) - Percent of all minelike contacts reacquired.
- NTA 1.3.1.1.2 - Identify Minelike Contacts (MILC) - To identify a MILC through various observation techniques (i.e. divers’ eyes-on, remotely operated vehicle (ROV)

pictures, and live or recorded video) as either a mine or non-mine: (Measure 1) - Percent accuracy of object identified; (Measure 2) - Percent of objects identified.

NTA 1.3.1 in the list above defines the overarching MCM task requirements. The second bullet point defines the overarching requirements for the mine hunting task, which is the subtask of MCM that is being considered for this research. The last two bullet points define the requirements for the reacquisition and identification subtasks that fall under the mine-hunting task. Nonetheless, the measures defined for the minehunting task should enable effectiveness in the high level MCM task, so they cannot be ignored. The measures defined for the MCM task (NTA 1.3.1) in particular are considered the three points of the MCM effectiveness triangle (percent residual risk to friendly forces, hours to complete clearing of mines, and cleared operations area in nm^2). In real world operations, MCM Commanders cannot actually know if an area has been completely cleared of all mine threats. Therefore, the measures that are directly calculated during a mission are time and residual risk. Then, “A given area will be declared clear of mines to a certain confidence level based on the search effort and the search results. A more confident declaration of a cleared area requires that more time and assets be applied in the operation” [146]. In general, however, the requirements outlined above from the UNTL provide direction for defining the measures of performance (MOPs) that establish individual system contributions. Requirements definitions for the relevant measures of performance that can be tracked through analysis will provide a direction for improvement in specific measures and desired capabilities. Requirements laid out by the Navy’s Program Executive Office of Littoral and Mine Warfare set the following performance requirements [17]: improve detection capability; decrease sensor false alarm rate; reduce or eliminate post mission analysis (PMA) detect, classify, identify and decide time; infuse automatic target recognition; improve neutralization time; improve network communications; achieve in-stride detect-to-engage capability.

Applicable constraints for the mine warfare mission are defined in terms of the total size of the SoS that will be utilized. Since MCM missions are to be operated off of the Littoral Combat Ship, the number of vehicles used at one time will be given a volume constraint.

In light of the points made in this section, potential trade-offs for the analysis of the

MCM task within this research will focus on improving performance requirements through perturbations around the baseline systems using advanced technologies (*i.e.*, modifying subsystem performance and utilization), varying the designs, and executing the missions with different operational concepts. It is likely that correlations will be seen between the efficiency in which energy of the systems is used and performance requirements. This will be an important trade-off to monitor.

5.1.2 What Level of Detail is Needed

This section will address the second question presented in defining the problem: “What level of detail is needed?”. The level of detail required is based on the types of trade-offs and/or optimizations that are desired. However, trade-offs can only be made if measures of effectiveness (MOEs) and performance (MOPs) are defined. Furthermore, MOEs and MOPs can only be evaluated if the appropriate parameters of the systems are manipulated and modeled (*i.e.*, the input variables). Also, sources of uncertainty and stochasticity must be brought to light.

5.1.2.1 Metrics Derivation

Defining the measures through which trade-offs, optimizations and analyses will be performed is not trivial. As was pointed out in Section 3.1, a critical part of the design process is being able to generate measures of goodness for products and processes. Such an abstraction is necessary to provide designers, decision makers and stakeholders with concrete values for assessing the combinations of design variables that result in the “best” design, for performing trade studies, and for selecting between alternatives.

Based on the requirements defined earlier, the overall goals are to produce a set of SoS alternative designs capable of performing the mine hunting mission and comparing the effectiveness and performance of each SoS alternative through analysis. While defining the customer requirements above, it was pointed out that the three overarching MOEs for the MCM mission are percent residual risk to friendly forces, clearance time in hours, and area cleared in nm^2 . Within the MCM mission exists the mine hunting task with its own set of MOEs, namely the area searched in nm^2 , the hunting time in hours, and the number of

mine-like objects found in the area. Furthermore, the reacquisition and identification tasks are categorized within the mine hunting task with associated MOEs. For the reacquisition task, the MOE is the percentage of mine-like contacts reacquired (MILC), and for the identification task the MOEs are the percent accuracy and the percent of objects actually identified. Not included in the UNTL are MOEs for the detection/classification (DC) task, although these can easily be deduced based on the other MOEs required. For example, in order to calculate the percentage of MILC reacquired during the reacquisition task, a number of MILC initially found during the DC task must be recorded. Furthermore, performance of the DC task should be tracked through a DC percent accuracy metric, the area actually searched in nm^2 , and the length of the search in hours. In summary, the MCM MOEs for this research task are succinctly shown in Table 3.

Table 3: MCM MOE Subset for this Research

| Task | Measures of Effectiveness (MOEs) | Units |
|-------------------------------|---|---------------|
| MCM Task | Residual Risk to Friendly Forces | % |
| | Clearance Time | hours |
| | Operations Area | nm^2 |
| Mine Hunting Task | Area Searched | nm^2 |
| | Hunting Time | hours |
| | MLO Found | # |
| Detection/Classification Task | MILC Found | # |
| | DC Accuracy | % |
| | Search Time | hours |
| | Search Area | nm^2 |
| Reacquisition Task | MILC Reacquired | % |
| Identification Task | Identification Accuracy | % |
| | Objects Identified | % |

The above measures are overall mission effectiveness measures. Subsystem and system level performance measures will subsequently be delineated in each of the next three chapters.

Lastly, from an analysis perspective the number of mines, the types of mines, any mine-like objects, and their placement and layout within the search area can be considered noise variables. This is because the SoS designer would have no control over these factors in the real-world. These noise variables can be manipulated in order to test the robustness of the SoS design, but that is not the initial goal of the design problem. Therefore, these factors

will be constrained as follows:

- Only bottom mines will be used.
- One bottom mine design will be included: the Italian MANTA mine.
- There will be a total of 50 mines placed randomly throughout the 100 km² clearance area.
- The randomly distributed locations of the mines will be the same for every experimental run.
- The depth of the sea floor will remain constant.
- The bottom type will be medium-sized sand granules.
- The water turbidity, current and sea-state will remain constant.

CHAPTER VI

EXPERIMENT SET A: SUBSYSTEM (SENSOR) LEVEL

Two particular subsystems of interest for a collaborative SoS are sensors and communications systems. Both of these subsystems have rich theoretical backgrounds with abounding applications in the real-world. Entire fields of science and engineering are committed to each. As was stated earlier, the perspective of this dissertation is that of a Systems Engineer methodically bringing together various disciplines in order to analyze alternative collaborative SoS design options. Each of the constituent disciplines would typically be modeled and analyzed by a disciplinary expert. However, since this dissertation is written by a single individual, scoping of the problem is necessary. Therefore, in this work, sensors (specifically sonar systems) are modeled with enough depth to map the energy of the subsystems up through the multiple levels of the SoS hierarchy. Consequently, communications are assumed to either be perfect or non-existent. However, future work could include communications modeled into the overall method developed by this thesis in a similar way in which the sensors are incorporated.

6.1 Modeling and Analyzing Sensors: A Review

6.1.1 Sensor/Sonar analysis

Sensor modeling is often approached from either the perspective of physical characteristics (transducer array design, sound propagation, reverberation, etc.) or from the perspective of statistical signal processing (beamforming, spectral analysis, matched filters, etc.) [85] [26]. As Ainslie referred to it, “The science of sonar performance modeling is traditionally separated into a ‘wet end’ comprising the disciplines of acoustics and oceanography and a ‘dry end’ of signal processing and detection theory” [3]. In terms of energy transfer, the disciplines of ‘acoustics and oceanography’ provide essential relationships for performance. This is usually approached through the sonar equation (or the radar equation for radar systems) which is detailed below. The signal processing analysis (*i.e.*, the ‘dry end’) is not so

much a function of the physical system itself as it is dependent on algorithmic considerations. Therefore, signal processing is not considered in this work beyond a few assumptions on the Detection Threshold parameter that will be introduced in a few paragraphs.

The sonar equation is a deterministic, physics-based performance model for passive and active sonar systems [119]. Fundamentally, it is “a specialized statement of the law of conservation of energy” [152]. It is also an abstraction of signal-to-noise ratio and is often expanded in logarithmic form. A version of the active sonar equation is given in Equation 14 below. Source Level (SL) is related to the acoustic power output, transmission loss (TL) is a negative effect based on acoustic spreading and environmental conditions, TS is the Target Strength of the expected target, NL is the noise level in the local environment, DI is the directivity of the sensor, and DT is the detection threshold for the signal processing equipment. The Reverberation Level, RL , is the result of unwanted reflections masking the target return signal.

$$S/N \equiv SL - 2TL + TS - (NL - DI) - RL > DT \quad (14)$$

It is important to rearrange the sonar equation from the form presented in Equation 14. The reason is that the Transmission Loss term, TL , is dependent on the distance that the signal will travel through the water. In fact, it is the only term that is dependent on the distance traveled by the signal, whereas all other terms are factors of the system itself, the target, or the environment. Therefore, TL is the tactically significant term that allows a designer or tactician to determine possible operational scenarios based on the transmission capabilities. The desire is to either design a system that has a Figure of Merit, FOM , greater than the total transmission loss, or if the sonar design is locked in (and subsequently the FOM), to operate at distances in which the Transmission Loss is not greater than the system FOM . The rearranged sonar equation is presented in Equation 15 which says that the FOM must be greater than the 2-way Transmission Loss in order for detection of the target to occur with some probability.

$$FOM = SL - DT + TS - (NL - DI) > 2TL \quad (15)$$

Sophisticated models of acoustic pulses interacting with the ocean environment are available, including the Applied Physics Laboratory High Frequency Ocean Environmental Acoustic Model [80], the Generic Sonar Model [175], and the Sonar Simulation Toolset [58]. The results of these simulations should not be considered accurate approximations of the real-world without validation against real experimental data. However, the results are expected to be verifiable representations of the physics of the problem that can be used to compare designs against each other and perform trade-offs according to accurate trends.

There is a dependence between sonar sensing operations and the energy required to perform the sensing task. Consequently, there is a dependence between the design of the sensor, the vehicle, and the operational concepts. A given operation is the task in which a sensor, or suite of sensors, must be implemented. The desired operational plan for a sensor is similar to a mission profile in aircraft design. Some sensors are required to remain static, and are subsequently designed for that purpose. The sensors in this work are expected to be dynamic in traversing a given area of interest. However, the sonar equation and the ‘wet end’ of sonar performance modeling do not usually consider the effects of dynamics on the overall sensor performance apart from the Doppler effect (which is really a dry end effect). For the performance of dynamic sensors, the field of Operations Analysis (OA) provides the relevant operational profiles and implementations of search theory. However, the modeling of sensors in OA is often simplistic and/or probabilistic, and lacking in the physics of the sensors. The application of sensors in OA will therefore be expanded on next, and the following section will provide a bridge between the two fields (sensor performance modeling and operations analysis). The bridge between these two fields through the use of a virtual experimentation environment is one of the significant contributions resulting from this dissertation.

6.1.2 Sensors in Operations Analysis

Search and Recovery (SAR) missions require the analysis of sensors to predict mission effectiveness [171]. Unfortunately, deterministic models of sensors (*e.g.*, the sonar equation)

do not capture the stochastic nature of operational environments [119]. In order to capture the stochastic nature of operational environments, a sensor designed according to the physics-based sonar or radar equation would be taken out into the real world where experiments can be performed. Experiments would be conducted by setting out targets up to the maximum theoretical sensor range calculated by the sonar equation. The sensor would be placed on a vehicle and operated through the test site at varying speeds. Data for the number of detections of the targets are collected, with the targets located at varying lateral ranges away from the vehicle search path. From the data, a *lateral range* curve is constructed which specifies the probability of detecting a target laterally away from the vehicle for the specific environment. This process is repeated in multiple environments for the single sensor to provide performance estimates through experimental data for specific combinations of sensors, targets, and environments. The result of this existing method is the generation of a probability of detection (P_D) curve for varying target ranges that can be applied to higher level calculations of mission effectiveness [89]. This process is shown in Figure 44. Unfortunately, this process is not economically viable for acquiring empirical data for varying sensors in the early stages of SoS design.

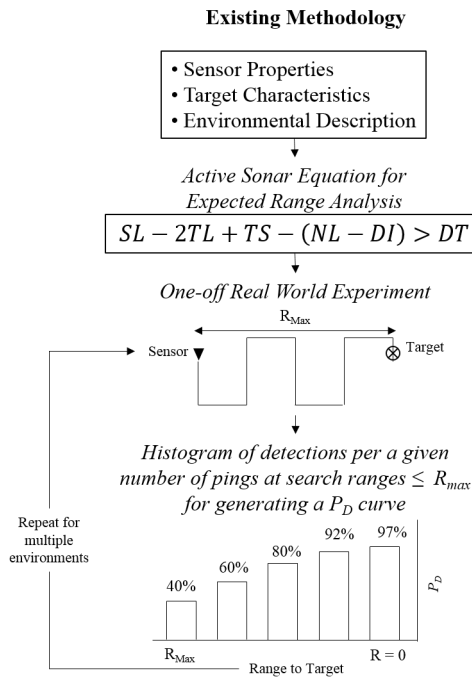


Figure 44: Existing P_D Generation Process

Due to the impracticality of performing the above experimental method during the conceptual design of sensors, vehicles and SoS architectures, empirical data is rarely available. As a result, analysts are often left with generating assumed probability curves or highly simplified estimates. Probabilistic models are usually employed. In a seminal book, *Naval Operations Analysis*, the motivation and implication of probabilistic models is stated for the radar equation as follows [119]:

The goal of a radar model is the prediction of a radar's ability to detect a target. A model which predicted this detection capability using only the elementary parameters of the radar system...would attempt to determine the range at which detection will occur, or the intensity of a signal returning to the antenna in terms of those basic parameters. Because of the elementary nature of its inputs, such a model is called absolute or deterministic. The radar equation is clearly an attempt to formulate an absolute theory, and were it not for the random nature of target, propagation, maintenance, operation and background noise, it might well succeed. In the presence of variations in these quantities, the radar equation can be expected to yield, at best, an estimate of an average range of detection in terms of the average values of the other quantities. It may also be used to determine maximum possible range of detection. Another approach to the formulation of a radar theory is to seek a less sophisticated model which accepts a certain amount of operational data and attempts its extrapolation to more general operational situations. Two such theories, the blip/scan and the direct method...will be referred to as relative or probabilistic.

The next approach is using highly simplified estimates. According to Gage, “it is common to approximate a detection sensor’s lateral range curve in order to facilitate analytical modeling of the search process” [57]. Figure 45 shows an example of how a “cookie cutter” approximation or an imperfect sensor approximation is made for a lateral range curve. However, without actual experimental data for the lateral range curve, the definite range and imperfect sensor models are simply assumptions with no associated sensor performance

model.

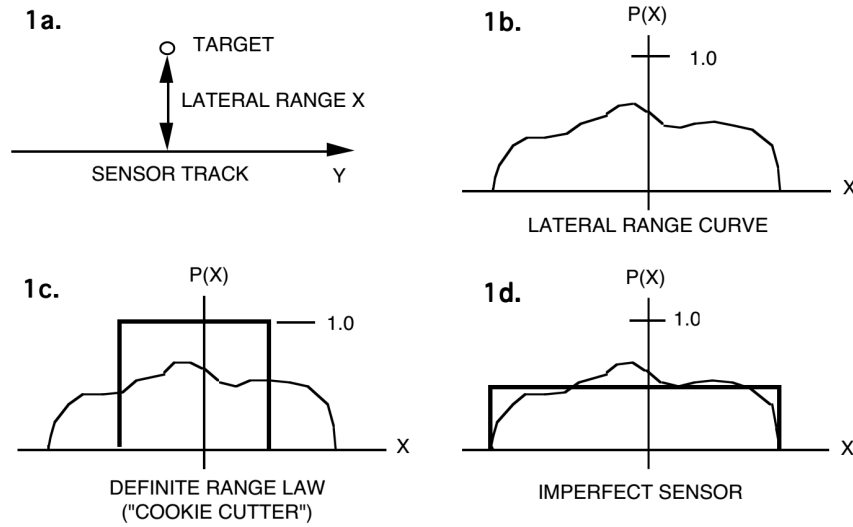


Figure 45: (1a) Definition of lateral range. (1b) Fictitious lateral range curve. (1c) Definite range law (“cookie cutter”). (1d) Imperfect Sensor. Adapted from Gage [57].

Koopman [89] provides additional lateral range curve models that are a bit more sophisticated, which are presented in Figure 46. Both of the curves are based on the inverse cube law, which was originally established to approximate visual search. The curve on the right contains a dip down the middle of the search path, which represents the effect of a sonar pinging directly over a target, which can cause difficulties in detection (similarly, a radar with sea return reflections). The parameter W is the effective sweep width. It is equivalent to the area under the curve (*i.e.*, the integral). The effective sweep width is interpreted as the lateral range out of both sides of the sensor at which the number of objects not detected within W is equal to the number of successful detections outside of W , in probability.

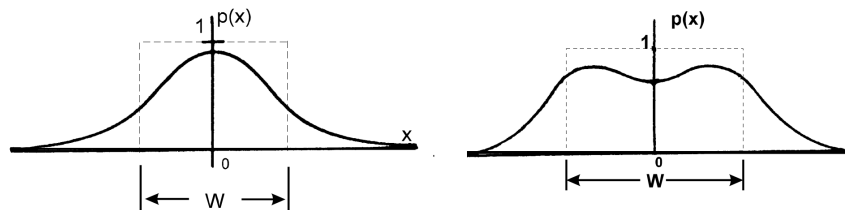


Figure 46: Inverse cube law approximations for the lateral range of a sensor [89, 155].

Finally, in much of the collaborative robotics literature, sensors are assumed to be

perfect and able to measure the full state of the environment [139]. Skoglar even states that “The Charnes and Cooper approach, complemented with the Markovian motion model and Stewarts search path constraint formulation, represents the state-of-the-art in computer based search planning, as found in tools in operational use today. This method, however, is not without limitations. In particular, the detection model is very simple, and neglects the strong dependency of detection performance on target location, terrain topography, and sensor position that exists in certain applications” [139, 32, 142].

These reviews demonstrate that there is a disconnect between the disciplines of sensor modeling and operations or robotics research. This is understandable since the separate disciplines are so rich individually. However, from a Systems Engineering perspective, the disciplines must be synthesized in order to better meet defined requirements, since without joining these disciplines, a significant amount of information is lost.

6.1.3 Filling the Gaps

The previous sections demonstrated that in the literature there are two general trends in modeling sensors: analysis without implementation and implementation without analysis. In other words, the sensor performance modeling subset of the literature focuses deeply on the analysis of sensors based on the physics of the problem, including acoustic interactions with the environment. Alternatively, Operations Analysis and robotics literature is focused on implementing sensors for specific applications, but tend to make generalized assumptions about the physics of the sensors due to a lack of empirical data and/or modeling capability. There is accordingly a gap in capability since without implementing the physics of the sensors into the operational analyses, energy conservation between the sensors and the operations cannot be mapped.

The following section will demonstrate a new formulation for acquiring empirical data. It builds a bridge between the detailed physics-based modeling of sensors and the required operational mission planning through virtual experimentation.

6.2 A New Formulation

The analysis and design of collaborative SoS alternatives requires the quantitative mapping of subsystem-level design trades up through system- and mission-specific effectiveness measures. Unfortunately, as was stated earlier, deterministic models of sensors (*e.g.*, the sonar equation) do not capture the stochastic nature of operational environments [119]. Probabilistic models are therefore employed to provide performance estimates through experimental data for specific combinations of sensors, targets, and environments. However, during the conceptual design of sensors, vehicles and SoS architectures, empirical data is rarely available. As a result, analysts are often left with generating assumed probability curves or highly simplified estimates (*e.g.*, the ‘cookie cutter’ sensor). Furthermore, functional relationships between the vehicle design, the sensor attributes, and the operational concepts are lacking. This section works to fill this gap through the bridging of a deterministic sonar model with an agent-based virtual experimentation environment and vehicle performance attributes. The proposed experimental augmentations are shown in Figure 47 below.

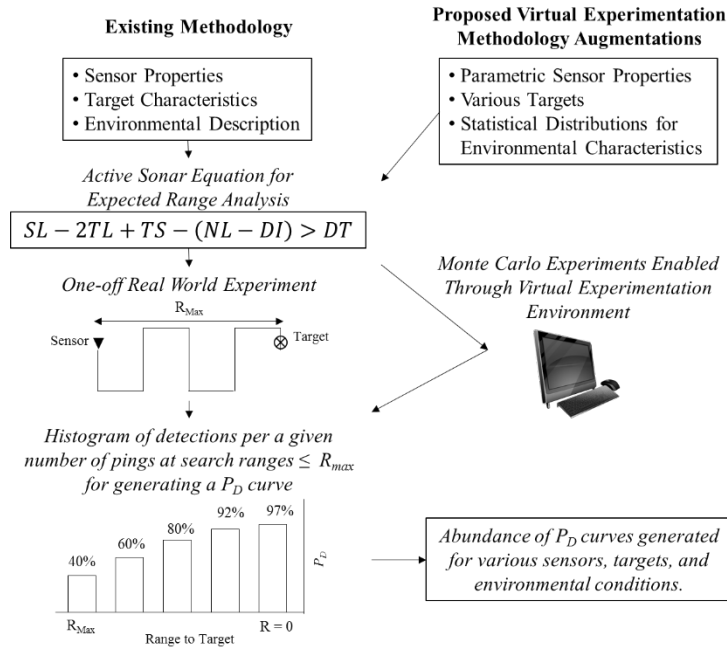


Figure 47: Existing P_D Generation Process Alongside Virtual Experimentation Augmentations.

This work is immediately relevant for the current vision of mine warfare in the U.S. Navy. More specifically, the mine hunting task of a mine countermeasures (MCM) mission is a challenging operation in which the Navy desires to decrease the tactical timeline and increase the use of autonomous robotic systems [17]. A key enabler to this is the use of nascent high frequency sonar capabilities which will allow the autonomous systems to detect, classify and identify mines and mine-like objects with a high degree of confidence and a minimal false alarm rate [62]. However, as was stated above, experimental data that can be associated with varying sonar designs is lacking.

Sensitivity of the sonar performance on the overall mission effectiveness is absent without an appropriate prediction of the sensor P_D curves. In order to fill this gap, this section is focused on the creation of a parametric sensor model based on the sonar equation which will be applied to an agent-based simulation for virtual experimentation. Agent-based simulation has been picking up steam in the last few decades as an alternative approach to costly real-world experiments. “Agent-based modeling and simulation (ABMS) is also an experimental technique, a framework for developing electronic laboratories in which the most detailed assumptions about individual agents, their behaviors and interactions can be varied and explored in silico. Some commentators have gone so far as to suggest that ABMS, with the computational experimental framework it offers, is a new way of doing science” [129, 10, 48].

The environment being utilized is the Autonomous Littoral Warfare Systems Evaluator Monte Carlo (ALWSE-MC) which has been provided by the Naval Surface Warfare Center Panama City Division (NSWC PCD). The acoustic model present in the simulation environment is a sophisticated approximation of acoustic pulses interacting with the ocean environment, based largely the High Frequency Ocean Environmental Acoustic Model [80]. The agent-based simulation environment calculates the sonar/ocean interaction at each time step. The results of the simulations should not be considered accurate approximations of the real-world without validation against real experimental data. However, the results are expected to be verifiable representations of the physics of the problem that can be used to compare designs against each other in capability. The virtual experiments provide data used

to define lateral range curves and sweep widths for each particular sensor design, resulting in a parametric design space of sensors and operational schemes. “Sweep width is a single number characterizing the average ability of a given sensor to detect a particular search object under a specific set of environmental conditions. Thus each combination of sensor, search object, and set of environmental conditions will have a particular associated sweep width. In the vernacular, sweep width might be called a measure of *raw detection power*” [88].

6.2.1 Modeling with the Sonar Equation

Significant parameters of the sonar equation include the Source Level, Transmission Loss, Target Strength, Noise Level, Directivity Index, Detection Threshold, and Reverberation Level. As was stated earlier, the sonar equation is “a specialized statement of the law of conservation of energy” [152], including energy output by the sensor (*e.g.*, acoustic power output defined by the Source Level) and energy losses through the environment (*e.g.*, the Transmission Loss). It is assumed in this work that the operations being modeled are limited by the ambient noise levels, even if just slightly, and are not limited by reverberations. Therefore, the *RL* term can be ignored while the *NL* will remain. This is not unusual in sonar modeling where either the *RL* or *NL* terms are often considered insignificant. The resulting sonar equation in terms of the Figure of Merit (FOM) is given in Equation 16. Figure 48 compares the power of the target echo, reverberations in the water, and ambient noise. From this figure it can be seen that at operational ranges considered to be relatively short, as in this work for the detection, classification and identification of small objects, the sonar system will be noise limited before it is reverberation limited.

$$FOM = SL - DT + TS - (NL - DI) > 2TL \quad (16)$$

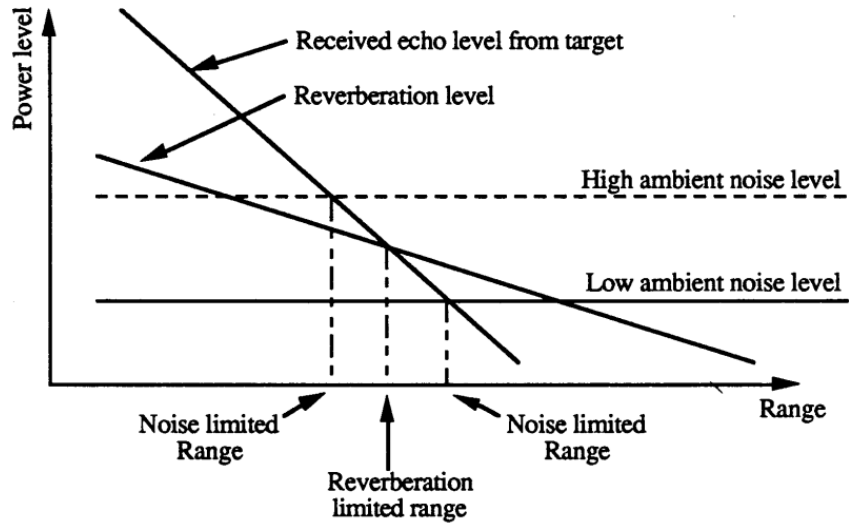


Figure 48: “An illustration of how echo level, reverberation and ambient noise behave as a function of range.” [39]

Each component of the sonar equation can be expanded based on the physics of the system and operating environment. By carefully selecting appropriate ranges for the sensor attributes, a parametric design space was generated. Expansion of the SL and DI drive the sizing of transducer elements as a function of operating frequency, f , (or wavelength, λ) and beam width, θ_{BW} . It should be noted that sensor sizing is highly dependent on the desired performance attributes such as frequency and beam width. The sensor design will drive some of the vehicle sizing and power requirements, as well as overall mission capability such as P_D . Other design variables that can be manipulated include DT , pulse length (pl), vehicle velocity (V_∞), and ping rate (pr). Inclusion of TL calculations will provide maximum range estimates. Sonar equation parameters such as TS and DT will be reviewed as well.

Reference Parameters: Every sensor requires a transfer or energy between its own sensing elements and the medium around it in order to operate. For a passive sensor, energy is transferred from the environment to the transducer in the form of acoustic waves for an underwater sonar system. For an active system, energy is transferred from the transducer into the surrounding water and vis-versa. For sonar, this energy is related to the frequency

and amplitude of vibration of the transducer elements, which is also related to the harmonic motion of a pressure wave in the surrounding water. The time rate of energy transfer, or power, is given in Equation 17 where P_{ac} is the acoustic power. The power divided by an area through which it flows is the intensity, I (*i.e.*, the power density). However, the average intensity of the sound waves in the water is related to the average pressure produced during a cycle of vibration of the transducer. More precisely, it is proportional to the root mean square pressure of the sound waves (p_{rms} , *i.e.*, the square root of the average instantaneous pressure squared during one cycle of vibration) as shown in Equation 18. The denominator of the p_{rms} term in Equation 18 includes the density of water, ρ , and the speed of sound in water, c .

$$\frac{dE}{dt} = P_{ac} \text{ (J/s)} \equiv \text{Watts (W)} \quad (17)$$

$$\frac{P}{A} = I \text{ (W/m}^2\text{)} = \frac{p_{rms}^2}{\rho c} \quad (18)$$

The equations above have been delineated in order to show the clear dependence between sonar sensing operations and the energy required to perform the sensing task. Because of that, there should be a dependence between the design of the sensor, the vehicle, and the operational concepts.

In acoustics, the applicable pressures and intensities encountered can have extreme variations, sometimes by many orders of magnitude. Therefore, logarithms are used in order to better manage the sensitivity of the sonar equation parameters. The difference between two pressures or intensities, generically termed x , would then be: $\log(x_1) - \log(x_2) = \log(\frac{x_1}{x_2})$. Conventionally, pressures and intensities in underwater acoustics are calculated against reference pressures and intensities, p_{ref} and I_{ref} respectively. The reference pressure underwater is taken as $1\mu Pa$, which can be used to derive the reference intensity:

$$I_{ref} = \frac{p_{ref}^2}{\rho c} = \frac{(1\mu Pa)^2}{\rho(\text{kg/m}^3) c(\text{m/s})} = \frac{1}{\rho c} \text{ (W/m}^2\text{)} \quad (19)$$

Accordingly, parameters from the sonar equation, such as the Source Level, are calculated relative to the reference pressure and intensity.

Omnidirectional Source Level: In underwater acoustic literature, the transducer producing the active sonar pulse is called the projector. The sound level of the projector is called the Source Level, which is a function of the intensity of the projector relative to the reference intensity, I_{ref} , defined above. More specifically, the omnidirectional Source Level is defined here as the sound level of the sonar in decibels where the numerator of the log term is the intensity of the source 1 meter from the projector and the denominator is the reference intensity, I_{ref} . Using Equation 18, the Source Level can be determined in metric system units as shown in Equation 20 below¹. The units on SL will usually be given as “dB re $1\mu Pa@1m$ ”, which is interpreted as *decibel quantities measured relative to a reference pressure of $1\mu Pa$ and at a fixed distance of 1 meter*. Finally, the acoustic power transmitted into the water is the result of an electrical input power converted to acoustic power at some efficiency, $P_{ac} = \eta_{ac}P_E$. The efficiency, depending on the particular sonar application, can vary from as little as 20% up to 70%. Trends for the Source Level of a sensor as a function of electrical power for varying efficiencies is given in Figure 49.

$$\begin{aligned}
 SL_{omni} &= 10 \log \frac{P_{ac}/\text{Area}_{\text{at 1 meter}}}{p_{ref}^2/\rho c} = 10 \log \frac{P_{ac}/4\pi(1\text{m})^2}{p_{ref}^2/\rho c} \\
 &= 10 \log \frac{P_{ac}\rho c}{4\pi(1 \times 10^{-6} \text{ Pa})^2(1 \text{ m})^2} \\
 &= 10 \log P_{ac}\rho c + 109\text{dB}
 \end{aligned} \tag{20}$$

$$SL_{omni} = 109\text{dB} + 10 \log \eta_{ac}P_E + 10 \log \rho c$$

¹A significant amount of available sonar data is usually given with reference to a 1 yard distance from the projector. Therefore, it is important to always check the data before assuming a reference distance.

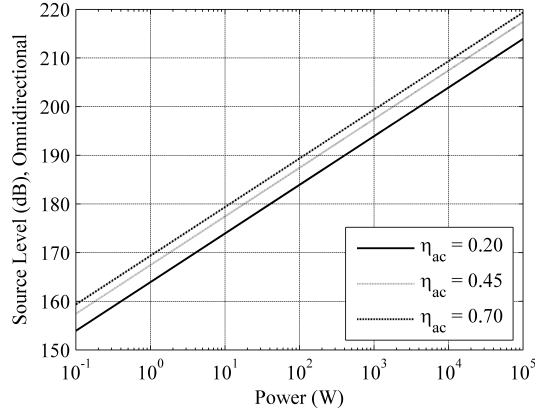


Figure 49: SL_{omni} as a function of Electrical Power, P_E .

Source Level Including Directivity Index: Sonar systems can be designed to generate various beam patterns depending on the number and arrangement of transducer elements. This can be accomplished for both transmitting and receiving arrays. In fact, the Principle of Reciprocity from acoustic theory shows as one of its conclusions that the beam pattern of a receiving array is equivalent to that of a transmitting array under certain conditions. Therefore, the directionality of an active sonar can have an equivalent beam width in both transmitting and receiving modes, which is the assumption applied to this work.

The Directivity Index, DI , of an array expresses the intensity of the directed beam as compared to an omnidirectional beam of the specific array. When added onto the Source Level equation, it is interpreted as an increase in the Source Level in a specific direction since transmission of the signal into other directions is canceled out. The directional SL function is presented in Equation 21 and the basic DI function is given in Equation 22. The Directivity Index of the system is dependent on specific design parameters, including the beam pattern of the particular sonar array. Without presenting the derivation here, the Directivity Index as a function of beam pattern is shown in Equation 23 below. This will be delineated further in the next section.

$$SL = 109\text{dB} + 10 \log \eta_{ac} P_E + 10 \log \rho c + DI \quad (21)$$

$$DI = 10 \log \frac{I_{omnidirectional}}{I_{directional}} \quad (22)$$

$$DI = 10 \log \frac{1}{\int_0^{\pi/2} b(\theta) \cos \theta d\theta} \quad (23)$$

...where $b(\theta)$ is the beam pattern function for varying beam angles, θ .

Directivity Index from Desired beam width: This research considers two specific sonar array designs: a linear array and a circular piston array. The linear array contains transducer elements along a single axis which provides a wide beam in the vertical direction and a small beam in the horizontal direction (or vis-versa). A linear array is the typical design for a side scan sonar (SSS). The circular piston array arranges transducer elements in an almost circular pattern so that there are an equivalent number of elements in both the horizontal and vertical axes. The results are equivalent beam widths in the vertical and horizontal directions. One design application of the circular piston array is the forward looking sonar.

Beam pattern functions can be derived for each array design in order to determine the array specific Directivity Index shown in Equation 23. It should be noted that most arrays are designed with transducer elements that are spaced evenly apart along the array, which is termed the separation distance, d . This is an important factor for the efficiency of the beam pattern since minimization of sidelobes requires $d \leq \lambda/2 = (c/f)/2$, where λ is the wavelength of the sound waves and f is the frequency. In order to minimize the number of transducer elements, the separation distance is then chosen to be the upper limit on the wavelength constraint, $d = \lambda/2$. With this in mind, beam pattern functions for the linear and circular piston arrays are shown in Equations 24 and 25, respectively. Again, derivations are not provided here as they can be found in the literature.

$$b(\theta)_{Linear} = \left[\frac{\sin \left(\frac{\pi L}{\lambda} \sin \theta \right)}{\frac{\pi L}{\lambda} \sin \theta} \right]^2 \quad (24)$$

$$L = nd$$

...where L is the total array length and n is the number of transducer elements.

$$b(\theta)_{Circ} = \left[\frac{2J_1 \sin \left(\frac{\pi D}{\lambda} \sin \theta \right)}{\frac{\pi D}{\lambda} \sin \theta} \right]^2 \quad (25)$$

...where D is the array diameter and J_1 is the Bessel Function of the first order and first kind.

From an operational perspective, it is more useful to define desired beam widths, θ_{BW} , and then size the physical attributes of the array to provide those beam widths². Subsequently, the beam patterns and the Directivity Index can be determined from the physical attributes of the array.

Feasible beam width angles are discrete since the size of the transducer must be able to fit an integer or half-integer (*e.g.*, 1.5, 2.5, etc.) number of wavelengths within the aperture. For a circular piston array, the beam width is a function of the wavelength and diameter of the transducer as shown in Equation 26.

$$\sin(\theta_{BW}/2) = 0.51(\lambda/D) \quad (26)$$

The number of wavelengths, nw , that fit within the aperture size are then equal to the diameter of the aperture over a single wavelength:

$$nw = D/\lambda \quad (27)$$

However, since the number of wavelengths that fit within the aperture must be an integer or half-integer, the desired beam widths are used to size the required aperture diameter and the subsequent number of wavelengths:

$$\frac{D_{req}}{\lambda} = nw_{req} = \left\lceil \frac{0.51}{\sin(\theta_{BW}/2)} \right\rceil - \frac{1}{2} nint \left\{ \left\lceil \frac{0.51}{\sin(\theta_{BW}/2)} \right\rceil - \left(\frac{0.51}{\sin(\theta_{BW}/2)} \right) \right\} \quad (28)$$

Equation 28 provides the actual aperture sizes that are possible based on a range of selected beam widths (*e.g.*, $\{\theta_{BW} | 0 < \theta_{BW} < \pi/2\}$). The $\lceil x \rceil$ symbol represents the *ceiling* function and the $nint(x)$ expression represents the nearest integer function³. The possible

²Horizontal and vertical beam widths are defined as θ_{HBW} and θ_{VBW} respectively in this work. However, θ_{BW} is used for generality when appropriate.

³The *nearest integer function* is also known as the *round* function. It is defined such that $y = nint(x)$, where y is the integer value closest to x . The definition is ambiguous for half-integers, therefore, half-integers are always rounded up in this work. Other conventions often round half-integers to even numbers. [176]

aperture sizes are therefore discrete. Consequently, the actual required beam widths are then calculated based on the sized aperture diameter. However, the required beam widths will often be different than what was originally desired because of the wavelength/aperture size constraint.

$$\theta_{BW_{req}} = 2 \arcsin \left(\frac{0.51}{nw_{req}} \right) = 2 \arcsin \left(\frac{0.51\lambda}{D_{req}} \right) = 2 \arcsin \left(\frac{0.51c}{fD_{req}} \right) \quad (29)$$

A similar aperture sizing process for desired beam widths of a linear array are provided below:

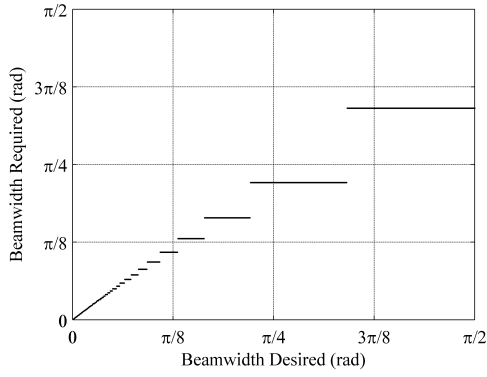
$$\sin(\theta_{BW}/2) = 0.442(\lambda/L) \quad (30)$$

$$nw = L/\lambda \quad (31)$$

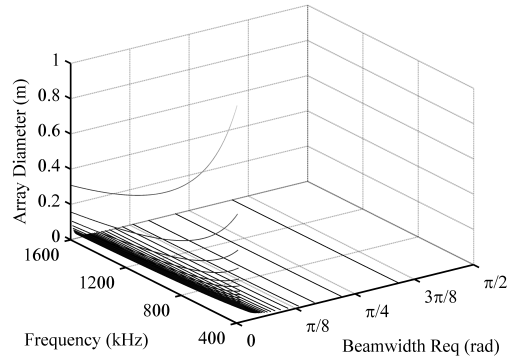
$$\frac{L_{req}}{\lambda} = nw_{req} = \left\lceil \frac{0.442}{\sin(\theta_{BW}/2)} \right\rceil - \frac{1}{2} \text{rint} \left\{ \left\lceil \frac{0.442}{\sin(\theta_{BW}/2)} \right\rceil - \left(\frac{0.442}{\sin(\theta_{BW}/2)} \right) \right\} \quad (32)$$

$$\theta_{BW_{req}} = 2 \arcsin \left(\frac{0.442}{nw_{req}} \right) = 2 \arcsin \left(\frac{0.442\lambda}{L_{req}} \right) = 2 \arcsin \left(\frac{0.442c}{fL_{req}} \right) \quad (33)$$

The discrete effect of the wavelength/aperture size constraint on the required beam width can be seen in Figures 50 and 51 below. The (a) plots show the desired beam widths against the required beam widths due to the wavelength/aperture size constraints. Similarly, a surface plot of the transducer diameter as a function of beam width and desired operating frequency is provided in the (b) plots.

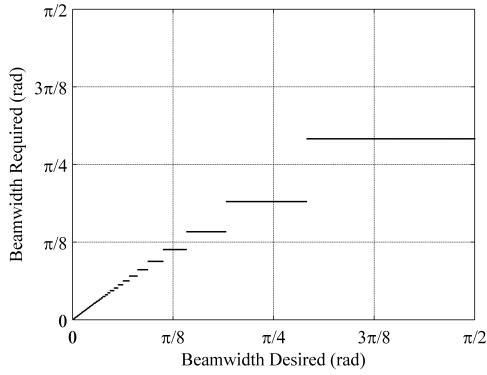


(a)

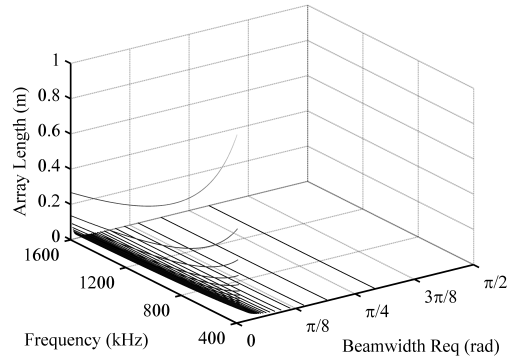


(b)

Figure 50: Required beam width Plots for a Circular Piston Array



(a)



(b)

Figure 51: Required beam width Plots for a Linear Array

Next, the Directivity Index functions can be estimated for each array type as given in Equations 34 and 35. Consequently, the Directivity Index is shown as a function of discrete array sizes and varying frequency in Figure 52.

$$DI_{Circ} = 20 \log(\pi D_{req}/\lambda) \quad (34)$$

...for a circular piston array with diameter $D \gg \lambda$.

$$DI_{Linear} = 10 \log(2L_{req}/\lambda) \quad (35)$$

...for a linear array with length $L \gg \lambda$.

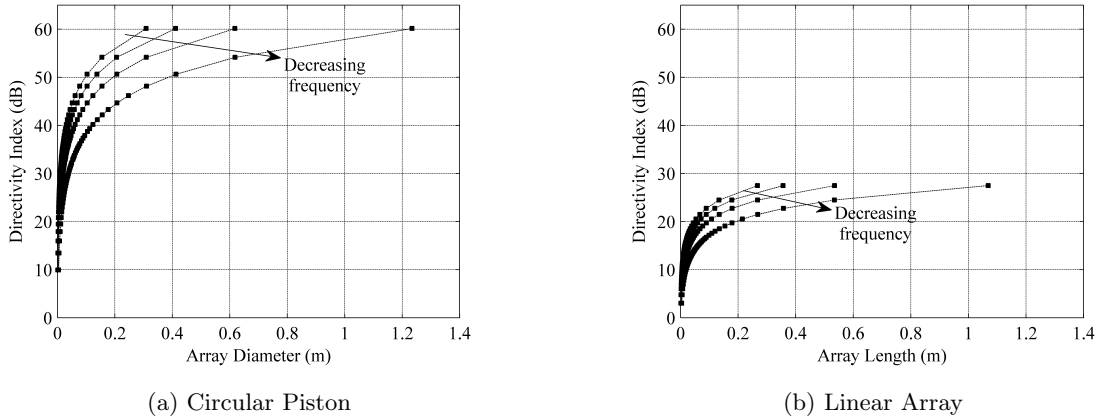


Figure 52: Directivity Index as a Function of Array Size

Finally, the Source Level for each active sonar array as functions of either array size or beam width are presented in Equations 36 and 37.

$$SL_{Circular} = 109\text{dB} + 10 \log \eta_{ac} P_E + 10 \log \rho c + 20 \log(\pi D_{req}/\lambda) \quad (36)$$

$$SL_{Circular} = 109\text{dB} + 10 \log \eta_{ac} P_E + 10 \log \rho c + 20 \log \left(\frac{0.51\pi}{\sin(\theta_{BW_{req}}/2)} \right)$$

$$SL_{Linear} = 109\text{dB} + 10 \log \eta_{ac} P_E + 10 \log \rho c + 10 \log(2L_{req}/\lambda) \quad (37)$$

$$SL_{Linear} = 109\text{dB} + 10 \log \eta_{ac} P_E + 10 \log \rho c + 10 \log \left(\frac{2(0.442)}{\sin(\theta_{BW_{req}}/2)} \right)$$

Figure 53 shows the influence of Directivity Index on Source Level as a function of electrical power provided to the system, P_E . Typical source levels can range from 160–280 dB for power inputs of 0.1 Watt up to 100 kW.

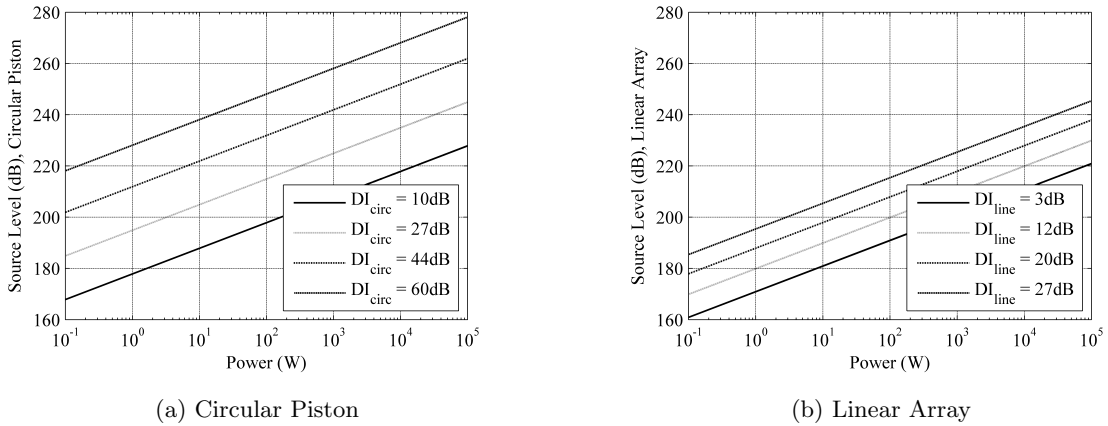


Figure 53: Source Level as a Function of Directivity and Electrical Power ($\eta_{ac} = 0.5$)

In order to assess multiple sonar designs through the parametric sensor model, discrete beam widths are chosen as the initial step in designing multiple experiments. For the circular piston array, the horizontal and vertical beam widths are equivalent. However, the linear array requires the definition of both the horizontal and vertical beam widths. The linear array designed in this work is meant to represent a side scan sonar (SSS), therefore the sonar beam will be wide in the vertical and small in the horizontal. The discrete beam width values chosen from Figures 50 and 51 as starting points for simulating various sonar designs are given in Equation 38.

$$\begin{aligned}
\theta_{BW_{circ}} &= \left[\frac{\pi}{12.29} \quad \frac{\pi}{7.65} \quad \frac{\pi}{4.53} \quad \frac{\pi}{2.93} \right] \\
\theta_{VBW_{line}} &= \left[\frac{\pi}{8.84} \quad \frac{\pi}{5.25} \quad \frac{\pi}{3.43} \right] \\
\theta_{HBW_{line}} &= \left[\frac{\pi}{167} \quad \frac{\pi}{35.70} \right]
\end{aligned} \tag{38}$$

The linear array SSS has 6 design combinations based on each vertical beam width being paired with a horizontal beam width. For each beam width or beam width-combination chosen from Equation 38, frequency and power settings are also assigned based on a 2-parameter, face-centered Central Composite design of experiment [111]. Minimum, maximum and center point values of the electrical power are taken from the range of 0.1 Watt to 100kW while the frequency settings are chosen as the minimum, maximum and center point values of 400kHz to 1600kHz. The initial set of experimental designs based on the specified discretizations are shown in Figure 54. One thing to notice is that the beam width (bw) settings for the FLS array are not evenly spaced because there are only specific discrete bw settings that can be chosen, as was pointed out through Figures 50 and 51. The vertical beam width (VBW) for the SSS design follows the same trend due to the discreteness. The horizontal beam width (HBW) has only been given two settings in this setup. The combinations of parameter settings results in $4 \times 3 \times 3 = 36$ experimental designs for the FLS and $3 \times 3 \times 3 \times 2 = 54$ experimental designs for the SSS.

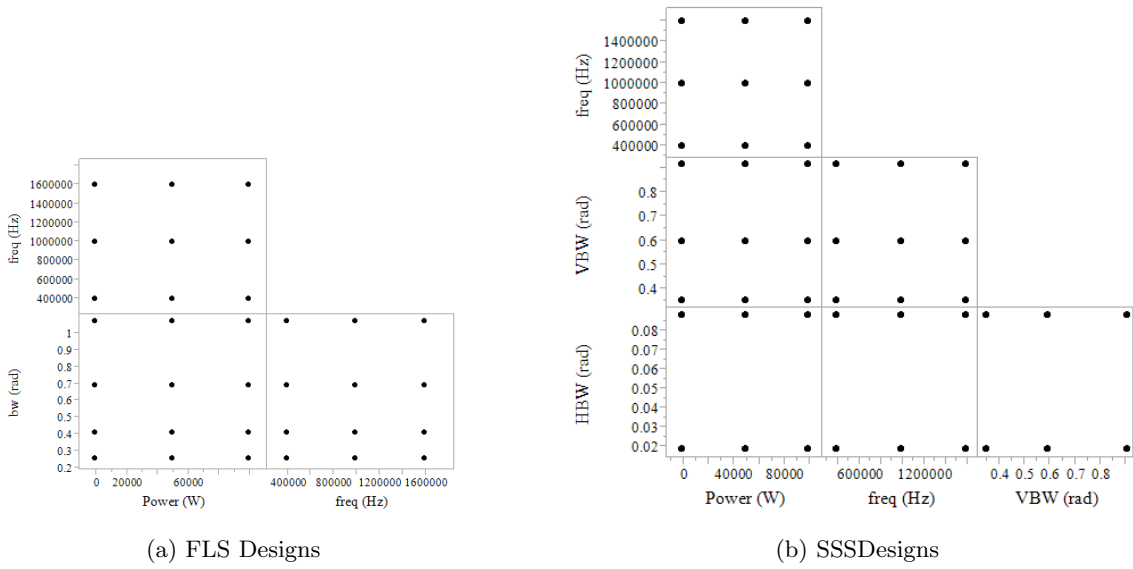
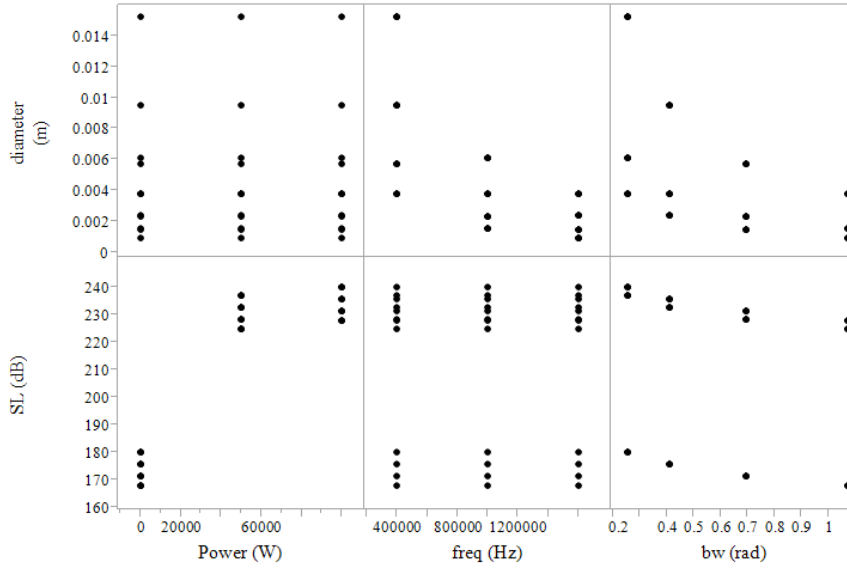
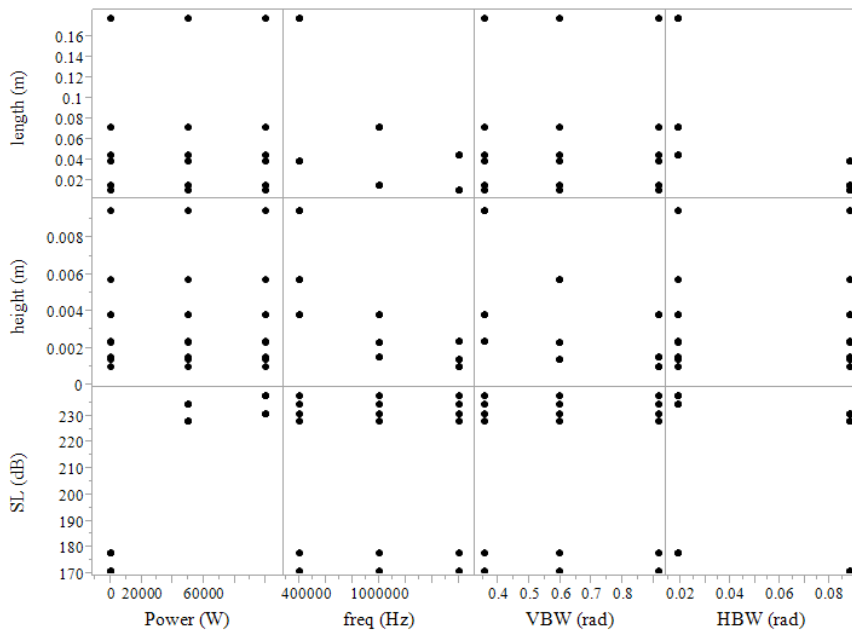


Figure 54: Initial Deterministic Sensor Design of Experiments

Each experimental design from Figure 54 can now be used to calculate array size (diameter or length) and Source Level as functions of power, frequency, and beam width. The functions were detailed in Equations 28, 32, 36 and 37. The results are shown in Figure 55.



(a) FLS Designs



(b) SSSDesigns

Figure 55: Initial Deterministic Sensor Design of Experiments

The calculations performed above allow the determination of sensor size which is important, but performance is not yet quantified. Source Level is only a single aspect considered so far. In order to fully calculate performance based on the sonar equation, the Figure of Merit function and the expected Transmission Loss must be considered. In fact, both of

the experimental setups shown so far will be expanded further to include the total Figure of Merit (FOM) and maximum range values after the Detection Threshold (DT), Noise Level (NL), Target Strength (TS) and Transmission Loss (TL) approximations are formulated.

It should be noted that the Source Level values for the linear array in Figure 55(b) are based on the horizontal beam width (or array length) as developed in Equation 37.

Detection Threshold The Detection Threshold of the sensor is the parameter which most depends on the computational and signal processing capabilities of the system. “The detection threshold is the decision level at which the observer decides ‘yes’ or ‘no’ as to whether a signal is present, based upon the criteria of the probability of making a correct detection and the probability of having a false alarm” [39]. The Detection Threshold can actually be varied based on sonar system parameters that can be controlled by the sonar operator such as the detection index, frequency bandwidth and integration time of the signal. However, the observer does not have to be a human but can alternatively be an automated computer algorithm. Therefore, for initial calculations of DT in this work, human factors are not considered.

Various definitions for DT are available throughout the literature. The definition used in this work is for the modeling of an active sonar as recommended by Dawe [39], but found in the Sonar Modelling Handbook as follows:

The detection threshold is defined as the ratio, in decibel units, of the signal power (or mean-squared voltage) in the receiver frequency bandwidth to the noise power (or mean-squared voltage) in the receiver frequency bandwidth, measured at the receiver input terminals, required for detection at some preassigned level of correctness of the detection decision...In this definition DT has units of dB re 1 μPa .

In the above definition, the signal power S and the noise power N are both in relation to the receiver frequency bandwidth. The Detection Threshold is then $DT = 10 \log(S/N)$. The detection index, d , has also been shown to be a function of the signal-to-noise ratio, S/N . Under certain assumptions such as Gaussian background noise distributions and

large sample sizes, the detection index can be given by $d = wt(S/N)^2$, where w is the receiver frequency bandwidth and t is the integration time of the signal (t is also the signal pulse length for an active sonar). The concept of the Detection Threshold is then clearly a statistical quantity based on the expected noise distributions and after substitution can be defined as: $DT = 10 \log(d/wt)^{1/2}$. Additionally, the integration time t can also be expressed as $t = T \cdot NP$, where NP is the minimum number of pings required for the detection algorithm to make a detection decision and T is the time between pings (*i.e.*, the period).

The resulting Detection Threshold function for the special case of Gaussian background noise and a single active pulse (or ping) is provided in Equation 39. In practical operations, the assumption of Gaussian background noise for the active sonar is not appropriate and at least two detected pings are required to accept a detection as valid. It is beyond the scope of this text to get into signal processing concepts such as frequency modulation versus continuous wave, fast fourier transforms, replica correlations, coherent or incoherent operations and the like. However, techniques are routinely used to uncorrelate ambient noise and reverberations from the transmitted pulse, and in these situations the replica correlated noise power can be described as an exponential distribution which does not become Gaussian because the statistical summations are carried out coherently. Subsequently, the wt term in Equation 39 becomes $(wt)^2$ [39]. In addition, an increased number of pings improves the detectability of the signal by decreasing the variability of the noise relative to the mean resulting in an effect of: $-5 \log(NP)$. The resultant active sonar Detection Threshold with multiple pings and exponential noise distribution is given in Equation 40. Active sonars can usually be modeled with $wt = 1$ and a requirement of 2 successive pings for target detection, $NP = 2$, which is given in Equation 41. Also, the bandwidth w , also known as the effective noise bandwidth or the equivalent noise bandwidth (ENBW) often takes on values from $w = 1Hz$ to $w = 10Hz$, but with most applications having $w < 5Hz$, as compiled by Harris [68]. Therefore, reasonable pulse lengths can range from $t = 1s$ to $t = 0.2s$.

$$DT = 5 \log(d/wt) = 5 \log(d/wT) - 5 \log(NP) \quad (39)$$

$$DT = 5 \log(d) - 10 \log(wt) - 5 \log(NP) \quad (40)$$

$$DT = 5 \log(d) - 5 \log(2) = 5 \log(d/2) \quad (41)$$

Next, the detection index, d , can be defined mathematically as given in Equation 42, where σ is the standard deviation of the noise power distribution and μ is the mean of the *signal+noise* and the *noise* distributions, μ_{S+N} and μ_N , respectively. Therefore, “values of d can be determined for specific probability density functions (pdfs) for a given probability of detection (P_D) and a given probability of false alarm (P_{FA})” [39].

$$d = \frac{(\mu_{S+N} - \mu_N)}{\sigma_N^2} \quad (42)$$

Since d is based on both the probability of detection and the probability of false alarm, DT only has significance when it is accompanied by the P_D and P_{FA} values which are relevant for the associated detection index, d . P_D is the probability that a signal will be detected if it is present, whereas P_{FA} is the probability that a noise signal will spike enough to cross the threshold of detection. The P_D and P_{FA} values do not sum to one in most situations, and are rarely meant to sum to one. The P_D is relevant if a signal is present that can be detected, and $1 - P_D$ is the probability that the signal will not be detected even though it is present. On the other hand, P_{FA} is relevant when a signal *is not* present, and then $1 - P_{FA}$ is the probability that a signal will not be detected when it is absent. A common value of P_D often used when modeling DT in order to perform analyses with the sonar equation is $P_D = 0.5$, although a value of $P_D = 0.9$ is sometimes used. Appropriate values of the probability of false alarm are often $P_{FA} = 10^{-3}$ or 10^{-4} . A baseline combination of $P_D = 0.5$ and $P_{FA} = 10^{-4}$ is quoted as appropriate, so those are the values that will be used as baselines for DT comparisons in this work.

Receiver-operating-characteristic (ROC) curves provide a relationship between P_D and P_{FA} with d as a parameter. These curves depend on the pdf of the noise distribution, which for this work is assumed to be exponential. The detection index, d , then falls out as a required parameter based on the desired P_D and P_{FA} . An example set of ROC curves under the assumptions of Rician *signal plus noise* distributions and exponential noise is

given in Figure 56. The chart shows the intersection of $P_D = 0.5$ and $P_{FA} = 10^{-4}$ results in $10 \log(d) \approx 18.5dB$. Then the Detection Threshold calculated from Equation 41 is: $DT = (10/2) \log(d) - 5 \log(2) = (18.5/2)dB - (1.5)dB = 7.75dB$. Similarly, for a combination of $P_D = 0.9$ and $P_{FA} = 10^{-4}$, the Detection Threshold would be $DT = 10dB$. The experiments to-be-performed in subsequent sections use DT values of $7dB$, which corresponds to $10 \log(d) = 17$, resulting in values such as $P_D = 0.5$ and $P_{FA} = 5 \times 10^{-4}$ or $P_D = 0.8$ and $P_{FA} = 10^{-2}$.

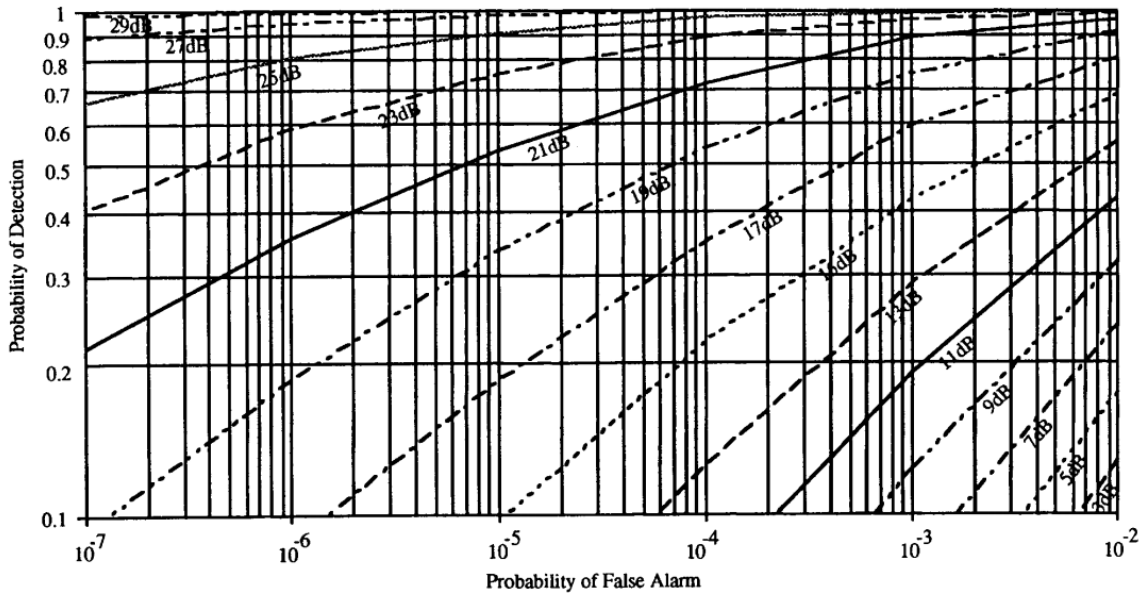


Figure 56: Active Sonar ROC Curves with Rician *Signal + Noise* pdf Statistics and Exponential *Noise* pdf Statistics [39]. (dB values on the curves are $10 \log(d)$)

Much more significant signal processing theory goes into deriving all applicable aspects of the Detection Threshold and its relevant parameters, but that was not the purpose of this section. Rather, the development above was meant to provide a sufficient amount of detail for identifying parameters that are relevant to creating a parametric sensor representation. The detection index, d , is relevant as was shown with appropriate probabilities of detection and false alarm. However, other properties such as the receiver bandwidth and integration time were appropriately defaulted to values common in sonar operation. The results from this section will be critical for running the agent-based virtual experimentation environment

(to be developed in later sections).

Noise Level There are various sources of ambient noise in the ocean environment. Historical testing and data has shown that the levels of specific noise sources are highly dependent on frequency range. This work is considering sonar operations above 400 kHz which is minimally affected by most noise sources. Shipping density, industrial activities and wind speed are the main sources of noise in the spectrum of $10\text{--}100\text{ Hz}$, and can have an affect over long ranges. Shipping and sea surface agitation dominate the frequency range of $100\text{--}1000\text{ Hz}$. The wind speed and sea state of the ocean environment have a major impact at frequencies of $1\text{--}100\text{ kHz}$, as well as some marine mammal factors. During World War 2, the acoustician V.O. Knudsen collected data on sea state noise which is often plotted as *Knudsen curves*. Above 100 kHz , which is the range of concern for this work, ambient noise is dominated by electronic thermal noise. Thermal noise is the result of molecular processes, and the NL function for this range of frequencies is given in Equation 43, adapted from Urick [154]. Figure 57 shows the thermal noise function within the relevant spectrum of frequencies greater than 100 kHz . Knudsen curves for the sea state effects are also shown. Self noise sources such as propeller noise, cavitation, flow noise, and machinery noise do not have an effect at the frequencies considered for this work.

$$NL = 20 \log(f) - 75 \quad (43)$$

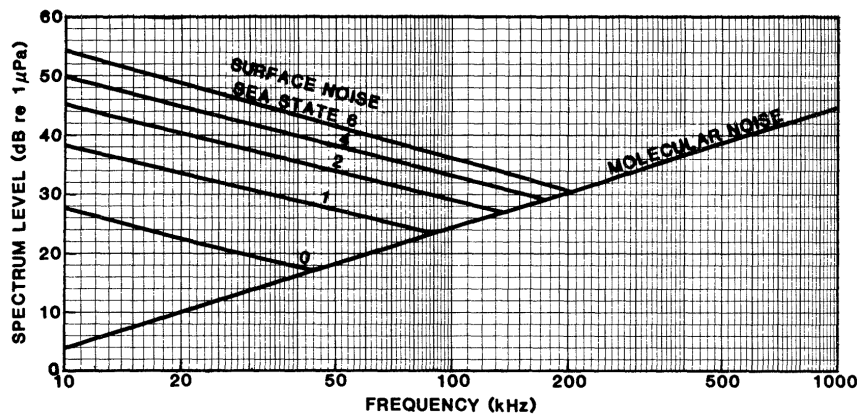


Figure 57: Thermal (Molecular) Noise and Knudsen Curves Adapted from Urick [154].

Target Strength For simple geometric shapes, the Target Strength of the object can be solved for analytically. The Target Strength, TS , is the power level of the acoustic reflection from the object of interest. For simple approximations, it is important that the radius of the target is much greater than the wavelength of the acoustic sound being used to reflect a signal off of the target, which is the case for this work. Therefore, the Target Strength will be modeled as given in Equation 44, where a is the expected radius of a class of objects of interest. In particular, the Italian made Manta mine will be used as a reference target for this work. The Manta mine is a shallow water bottom mine whose “shape, low target strength and low magnetic signature make the mine very difficult to detect, even with side scan sonars” [55]. The shape of the Manta mine makes it an appropriate reference target for using Equation 44 with a diameter of approximately 1 meter. Computer generated images of the Manta mine are shown in Figure 58.

$$TS = 10 \log \left(\frac{a^2}{4} \right) \quad (44)$$

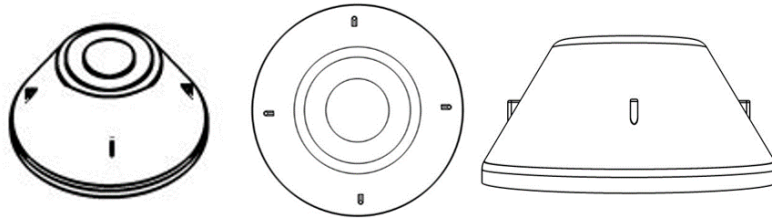


Figure 58: Three Computer Generated Views of the Manta Mine.

The Expanded Sonar Equation and Figure of Merit The sonar equation in the form of the Figure of Merit (FOM) is now expanded as shown in Equations 45 and 46. These equations are functions of the parameters developed in the previous sections. The FOM of the sonar conveys the transmission capability of the system in decibels. In contrast, the Transmission Loss (TL) expresses the loss in signal as it travels a particular distance based on the properties of the environment. Therefore, to detect a target at a particular range, the FOM of the sonar must be greater than or equal to the expected TL at that range (see Equation 47). The TL function will be developed in the next section along with the

solutions for maximum sensor range based on FOM equivalence with the TL .

$$\begin{aligned}
FOM_{Circ} &= SL_{Circ} - DT + TS - (NL - DI) \\
&= SL_{Circ} + DI - DT + TS - (NL) \\
&= 109\text{dB} + 10 \log \eta_{ac} P_E + 10 \log \rho c + \\
&\quad 2(20 \log(\pi D_{req}/\lambda)) - 5 \log(d/2) + 10 \log\left(\frac{a^2}{4}\right) - (20 \log(f) - 75) \\
&= 109\text{dB} + 10 \log \eta_{ac} P_E + 10 \log \rho c + \\
&\quad 40 \log\left(\frac{0.51\pi}{\sin(\theta_{BW_{req}}/2)}\right) - 5 \log(d/2) + 10 \log\left(\frac{a^2}{4}\right) - (20 \log(f) - 75)
\end{aligned} \tag{45}$$

$$\begin{aligned}
FOM_{Linear} &= SL_{Linear} - DT + TS - (NL - DI) \\
&= SL_{Linear} + DI - DT + TS - (NL) \\
&= 109\text{dB} + 10 \log \eta_{ac} P_E + 10 \log \rho c + \\
&\quad 2(10 \log(2L_{req}/\lambda)) - 5 \log(d/2) + 10 \log\left(\frac{a^2}{4}\right) - (20 \log(f) - 75) \\
&= 109\text{dB} + 10 \log \eta_{ac} P_E + 10 \log \rho c + \\
&\quad 20 \log\left(\frac{0.884}{\sin(\theta_{BW_{req}}/2)}\right) - 5 \log(d/2) + 10 \log\left(\frac{a^2}{4}\right) - (20 \log(f) - 75)
\end{aligned} \tag{46}$$

$$\begin{aligned}
FOM &\geq TL_{total} \equiv f(r) \\
&\dots\text{required in order to detect a target at a specific range, } r
\end{aligned} \tag{47}$$

Transmission Loss The Transmission Loss (TL) is the final parameter needed in this work for assessing the sonar equation. For an active sonar system, the Transmission Loss is quantified as a two-way TL parameter which is compared to the FOM , as shown in Equation 47.

Transmission Loss is a function of range, modeled in this work as the result of spreading losses and attenuation due to water viscosity and molecular effects. The spreading loss can be modeled as a loss of intensity due to spreading of the sound wave either spherically or cylindrically over the range of interest. Cylindrical spreading is a useful approximation because the sound cannot spread spherically in the ocean forever; it will eventually encounter the sea surface and/or sea floor. The $TL_{spreading}$ function in general is defined logarithmically as the difference of intensity from the source reference range (1 meter) to the sonar range, r . The intensities can be equated as the power of the source, P , over the area which the sound has been spread. Also, the power of the signal is equivalent at any range. The

general expression is then:

$$TL_{spreading} = 10 \log \left(\frac{I_{1m}}{I_r} \right) = 10 \log \left(\frac{P/A_{1m}}{P/A_r} \right) = 10 \log \left(\frac{A_r}{A_{1m}} \right) \quad (48)$$

For spherical spreading, the area is defined as: $A_r = 4\pi r^2$. Alternatively, the area for cylindrical spreading is defined as: $A_r = 2\pi r h$, where h is the height of a cylinder equivalent to the water depth. Note that the entire area of a cylinder was not included in the cylindrical calculation because the sound is not distributed over the area of the top and bottom of the cylinder (the sea surface and sea floor). The specific spreading laws are calculated as follows:

$$TL_{spherical} = 10 \log \left(\frac{4\pi r^2}{4\pi(1)^2} \right) = 20 \log r \quad (49)$$

$$TL_{cylindrical} = 10 \log \left(\frac{2\pi r h}{2\pi(1)h} \right) = 10 \log r \quad (50)$$

Both the spherical and cylindrical spreading laws are simple approximations often used in modeling underwater sound propagation. A practical model to be used in this work is an average of each of the models and is given in Equation 51.

$$TL_{spreading} = 15 \log r \quad (51)$$

Attenuation of the signal is a complex function of the properties of the underwater environment. Ainslie [3] provides adequately accurate empirical relations for the attenuation of sound in sea water as is given in Equation 52, where a_{visc} is due to viscosity and a_{chem} is due to the chemical relaxation effects of boric acid and magnesium sulfate.

$$\begin{aligned} a_{water} &= a_{visc} + a_{chem} && (dB/km) \\ &= A_{visc} f^2 + A_B \frac{f^2 f_B}{f^2 + f_B^2} + A_{Mg} \frac{f^2 f_{Mg}}{f^2 + f_{Mg}^2} && (dB/km) \end{aligned} \quad (52)$$

The term f in Equation 52 is the operating frequency of the sonar, whereas f_B and f_{Mg} are the relaxation frequencies of boric acid and magnesium sulfate, respectively. Expressions for each of the relaxation frequencies are given in Equations 53 and 54. The coefficients for Equation 52 are given in Equations 55–57, where T , z , S and pH are the local temperature, depth, salinity, and acidity. This full attenuation function given by Ainslie is appropriate

within the parameter ranges given in Equation 58.

$$f_B = (0.78)e^{T/26} \sqrt{\frac{S}{35}} \quad kHz \quad (53)$$

$$f_{Mg} = (42)e^{T/17} \quad kHz \quad (54)$$

$$A_{visc} = 4.9 \times 10^{-4} \exp \left[- \left(\frac{T}{27} + \frac{z}{17,000} \right) \right] \quad dB / (km \cdot kHz^2) \quad (55)$$

$$A_B = 1.06 \times 10^{-4} \times 10^{0.776(pH-8)} \times 10^3 \quad dB / (km \cdot kHz) \quad (56)$$

$$A_{Mg} = 5.2 \times 10^{-4} \left(1 + \frac{T}{43} \right) \left(\frac{S}{35} \right) e^{-z/6,000} \times 10^3 \quad dB / (km \cdot kHz) \quad (57)$$

$$\left. \begin{array}{l} 200 < f < 10^6 \quad (Hz) \\ 7.7 < pH < 8.3 \quad (-) \\ 8 < S < 40 \quad (g/kg) \\ -2 < T < 30 \quad (^\circ C) \\ 0 < z < 3000 \quad (meters) \end{array} \right\} \quad (58)$$

Finally, the total one-way Transmission Loss due to spreading and attenuation is given in Equation 59 where the range, r , is in meters. Then the active sonar total two-way Transmission Loss given in Equation 60 is found by doubling the one-way loss, not by doubling the range r . Figure 59(a) graphically displays the attenuation behavior of Equations 52-57 as a function of sonar operating frequency. The total attenuation is shown as the a_{water} trend line which depends on the individual attenuation functions for viscosity and chemical relaxation depending on the frequency range. Figure 59(b) expands on the attenuation function by including operating range as a dimension which results in the total TL from Equation 60. The main takeaway from Figure 59 is that there is a clear trade-off between operating frequency and sonar range due to the Transmission Loss incurred. High operating frequencies are desired for better resolution in detecting a target, but this comes at a cost of the range capability.

$$TL_{one-way} = TL_{spreading} + TL_{attenuation} \quad dB \quad (59)$$

$$= 15 \log r + r \cdot a_{water} \left(\frac{dB}{km} \frac{km}{1000m} \right) \quad dB$$

$$TL_{total} = 2TL_{one-way} \quad dB \quad (60)$$

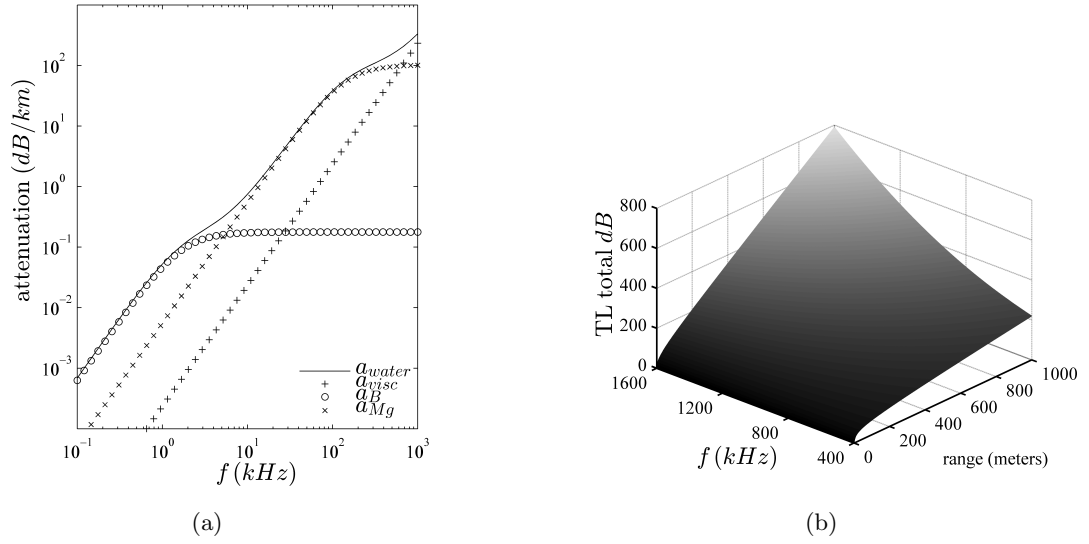


Figure 59: Attenuation and Total Transmission Loss as functions of operating frequency and range over which the signal spreads. The environmental properties are: $\{z = 10m, T = 20^\circ C, S = 34.7g/kg, pH = 8\}$.

The experimental designs initially established were displayed in Figure 54, with 36 FLS sonar designs and 54 SSS designs. The physical dimensions of the sensors and the Source Levels were subsequently calculated and presented in Figure 55. Now, with the FOM and TL_{total} relationships developed, the maximum range capability for each sensor design can be determined. This is accomplished by equating the FOM to the total Transmission Loss, TL_{total} , and solving for r_{max} as is shown in Equation 61. Solutions for Equation 61 require an iterative numerical analysis, such as the Newton-Raphson method.

$$FOM \geq TL_{total} \equiv f(r) \tag{61}$$

$$FOM - 2(15 \log r_{max} + r_{max} a_{water}) = 0$$

With the FOM and Transmission Loss firmly established, each sensor design is now characterized by its theoretical capabilities within a specific environment. Experimental designs were specified earlier for the power, frequency and beam width settings which resulted in 36 forward looking sonar (FLS) and 54 side scan sonar (SSS) designs. Additional

variable ranges and settings must also be considered based on each sonar equation parameter that was reviewed. Accordingly, the variable ranges and parameter settings used for the experimental setup of each sensor along with environmental assumptions are given in Table 4. Note that the last variable presented in Table 4 is the sensor velocity. This variable will be utilized in the next section when the virtual experimentation environment is initiated.

Table 4: Constants and Variable Ranges for the Parametric Sonar Experimental Setup

| Parameter | Range or Value | Units | Notes |
|------------------------------|--------------------------|---------------------|--|
| $\{z, T, S, pH\}$ | $\{10, 20, 34.7, 8\}$ | $\{m, C, g/kg, -\}$ | Estimates near the surface of sea water [3]. |
| p | 202.78 | kPa | $p = f(z)$, pressure of sea water as derived by Leroy, restated in [3]. |
| ρ | 1024.86 | kg/m^3 | $\rho = f(S, T, p)$, density of sea water as given in [3]. |
| c | 1521.29 | m/s | $c = f(z, S, T, p)$, speed of sound in sea water as given in [3]. |
| θ_{BW} | $(0, \pi/2)$ | <i>radians</i> | Values are discrete within specified range. |
| DI_{Circ} DI_{Linear} | (9, 61) (3, 28) | dB | Values are discrete within specified range due to behavior of Equations 28 and 32. |
| SL | (170, 280) | dB | Expected range from empirical data. |
| η_{ac} | (20, 70) | % | Expected range from empirical data, and a value of 0.5 is used for the set of experiments in this section. |
| P_E | $(0.1, 100 \times 10^3)$ | Watts | Expected range from empirical data. |
| a | 1/2 | <i>meters</i> | Manta mine radius as a reference [55]. |
| DT | (6, 10) | dB | Detection Threshold value held constant at 7 dB for experiments in this section. |
| V_∞ | (2, 5, 8) | m/s | Vehicle velocities chosen as discrete low, medium and high speeds. |

Based on the parameterization given in Table 4, the FOM and maximum range for each sensor can be calculated, resulting in Figures 60 and 61. The results display the required sensor dimensions and the maximum range capabilities as functions of power, frequency, and discrete beam width. In total, the results include 90 designed FLS and SSS array experiments. It can be seen that increased power is positively correlated with sensor range in general. However, it is clear that the main driver in performance capability according

to the sonar equation is frequency, which is negatively correlated with sensor range. It can also be seen that better range by performance through low frequency and high power also means an increase in aperture size. Therefore, physical constraints would potentially be a consideration.

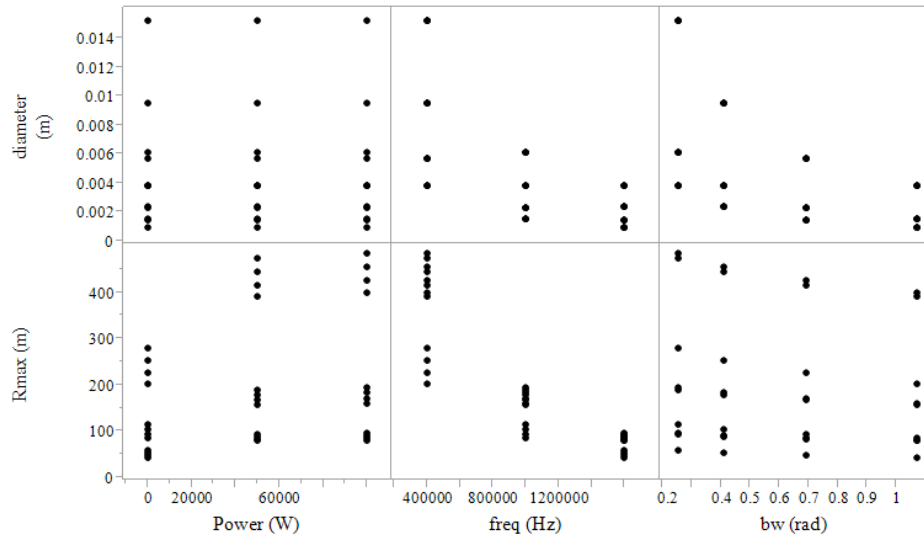


Figure 60: FLS Deterministic Results

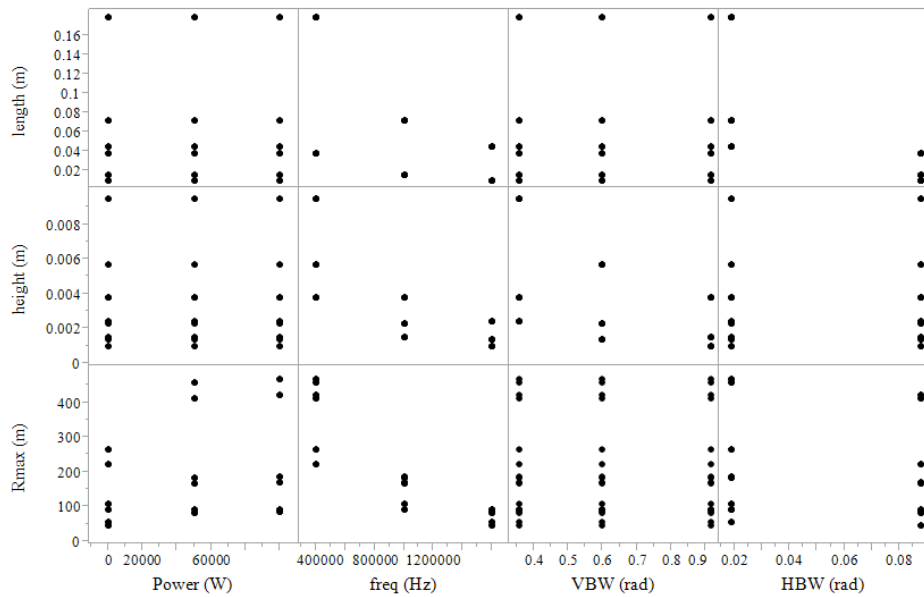


Figure 61: SSS Deterministic Results

Up to this point, results based on the sonar equation are completely deterministic. The next section will describe the setup of the virtual experimentation environment through

which each sensor design is tested. The results of those experiments provide functional relationships between the vehicle design, the sensor attributes, and the operational concepts through the generation of lateral range curves and effective sweep widths. After the results are generated, comparisons will be shown between the performance capabilities of the sensors based on the virtual experiments versus the sonar equation analysis alone.

6.3 Virtual Experimentation Environment and Geometric Orientations

The virtual experiments for each sensor can now be setup according to the virtual experimentation method expressed in Figure 47, which has been regenerated in Figure 62 below. Up to this point, the sonar equation range analysis has been performed for each selected sensor design, resulting in Figures 60 and 61. Therefore, the next step is to run Monte Carlo experiments through the ALWSE-MC experimentation environment, which is an agent-based simulation environment. As was mentioned earlier, the acoustic model present in the simulation environment is based largely on the sophisticated High-Frequency Ocean Environmental Acoustic Model [80]. It takes in sensor model parameters and emulates their propagations through the underwater environment.

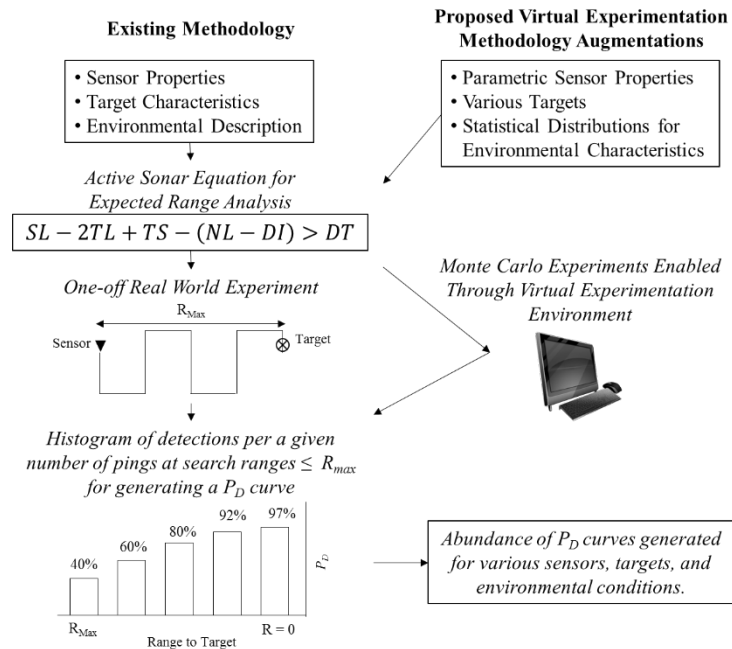


Figure 62: Existing P_D Generation Process Alongside Virtual Experimentation Augmentations

After running each sensor through the ALWSE-MC simulation environment, probability of detection (P_D) curves (*i.e.*, lateral range curves) are generated. The lateral range curves generated for each sensor design are then used for defining sweep widths for search operations and higher level calculations of mission effectiveness. In order to execute the virtual experiments for each sensor design, the environment has been setup to emulate the operations shown in Figure 63.

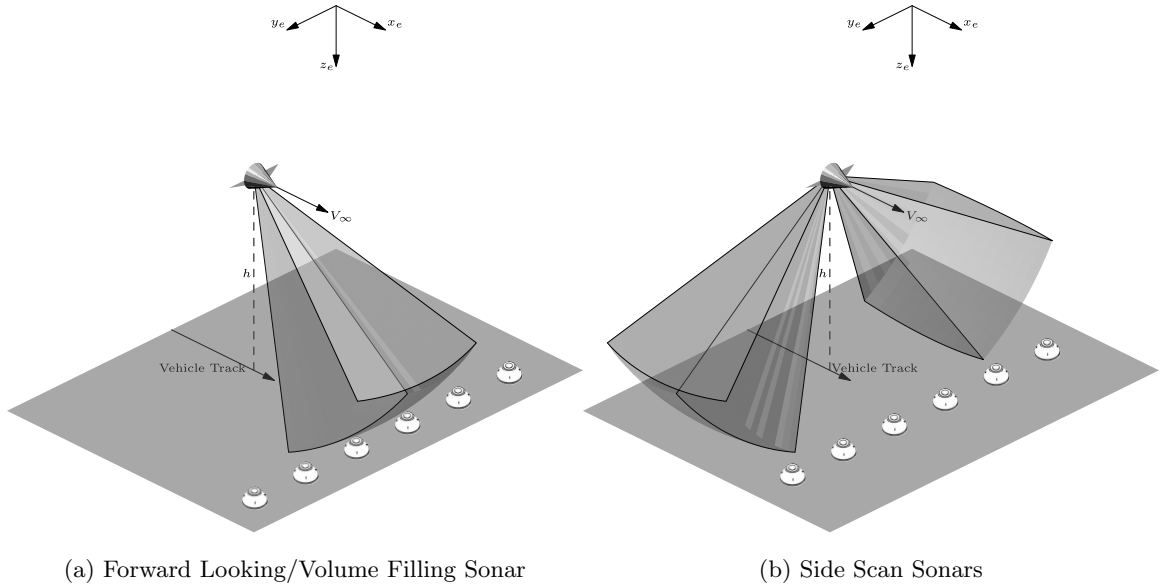


Figure 63: Lateral Range Curve Experimental Setup

$$V_\infty = \{2, 5, 8\} \quad m/s \quad (62)$$

Each sensor is simulated at three velocities as given in Equation 62. Figure 63 displays the circular piston forward looking sonar in part (a) and the linear array side scan sonar (SSS) in (b). In order to execute the virtual experiments, each sensor design is defined in the ALWSE-MC environment. The sensors are placed on point mass vehicles that are not currently affected by the environment in terms of vehicle performance; instead, only the sensors are affected by the environment. Sensor orientation is important for defining the sensor beam widths and grazing angles. The mathematical details for specifying and calculating orientations is given in Appendix C. Each sensor is operated along a vehicle track that intersects a line of Manta mine targets, and this is repeated in a Monte Carlo

fashion 25 times. The number of detections for a specific target at a specific range over the full set of 25 repetitions becomes the probability of detection at that range. The altitude (or depth) of each sensor is calculated as a function of maximum sensor range to ensure that the beam can intersect the sea floor with a grazing angle of $\pi/4$.

The results of the virtual experiments described above provide probability of detection curves for each of the 90 sensor designs at three discrete velocities, resulting in 270 lateral range curves. Three of the lateral range curves for one FLS design executed at three velocities is shown in Figure 64. The ESW values above each plot is calculated by integrating the area under each probability of detection curve. The total number of virtual experiments executed to produce all 270 curves was: $90 \text{ designs} \times 3 \text{ velocities/design} \times 15 \text{ targets/design/velocity} \times 25 \text{ Monte Carlo runs/target} = 101,250 \text{ experiments}$. The total computational run-time for these experiments took more than a month.

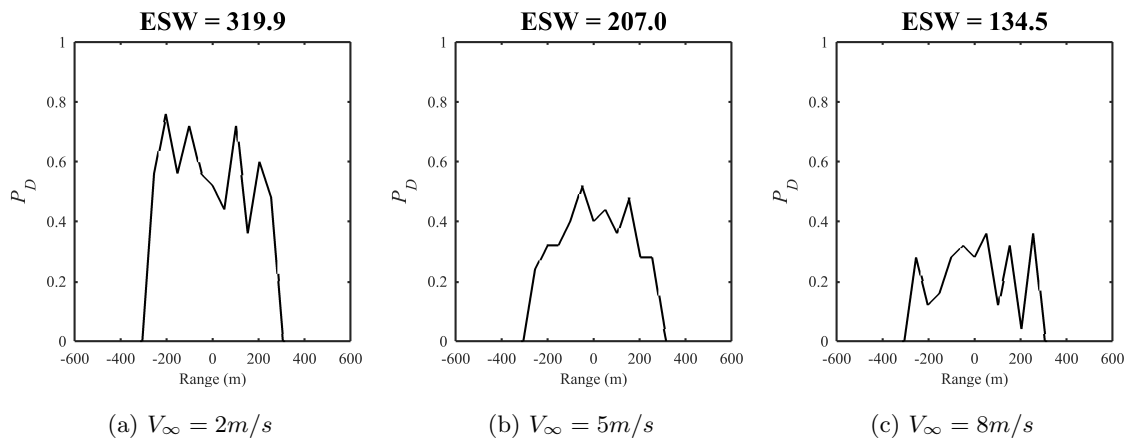


Figure 64: One set of FLS lateral range curve experimental results at discrete velocities

More examples for both types of sonar are shown in Figures 65 and 66. The full set of 270 curves are provided in Appendix D. The curves are also called lateral range curves because they define the probability of detecting a target laterally from the direction of vehicle motion. By calculating the area under each curve, the Effective Sweep Width (ESW) is determined. The ESW is a useful metric which can be used to define lane widths for the search missions. Interestingly, the ESW can be interpreted as providing a lane width where the number of objects not detected within the sweep lane is probabilistically equivalent

to the number of objects that are detected outside of the sweep lane [88]. Note that the ESW ranges both sides of the vehicle, so it is equivalent to a sensor diameter around the vehicle. On the other hand, the sensor range is one sided. In other words, the sensor range is equivalent to a radius around the vehicle.

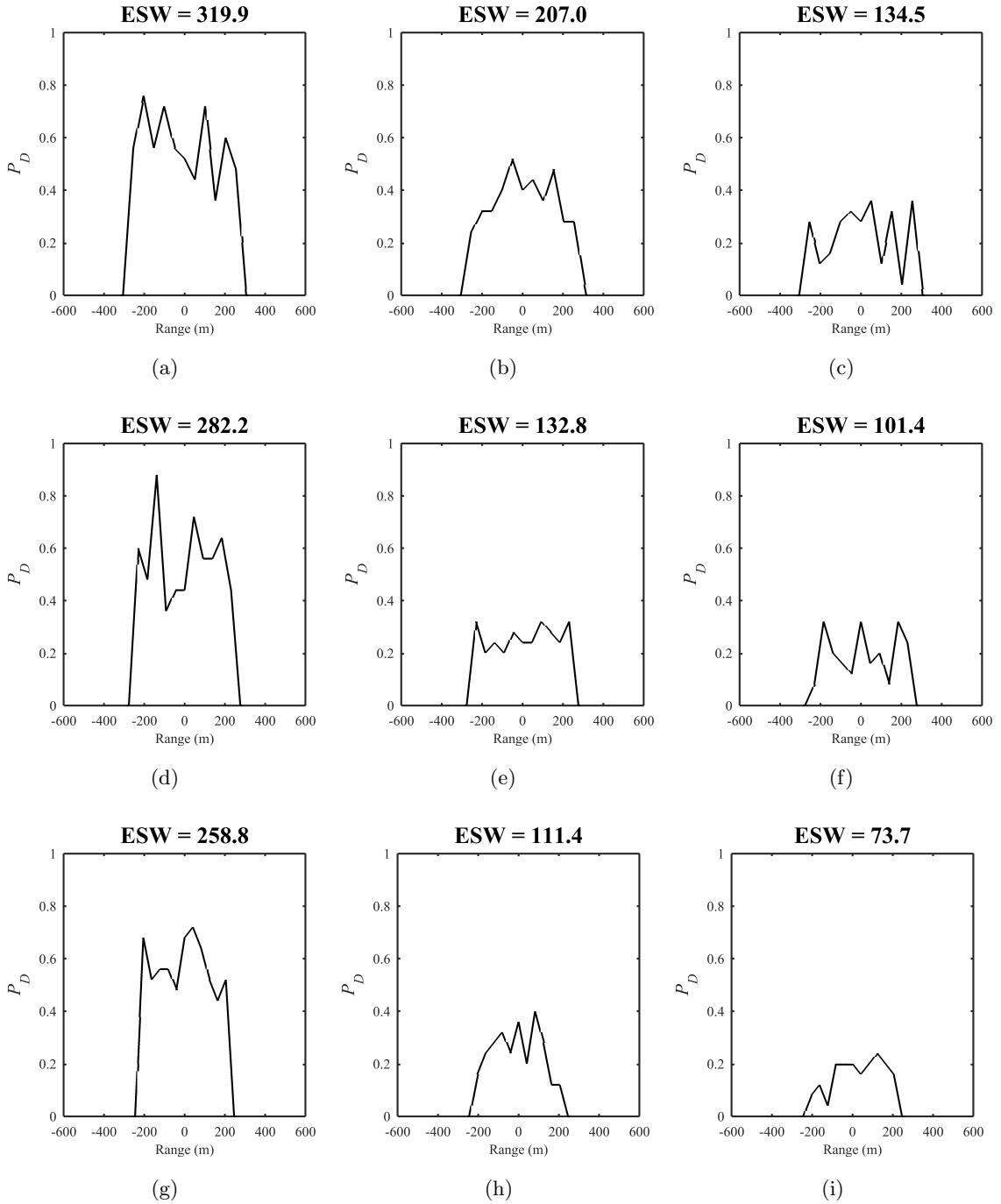


Figure 65: Subset of FLS Lateral Range Curves

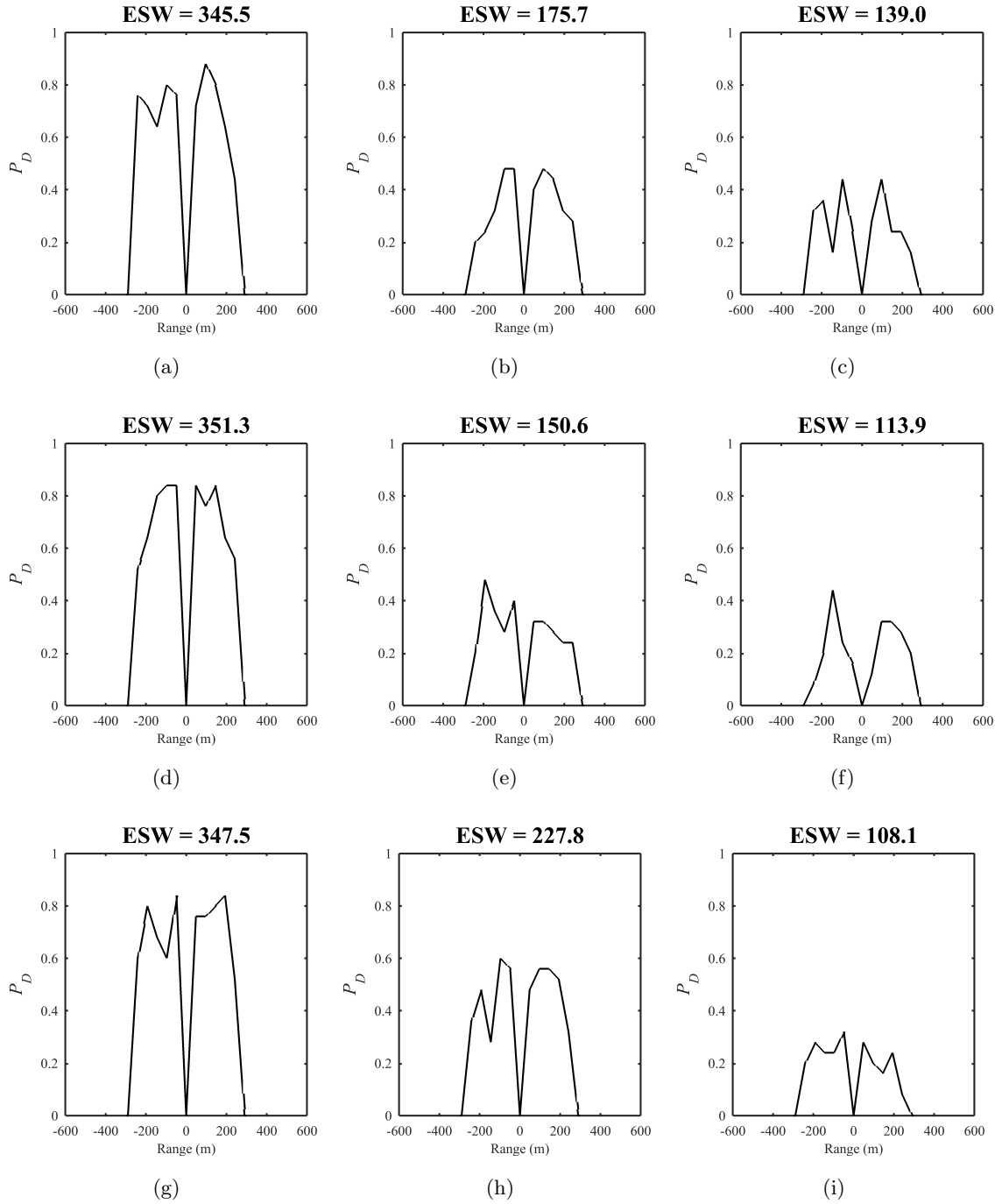


Figure 66: Subset of SSS Lateral Range Curves

6.4 Experimental Approach and Results

The experimental setup for the subsystem level analyses originally presented in Chapter 4 is shown again in Figure 67. For Experiment Set A, data is acquired to compare the

three different approaches presented through three different analyses. Through a design of experiments and a set of physical constraints, 90 sonar designs were selected earlier in this chapter to be tested through each analysis path. In context of the *Sensor Performance* path, the 90 sensor designs are analyzed deterministically through the sonar equation (SE) which provides characteristics such as the theoretical maximum sensor range. Along the *Operations Analysis* (OA) path, sensor designs are explored probabilistically in a way which is common in OA. In particular, the sensors are defined as generic probability distributions which will detect a target within some probability as a function of range away from the sensor. Finally, through the third subsystem level path, sensor designs are explored through the new virtual experimentation (VXE) approach developed in this work, which is one of the major contributions of this dissertation. The next two sections will provide data visualization and analysis for Experiments 1 and 2.

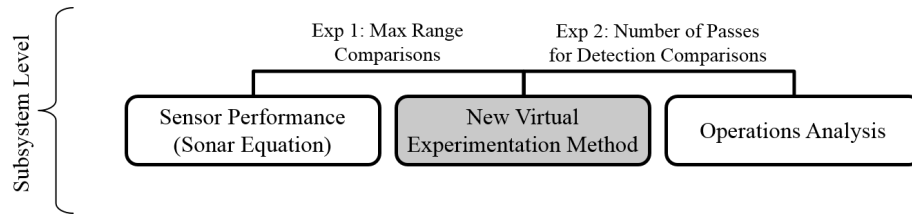


Figure 67: Subsystem Level Experimental Setup

6.4.1 Experiment 1: Maximum Range Comparisons

Figures 68 and 69 display the ESW results from the virtual experiments, along with the R_{max} calculations from the sonar equation. *Recall that the R_{max} values here are NOT from the virtual experiments. They are from the deterministic sonar equation calculations.* Therefore, it can be seen in the V_{∞} column that the ESW values are affected by velocity, whereas R_{max} is not. This shows the dependence of sensor performance on the kinematics of the sensor, not just the theoretical maximum ranges based on the sonar equation.

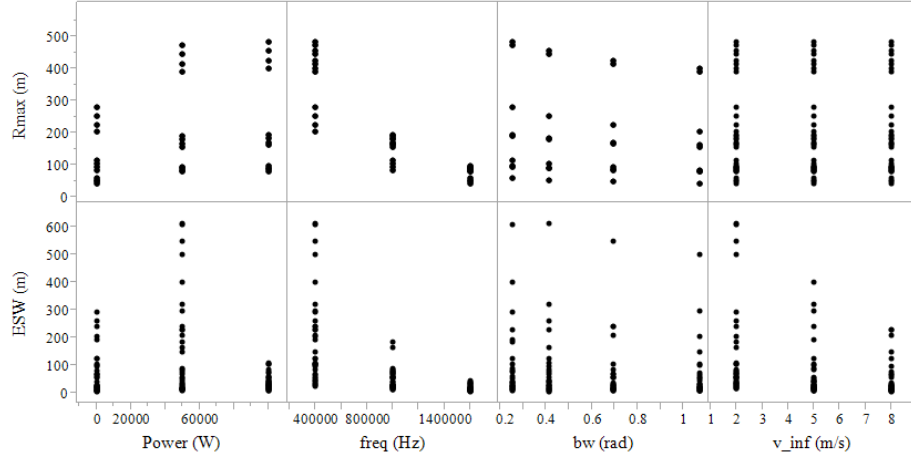


Figure 68: FLS R_{max} from the sonar equation and ESW experimental results

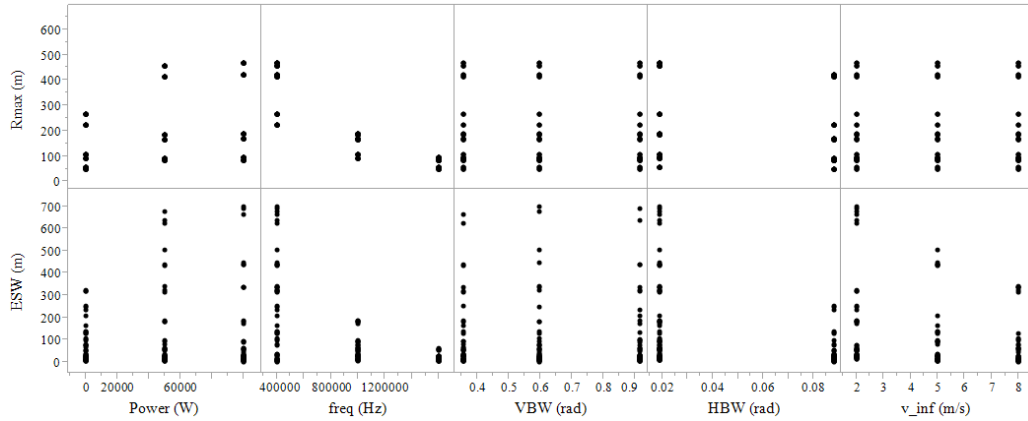


Figure 69: SSS R_{max} from the sonar equation and ESW experimental results

The development of Hypothesis 3 was born out of the observation that without experimental operational data, the sonar equation over-predicts the sensor range for sensors in motion. Therefore, there was no functional link between the sensor energy-based performance (the sonar equation) and the sensor energy-based motion (vehicle velocity). The hypothesis postulated that a relationship could be formed, and this chapter formed that link through a virtual experimentation environment. This was shown to be true through the previous results given above. Below, additional results are shown to further support the hypothesis.

As was outlined earlier, 90 sensor designs were executed through the virtual experimentation environment at 3 different velocities. This resulted in 270 designed experiments that

were executed. Figure 70 below directly compares the maximum range estimated in Experiment 1 through both the sonar equation approach and the VXE approach. The linear trend-line in each plot is simply a perfect fit line. If a data point is on the line, then the sonar equation predicted the experimental maximum range. If a point is below the line, then the sonar equation over predicted. Points over the line had better range than the sonar range predicted. For the FLS, 69 out of 108 experiments were *over predicted* ($\approx 64\%$) and 3 designs were accurately predicted ($\approx .03\%$). For the SSS, 147 out of 162 design ranges were over predicted by the sonar equation ($\approx 91\%$) and 6 were perfectly predicted ($\approx 0.04\%$).

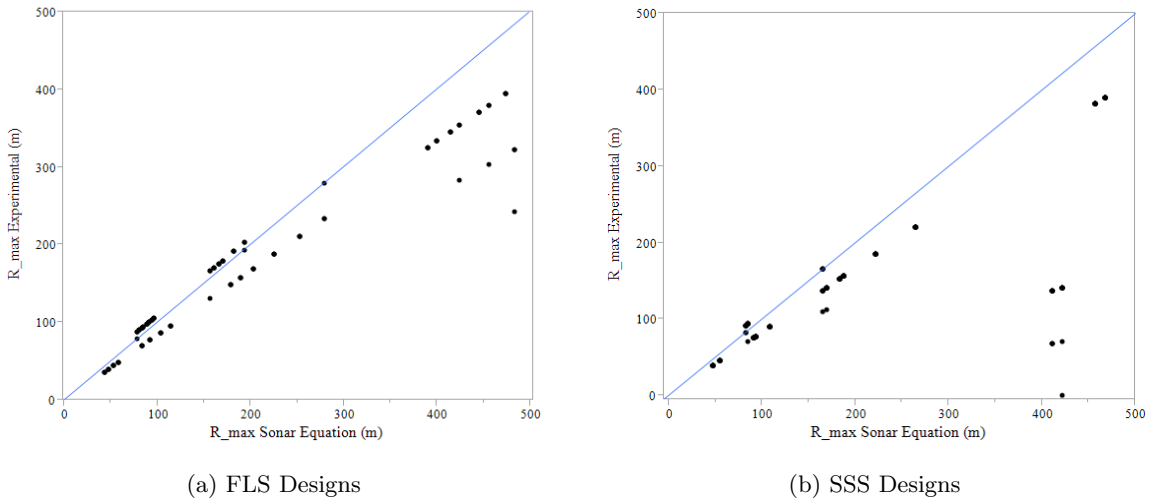


Figure 70: Sonar Equation predicted maximum range versus VXE Maximum Range

Note that the experimental range results shown are *not* equivalent to half the sensor experimental effective sweep width. The experimental range shown in Figure 70 is the maximum range at which the sensor detected anything, even if the target at that range was detected once out of the 25 Monte Carlo runs. Also, it is important to understand that the experimental range results occurred both due to the stochastic nature of the environmental variables in the simulation environment *and* the motion of the vehicles.

The hypothesis is further substantiated by this data, since there is statistical significance showing the effect of sensor movement on the performance. Without the sensor experimentation method developed here, these results would not have been observable. Additionally, vehicle trade-offs will be better established after knowing the effect that vehicle operations

will have on the ability to detect targets.

Although it was shown that in the majority of cases the sonar equation over predicted the sensor performance, there were a few cases that were actually under predicted. These cases should be investigated to see what caused this. Figures 71 and 72 provide scatter plots of the sensor design parameters (power, frequency, and beam width), the operational parameter (velocity) and the outputs (the sonar equation calculated range and the virtual experimentation effective sweep width). In these charts, the data points labeled with dark black squares are the experimental runs which were under predicted by the sonar equation. The faded dots are all other designs. By investigating each input against every other input, it can be determined if there are certain combinations of inputs that caused the under prediction. For example, in each chart, every operational velocity input has a black square associated with it. Consequently, velocity did not drive the under prediction. In the FLS chart (Figure 71), it becomes obvious that combinations of the middle and upper power inputs along with the middle and upper frequency inputs caused the under prediction. Furthermore, all experiments with upper power and upper frequency inputs for the FLS were under predicted by the sonar equation. These observations are highlighted by the circle in the chart. The SSS followed a similar trend as can be seen in Figure 72. However, the SSS has an additional input driving the under prediction of performance: the horizontal beam width (HBW) of the sensor.

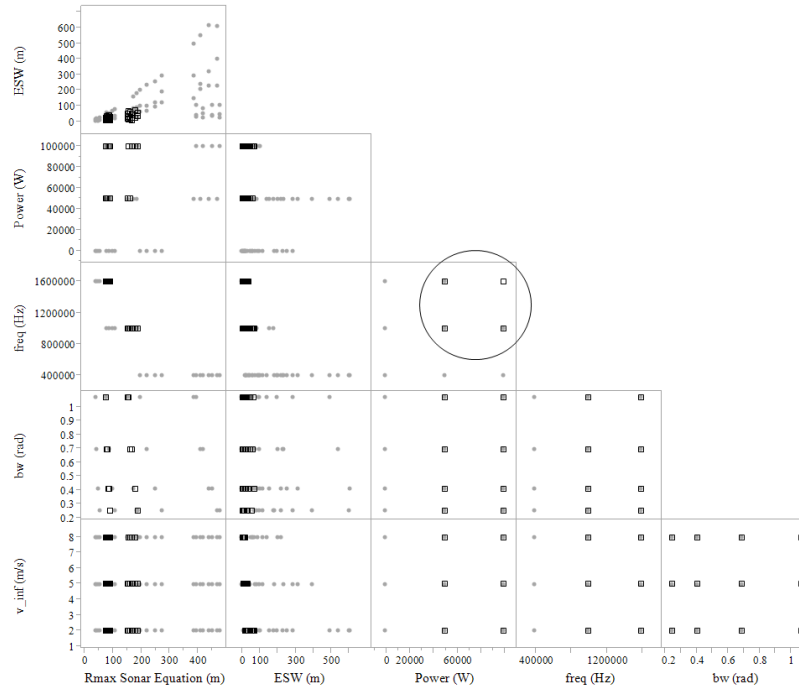


Figure 71: FLS predicted maximum range versus actual maximum range

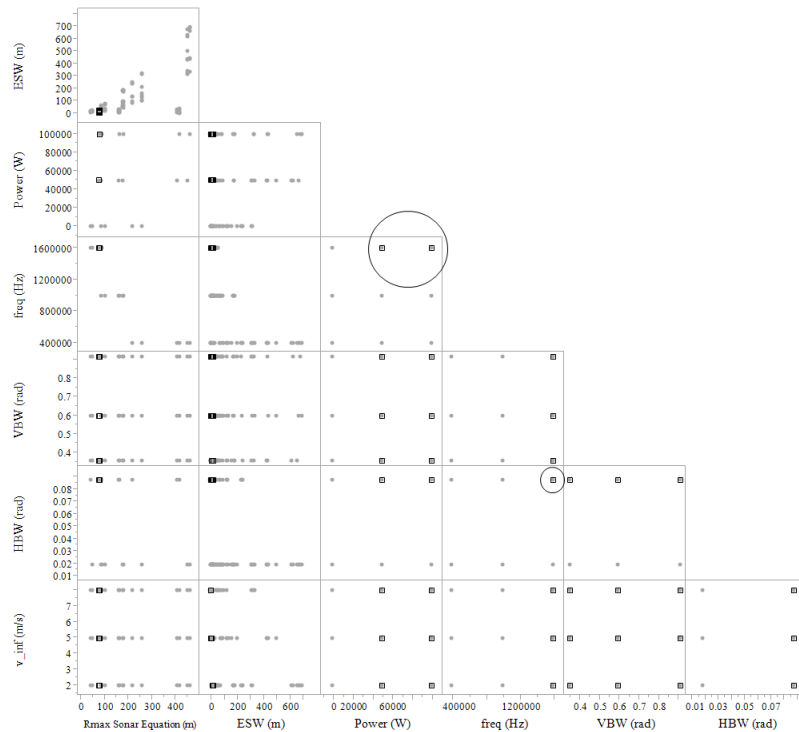


Figure 72: SSS predicted maximum range versus actual maximum range

The purpose of these explanations is to reveal that sensor modeling without operational considerations can handicap the expected sensor performance. In most cases, the sonar

equation model over predicted the virtual experiments (*i.e.*, the sonar equation was more ‘idealistic’). In a handful of cases, the sonar equation under predicted the performance. Either way, this has established an argument for combining operational experimentation along with sensor performance in a method for analyzing sensors that will be utilized in a collaborative SoS. Additionally, this provides a link between the sensor performance and the operations of the vehicle carrying the sensor.

6.4.2 Experiment 2: Number of Pass Comparisons

In order to set up this experiment, a baseline ‘cookie cutter’ sensor is defined as a uniform distribution of 80% probability of detection across its range. Alternatively, the average probability of detection for all 90 of the VXE sensors is calculated. Then, the number of passes required to obtain at least 98% detection probability for both the ‘cookie cutter’ sensor and the VXE sensors are calculated. A portrayal of the ‘cookie cutter’ sensor is shown in Figure 73(a) and the first of 90 VXE sensors is shown in Figure 73(b). The average probability of detection for the FLS design in Figure 73(b) is $P_{D,ave} = 57\%$. An initial comparison of the number of passes required to achieve 98% confidence is shown in Figure 74(a) and (b). The (a) plot shows the uniform versus the VXE sensor tested at 2 m/s , whereas the (b) plot shows the effect of operational speed on the VXE sensor. It is clear that the effectiveness of the sensor is highly dependent on sensor operational considerations such as speed.

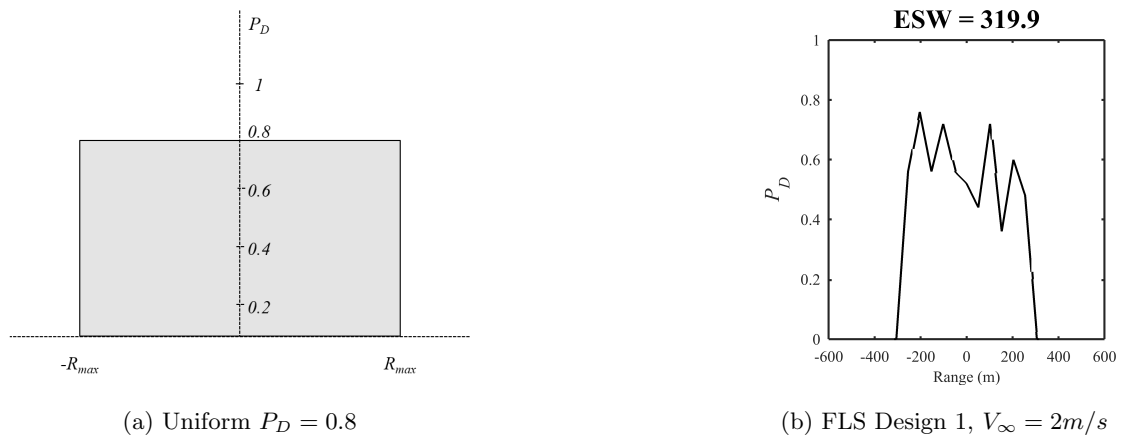


Figure 73: Operations Analysis vs. VXE Generated Detection Curves

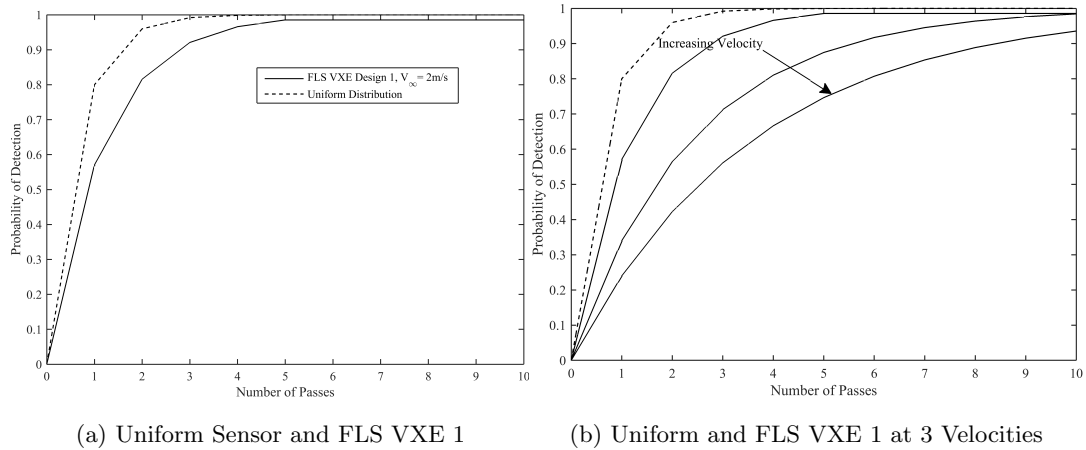


Figure 74: Number of Passes Required for $P_D = 98\%$

The 90 VXE sensor designs are additionally compared against the uniform sensor. Again, each of the 90 sensor designs are executed at 3 different velocities in the virtual experimentation environment. Figure 75 shows the wide variations in required number of passes across all 90 sensors at varying velocities. The results in part (a) are for the 36 FLS designs each at three different velocities and the results in part (b) are for the 54 SSS designs each at three different velocities. It is clear that some of the sensor designs cannot get even close to the desired confidence with ten passes over a target. This type of information would not be available without the energy-based link that was created through the sensor virtual experimentation environment (VXE).

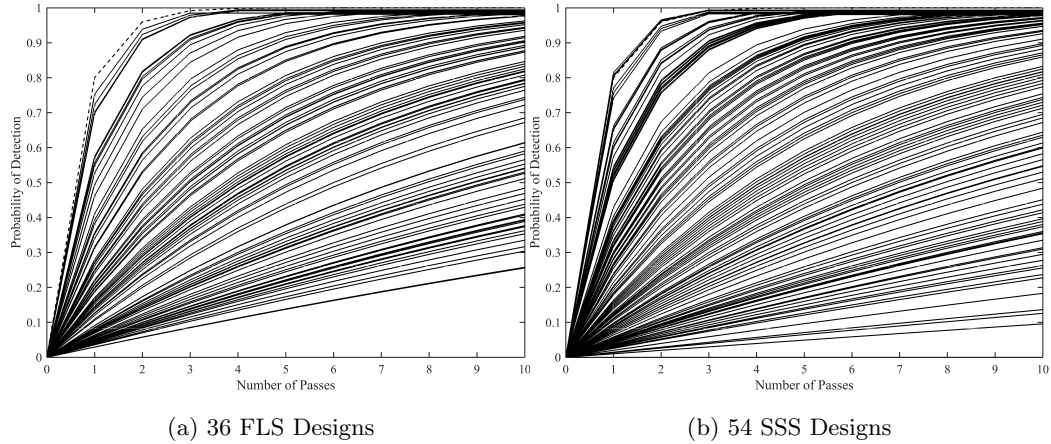


Figure 75: Number of Passes Required for $P_D = 98\%$: Uniform Sensor and all 90 VXE Sensor Designs at Varying Velocities ($V_\infty = \{2, 5, 8\} m/s$)

6.5 Recapitulation: A New Sensor Experimentation Method

Part of the overarching hypothesis of this dissertation is that the analysis of alternative multi-agent collaborative systems is better enabled by energy-based analyses at each level of the SoS design. This chapter has presented and analyzed detailed in-depth energy-based relationships for the subsystems applicable to this work, namely the sensors. As was pointed out early in this chapter, the sonar equation (when modeled in depth) provides an energy-based estimation of sonar performance. However, the sensors in a collaborative search mission are not static, and the sonar equation does not capture kinematic effects. Accordingly, it was pointed out that Operations Analysis and mobile robotics research each take kinematics into consideration, but they tend to negate sensor performance. The method presented in this chapter bridges the gap. The approach of modeling the sensor from the sonar equation and simulating its motion in a virtual experimentation environment provides energy-based functionals for both the sensor performance and the sensor kinematics. A flow chart of the new approach is shown in Figure 76. The standard approaches currently commit resources to either the left-side of Figure 76 (sensor modeling) or the right-side (probabilistic sensor estimates for the analysis of operations). The new approach developed in this work bridges the two.

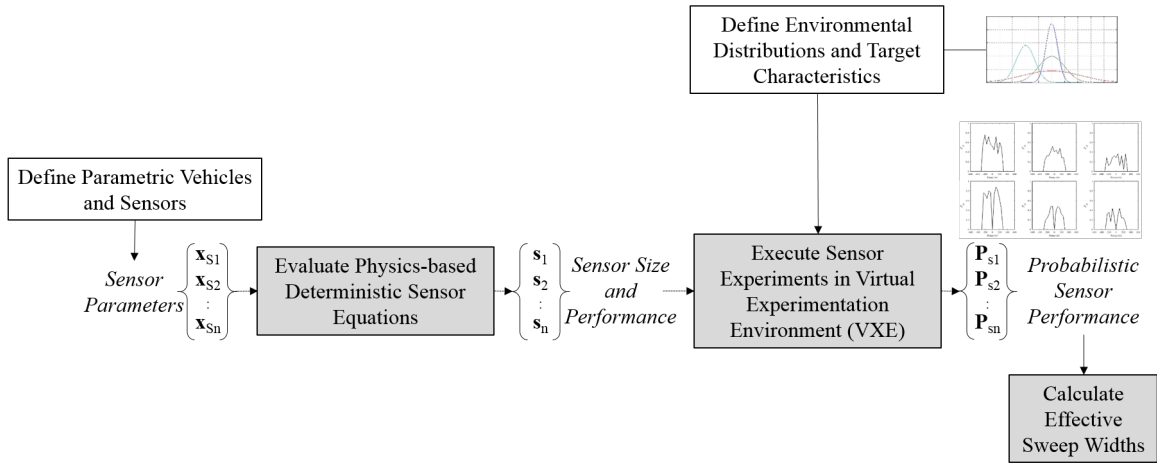


Figure 76: A New Sensor Experimentation Method - The VXE Approach

Experiment Set A provided data and analyses for comparing the new sensor modeling approach (the VXE approach) with two of the most common processes currently used. The motivation for developing the new VXE approach was in part due to the two general trends common in modeling sensors: analysis without implementation and implementation without analysis. In other words, the sensor performance modeling subset of the literature focuses deeply on the analysis of sensors based on the physics of the problem, including acoustic interactions with the environment. Alternatively, Operations Analysis and robotics literature is focused on implementing sensors for specific applications, but tend to make generalized assumptions about the physics of the sensors due to a lack of empirical data and/or modeling capability. Therefore, it was observed that there is a gap in capability since without implementing the physics of the sensors into the operational analyses, energy conservation between the sensors and the operations cannot be mapped. The results of Experiments 1 and 2 show that the VXE approach can provide an energy-based link between detailed sensor performance modeling and sensor operations. Even more so, there are clear benefits in performing trade-offs between sensors when using the VXE approach that were not available with the previous existing analyses.

The possibility of creating this link between sensor energy, detection capability, and velocity, along with the experiments executed to show the impact of this energy-based

relationship, has substantiated Hypothesis 3 which is restated here:

Hypothesis 3 *If a relationship is formed between sensor energy, sensor detection capability, and sensor velocity, then an energy-based link will be established between the effective sweep width parameter at the subsystem level and the vehicle performance at the system level.*

Hypothesis 3 led to creating the link between sensor energy, performance, and operational motion. Experiment Set A which included Experiments 1 and 2 in this chapter resulted in the subsystem level analysis and design process presented in Figure 76. The developed process is just the first level of the overall SoS analysis of alternatives method produced through this dissertation. Right now the subsystem level process is specific to the example problem at hand, but later on it will be generalized for the analysis of any collaborative SoS.

6.6 Motivation for Experiment Set B

The subsystems (sensors) in this chapter have been modeled and analyzed through an energy-based approach. Specifically, the sensor range performance and probability of detection are functions of sensor power (which is energy rate) and vehicle velocity, which is itself dependent on vehicle energy. However, in this chapter, the vehicle (system-level) velocity is not calculated based on any energy functionals. Therefore, it is simply an independent variable with no dependencies. This motivates the next chapter, which will develop the system-level analyses for vehicle design. The vehicles will be designed based on an initial energy requirement to power the sensors. However, the designs will have to be iterated through a sizing and synthesis process in order to produce vehicles that are balanced in terms of energy available, energy required, and volume required for the payload. Each sized vehicle will have an attributed velocity function which relates the speed it can obtain with the energy it will expend to move at that speed. After each vehicle is sized, there will be a functional relationship between energy and vehicle velocity which then maps down to sensor capabilities as a function of velocity. It will partially substantiate Hypothesis 4 and set the ground work for the final set of experiments in Chapter 8. Hypothesis 4 which will

be substantiated in the following chapters is restated below:

Hypothesis 4 *If the coverage effort is defined as a function of linked energy-based parameters from the subsystem level up through the SoS level, then the coverage effort can be formulated as a cost function within a mixed-integer linear programming optimization for the selection of alternative SoS designs.*

CHAPTER VII

EXPERIMENT SET B: SYSTEM (VEHICLE) LEVEL

The vehicle sizing and synthesis process consists of bringing together multiple disciplines (hence the synthesis) in order to find a vehicle design which has enough energy and volume to perform a required mission. Relevant vehicle design processes and methods have been developed by various author's in the areas aircraft design, ship design, and underwater vehicle design. Vehicle performance and stability analyses are also important for each designed vehicle. For the underwater vehicles in this dissertation, the sizing and synthesis process will begin with defining desired subsystems and required power systems to sustain those subsystems. Then an estimate of the required hull volume and dimensions will be acquired. Therefore, the main driver in designing the vehicle will be the ability to contain, carry, and utilize these subsystems and components over the entire required mission time. The implemented method for the underwater vehicles in this work will take appropriate information from the sensor design chapter as well as the mission requirements.

7.1 Sizing and Synthesis Methods

Vehicle design and research consists of distinct disciplines including aerodynamics and hydrodynamics, structures, propulsion, performance, stability and control and various others. However, the distinction often creates isolation [131]. Synthesizing a vehicle largely consists of integrating the disciplines in an appropriate way. Furthermore, there may be varying fidelity analyses available which incorporate an increasing amount of physics-based design. "Reduced reliance on historical data and a thorough understanding of the physics of the problem is required to ensure that unconventional systems are correctly modeled. The synthesis and sizing-centric design process involves the linking of each of the traditional disciplines to a single controlling routine" [103]. A varying fidelity sizing and synthesis process is shown in Figure 77.

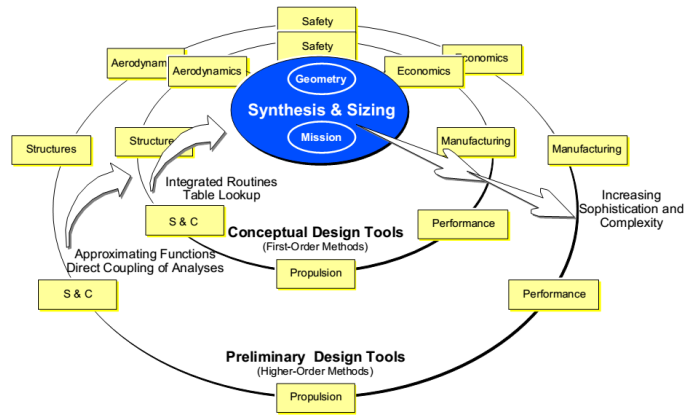


Figure 77: Varying Fidelity Sizing and Synthesis Approach [103]

In Appendix E, various sizing and synthesis methods for aircraft and surface vessels are reviewed and some important theories are presented. However, in this chapter, some comments on underwater vehicle sizing is provided and then the implemented method is developed.

Underwater Vehicle Design Process Underwater vehicle design requires a new set of requirements. These include the ability to submerge and stay submerged, to have a hull thick enough to withstand the depths of the sea, to operate with little to no communications, and to integrate a greater array of sensor suites for navigation, control, and target search. Also, a fully submerged vehicle cannot utilize fuel that requires exhaust off-board or air-breathing capabilities. Therefore, without a snorkel installed, the vehicle will likely use batteries or hold fuel byproducts on board.

Allmendinger [5] provides an interesting perspective on the design process. It takes into consideration the fact that a system will usually not operate in isolation. Instead, there are *boundaries* through which the vehicle must interact with the surrounding environment and with other vehicles/systems in order to accomplish a mission. The process is shown in Figure 78.

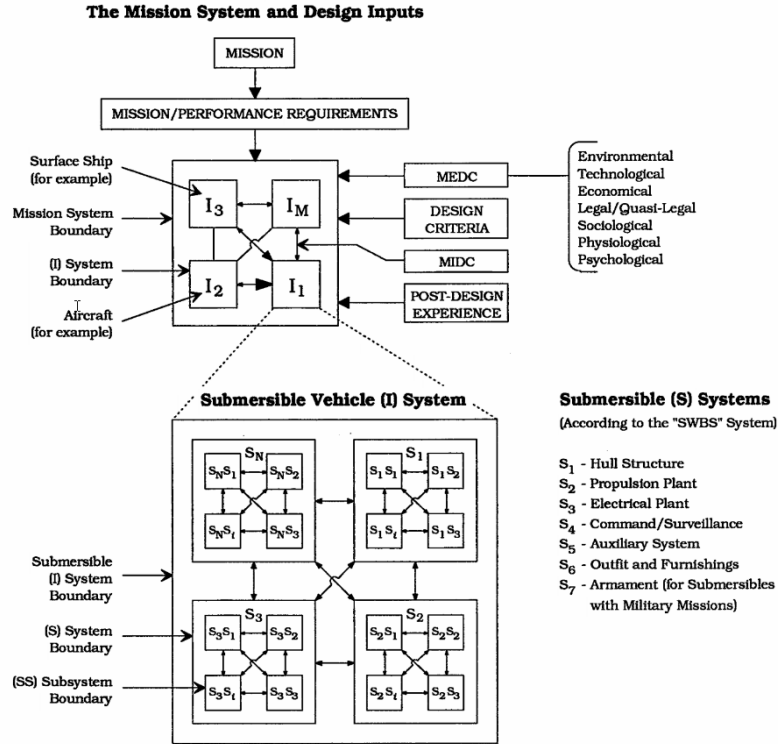


Figure 78: Allmendinger’s Submersible Design Process with Mission Systems Considered [5]

The concept of assuring that mission considerations are part of the design process is recognized by many. As was stated earlier, the DoD in particular has increased their focus on designing for capabilities. Therefore, it is imperative that the design of a UUV is coupled with the required tactics and operations. As Frits argues in relation to his design process for an underwater torpedo, “by simultaneously designing the torpedo and the tactics with which the undersea weapons are used, a more effective overall weapon system can be created” [54].

7.2 Filling the Gaps

One of the main difficulties in sizing a vehicle is knowing where to start from. Since the process is iterative in nature, there must be an initial condition, including weight/volume estimation, aerodynamic/hydrodynamic coefficient estimates, propulsion/fuel thermodynamic parameters, and potentially an engine deck. These estimates often come from historical data of similar vehicles. However, for revolutionary vehicles historical data is inherently not available, and the estimates must be initiated from higher-fidelity, physics-based analyses.

The area of underwater unmanned vehicle design is a relatively new area. Subsequently, there is a lack of hydrodynamic coefficient data available in the public literature for varying vehicle sizes and velocities (there is some data available for specific configurations at limited velocity ranges, which will be shown). Therefore, Appendix F presents fundamental theory for the development of the hydrodynamics of the vehicles. The theory provides a good feel for the types of coefficient values that should be expected.

Ultimately, the Air Force Research Laboratory's Missile Data Compendium (DATCOM) is implemented in this work as a physics-based analysis for hydrodynamics. Although Missile DATCOM is usually used for estimating the aerodynamic data of airborne missile shaped projectiles, it has been applied here by matching Reynold's number and Mach number with the underwater environment. The missile DATCOM results provide values similar to those from the theories presented in Appendix F.

7.3 Applied Formulation

The vehicle sizing and synthesis process consists of bringing together multiple disciplines (hence the synthesis) in order to find a vehicle design which has enough energy to perform the required mission. The need for energy inherently correlates with the size of the vehicle, as more fuel will require more internal volume to house the energy source. However, as fuel is added and the volume and weight are increased, more fuel is necessary to power the larger, heavier system. When a balanced solution between volume and energy is found, the vehicle is considered a sized vehicle. For this work, the pertinent requirements are for each vehicle to have an energy endurance of 24 hours and carry one of the sensors developed in the previous chapter. In the overall hierarchical SoS design process, the vehicle sizing and synthesis step fits within the vehicle analysis level. The vehicle analysis level is shown in Figure 79, which represents the information fed into the vehicle sizing process, and the information to come out of it. Additionally, a detailed view of the synthesis of disciplinary processes that must occur within the sizing process to iterate and converge on a sized vehicle for this work is shown in Figure 80.

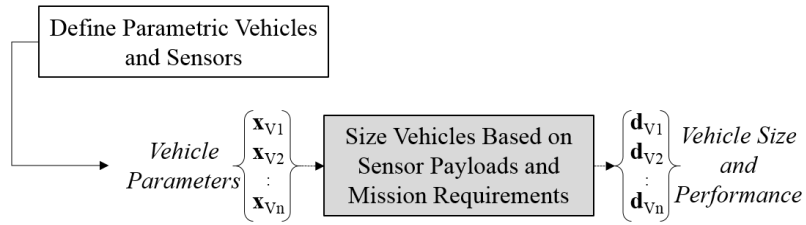


Figure 79: System (Vehicle) Level Considerations for the SoS Design Process

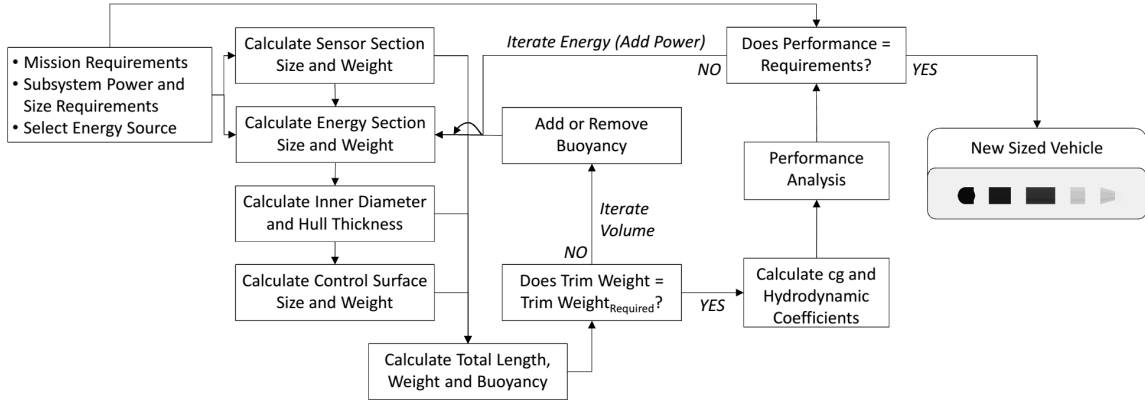


Figure 80: Implemented Sizing and Synthesis Process

7.3.1 Section Sizing Loop

The outer diameter of the vehicle is an important factor in the performance and payload capabilities of the overall system. The vehicle drag (*e.g.*, resistance) scales with the square of the radius of the vehicle, so any increase in diameter will have a detrimental effect on performance. Therefore, minimizing diameter can be beneficial, but a small diameter may not be able to house the necessary components and fuel. Increasing the length of the vehicle instead of the diameter can be beneficial in overcoming the issue of drag. However, a maximum length should be defined since the system will need to perform operational maneuvers that may be limited by vehicle length. Similarly, transportation constraints must be considered as well. It is helpful to define minimum and maximum values for the diameter and length based on historical data as shown in Equations 63 and 64. For this work, an inner diameter is first calculated based on the payload requirements of each section and then a hull thickness is calculated, which leads to a total outer diameter. Therefore,

the minimum and maximum diameter constraints are defined relative to the inner diameter, d_{inner} . Accordingly, the actual outer diameter of the vehicle may be slightly larger due to the hull thickness calculation.

$$\{d : d_{min} \leq d_{inner} \leq d_{max}\} \quad (63)$$

$$\{l : l_{min} \leq l \leq l_{max}\} \quad (64)$$

The sonar section is the first section to be sized since the length and diameters were provided by the sensor sizing step. In addition to the transducer array diameters and lengths, there is significant computing and processing equipment that must be packed inside of the sensor section. Useful estimates of the computing boards and other electronics as a function of transducer array size are provided by McAllister [104]. If the inner diameter of the sensor section is calculated to be less than d_{min} , then d_{min} is used as the current diameter. If the inner diameter is greater than the diameter required for the sonar system then there is void volume within the sensor section.

The hull thickness, t_{hull} , is calculated based on the maximum depth requirement for the vehicle. The thickness can be established on the von Mises criterion for unstiffened shells as shown in Equation 65, where d is the outer diameter of the vehicle, p is the local pressure of the sea water, U is the ultimate strength of the hull material and FS is a factor of safety. Since the outer diameter is not yet known, an initial guess can be made by using the inner diameter to calculate the hull thickness and then calculating a new outer diameter from Equation 66. The thickness calculation is then recalculated in an iterative fashion until convergence.

$$t_{hull} = \frac{0.56 \cdot d_{outer} \cdot p}{U \cdot (1 - FS) + 1.12 \cdot p} \quad (65)$$

$$d_{outer} = d_{inner} + 2t_{hull} \quad (66)$$

The parametric sensor sizing formulation in Section 6.2.1 provided power requirements for each sonar in addition to the diameter and length. Therefore, after the sensor section

is sized, an initial calculation of the energy section is made based on the sensor power requirements and the required operational time of the vehicle, T_{req} . The total energy of the system can be decomposed as shown in Equation 67. The vehicle motion component, E_{motion} , is based on the energy required to perform the mission in terms of requirements such as range, endurance, sprint speed, etc. The other component, E_{other} , can be used to specify any additional energy requirements expected, such as communications, guidance navigation and control (gnc), etc.

$$E_{total} = E_{sensor} + E_{motion} + E_{other} = (P_{total} \cdot T_{req}) \quad (67)$$

If the thermodynamic properties of the energy source are known, the required size of the energy section can be estimated. The pertinent factors are the specific energy, \dot{e} ($W - hr/kg$), the energy density, u ($W - hr/m^3$), and the mass density, ρ_{fuel} (kg/m^3). Either the energy density or the specific energy and mass density are necessary along with a required endurance for the vehicle. It is assumed in this work that the energy source will completely fill a cylindrical volume with a diameter equal to the inner diameter of the vehicle. This assumption can be adjusted to account for actual battery cell geometries or fuel tank requirements. The length of the energy section is varied until there is enough volume for the required fuel source. If the total length of the vehicle approaches an active constraint (*i.e.*, $l_{total} = l_{max}$), then the diameter is subsequently adjusted until the fuel volume requirement is met. The appropriate conditions are given in Equation 68, where $u = \dot{e}/\rho_{fuel}$.

$$l_{energy} = \begin{cases} \frac{(P_{total} \cdot ED)/u}{(\pi/4)d_{inner}^2} & , \quad l_{total} < l_{max} \\ l_{total} - l_{sensor} - l_{other} & , \quad l_{total} = l_{max} \\ \therefore d_{inner} = \sqrt{\frac{(P_{total} \cdot ED)/u}{(\pi/4)l_{energy}}} & \end{cases} \quad (68)$$

Next, the nose of the vehicle is given a spherical shape with the radius equal to half the outer diameter of the vehicle. The tail section is defined as a converging cone which houses the motor and propeller shaft with a pusher-prop at the back. For the REMUS style UUV,

four control surfaces are placed on the tail at equidistant rotation angles around the tail. For the RMMV style vehicle, two sets of two control surfaces are placed along the vehicle body. The four sections discussed so far (nose, sensor, energy, and tail) make up the initial vehicle. Before performance of the vehicle is calculated, buoyancy is checked in order to try and match the required trim weight. If the trim weight requirement is not met then a buoyancy section is added to the vehicle equal to the volume required to meet the trim weight desired. An example of both the REMUS and RMMV style vehicles are shown in Figure 81. It should be noted that the two vehicles in Figure 81 are not to-scale with each other. The REMUS style vehicle on the left is actually 4x smaller in length and diameter than the RMMV vehicle on the right.

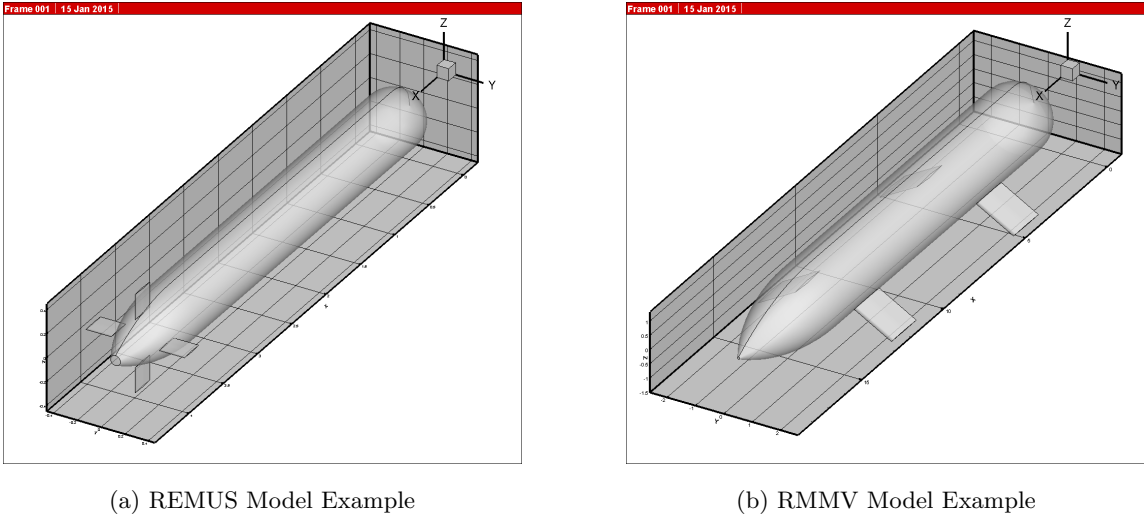


Figure 81: REMUS and RMMV Sized Vehicle Examples, produced by Missile DATCOM.

7.3.2 Vehicle Performance Loop

After the initial section sizing loop which was described in the previous section, the vehicle is only able to meet the sensor power and volume requirements. During the performance loop, the forces that act on the vehicle while in motion must be considered in order to determine the power and thrust required to operate in motion. The forces acting on the vehicle are shown in the free-body diagram in Figure 82. Since most of the operational mission of a search vehicle is occupied by constant velocity steady cruise, it is appropriate to consider a free-body diagram in which the thrust of the vehicle must equal the drag. Also, it is

assumed in this work that the vehicles are to be designed with positive trim weight (trim weight is equal to the difference between the vehicle buoyancy and the vehicle weight). If the vehicle motion stops it will therefore float to the surface of the water. Therefore, a negative lift vector is required to keep the vehicle at a constant depth during operation, which is a function of the angle of attack, α . It is also assumed that since the angle of attack will be small, the impact of the thrust vector in the z -direction is approximately zero (*i.e.*, $T \sin(\alpha) \approx 0$ by the small angle approximation). An alternative approach would be to design ballast tanks that would keep the vehicle at a specific depth, but that approach is not considered here.

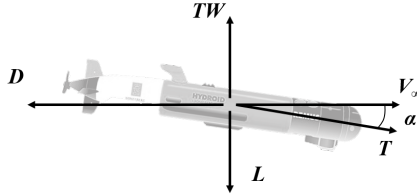


Figure 82: Steady Level Search Free-Body Diagram, $TW = L$, $D = T$ with $\sin(\alpha) \approx 0$

The vehicle performance will be highly dependent on estimates of the vehicle drag coefficient and the associated drag polar. For this work, access to the Air Force Research Laboratory’s Missile DATCOM program was utilized, which provides aerodynamic coefficients for missile shaped vehicles. By setting the Reynolds and Mach numbers to values appropriate for the underwater environment, Missile DATCOM was able to provide impressive results as a function of vehicle reference area, especially considering the range of theoretical values presented in Appendix F. It is assumed in this work that the drag polar for the vehicles is as shown in Equation 69, where C_{D_o} is the zero-lift drag and kC_L^2 is the drag due to lift. It is also assumed that the coefficient k is approximately equal to unity [95]. The lift coefficient, C_L , can be expanded as shown in Equation 70. Also, the reference area utilized is the area of the vehicle determined by looking at the vehicle from directly in front of it as given in Equation 71.

$$C_D = D_{D_o} + kC_L^2 \quad (69)$$

$$C_L = \frac{2L}{\rho_\infty V_\infty^2 S_{ref}} = \frac{2TW}{\rho_\infty V_\infty^2 S_{ref}} \quad (70)$$

$$S_{ref} = \pi d_{outer}^2 / 4 \quad (71)$$

The power required for motion of the vehicle is equal to the thrust required times the velocity. Since thrust is equal to drag for the search cruise condition, the power required function can be expanded using Equations 69 and 70 as shown in Equation 72. Furthermore, the power required is also equal to the change in energy with time. If the thrust and velocity are assumed to remain constant during the search segment, than the power required is also constant and the endurance can be solved for as given in Equation 73. It is easy to see that a minimum power condition will provide a maximum endurance. The velocity condition for maximum endurance can be found by differentiating the power function from Equation 72 with respect to velocity and solving for the velocity when the differential is equal to zero. The resultant velocity for minimum power, and thus maximum endurance, is shown in Equation 74. Similarly, the maximum range of the vehicle can be found by differentiating the thrust required function with respect to velocity (the thrust required is just the power required divided by velocity). The resultant velocity for maximum thrust is given in Equation 75.

$$\begin{aligned} P_{req} &= T_{req} V_\infty = D V_\infty = \left(\frac{1}{2} \rho_\infty V_\infty^2 S_{ref} C_D \right) V_\infty \\ &= \left(\frac{1}{2} \rho_\infty S_{ref} C_{Do} \right) V_\infty^3 + \left(\frac{2TW^2}{\rho_\infty S_{ref}} \right) \frac{1}{V_\infty} \end{aligned} \quad (72)$$

$$\begin{aligned} P_{req} &= \frac{dE_{req}}{dt} \rightarrow dt = \frac{dE_{req}}{P_{req}} \\ \int dt &= \frac{\int dE_{req}}{P_{req}} \rightarrow Endurance = \frac{E_{req}}{P_{req}} \end{aligned} \quad (73)$$

$$V_\infty|_{maxEnd} = \sqrt{\frac{8TW}{\pi \rho_\infty d_{outer}^2 \sqrt{3C_{Do}}}} \quad (74)$$

$$V_\infty|_{maxRange} = \sqrt{\frac{8TW}{\pi \rho_\infty d_{outer}^2 \sqrt{C_{Do}}}} \quad (75)$$

The maximum endurance and range conditions are important since the purpose of search missions is usually to cover as much area as possible, but to do so at a high rate. If the rate of motion, and therefore the area coverage rate, is too low with the velocities given in

Equations 74 and 75, then the velocity can be increased, but at the detriment to both range and endurance. The maximum velocity condition is found by calculating the velocity when the power required is equal to the power available through the motor and shaft. The power available is equal to the power transmitted through the motor shaft times the efficiency of the propeller, η_{prop} , as shown in Equation 76. If the propeller is assumed to have variable pitch capability, then the propeller efficiency can be expected to be constant [8]. This is a reasonable assumption, but can be corrected for by calculating the propeller efficiency at varying speeds of rotation and vehicle velocities. Also, the power transmitted through the shaft is a function of the motor or engine installed on the vehicle. It is assumed in this work that the power capabilities of the motor or engine are more than enough for the desired operating conditions. Figure 83 shows both the required shaft power and required thrust for one of the sized vehicles. The minimum values of the solid line functions represent the velocities for minimum power and minimum thrust. The dotted lines express the trend of power available and thrust available. The intersection of the available and required curves represents that maximum possible velocity of the vehicle.

$$P_{available} = \eta_{prop}P_{shaft} \quad (76)$$

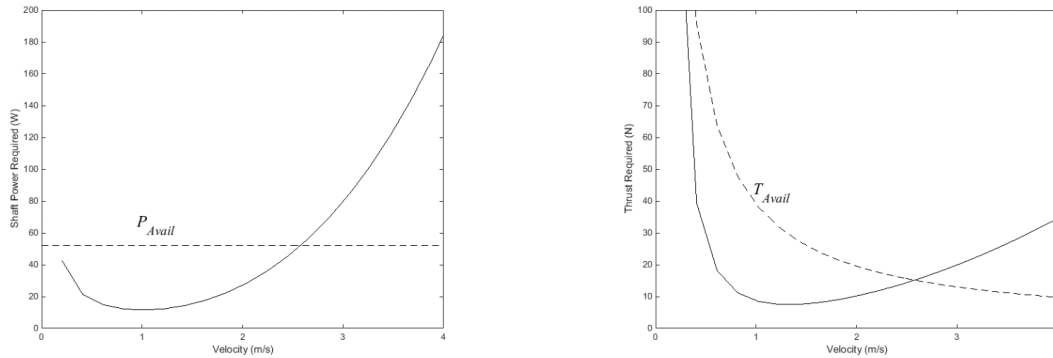


Figure 83: Required and Available Power and Thrust Examples

The last velocity condition to consider is the maximum velocity desired. This is a desired sprint speed that will likely be much less than the maximum velocity that is possible. The sprint speed will usually only be operated for a fraction of the total mission time. The total

required power for motion is then the power required for maximum range or endurance plus a fraction of the power for maximum desired velocity, as shown in Equation 77 (σ is the fraction of time desired for sprint operation). Since the range is more limiting than the endurance, the power for maximum range is used here. Finally, the total required energy for motion is calculated by multiplying the total power of motion by the desired time of operation, T_{req} , which may be less than the maximum endurance capability of the vehicle.

$$P_{motionTotal} = (1 - \sigma)P_{maxRange} + \sigma P_{V_{\infty},sprint} \quad (77)$$

$$E_{motionTotal} = P_{motionTotal}T_{req} \quad (78)$$

On the first iteration through the performance sizing, the energy required for motion will be less than the energy available. Therefore, the vehicle is resized by expanding the energy section of the vehicle. Since the vehicle has grown in size due to the added energy, the volume will likely need to be readjusted. The drag on the vehicle may then be affected, and therefore more energy will be required to overcome the performance decrement. This process continues until volume and power are balanced, in which case the vehicle is considered to be sized. The process is regenerated in Figure 84 below.

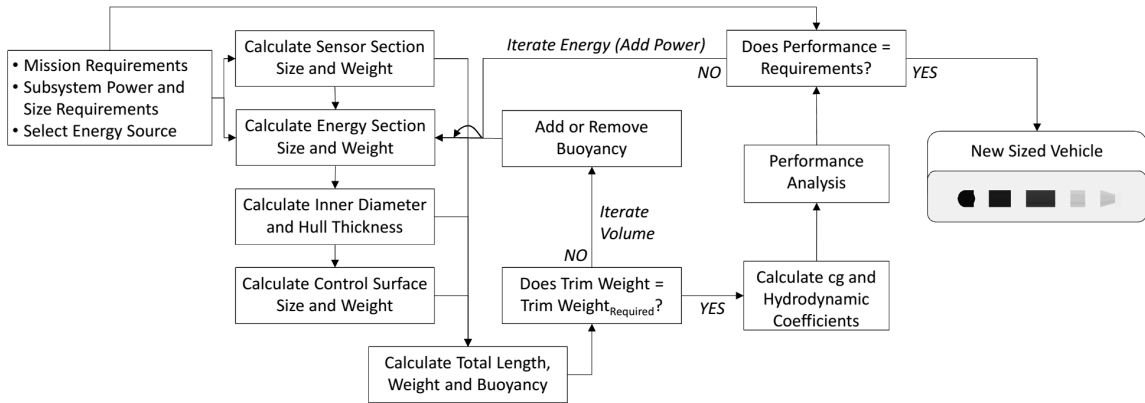


Figure 84: Implemented Sizing and Synthesis Process

7.3.3 Results of the Vehicle Sizing Process

Two vehicles (a REMUS and an RMMV style) were sized for each of the 90 sensor designs delineated earlier (36 FLS and 54 SSS). This resulted in a total of 180 vehicle design attempts

based on carrying a single sensor on either the REMUS or the RMMV style vehicles. The sizing and synthesis iterations progressed for each vehicle in similar fashions to what is shown in Figure 85 and Figure 86. In each of these figures, the left most plot displays volume-iteration versus total length of the vehicle. The middle plot shows volume-iterations versus the energy available to the vehicle. Finally, the plot on the right conveys the iterative growth of power onboard the vehicle (dotted line) along with the power required (solid line) for the sensors and motion.

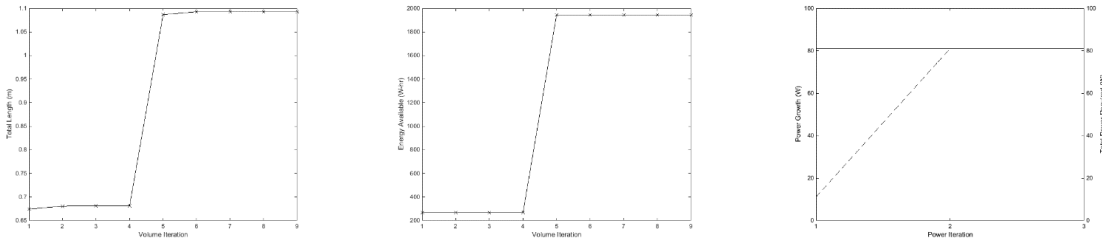


Figure 85: Vehicle Sizing Iterations with an FLS, $P_{ac} = 0.1W$

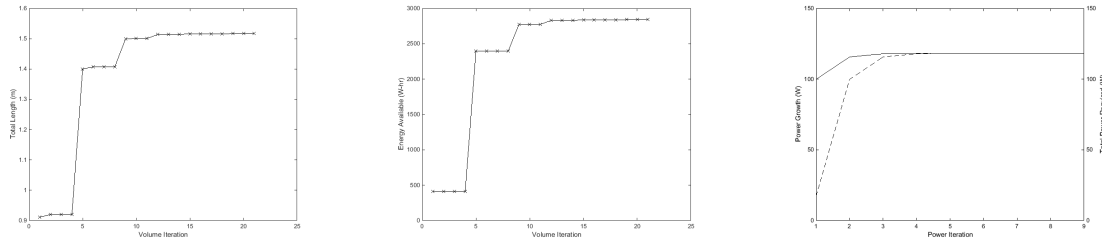
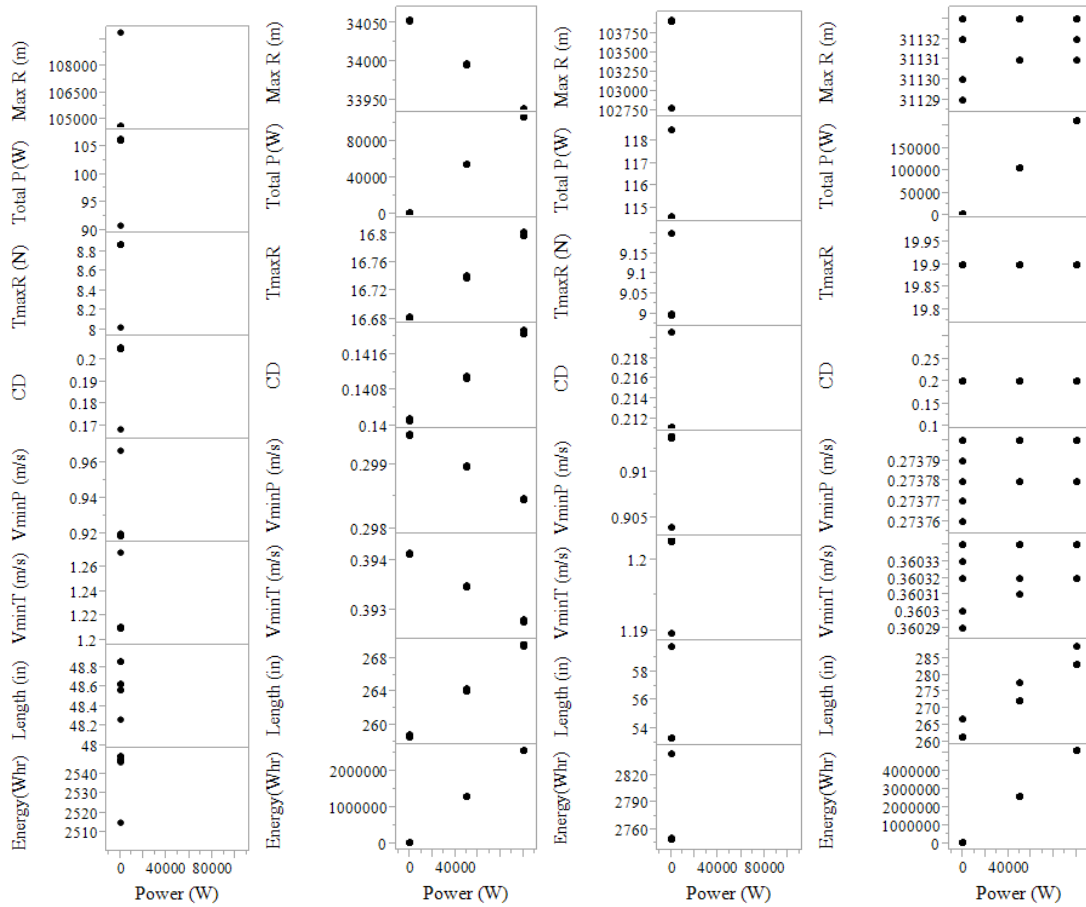


Figure 86: Vehicle Sizing Iterations with an SSS, $P_{ac} = 0.1W$

The REMUS style vehicles were able to converge on sized solutions for the sensors that had P_{ac} requirements of 0.1W. However, convergence was not obtainable for 50kW and 100kW sensor power requirements; that equates to 30 out of 90 successfully sized REMUS style vehicles. This is due to the limited volume available in the REMUS style vehicles along with batteries (li-ion) with relatively low energy density ($\approx 4.5W \cdot hr/in^3$). The RMMV vehicles, on the other hand, were able to converge on sized solutions for all of the power requirements; that equates to 90 out of 90 successfully sized RMMV style vehicles. This is not surprising since the RMMV has more available volume and uses diesel fuel with a relatively high energy density ($\approx 160W \cdot hr/in^3$).

Figure 87 shows the sizing results of the forward looking sonars (FLS) installed on the

REMUS style vehicles (a) and the RMMV style vehicles (b), along with the side-scan sonars (SSS) installed on the REMUS (c) and the RMMV (d). Notice the difference of scale on the left axes. The requirements for the RMMV are much greater, which is obvious in analyzing the energy, length, and total power. The RMMV is a much larger vehicle with better payload capabilities, but that does not necessarily correlate with greater range as is shown. On the other hand, the REMUS' have better range capability, but they are limited in their sensor payloads because of the lack of energy they can carry. However, the size requirements for the REMUS are much more reasonable; in other words they are easier to transport.



(a) REMUS w/ FLS (b) RMMV w/ FLS (c) REMUS w/ SSS (d) RMMV w/ SSS

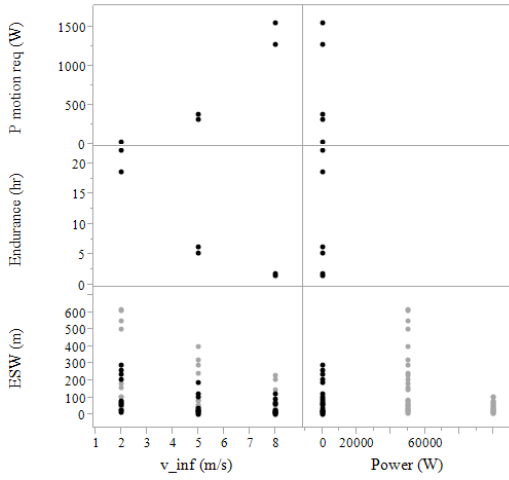
Figure 87: Sizing results for one sensor type per vehicle

The inability for the REMUS vehicles to converge on sized solutions for the middle and

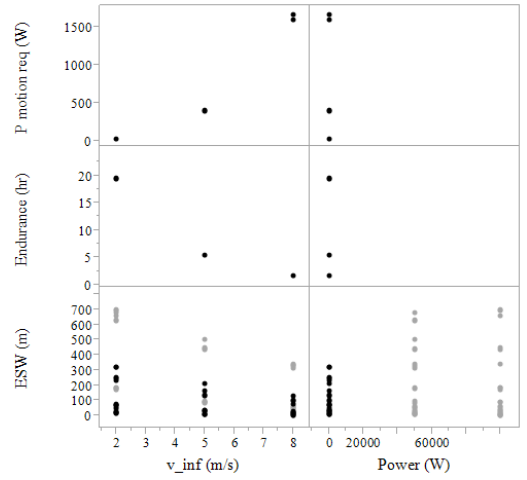
upper sensor power requirements should be clear. This is apparent in that there are no data points for those designs in Figure 87(a) and (c). This fact is the first clue in discovering the necessity of considering an energy-based approach to vehicle-sensor compatibility. Without analyzing the vehicle installation, a designer might easily assume all of the sensor designs that are available are feasible in operation. However, this shows that sensors are not feasible unless the vehicle they are installed on have the energy capability necessary to power them and move them through the environment.

In addition, Figure 87 shows that the RMMV style vehicles may have enough energy to complete a mission on their own (*i.e.*, without collaboration). This is another aspect of the SoS design that can, and will, be investigated further after some more sizing data is presented.

With sized vehicles available as is shown in Figure 87, it is now imperative to analyze performance capabilities. The sensor designs were each tested at three different velocities in the subsystem chapter: $V_\infty = \{2, 5, 8\} m/s$. Similarly, the performance of each sized vehicle is established at the same velocities. Figure 88 shows the REMUS style vehicles' endurance and power required for motion. The ESW (effective sweep width) values are from the subsystem chapter. The dark data points represent the installed sensor-vehicle designs that were feasible for the REMUS style vehicles. The lighter, grayed out, data points are infeasible sensors for the REMUS style vehicles. Figure 89 presents the same type of performance analysis for the RMMV vehicles.

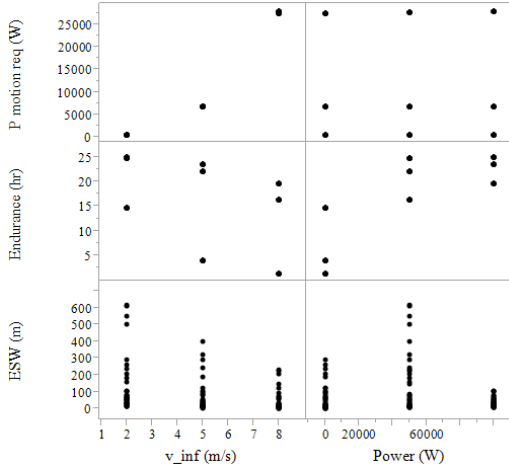


(a) Performance w/ FLS

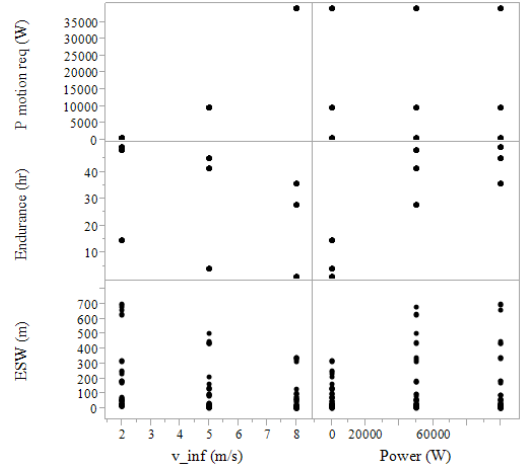


(b) Performance w/ SSS

Figure 88: Endurance and power required for REMUS style vehicles with installed sensors



(a) Performance w/ FLS



(b) Performance w/ SSS

Figure 89: Endurance and power required for RMMV style vehicles with installed sensors

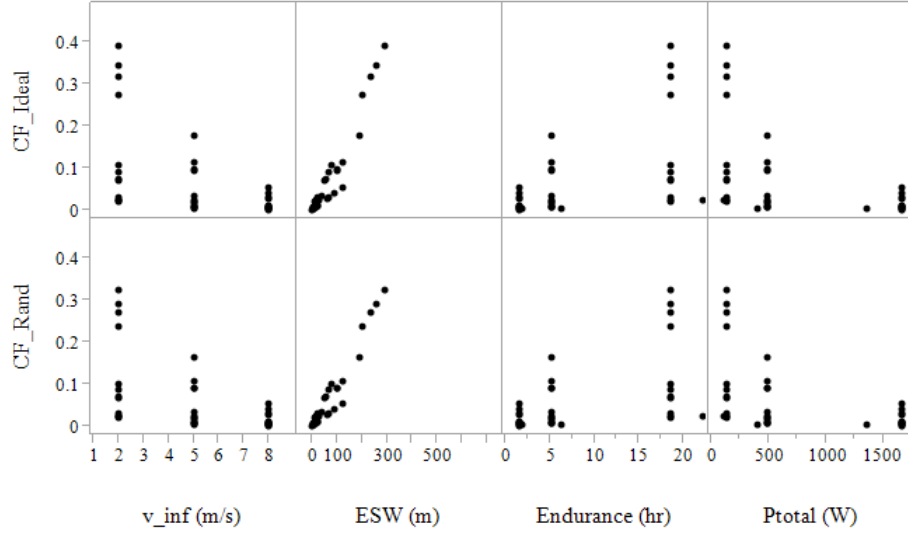
7.3.4 Insights from the Coverage Factor

Figures 88 and 89 displayed the endurance and ESW capabilities of each sized vehicle as a function of vehicle velocity. This leads to the ability to examine the coverage capability of each vehicle. Recall that the coverage factor is:

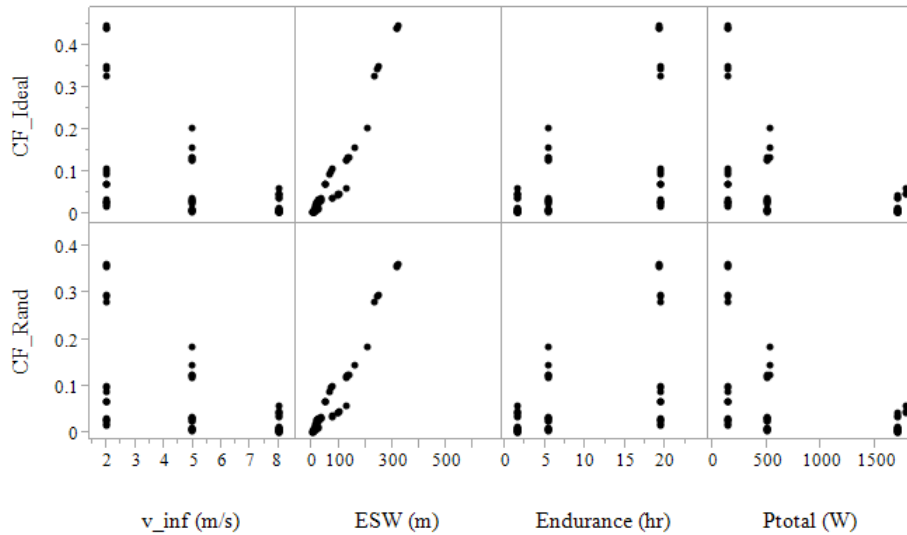
$$\lambda_{i,ideal} = V_{\infty,i} S_i T_i / A_s$$

$$\lambda_{i,ran} = 1 - e^{-\frac{V_{\infty,i} S_i T_i}{A_s}}$$
(79)

...for both the ideal and worst case scenarios, where S_i is the ESW of vehicle i , T_i is the endurance of vehicle i , and A_s is the required search area. Figure 90 shows the total coverage factor for both the ideal and limiting cases, where CF is λ .



(a) REMUS coverage factor w/ FLS installed

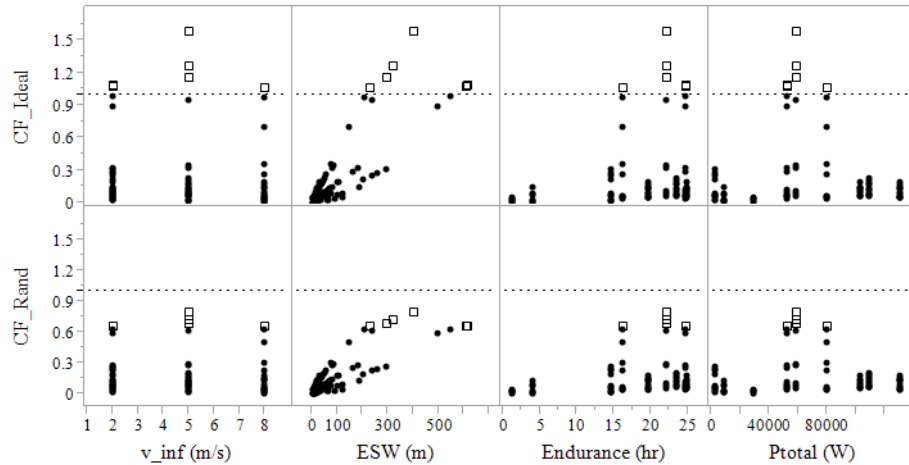


(b) REMUS coverage factor w/ SSS installed

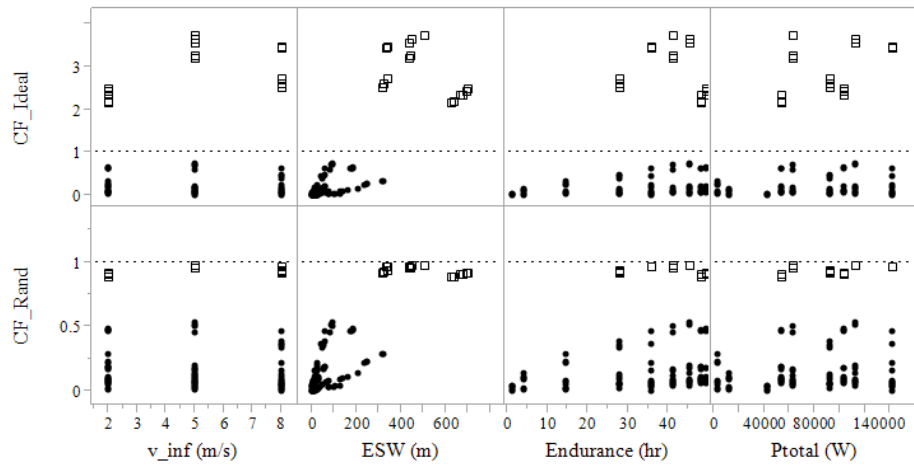
Figure 90: Coverage Factor Scatter Plots for REMUS Style Vehicles

Some of the RMMV vehicles have greater endurance and ESW capabilities than most of the other vehicles. This is because the RMMV has a much higher energy density and volume. This is seen in Figure 91, where some of the vehicle designs can almost complete

the entire area search by themselves. The ideal coverage is not likely to occur, but for some of the designs, the lower bound of expected capabilities in coverage is still close to full coverage before the 24 hour mission requirement. The dotted reference line in Figure 91 is the full coverage limit, and the data points with square markers exceed full coverage for the ideal situation. However, not all of the square markers get to complete coverage before the 24 hour mission requirement.



(a) RMMV coverage factor w/ FLS installed



(b) RMMV coverage factor w/ SSS installed

Figure 91: Coverage Factor Scatter Plots for RMMV Style Vehicles

A more interesting view of the coverage factor is how it changes over time. This is shown for the REMUS style vehicles with FLS installed in Figure 92. Similarly, the REMUS vehicles with SSS installed is shown in Figure 93.

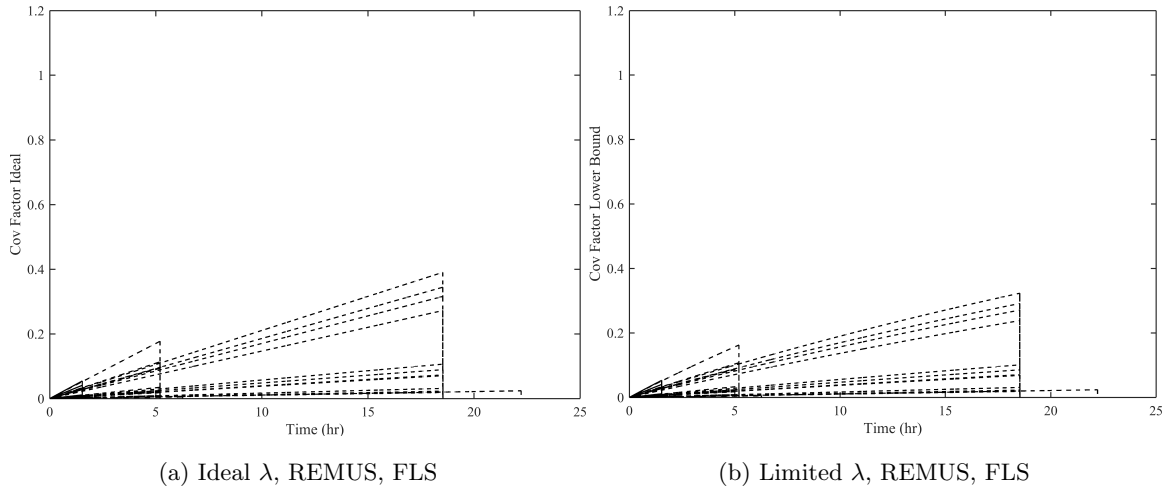


Figure 92: Coverage Factor over time for REMUS Style Vehicles w/ FLS

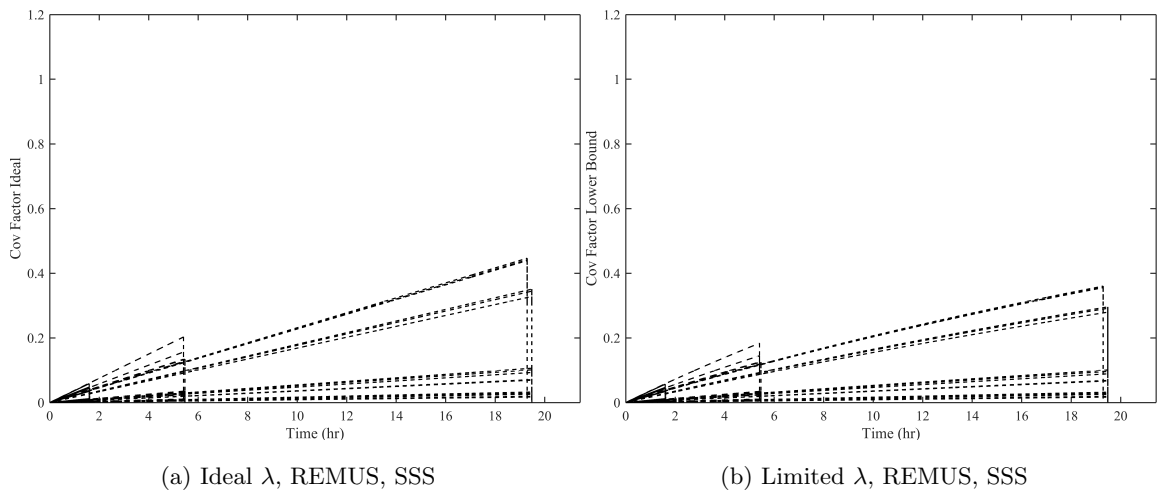


Figure 93: Coverage Factor over time for REMUS Style Vehicles w/ SSS

In the plots above, it is clear that the REMUS vehicles are incapable of performing the full mission on their own. The results for the RMMV can be drastically different. This is presented in Figures 94 and 95.

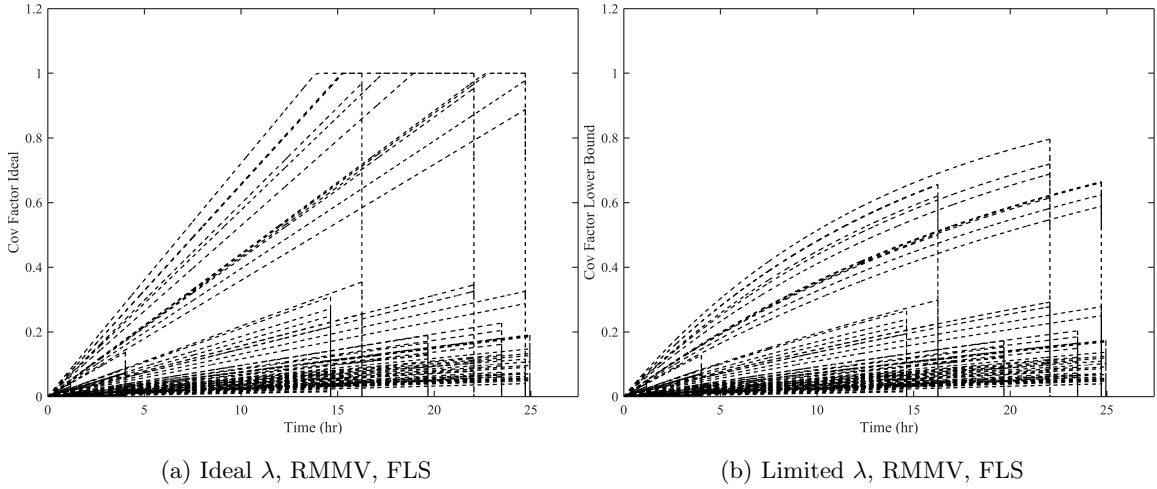


Figure 94: Coverage Factor over time for RMMV Style Vehicles w/ FLS

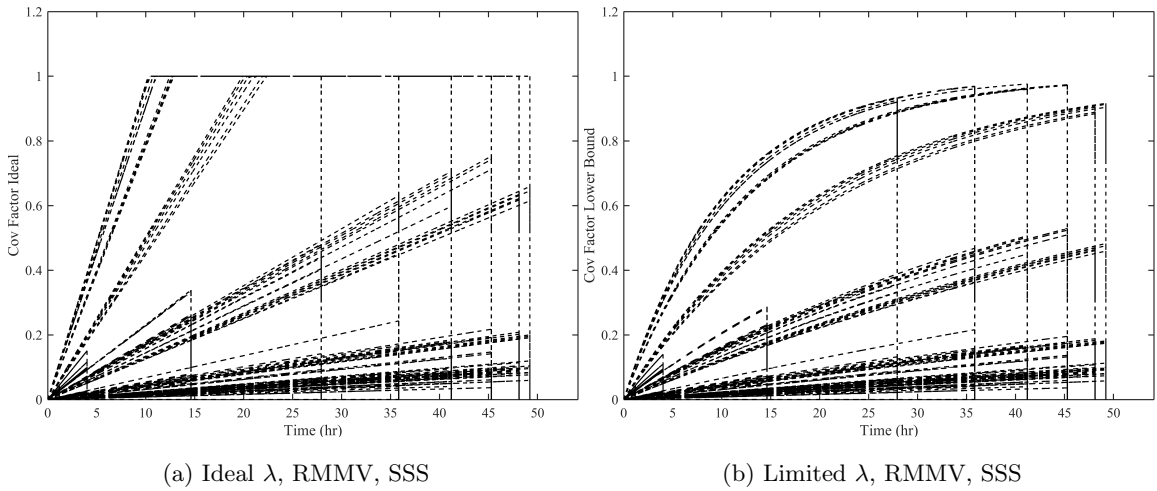


Figure 95: Coverage Factor over time for RMMV Style Vehicles w/ SSS

7.4 Experimental Approach and Results

The previous few sections have delineated a multi-level design method for generating alternative sensor and vehicle designs that are to be utilized within a collaborative system-of-system mission. The vehicle and sensor performance has been calculated through a parametric representation of the sensor and vehicle design space. As was stated earlier, varying design considerations can prove to be either beneficial or detrimental to the cooperative operations of a grouping of unmanned systems. Therefore, delineation of the single vehicle capabilities at both the subsystem and system level is an imperative step in determining

overall effectiveness. The need for energy-based delineation at the system-level along with the subsystem-level is supported by the subsequent experimental approach of this chapter. The experimental setup for the system level analyses originally presented in Chapter 4 is shown again in Figure 96. The next three sections will provide the details for Experiments 3, 4 and 5, and the subsequent results. The arrows at the top of Figure 96 portray data and analysis flowing from the subsystem-level experiments.

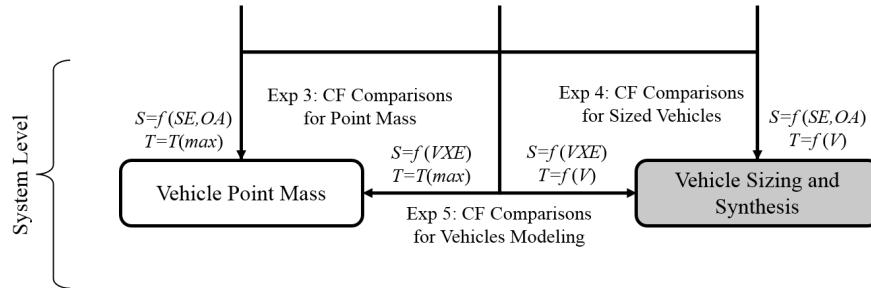


Figure 96: System Level Experimental Setup

The coverage factor was deemed an appropriate means for measuring the system-level experiments since it mostly combines energy-based parameters from each level of the SoS hierarchy. Specifically, the velocity (which is a function of vehicle energy), and the total coverage of multiple vehicles at the SoS level. Unfortunately, a link between sensor width, S_i , and the energy of the vehicle had not been formally established in the literature to the knowledge of the author. However, the results of the VXE approach to sensor modeling provided the necessary link, which again is a major contribution of this work.

7.4.1 Experiment 3: Point Mass Comparisons

Experiment 3 demonstrates the gap in separate approaches to sensor analysis when applied at the vehicle level. For a point-mass vehicle assumption, T_i is just the allowable mission time. In this experiment, a comparison is made between point-mass vehicles with sensors that are specified by the sonar equation and operations analysis versus sensors developed through the new virtual experimentation approach. The flow chart for Experiment 3 is shown in Figure 97.

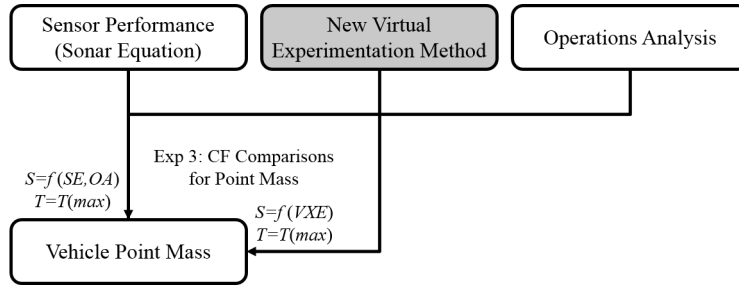


Figure 97: Experiment 3: Coverage Factor Comparisons for Point Mass Vehicles

The 90 sensor designs established in Chapter 6 are each placed on a point-mass vehicle for Experiment 3. The coverage factor is calculated for each sensor-vehicle combination at three discrete velocities. Since the vehicles are point-masses, the operational time is set as 24 hrs for each system. Then, the sweep width, S_i , of each vehicle is either twice the theoretical maximum range for a static sensor according to the SE plus OA approach, or it is the experimentally calculated sweep width according to the VXE approach, which varies with velocity. Figure 98 shows the comparison of each approach at the three distinct velocities.

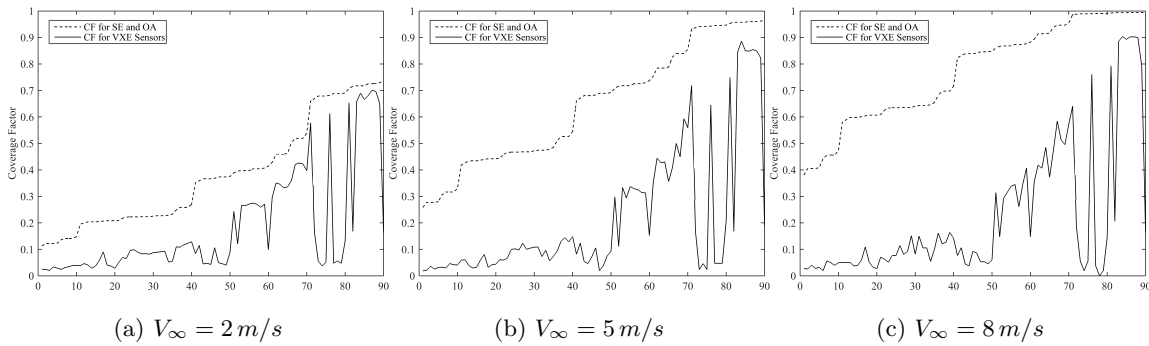


Figure 98: The Sonar Equation and Operations Analysis over-predicts coverage due to a lack of information linking sensor performance to vehicle operations.

The $x - axis$ displays the vehicle-sensor index, which has been sorted according to increasing sweep width calculated by the SE plus OA approach. The results of the charts are very telling. In particular, the effect of experimental sweep width on overall mission performance of the sensor is isolated and clearly seen. The CF for SE and OA trend lines increase in each chart as velocity increases, since the sensor performance in that approach

is not affected by the operations of the vehicle. However, the *CF for VXE Sensors* trend line remains relatively constant. This is because even though velocity is increasing (which would normally increase the coverage factor), the performance of the sensors degrade with increased velocity. Therefore, simply increasing vehicle velocity does not provide as much of an impact. This is a significant observation for collaborative operational planning of vehicles in a search mission.

7.4.2 Experiment 4: Sized Vehicle Comparisons

Experiment 4 demonstrates the gap in separate approaches to sensor analysis when applied at the vehicle level, but now without the point-mass vehicle assumption. Instead, the vehicle time, T_i , is dependent on the vehicle design and velocity. Accordingly, the vehicle endurance is a function of vehicle design parameters and velocity. The details of the sizing and synthesis process applied to these vehicles were given earlier in this chapter. Similar to Experiment 3, the sensor analyses for Experiment 4 are specified by either the sonar equation and operations analysis or the new virtual experimentation approach. The flow chart for Experiment 4 is shown in Figure 99.

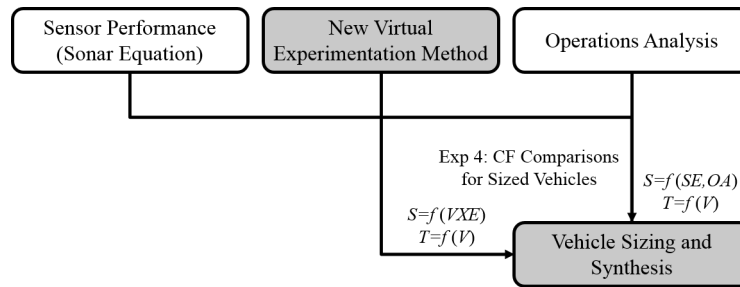


Figure 99: Experiment 4: Coverage Factor Comparisons for Sized Vehicles

The 90 sensor designs are each placed on either the REMUS-style vehicles or the RMMV style vehicles. However, as was demonstrated earlier, the REMUS vehicles can only carry one-third of the 90 sensors due to limited energy capacity of the batteries.

The coverage factor for each vehicle-sensor combination is calculated at three discrete velocities. Since the vehicles are sized based on payload and baseline design considerations, the operational time for each vehicle is set as the calculated endurance. The sweep width,

S_i , of each vehicle is either twice the theoretical maximum range for a static sensor according to the SE plus OA approach, or it is the experimentally calculated sweep width according to the VXE approach, which varies with velocity. These are the same sensor comparisons presented in Experiment 3. Figures 100 and 101 show the comparison of each sensor modeling approach at the three distinct velocities for vehicles that are endurance limited.

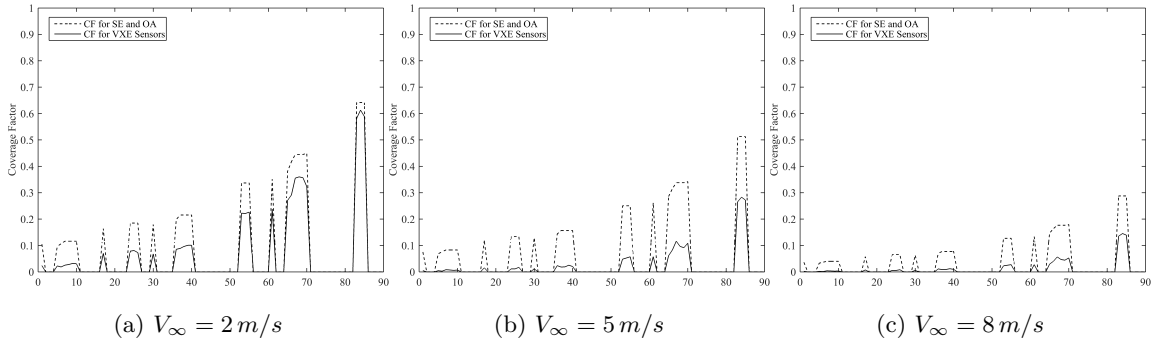


Figure 100: Coverage Factor comparisons for sized-REMUS style vehicles with sensors modeled through the old approach versus the new approach

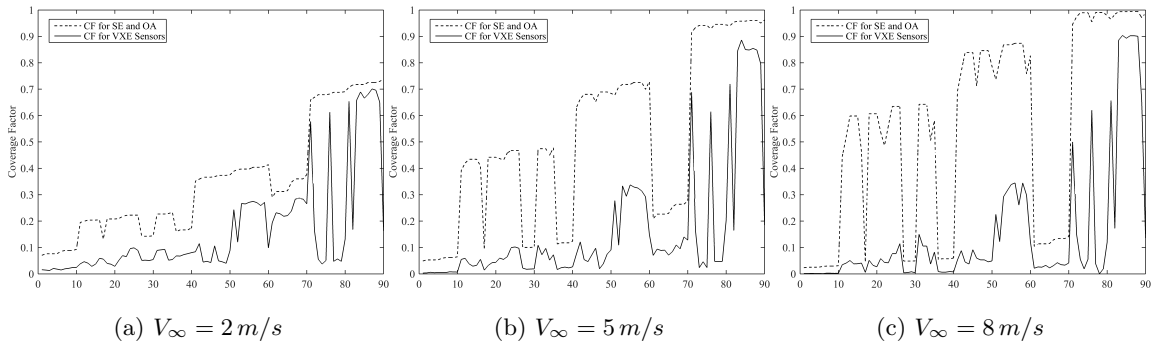


Figure 101: Coverage Factor comparisons for sized-RMMV style vehicles with sensors modeled through the old approach versus the new approach

The results of the charts show the significant effect of vehicle endurance on the operational capabilities, especially when compared with the point-mass vehicle data of Experiment 3. For the REMUS-style vehicles, it is clear that endurance is the main effect in capability as velocity increases. For the RMMV-style vehicles, endurance has a moderate

effect, but the specific sensor-modeling approach has the major impact. This is another significant observation for collaborative operational planning of vehicles in a search mission. It shows that energy-based design and analysis of sensors *and* vehicles have a significant impact on overall mission effectiveness.

7.4.3 Experiment 5: Vehicle Modeling Comparisons w/ VXE Sensors

Experiment 5 demonstrates the gap in separate approaches to *vehicle analysis* when utilizing the sensors developed through the virtual experimentation environment. This is different from Experiments 3 and 4 in that each of those experiments used varying sensor analyses with a constant vehicle modeling approach (point-mass vehicles in Experiment 3 and energy-limited sized vehicles in Experiment 4).

The first approach for the vehicle analysis in Experiment 5 is the point-mass approach, and the second approach is the sizing and synthesis method built on energy-limited analyses. The vehicle time, T_i , for the point-mass approach is just the allowable mission time whereas the sizing approach determines a different endurance time for each vehicle design. The flow chart for Experiment 5 is shown in Figure 102.

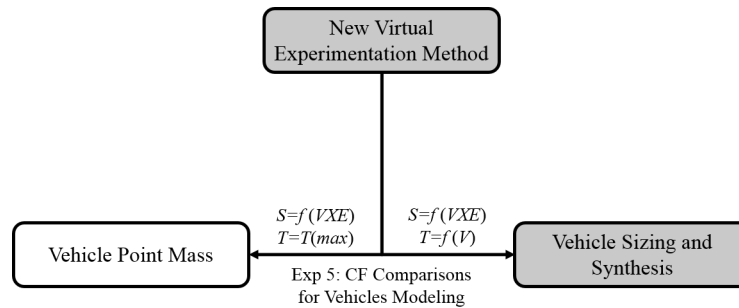


Figure 102: Experiment 5: Coverage Factor Comparisons for Competing Vehicle Analyses with VXE Sensors

The 90 sensor designs are once again placed on either the REMUS-style vehicles or the RMMV-style vehicles for Experiment 5, except all of the sensors now have sweep widths (S_i) that are calculated according to the VXE sensor modeling approach. The coverage factor for each vehicle-sensor combination is calculated at the three discrete velocities. Figures 103 and 104 show the comparison of each *vehicle* modeling approach at the three distinct

velocities with sensors developed through the VXE.

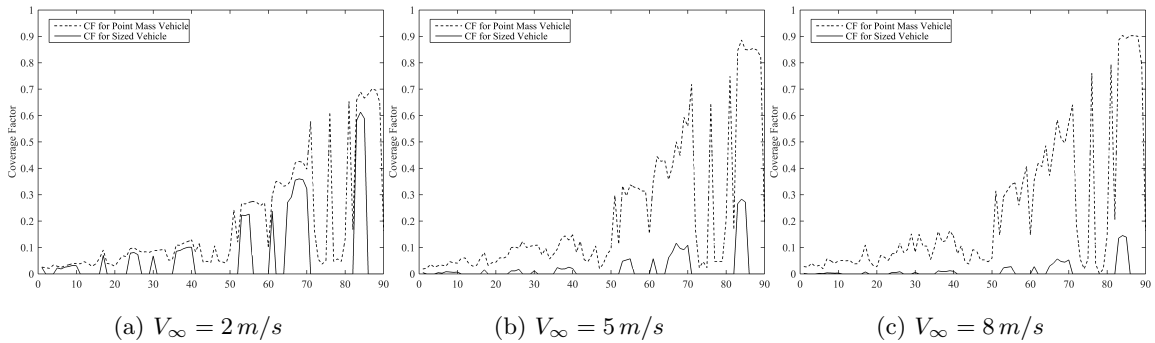


Figure 103: Coverage Factor comparisons for REMUS style vehicles modeled as point masses versus sizing and synthesis

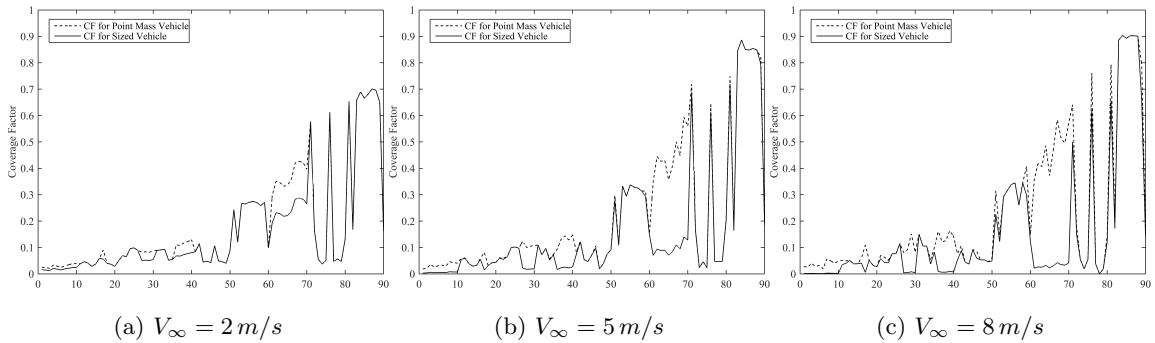


Figure 104: Coverage Factor comparisons for RMMV style vehicles modeled as point masses versus sizing and synthesis

The results of the charts show that the effect of vehicle endurance on the operational capabilities of the systems is not as large when the sensors are modeled according to the VXE approach. However, there are still significant effects, especially for the REMUS-style vehicles. The RMMV-style vehicles do not show as much of an endurance-limited effect because most of the RMMV-style vehicles have an endurance which is greater than or equal to the mission time. Once again, this is another significant observation for collaborative operational planning of vehicles in a search mission. It shows that trade-offs between vehicle designs can have a large impact on overall effectiveness when the vehicles are energy-limited. Trade-offs can therefore be made between vehicle performance capabilities and other requirements, such as transportability, reliability, cost, etc.

7.5 A Foundation for SoS Analysis and Design

Experiment Set B provided data and analyses for expressing the importance in modeling systems through an energy-based approach. Often in SoS analysis and design, vehicles and systems are modeled as little more than point-masses as was pointed out throughout this dissertation. In some situations, that level of detail may be fine. However, for analyzing alternative SoS which must collaboratively accomplish a mission under constrained requirements, system capability as a function of energy-limited processes is important.

As can be seen, there are significant trade-offs that can be considered in choosing a vehicle with the appropriate sensing and maneuvering properties to best complete a mission. Most of the designs delineated here have varying performance capabilities in terms of not only range, endurance and speed, but also in terms of probabilistic sensor capability. Consequently, the question stands as to which vehicle-sensor combination will best be capable of performing the search mission? Even more so, what combination of vehicles with associated sensors would best provide the desired search capabilities (or confidence) with a minimal amount of time and effort?

CHAPTER VIII

EXPERIMENT SET C: SYSTEM-OF-SYSTEMS LEVEL

The previous two chapters supported the fact that there are significant trade-offs that can be considered in choosing a vehicle with the appropriate sensing and maneuvering properties to best complete a mission. The system-level designs considered had varying performance capabilities in terms of not only range, endurance and speed, but also in terms of probabilistic sensor capability. The system-level performance variations were built on the accepted approach of sizing a vehicle to balance volume and energy in order to complete a set of requirements. The requirements included payload capacity and available energy to meet the demands of the subsystems and vehicle kinetics. The variations in subsystem-level design were due to an energy-based approach of bridging the gap between sensor performance and vehicle operations. By simulating the sensors in a physics-based virtual experimentation environment, relationships were created that mapped the probabilistic detection capability of the sensors with power and motion requirements.

Analysis and design at the SoS and mission level can be approached in many ways and take many perspectives. The existing statements for defining the overarching goals in designing a system-of-systems are numerous, but one relevant to this dissertation and this chapter is that “systems-of-systems are large-scale integrated systems which are heterogeneous and independently operable on their own, but are networked together for a common goal. The goal...may be cost, performance, robustness, etc...” [81]. As others have pointed out, the evaluation of technologies for an SoS determines the relative benefit of a proposed technology on one or more metrics [19]. Some authors have looked at the development of robotic swarms as a system-of-systems, applying ant colony optimization and artificial immune systems to describe the individual system performance [128].

In this chapter, the energy-based approach applied to the subsystem and system levels of the previous two chapters will now be administered at the system-of-systems level. Through detailed SoS level experiments, this chapter will provide substantiation to the overarching hypothesis of this dissertation, namely that *an energy-based approach to analyzing system-of-system (SoS) components across multiple levels of the SoS hierarchy will enable more accurate and transparent trade-offs for SoS analysis of alternatives.* Accordingly, this chapter will not only present the energy-based approach developed for this work, but it will present other techniques that have become ubiquitous with SoS analysis. These other approaches have been highlighted throughout this dissertation repeatedly up to this point, so a concise synopsis of the shortcomings is provided here:

- The subsystem level of SoS analysis and design is often simplified to a set of homogeneous sensors that are not affected by operational considerations such as vehicle velocity.
- The system level of SoS analysis and design is often simplified to a set of point-mass vehicles which are not affected by sensor-payload requirements or fuel considerations.
- SoS level analyses often include limitations due to the above two bullet points, or the SoS is characterized by a global metric that does not provide specific mission performance quantification.
- The number of systems utilized within the SoS mission is often chosen either arbitrarily, or based strictly on the availability of systems.

This chapter will present results of the developed method in comparison with the shortcomings stated above. The application of the developed method will demonstrate new trade-off insights not gleaned through the other processes. After experimentation, the method will be formalized in a complete flowchart and placed alongside the generic top-down decision support process. In this way, the method will be made transparent so that it will be a process that is clear and repeatable by others. After all, a dissertation built around the development of a new method must inherently provide a clear road map for

others to not only use the method, but to understand the new benefits it provides. This chapter will highlight those benefits and answer the questions: “What are the differences between the results of the new approach and other techniques?”, and “What is the reason for those differences?”.

One final piece of the puzzle needed before those questions can be answered is a way to choose the number of vehicles that will be utilized in the SoS mission. In particular, how many vehicles will best cover the mission area? In the control systems and robotics literature, this problem is often simplified by assuming a number of robots, and then optimizing their movement to cover an area within a maximum cost (the cost is often time). Some research has been found which approaches the problem from a graph theory perspective in which a minimum number of tours is calculated for traveling a gridded area. However, solutions to this problem can be *NP*-hard and once again, the technique assumes all sensors and vehicles are homogeneous. Therefore, significant work has been put into developing a heuristic technique for determining the number of systems that should be used to cover an area when the systems have non-homogeneous sensing and vehicle performance capabilities. In this work, the vehicles are required to perform a single pass over the entire search area, but the requirement of multiple passes is arbitrary to add. This chapter will unfold as follows:

- Optimal control for an area coverage problem will be reviewed which leads to Experiment 6, which is exploratory in nature. It will present various point-mass multi-vehicle search simulations and observations will be noted.
- Multi-Integer Linear programming will be presented as an optimization scheme for subsystem and system level trade-offs as a function of SoS level effectiveness goals. The need for this optimization scheme comes out of the shortcomings presented in Experiment 6.
- A new heuristic approach to defining a number of systems to cover a search area will be presented.
- The full trade-off method for analyzing collaborative system-of-system alternatives

will be formalized, and Experiment 7 will demonstrate the full approach.

- Results and substantiation of the overarching hypothesis of this dissertation will be discussed.

8.1 Optimal Control for Area Coverage

Systems engineers usually approach the problem from a systematic, decomposition then recomposition perspective. Alternatively, a roboticist will often investigate the control of the individual systems along with an aggregation of control for the multi-robot collaboration. Research relevant to this dissertation includes work in the realm of optimal or complete *area coverage*. However, it is important to start from the simplest case and build up from there, so area coverage with a single vehicle is pertinent.

Complete coverage with single robots has been researched extensively. Some research efforts include spiraling algorithms [59] and back tracking [60]. It has also been suggested that the simplest routine is to move in a single direction until a border or object is encountered, and then turn around until another border is reached in a lawn-mower fashion [69]. Road-map coverage techniques (using graph theory and topological mathematics) can be useful, although solving for minimum paths can be *NP*-hard. A coverage algorithm for determining minimum tours and then defining the number of robots is given in [110]. Ultimately, however, determination of efficient and complete search and exploration strategies can be computationally intractable [126].

If some amount of *a priori* information is available for possible target locations in the form of probability distributions, then the search can be directed in more efficient paths [126, 180, 25, 71]. If communication is possible (which can be extremely limited in the underwater environment), then information can be shared among collaborative systems as the search progresses. In that way, the overall mission effectiveness can be significantly greater [34]. For multi-vehicle search schemes, other researchers have worked towards either centralized or decentralized control schemes [56]. Various factors strongly influence the overall effectiveness of the collaborative operation, including vehicle avoidance, separation distances, etc.

There are two main perspectives outlined above, which can come off as qualitative versus quantitative. The systems engineering approach can be extremely detailed in defining and decomposing the problem and offering architectural solutions that should be analyzed. On the other hand, the field of collaborative control can be very quantitative in analyzing particulars of control theory. However the full system integration is often lacking, with various simplifying performance assumptions made at the subsystem and system levels.

The rest of this section will demonstrate area coverage utilizing single- and multi-vehicle search schemes. It is shown through simulation without subsystem and system effects considered very deeply. In subsequent sections of this chapter, the experiments from the subsystem and system chapters are brought back into the fold for new collaborative vehicle experiments. Various linear programming optimization goals are delineated and the overarching hypothesis of this dissertation is substantiated.

8.1.1 Defining the System Dynamics

The movement of the systems are assumed to be constrained over the region:

$$R = \{(x, y) \in \mathbb{R}^2 : x_{min} \leq x \leq x_{max}, y_{min} \leq y \leq y_{max}\} \quad (80)$$

Note the assumption of no movement in the z -direction. The system level vehicles are defined by the set:

$$\bar{\mathbf{X}} = [X_1(\bar{d}_1, \bar{s}_1), X_2(\bar{d}_2, \bar{s}_2), \dots, X_n(\bar{d}_n, \bar{s}_n)] \quad (81)$$

where $\bar{\mathbf{X}}$ is a set of n specified systems, X_1, \dots, X_n , which are each a function of the system design variables, \bar{d}_n , and the subsystem design parameters, \bar{s}_n . Similarly,

$$\bar{\mathbf{p}} = [\bar{p}_1(t), \bar{p}_2(t), \dots, \bar{p}_n(t)] \quad (82)$$

is a set of n state vectors for each of the n systems as they progress throughout the mission (or process) time, t . The states of each system can also be specified in relation to position within the m -dimensional space, \mathbb{R}^m , where $\bar{p}_n(t) = f(p_{n,x}, p_{n,y})$, if $x, y \in \mathbb{R}^m$. The operational control of each system throughout the mission is defined by the set:

$$\bar{\mathbf{u}} = [\bar{u}_1(t), \bar{u}_2(t), \dots, \bar{u}_n(t)] \quad (83)$$

which are the control vectors for each of the n systems. The design of the systems, $\bar{\mathbf{X}}$, along with the permissible excitation inputs of the systems, $\bar{\mathbf{u}}(\mathbf{t})$, are fundamental in describing the dynamics of the systems in order to calculate the states over time, $\bar{\mathbf{p}}(\mathbf{t})$. A state-based approach allows the system designs and behaviors to be mapped to the mission processes through first-order differential equations [52].

The equations of motion over the $m = 2$ -dimensional space for a single vehicle can be written as:

$$\begin{aligned} M(\ddot{p}_x - \dot{r}\dot{p}_y) &= \sum F_x = -D \cos \theta + T \cos \theta \\ M(\ddot{p}_y + \dot{r}\dot{p}_x) &= \sum F_y = -D \sin \theta + T \sin \theta \\ \ddot{r}I_{zz} &= N_A \end{aligned} \quad (84)$$

where \dot{r} is the angular velocity around the z -axis of the vehicle, I_{zz} is the moment of inertia around the same axis, N_A is the moment induced, M is the mass of the system, D is the drag of the vehicle, T is the thrust, and θ is the heading angle. The drag is expanded as:

$$\begin{aligned} D &= k\dot{p}^2 \\ \text{where } k &= \frac{1}{2}\rho_\infty S_{ref} C_D \\ \text{and } \dot{p} &= \dot{p}_x / \cos \theta = \dot{p}_y / \sin \theta = \sqrt{\dot{p}_x^2 + \dot{p}_y^2} \end{aligned} \quad (85)$$

As a matter of simplification, it is assumed that the rates of rotation are negligible (therefore turns are instantaneous). The differential dynamic equations are then:

$$\begin{aligned} \ddot{p}_x &= -\frac{k}{M \cos \theta} \dot{p}_x^2 + \frac{T}{M} \cos \theta \\ \ddot{p}_y &= -\frac{k}{M \sin \theta} \dot{p}_y^2 + \frac{T}{M} \sin \theta \end{aligned} \quad (86)$$

which are non-linear. In order to linearize the equations of motion, the equilibrium point is defined as a velocity, \dot{p}_e , which is independently chosen depending on the operational requirement¹. In accordance with Equation 86, the directional velocities \dot{p}_x and \dot{p}_y can be redefined as the total velocity, $\dot{p} = \dot{p}_e$, which also allows the $\cos \theta$ and $\sin \theta$ terms to drop out.

¹The operational requirement may be based on desired range, endurance, speed, sensor performance, etc. For maximum range of a propeller driven vehicle the Carson speed may be a useful equilibrium velocity due to the gradient of the velocity versus power required curve around the Carson velocity [8].

After linearization through the Taylor series expansion, the A and B state-representation matrices result in the forms shown in Equation 87. The state and control vectors are shown in Equation 88.

$$\mathbf{A}(t) = \begin{bmatrix} 0 & 0 & 1 & 0 \\ 0 & 0 & 0 & 1 \\ 0 & 0 & -\frac{2k}{M}\dot{p}_e & 0 \\ 0 & 0 & 0 & -\frac{2k}{M}\dot{p}_e \end{bmatrix} \quad \mathbf{B}(t) = \begin{bmatrix} 0 & 0 \\ 0 & 0 \\ \frac{T}{M} & 0 \\ 0 & \frac{T}{M} \end{bmatrix} \quad (87)$$

$$\mathbf{p}(t) = \begin{bmatrix} p_x \\ p_y \\ \dot{p}_x \\ \dot{p}_y \end{bmatrix} \quad \mathbf{u}(t) = \begin{bmatrix} \cos \theta \\ \sin \theta \end{bmatrix} \quad (88)$$

Therefore, $\dot{\mathbf{p}} = \mathbf{A}(t)\mathbf{p}(t) + \mathbf{B}(t)\mathbf{u}(t)$ is linear and time-varying. According to this setup, the thrust T is assumed constant throughout the mission. The controlled heading, θ , is determined through specified path planning strategies evaluated at each time step. Similarly, other control input excitations can be defined, including control surface deflections and attitude control thrusters if installed. However, the scope of this work is not to implement vehicle control strategies, but rather to observe the effect of varying subsystem and system designs on the overall mission capabilities of a group of collaborative systems. Therefore, the kinematics of the systems, as was outlined above, is relevant, along with the operational control (*i.e.*, path planning), but the underlying layers of system control are outside of the scope. Nonetheless, this is a very interesting area that can, and should, be investigated through future work.

Energy consumption throughout the mission and the rate at which it is consumed (power) can be modeled. Since the power required for motion is a function of the dynamics of the system, the energy consumption is calculated throughout the full simulation time. Also, if it is assumed that sensor power is the only relevant subsystem on-board for now (implying perfect or no communications), then the total energy consumed over time

(*i.e.*, the total power) is calculated as shown in Equation 89.

$$\begin{aligned}
 P_{total} &= P_{motion} + P_{sensor} = \frac{dE_{total}}{dt} \\
 \dot{E}_{total} &= D\dot{p} + P_{sensor} = k\dot{p}^3 + P_{sensor} \\
 \dot{E} &= k\dot{p}_e^3 + P_{sensor}
 \end{aligned} \tag{89}$$

8.2 *Experimental Approach*

The experimental setup across all levels of the SoS hierarchy originally presented in Chapter 4 is shown again in Figure 105. At the system-of-systems (SoS) level, which is the subject of this chapter, two experiments are provided: 6 and 7. Experiment 6 explores the mission behavior of systems-of-systems developed through the *old* approach. In particular, the subsystems are based on the old modeling processes, and the vehicles are represented by point-masses. This should be evident since Experiment 6 follows the left hand path in Figure 105. From Experiment 6, shortcomings will be observed in the old approach. That will lead to the development of an optimization scheme and a new path planning approach. Finally, Experiment 7 will use the new energy-based methods produced and formalized by this dissertation, along with the optimization and path planning schemes, to provide a final platform for testing all of the developments of this work. In other words, Experiment 7 demonstrates the full substance of this dissertation.

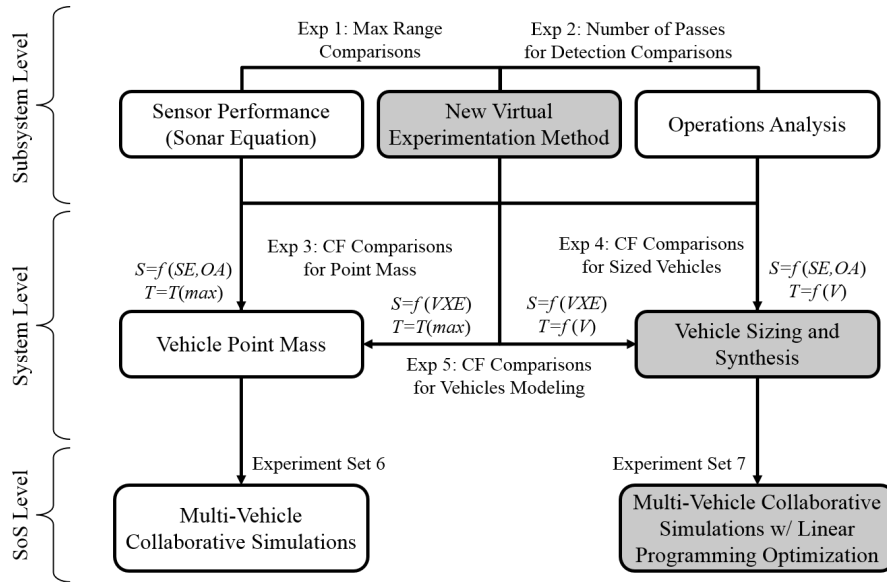


Figure 105: Decomposed Level-by-Level Experimental Approach

8.3 Experiment 6: SoS Modeling of Point-Masses and Simplified Sensors

As an example, it is appropriate to begin with a single vehicle and simple path planning logic. For subsequent examples, the number of vehicles and complexity of operational control (*e.g.*, vehicle avoidance, way-point sharing) will be increased. Sensor power is initially scaled as a function of sensor radius. This simplification will later be appended with actual sensor power-range relationships. These examples are intended to provide a feel for the effect of parameter variations on potential performance (*i.e.*, area coverage as a function of time).

It is assumed that full coverage of the area, R , is desired and there are no obstacles or barriers within the area that must be avoided. In addition to area coverage, maximum area coverage rate is desired. Therefore, *Brownian* motion and random walks are likely inefficient [41]. In order to simplify the path planning for this example, the region R is discretized into a grid dependent on the sensor radii. For a sensor on vehicle n with radius σ_n , the grid points of interest are distributed among r points in the x -direction and s points

in the y -direction:

$$\begin{aligned}
q_{i=1,\dots,r} &= x_{min} + (2i - 1)\sigma, \quad \text{where } r = \left\lfloor \frac{2\sigma_n}{x_{max} - x_{min}} \right\rfloor \\
q_{j=1,\dots,s} &= y_{min} + (2j - 1)\sigma, \quad \text{where } s = \left\lfloor \frac{2\sigma_n}{y_{max} - y_{min}} \right\rfloor \\
\text{and } q_{ij} &= (q_i, q_j)
\end{aligned} \tag{90}$$

The sensor radius, σ_n , is the sensor range defined on one side of the vehicle. Therefore, it would be half of an effective sweep width calculation.

Next, logic for determining the grid points to be searched and in what order must be defined. It is assumed that single pass search is sufficient, so each q_{ij} only needs to be visited once by the associated vehicle. Therefore, a set $\mathbb{Q}(t)$ is defined which contains the grid points to be searched at time t . Subsequently, at time $t = 0$, $q_{\forall i, \forall j} \in \mathbb{Q}(t_0)$. The goal of the search is that at time $t = t_f$, $q_{\forall i, \forall j} \notin \mathbb{Q}(t_f) = \emptyset$. The initial conditions are:

$$\begin{aligned}
(p_x(0), p_y(0)) &= (p_x(t_f), p_y(t_f)) = (0, 0) \\
\dot{p}(0) &= \dot{p}(t_f) = 0 \\
u_1(0) &= \theta(0) = \pi/4
\end{aligned} \tag{91}$$

The heading, $\theta(t)$, is calculated as the angle in the direction of the closest $q_{i,j} \in \mathbb{Q}(t)$. If more than one q_{ij} is available, the heading angle is selected to minimize $\theta(t+1) - \theta(t)$ (*i.e.*, continue in the current direction if possible). When $\mathbb{Q}(t) = \emptyset$, the heading is set towards $(p_x, p_y) = (0, 0)$.

The first example simulation was executed with one vehicle as shown in Figure 106. The results make intuitive sense in that the search tracks follow the path for the nearest point, q_{ij} . The vehicle decided to head in the $\theta = \pi/2$ direction after arriving at the first point of the grid. It returns to the starting point after completing all points, which occurred near the center of the grid. The yellow circles in the chart represent the sensor radius. They are *not* plotted at every time step.

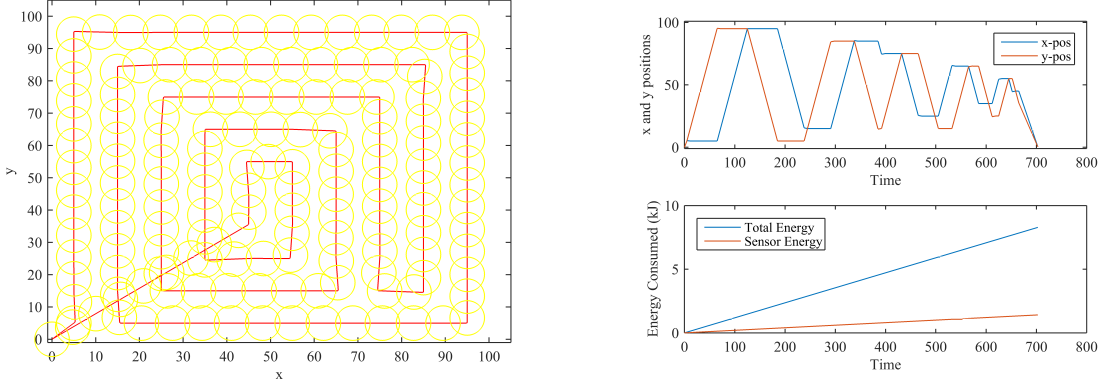


Figure 106: One Vehicle, $V_{\infty} = 3 \text{ m/s}$, $\sigma = 5 \text{ m}$, $t_f = 0.2 \text{ hr}$, $P_s = 2 \text{ W}$, $E_f = 8.3 \text{ kJ}$

Now, the coverage factor will be presented for the above simulation. Recall that according to the ideal coverage factor equation, the amount of time for a vehicle to ideally cover 100% of a region is $T = A_s/(V_{\infty}S)$, where A_s is the total search area and S is the effective sweep width of the vehicle. This was solved for from the ideal coverage factor shown in Equation 92 with $\lambda_I = 1$. The random motion coverage factor is shown in Equation 93. The ideal coverage can be considered an upper bound on performance, whereas the random coverage is a lower bound. The time for random coverage is $T_r = -A_s \ln(1 - \lambda_r)/(V_{\infty}S)$, where a percent coverage needs to be selected as less than unity due to the asymptotic nature of the logarithm.

$$\lambda_I(t) = \frac{A(t)}{A_S} = \frac{V_{\infty}St}{A_S} \quad (92)$$

$$\lambda_r(t) = 1 - e^{-\frac{V_{\infty}wSt}{A_S}} \quad (93)$$

For the first simulation provided above (Figure 106), the *calculated*, theoretical time for ideal coverage is $T_I = 0.1 \text{ hr}$. The theoretical random coverage time for 98% coverage is 0.36 hr . According to the coverage factor, the search pattern produced by proceeding to the nearest way-point is not ideal, but it is much closer to ideal than the random pattern. Part of the increased time is due to the vehicle traveling back to the initial starting point, which causes the search pattern to overlap some of the already searched region. Accordingly, $T_I = 0.1 < T = 0.2 < T_r = 0.36$ hours.

The second simulation was executed with two vehicles as shown in Figure 107. The sensor on the second vehicle has twice the range of the first vehicle. However, the vehicles

have no knowledge of each other or each other's search grids. Therefore, the first vehicle performs exactly the same as in the first case. Obviously, without collaboration the total energy will be greater, although the probability of detecting objects would also be greater because of multiple vehicles passing over the same area. Note that the vehicle velocities are the same for both vehicles, but since the second vehicle has greater sensor range, it is able to complete the mission faster and with less total energy. Also, the coverage factor time for the first vehicle is the same as in the first simulation, but now the second vehicle coverage factor time are different. In particular, $T_I = 0.05 < T = 0.1 < T_r = 0.18$ hours.

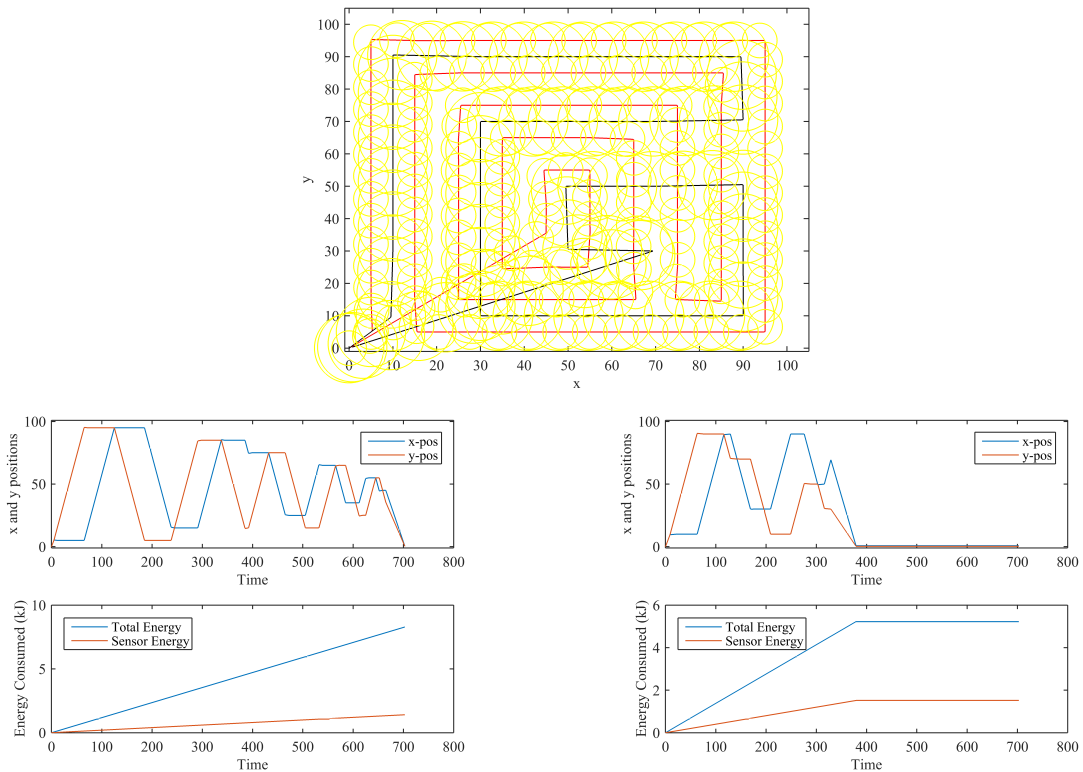


Figure 107: Two Vehicles, $V_{\infty, \forall i} = 3 \text{ m/s}$, $\sigma = (5, 10) \text{ m}$, $t_f = (0.2, 0.1) \text{ hr}$, $P_s = (2, 4) \text{ W}$, $E_f = (8.3 + 5.2) = 13.5 \text{ kJ}$. No way-point collaboration; No vehicle avoidance.

The third simulation shown in Figure 108 includes all of the same settings as the test case above, except the vehicles now have a complete knowledge of each other's search assignments. Therefore, if a vehicle sensor passes a way-point within 10% of the sensor range, that way-point will be removed from the other vehicle's queue. The total time is decreased compared to the second simulation when the vehicles were not collaborating.

In particular, the total time almost splits the time of the individual vehicle times from the non-collaborative simulation. The total energy is increased, but not by much. The energy increase is likely due to inefficient collaboration among the vehicles. In particular, the vehicles are sharing information about the way-points, so the actual path taken is not pre-planned. Accordingly, one vehicle can be on its way to a way-point, but if the other vehicle gets there first, the first vehicle has to turn away to a new way-point. This turns out to be an inefficient means of decentralized collaboration as compared to a centralized scheme in which all way-points are pre-planned and must be attended. As it turns out, the energy required to collaborate can actually make collaboration less efficient than not collaborating. Therefore, collaboration should be analyzed and designed to achieve more efficient results if it is to be implemented.

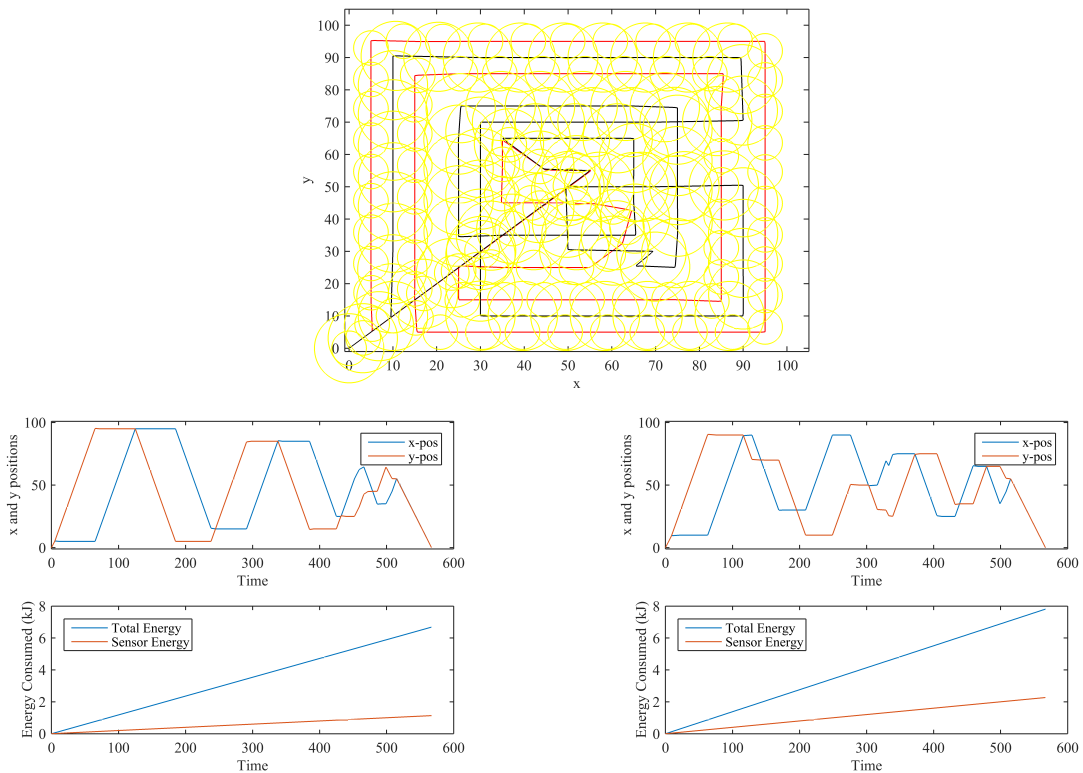


Figure 108: Two Vehicles, $V_{\infty, \forall i} = 3 \text{ m/s}$, $\sigma = (5, 10) \text{ m}$, $t_{f, \forall i} = 0.16 \text{ hr}$, $P_s = (2, 4) \text{ W}$, $E_f = (6.7 + 7.8) = 14.5 \text{ kJ}$. With way-point collaboration; No vehicle avoidance.

Another interesting result of the above simulation is the total time of the mission, which was 0.16 hrs for each vehicle. For the first vehicle, the ideal, actual and random coverage

factor times were $T_I = 0.1 < T = 0.16 < T_r = 0.36$ hours (recall the previous simulation had 0.2 hrs for the first vehicle). The bounds around the actual time for the second vehicle are different, but the actual time was still within the bounds. The lower theoretical bound for the second vehicle is $T_I = 0.05 \text{ hr}$ and the upper bound for random motion is $T_r = 0.18 \text{ hr}$. The actual time was $T = 0.16 \text{ hr}$. However, even though both vehicles' actual times were within the theoretical coverage factor bounds, there is no guarantee that they will be bounded by the theoretical limits in the presence of collaboration. The bounds are truly relevant if the vehicles' search paths are independent and the search areas are completely separate for each vehicle.

In the fourth simulation shown in Figure 109, the vehicles do not collaborate, but they do try to avoid each other. This is clear in the beginning of the mission when they separate into different directions. For this case, the avoidance without collaboration did not have a large impact on time or energy as compared to the previous two simulations (no avoidance or collaboration and just collaboration, respectively). In this simulation the time was slightly increased for the second vehicle as compared to the simulation with no collaboration or avoidance, along with slightly more energy used. On the other hand, the total energy used was about the same as the simulation with just collaboration.

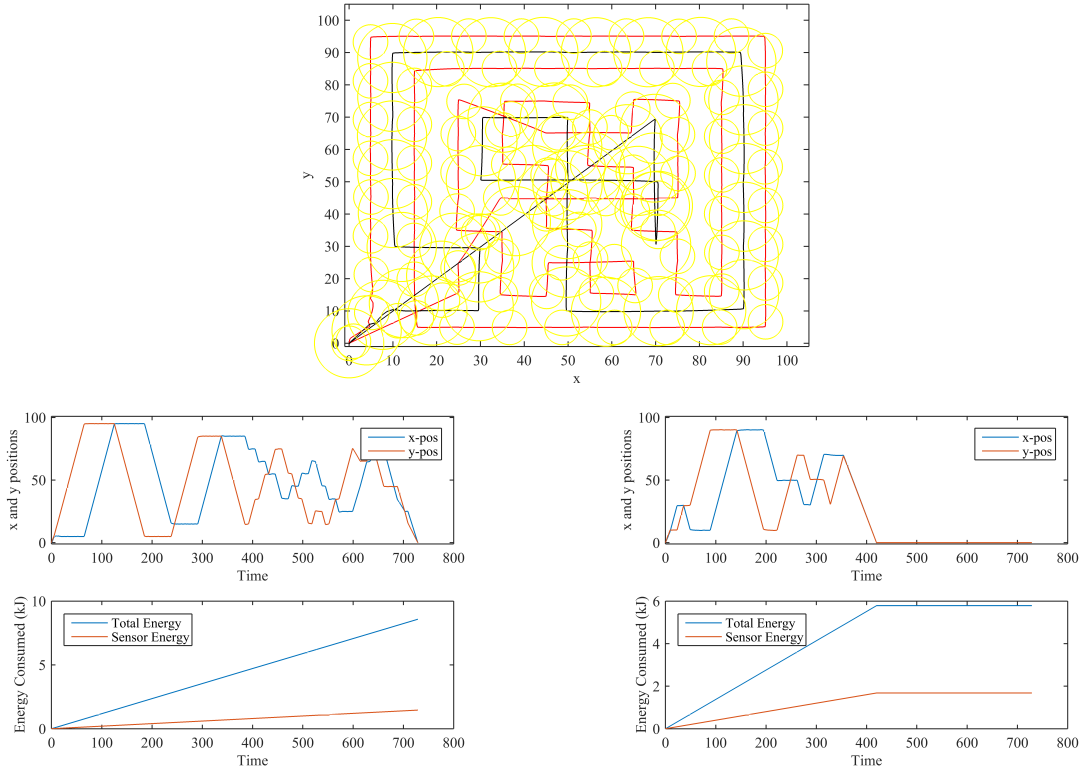


Figure 109: Two Vehicles, $V_{\infty, \forall i} = 3 \text{ m/s}$, $\sigma = (5, 10) \text{ m}$, $t_f = (0.2, 0.12) \text{ hr}$, $P_s = (2, 4) \text{ W}$, $E_f = (8.6 + 5.8) = 14.4 \text{ kJ}$. No way-point collaboration; With vehicle avoidance.

In the fifth simulation shown in Figure 110, the vehicles collaborate and avoid each other. For this case, collaboration with avoidance took a similar amount of time as compared with the previous cases, however there was a slight increase in energy consumption. The energy increase is counterintuitive since it is expected that collaborative operations should help groupings of systems to be more efficient at their task. By more closely examining this simulation, it becomes evident that the increase in energy consumption is due to the vehicle queues being constantly updated by each other. Therefore, while a vehicle is on its way to one way-point, if that way-point is acquired by the other vehicle, the first vehicle has to then back-track to a new way-point.

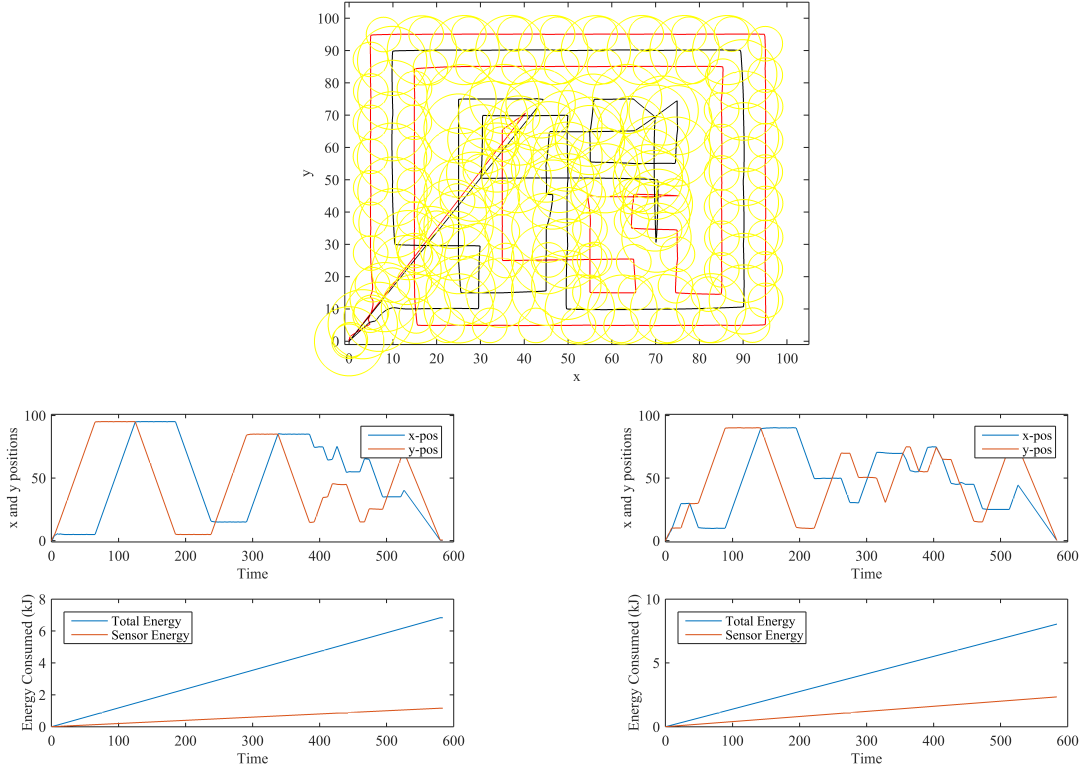
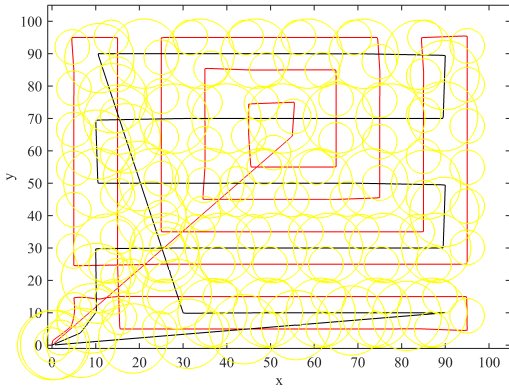
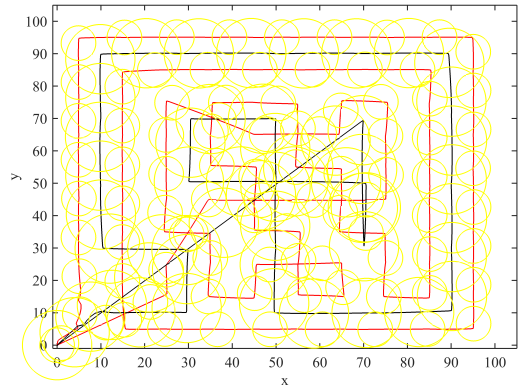


Figure 110: Two Vehicles, $V_{\infty, \forall i} = 3 \text{ m/s}$, $\sigma = (5, 10) \text{ m}$, $t_{f, \forall i} = 0.16 \text{ hr}$, $P_s = (2, 4) \text{ W}$, $E_f = (6.8 + 8.0) = 14.8 \text{ kJ}$. With way-point collaboration; With vehicle avoidance.

The avoidance scheme used in the previous simulations utilized the concept of specular reflection for *both* vehicles involved in the interaction. In other words, each vehicle would reflect away from the other vehicle specularly, as if the other vehicle was a plane wall. For the next two simulations, a different type of avoidance scheme was implemented in order to see how another small change in operations would impact the overall mission effectiveness. The new avoidance scheme includes a right-of-way rule in which the vehicle with the larger sensor always continues in its desired direction of travel, but the other vehicle must reflect specularly when an interaction occurs. The results of the new avoidance scheme compared to the old avoidance scheme without and with collaboration are shown in Figures 111 and 112, respectively.



(a) New avoidance, no collaboration



(b) Original avoidance, no collaboration (from Fig. 109)

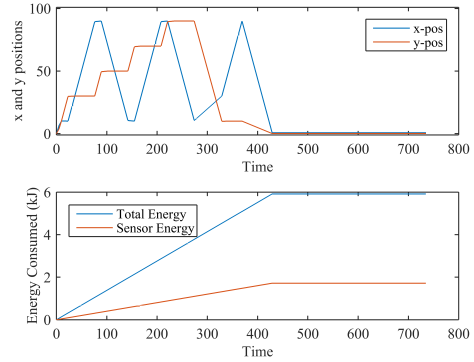
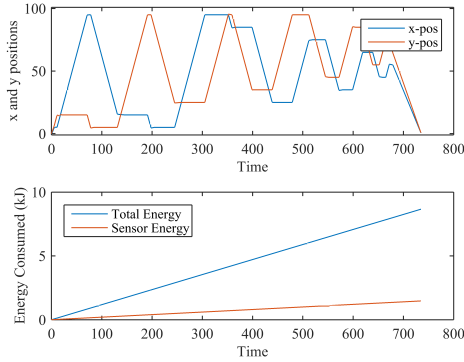
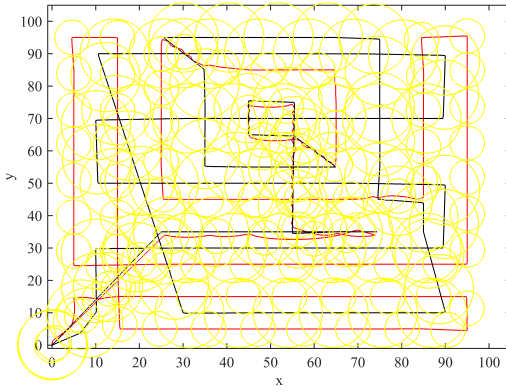


Figure 111: Two Vehicles, $V_{\infty, \forall i} = 3 \text{ m/s}$, $\sigma = (5, 10) \text{ m}$, $t_f = (0.2, 0.12) \text{ hr}$, $P_s = (2, 4) \text{ W}$, $E_f = (8.6 + 5.9) = 14.5 \text{ kJ}$. No way-point collaboration; With new vehicle avoidance. Position and energy plots are associated with plot (a).

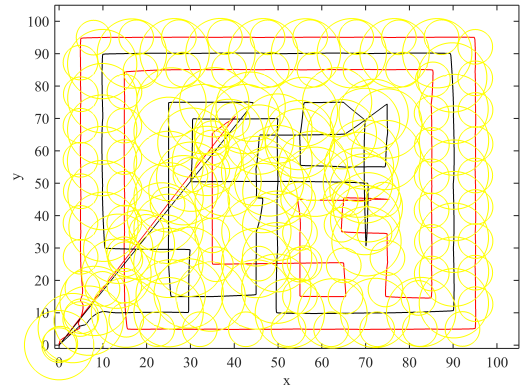
The behavior that emerged in Figure 111 for the new avoidance scheme with no collaboration is very interesting. The vehicle with the larger sensor range is shown with the black track-line in Figure 111(a); it is the vehicle with the right-of-way. In this simulation, the search pattern that emerged for the right-of-way vehicle was a structured lawn-mower pattern. In comparison, the typical type of pattern that emerged under the old scheme was a concentric square pattern such as shown during the beginning of the mission in Figure 111(b). This pattern also emerged for the single-vehicle and two-vehicle scenarios in all of the previous simulations (Figure 106-110). Also, the secondary vehicle with the smaller sensor range in Figure 111(a) resolves into the typical concentric square pattern after it has

reflected away from the other vehicle. Once again, this change in avoidance scheme demonstrates how seemingly simple perturbations at one level of the SoS hierarchy can have large impacts on how the mission will progress. However, for this example, the mission time and energy consumption were very similar to the results from the previous avoidance scheme.

In Figure 112, the new avoidance is applied along with vehicle collaboration. The difference in mission progression over time between the new and old avoidance schemes can be seen by comparing the (a) and (b) tracks in Figure 112. In this case, the average mission time and energy consumption actually increased significantly compared to all of the previous simulations, including the new avoidance simulation with no collaboration. The counterintuitive observation of greater energy consumption for utilizing a collaborative scheme is apparent.



(a) New avoidance, with collaboration



(b) Original avoidance, with collaboration (from Fig. 110)

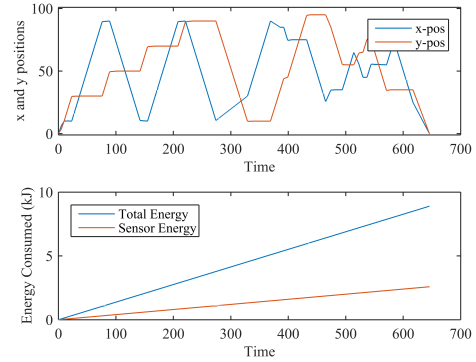
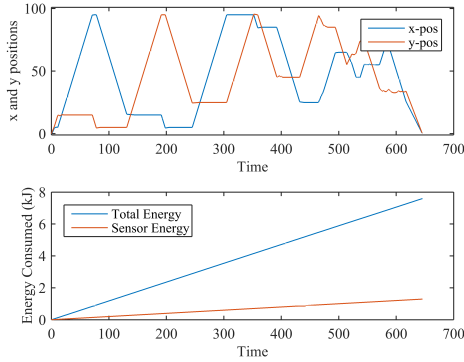


Figure 112: Two Vehicles, $V_{\infty, \forall i} = 3 \text{ m/s}$, $\sigma = (5, 10) \text{ m}$, $t_{f, \forall i} = 0.18 \text{ hr}$, $P_s = (2, 4) \text{ W}$, $E_f = (7.6 + 8.9) = 16.5 \text{ kJ}$. With way-point collaboration; With new vehicle avoidance. Position and energy plots are associated with plot (a).

Next, in the simulation shown in Figure 113, the thrust of each vehicle was increased which subsequently raised the velocity of each vehicle. The original avoidance scheme (both vehicles reflecting specularly) is implemented. It is clear by examining the results of the simulation that increasing the vehicle velocities helped to decrease the time of the mission. However, the energy consumption is significantly greater than the previous simulations since the energy of motion grows at the rate of velocity cubed.

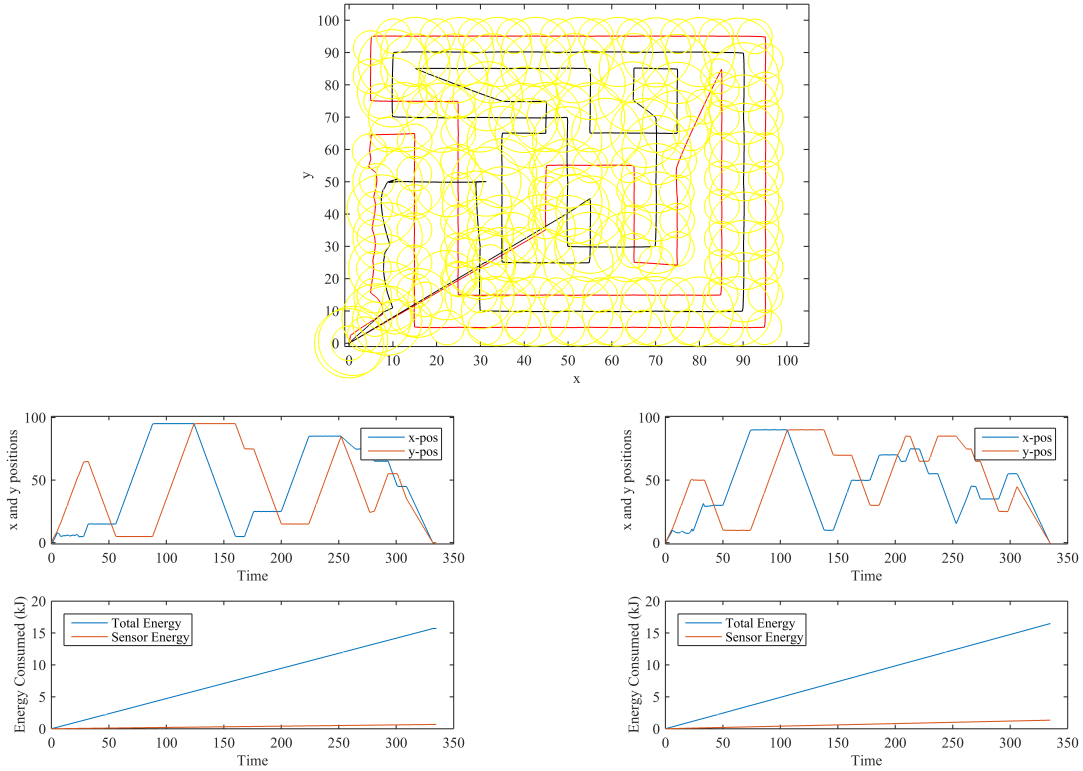


Figure 113: Two Vehicles, $V_{\infty,vi} = 5 \text{ m/s}$, $\sigma = (5, 10) \text{ m}$, $t_f = 0.1 \text{ hr}$, $P_s = (2, 4) \text{ W}$, $E_f = (15.7 + 16.5) = 32.2 \text{ kJ}$. With way-point collaboration; With vehicle avoidance.

The quantitative variables and results of the 8 simulations shown so far are given in Table 5. The table conveys the number of vehicles in each simulation, n , whether or not collaboration and/or avoidance is implemented, *coll.* and *avoid.*, the sensor ranges, σ , the vehicle velocities, V_{∞} , the simulation area, A , the mission time for each vehicle, t , and the energy consumption for each vehicle, E_T . The values on the left-side of the energy column are total energy, and the values on the right-side are the sensor energy: total/sensor. The energy values for each vehicle are shown, and the sum of the energy of all vehicles is shown under each horizontal bar.

Table 5: Single- and Dual-Vehicle Simulation Data

| Case | n | coll. | avoid. | σ (m) | V_{∞} (m/s) | A (km ²) | t (hr) | E_r (kJ) Veh/Sen |
|------|-----|-------|---------|--------------|--------------------|------------------------|------------------|----------------------------------|
| 1 | 1 | N/A | N/A | 5 | 3 | 0.01 | 0.2 | 8.3/1.4 |
| 2 | 2 | N | N | {5,10} | $3 \forall i$ | 0.01 | {0.2,0.1} | 8.3/1.4 5.2/1.5 13.5/2.9 |
| 3 | 2 | Y | N | {5,10} | $3 \forall i$ | 0.01 | $0.16 \forall i$ | 6.7/1.1 7.8/2.3 14.5/3.4 |
| 4 | 2 | N | Y | {5,10} | $3 \forall i$ | 0.01 | {0.2,0.12} | 8.6/1.5 5.8/1.7 14.4/3.2 |
| 5 | 2 | Y | Y | {5,10} | $3 \forall i$ | 0.01 | $0.16 \forall i$ | 6.8/1.2 8.0/2.3 14.8/3.5 |
| 6 | 2 | N | Y (new) | {5,10} | $3 \forall i$ | 0.01 | {0.2,0.12} | 8.6/1.5 5.9/1.7 14.5/3.2 |
| 7 | 2 | Y | Y (new) | {5,10} | $3 \forall i$ | 0.01 | $0.18 \forall i$ | 7.6/1.3 8.9/2.7 16.5/4.0 |
| 8 | 2 | Y | Y | {5,10} | $5 \forall i$ | 0.01 | $0.1 \forall i$ | 15.7/0.7 16.5/1.3 32.2/2.0 |

Key Points to Note The simulations above have supported the statements made throughout this work that multiple levels of the SoS hierarchy should be closely examined in designing a collaborative SoS. In particular, the operational concepts were varied in the simulations in a simple fashion, and yet performance varied significantly. At the system-level, a small change in velocity caused better mission time but also resulted in twice as much energy consumption. Furthermore, it must be noted that the greater velocity present in the eighth simulation shown in Figure 113 has no functional link to the sensor performance. There should be a larger effect on mission performance which is not present due to this simplification. This is often a simplifying assumption made implicitly in operational planning and robotics literature. Therefore, the overall mission effectiveness is over-estimated. This shortcoming will be substantiated further through experiments provided in later sections in this chapter to be presented. But for now it is important to point out that this type of overestimation of mission effectiveness was one of the main drivers and observations in developing the overarching hypothesis of this dissertation, namely that *an energy-based approach to analyzing system-of-system (SoS) components across multiple levels of the SoS hierarchy will enable more accurate and transparent trade-offs*

for SoS analysis of alternatives. The next few simulations show results similar to those presented above, except with larger search areas implemented, and therefore greater numbers of vehicles.

Increased Search Area The next simulation, shown in Figure 114, includes an increased search area of $1000 \times 1000 m^2$. The previous simulations used a $100 \times 100 m^2$ search area. Accordingly, the mission below includes more vehicles, but there is no direction on how many vehicles exactly to use at this point. The sensor ranges have also been increased to *25 meters*, and the sensor power is scaled up to *10 Watts*. The search time has increased significantly, from a scale of minutes to hours. Similarly, the energy expended has jumped up an order of magnitude compared to the previous simulations.

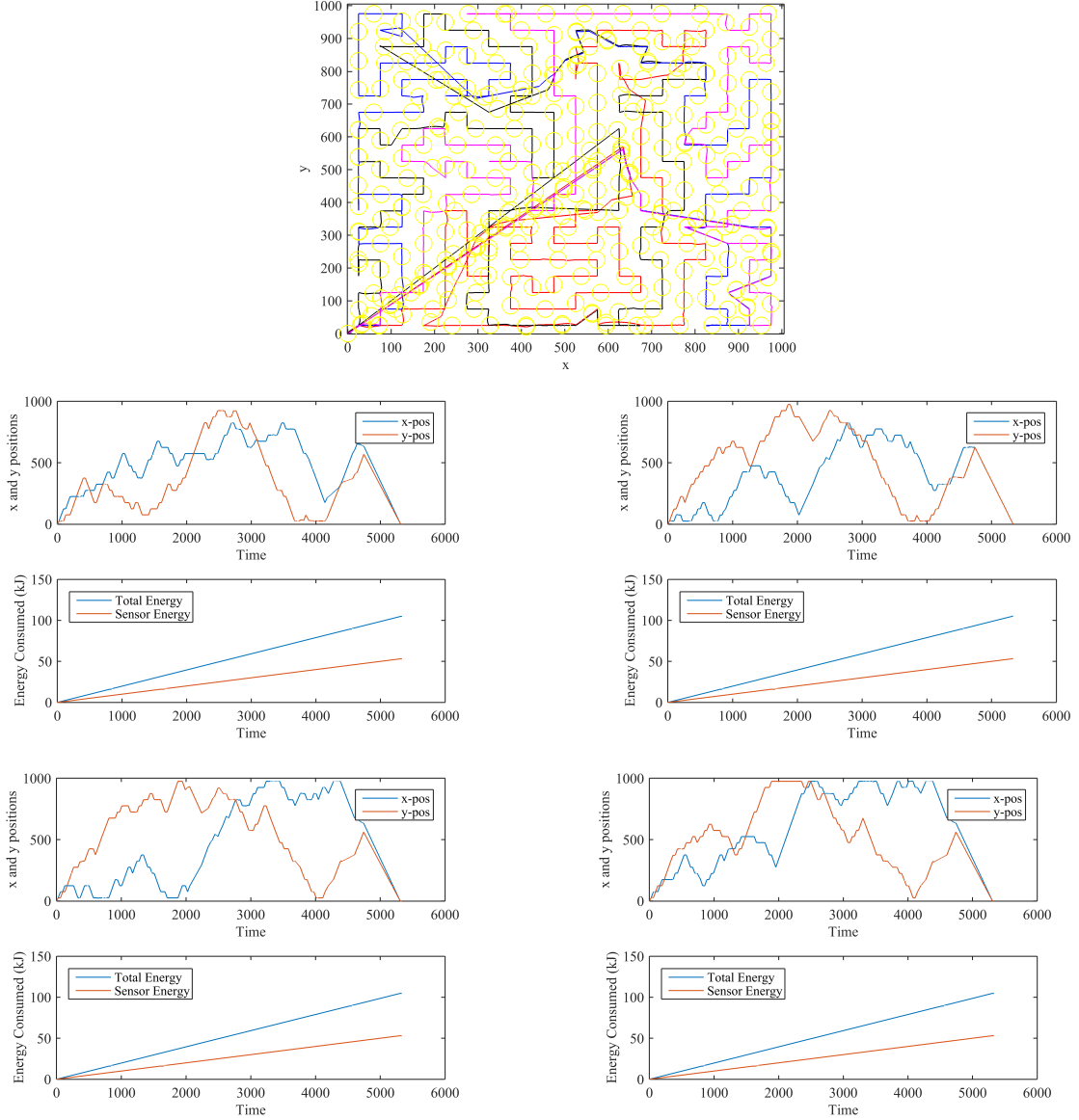


Figure 114: Four Vehicles, $V_{\infty, \forall i} = 3 m/s$, $\sigma_{\forall i} = 25 m$, $t_f = 1.48 hrs$, $P_{s, \forall i} = 10 W$, $E_f = (105 + 105 + 105 + 105) = 420 kJ$. With way-point collaboration; With vehicle avoidance.

The next simulation shown in Figure 115 includes all of the same characteristics as the previous simulation *except* for the sensor parameters. In the previous simulation, the sensors were homogeneous with a range of 25 meters and a power consumption of 10 W. In the following simulation, two vehicles have a sensor range of 20 meters with a power consumption of 8 W, and the other two vehicles have a sensor range of 30 meters with a power consumption of 12 W. The results were unexpected. In particular, the mission

time has almost doubled from 1.48 hrs to 2.6 hrs and the energy expended has similarly almost doubled from 420 kJ to 733 kJ. However, the only difference applied that caused the decrement in mission effectiveness was sensor range, and even that difference was not large. Two sensors had 5 m less range, and two sensors had 5 m more range. This is another example of the large impact that is possible on SoS performance due to a relatively small change in subsystem or system capability.

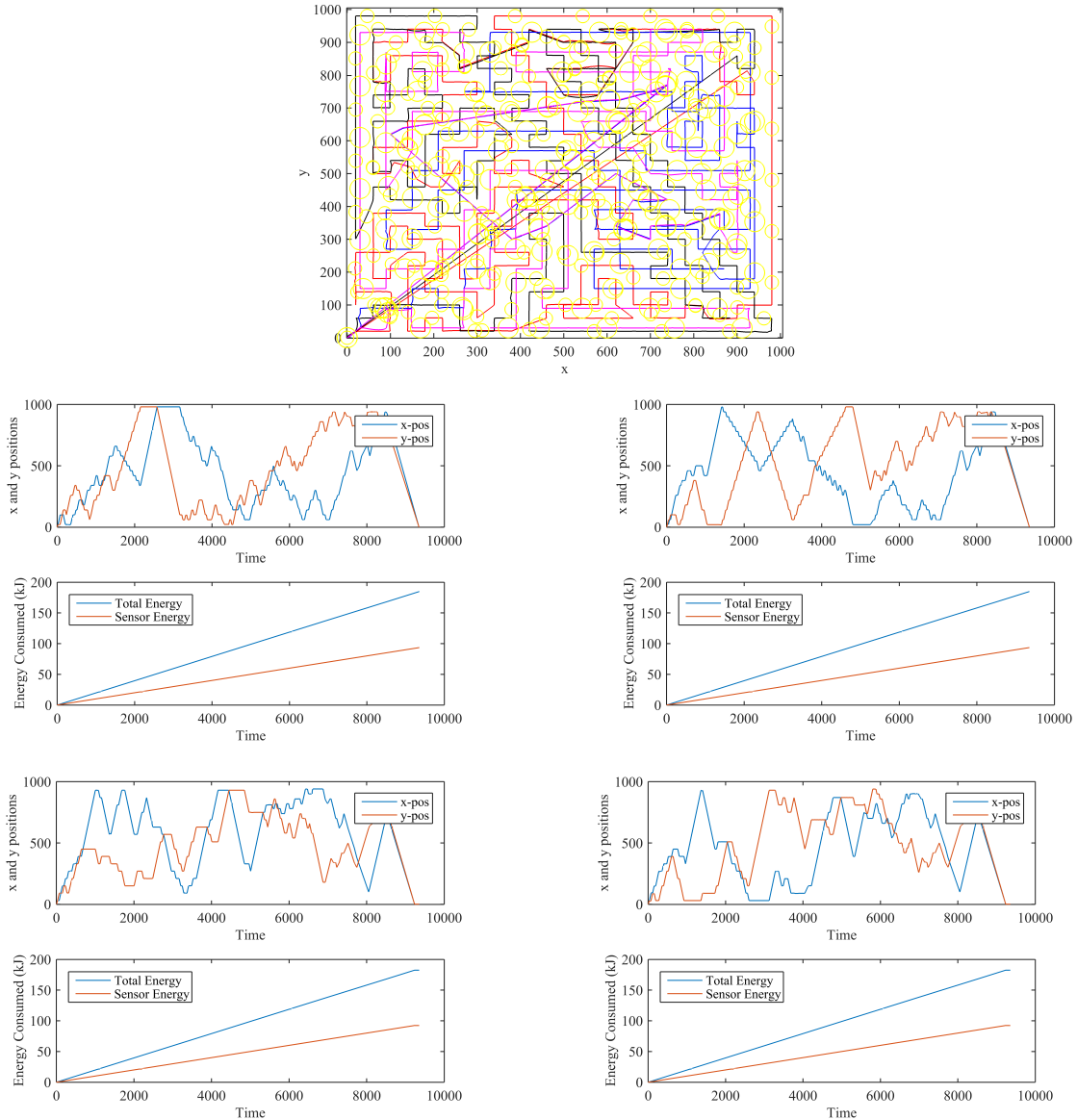


Figure 115: Four Vehicles, $V_{\infty,Vi} = 3\text{ m/s}$, $\sigma = (20, 20, 30, 30)\text{ m}$, $t_f = 2.6\text{ hrs}$, $P_s = (8, 8, 12, 12)\text{ W}$, $E_f = (184 + 184 + 182 + 183) = 733\text{ kJ}$. With way-point collaboration; With vehicle avoidance.

8.3.1 Recapitulation of Experiment 6 and Further Developments

The content of this section described an analytical formulation for analyzing alternative sensors and vehicles in a collaborative search mission. Experiments were executed for one, two and four vehicle architectures. In addition, sensor radius, sensor power, vehicle interactions, and vehicle thrust were minimally manipulated. It is apparent that even for a simple set of initial experiments, variations in performance can be significant, and sometimes counterintuitive.

A major take-away from Experiment Set 6 is that multiple factors influence the overall effectiveness of the collaborative mission. Factors such as the number of vehicles, sensor radii, sensor power, vehicle interactions, and vehicle thrust were minimally manipulated, and the impact was assessed. However, the simulations utilized the concept of point-mass systems in which the multiple-levels of the SoS hierarchy were not linked through an energy-based approach. Therefore, vehicle performance did not affect sensor performance or vis-versa. Consequently, trade-offs could not be effectively made between sensor selection, vehicle designs, and operational concepts.

Determining the combinations of sensors and vehicles that best perform the mission is not trivial. For that reason, the next section will systematically step through various performance measures for optimizing the effectiveness of the mission through combinations of sensors and vehicles that were designed in the subsystem and system analysis chapters.

8.3.2 Optimization Through Linear Programming

The desire is to minimize a set of performance measures, $\bar{\mathcal{F}}$, which are functions of the system designs, subsystem designs, the number of systems, the discretized states of the systems during a mission, and the operational control of the systems. Therefore,

$$\bar{\mathbf{X}} = [X_1(\bar{d}_1, \bar{s}_1), X_2(\bar{d}_2, \bar{s}_2), \dots, X_n(\bar{d}_n, \bar{s}_n)]$$

is a set of n specified systems, X_1, \dots, X_n , which are each a function of the system design variables, \bar{d}_n , and the subsystem design parameters, \bar{s}_n . Similarly,

$$\bar{\mathbf{p}} = [\bar{p}_1(t), \bar{p}_2(t), \dots, \bar{p}_n(t)]$$

is a set of n state vectors for each of the n systems as they progress throughout the mission (or process) time, t . The states of each system can also be specified in relation to position within an m -dimensional space, \mathbb{R}^m , where $\bar{p}_n(t) = f(p_{n,x}, p_{n,y})$, if $x, y \in \mathbb{R}^m$. The operational control of each system throughout the mission is defined by the set

$$\bar{\mathbf{u}} = [\bar{u}_1(t), \bar{u}_2(t), \dots, \bar{u}_n(t)]$$

which are the control vectors for each of the n systems. The design of the systems, $\bar{\mathbf{X}}$, along with the permissible excitation inputs of the systems, $\bar{\mathbf{u}}(\mathbf{t})$, are fundamental in describing the dynamics of the systems in order to calculate the states over time, $\bar{\mathbf{p}}(\mathbf{t})$. A state-based approach allows the system designs and behaviors to be mapped to the mission processes through first-order differential equations [52].

The set of performance measures to be minimized are functions of the variable sets specified above, subject to functional constraints, $\bar{\mathbf{G}}$. Side constraints can also be included.

$$\begin{aligned} \min \quad & \bar{\mathcal{F}} = f(\bar{\mathbf{X}}, \bar{\mathbf{p}}, \bar{\mathbf{u}}) \\ \text{subject to} \quad & \bar{\mathbf{G}} = g(\bar{\mathbf{X}}, \bar{\mathbf{p}}, \bar{\mathbf{u}}) \leq 0 \end{aligned} \tag{94}$$

The set of performance measures $\bar{\mathcal{F}}$ may result in a single- or multi-objective optimization scenario. The performance measures may include effectiveness metrics such as area coverage rate, fuel efficiency, minimum energy expenditure, and maximum situational awareness among others. Most practical engineering problems, especially on the scale of a collaborative grouping of systems, are multi-objective in nature. Therefore, there is likely not a single “best” solution, but rather a set of potential solutions that must be analyzed and decided between. If the control inputs are varied throughout the mission, then performance is also a function of time. If that is the case, the problem can be restated as an attempt to minimize the integral of the performance over the mission, task or process. The final time, t_f , may or may not be constrained.

$$\min \quad \bar{\mathcal{F}} = \int_0^{t_f} f(\bar{\mathbf{X}}, \bar{\mathbf{p}}, \bar{\mathbf{u}}) dt \tag{95}$$

Furthermore, the allowable variations of the system, subsystem, and operational control parameters ($\bar{\mathbf{X}}(\bar{\mathbf{d}}, \bar{\mathbf{s}}), \bar{\mathbf{u}}(\mathbf{t})$), have no guarantee of continuity. Similarly, the number of systems, n , utilized in the collaborative grouping is inherently discrete. Therefore, it cannot be

automatically assumed that any of the performance measures in the performance vector $\bar{\mathcal{F}}$ are smooth. An overarching question from a mathematical perspective is then: *how should changes be made to $\bar{\mathbf{X}}(\bar{\mathbf{d}}, \bar{\mathbf{s}})$, $\bar{\mathbf{p}}(\mathbf{t})$, and $\bar{\mathbf{u}}(\mathbf{t})$ in order to obtain minimized solutions for $\bar{\mathcal{F}}$?*

The subsystem and system analysis chapters produced hundreds of alternative vehicle and sensor combinations that can be included in the SoS operations. The system set $\bar{\mathbf{X}}$ is made up of the 120 sized vehicles from the system analysis chapter. There were actually 180 designs initially in the system set in accordance with the 180 sensor designs from the subsystem chapter, which make up the set $\bar{\mathbf{s}}$. However, 60 of the REMUS style vehicles could not converge on a sized solution for the associated 60 sensors with medium and high power requirements. Additionally, the design variables for each vehicle, $\bar{\mathbf{d}}$, include parameters such as the vehicle diameters, length, and fuel type (battery or diesel fuel).

The desire is to maximize mission effectiveness as a function of the vehicles, $\bar{\mathbf{X}}$. Since the set $\bar{\mathbf{X}}$ is discrete in nature, mixed-integer linear programming provides an appropriate path. The original problem formulation without control inputs is:

$$\begin{aligned} \min \quad & \bar{\mathcal{F}} = f(\bar{\mathbf{X}}(\bar{\mathbf{d}}, \bar{\mathbf{s}})) \\ \text{subject to} \quad & \bar{\mathbf{G}} = g(\bar{\mathbf{X}}(\bar{\mathbf{d}}, \bar{\mathbf{s}})) \leq 0 \end{aligned} \tag{96}$$

The general format for a mixed-integer linear programming problem with a single objective is:

$$\min \quad \mathbf{f}_x^T \quad \text{subject to} \quad \begin{cases} x(\gamma) \\ A \cdot x \leq b \\ Aeq \cdot x = beq \\ lb \leq x \leq ub \end{cases} \tag{97}$$

...where \mathbf{f} is a vector of cost coefficients, γ is a vector of integers, A is the linear inequality constraint matrix, b is the linear inequality constraint vector, Aeq and beq are similar for equality constraints, and lb and ub are vectors of lower and upper bounds for each variable, x .

In order to use the set of vehicles, $\bar{\mathbf{X}}$ in this problem, they must be reformatted to fit

the mixed-integer linear programming problem. This is done as follows:

$$x = [x(1)\bar{\mathbf{X}}_1, x(2)\bar{\mathbf{X}}_2, \dots, x(n)\bar{\mathbf{X}}_n] \quad (98)$$

...where $x(1) = 1$ means that vehicle $\bar{\mathbf{X}}_1$ has been chosen, and $x(1) = 0$ means that vehicle $\bar{\mathbf{X}}_1$ is not used. Recall that the subsystem chapter established 90 sensor designs with varying design and performance properties. The breakdown was 36 specific forward looking sonar (FLS) designs and 54 specific side scan sonar designs. Each sensor was executed through the virtual experimentation environment at 3 discrete velocities in order to create an energy-based functional link between sensor operations and sensor performance. In the system chapter, REMUS style and RMMV style vehicles were used as baselines for sizing new vehicles that could carry each of the 90 sensor designs. As it turned out, only 30 REMUS style vehicle were able to converge out of 90 attempts. The breakdown was 12 REMUS style vehicles with an FLS, and 18 with an SSS. The RMMV did much better in terms of convergence. All 90 of the sizing attempts were successful for the RMMV, resulting in 36 RMMV style vehicles with FLS installed and 54 with SSS installed. In total, there are $n = 120$ vehicles available for the optimization set $\bar{\mathbf{X}}$.

As was stated earlier, SoS design problems are multi-objective in nature. However, mixed-integer linear programming (MILP) desires a single cost function. Therefore, the SoS design problem can be restated to minimize a single cost function while other requirements are defined as constraints, either equality or inequality. Multi-objective mixed-integer linear programming techniques do exist and can be applied if desired, however development and application of such a technique is beyond the scope of this text.

Various cost coefficients can be tested and analyzed. Naturally, the desire is to maximize area coverage. The coverage effort was defined as:

$$ce_i = V_{\infty,i} S_i T_i \quad (99)$$

...where $V_{\infty,i}$ is the velocity of vehicle i , S_i is the effective sweep width, and T_i is the vehicle endurance. Note that T_i can be defined as either the vehicle endurance or the maximum allowed mission time, whichever is less. Also, for these experiments, each of the 120 vehicles can be defined to operate at any of the three discrete velocities defined earlier:

$V_\infty = (2, 5, 8) m/s$, which are the velocities at which effective sweep width experiments were executed. Accordingly, the full set of vehicles to be used in the linear programming optimization problem is $n = 360$, where every three vehicles are the same design, but with a different operational speed. Subsequently, both sensor and vehicle performance are affected since the design alternatives have energy-based functional links between the subsystem and system levels.

8.3.3 Cost Function Investigation

Maximize Coverage Effort: In order to maximize coverage effort, the cost function can be defined to minimize the negative of the aggregate coverage effort as shown in Equation 100. Without any constraints, the optimization would converge on a solution of unity for all integer variables, \mathbf{x} . An arbitrary constraint is to desire the ten vehicles with the greatest coverage effort. Accordingly, $Aeq \cdot x = 10$, where Aeq is just a unity vector. Recall that there are $n = 360$ designs to choose from when including operational speed as a variable.

$$\begin{aligned}
 \text{minimize } \mathbf{f}(\mathbf{x}) &= -\sum_{i=1}^n ce_i x(i) = -\sum_{i=1}^n V_{\infty,i} S_i T_i x(i) \\
 \text{subject to : } &\sum_{i=1}^n x(i) = 10 \\
 T_i &= \begin{cases} t_{i,endurance}, & t_{i,endurance} < T_{MissionMax} \\ T_{MissionMax}, & t_{i,endurance} \geq T_{MissionMax} \end{cases}
 \end{aligned} \tag{100}$$

The results of the ten vehicles with the greatest coverage effort are shown in Figure 116. In the chart shown, the solid diamond data points are the REMUS style vehicles while the open-circle data points are the RMMV style vehicles. The highlighted data-points represent the ten selected maximum *coverage effort* vehicles. Note that the $y - axis$ is the *coverage factor* for both the random and ideal cases. Therefore, the calculated coverage factors are the coverages for a single vehicle. All ten vehicles were RMMV style vehicles with SSS sensors installed. This intuitively makes sense since the RMMV vehicles have the greatest endurance capabilities (T). However, there is a subtle behavior in this data that immediately starts to reveal some effects of considering trade-offs at all levels of the SoS hierarchy through energy-based functionals. For example, the sensor-vehicle combinations

with the greatest ESW are not the best in terms of coverage effort and factor. This is because the vehicles with the greatest velocities were not the vehicles with the greatest endurance or the best effective sweep widths. This was the premise of Hypothesis 3 which was substantiated through the experiments and analyses provided in Chapter 6. Recall that Hypothesis 3 was established after observing that there is a missing link between sensor performance at the subsystem level and the operational components of the other levels of the hierarchy (vehicle performance and multi-agent grouping effects). Therefore, *if the SoS design space was not built-up through the subsystem and system levels using an energy-based approach, the trade-offs shown here would not be evident.* A representative example of one of the RMMV style designs that was a result of this optimization is shown in Figure 117.

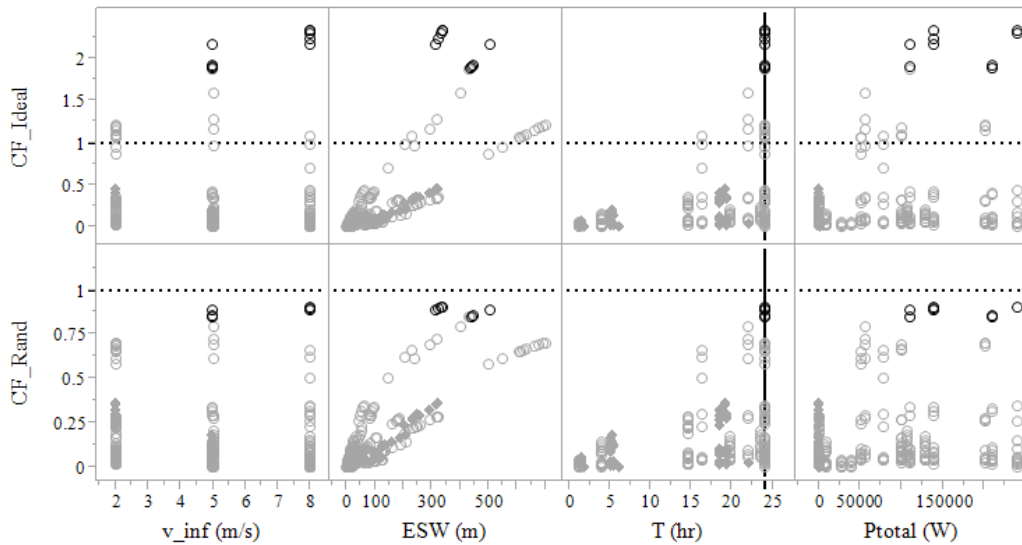


Figure 116: Maximum Coverage Effort Results for Ten Vehicles

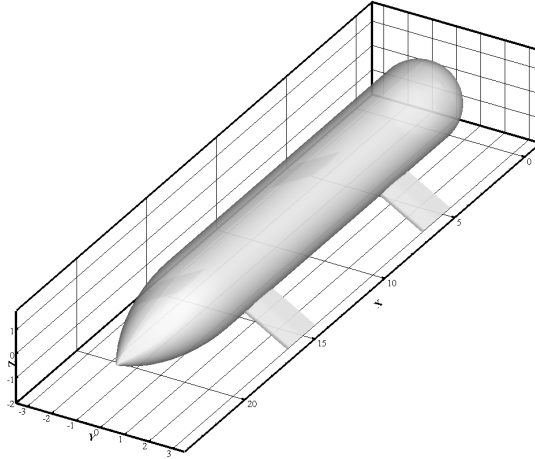


Figure 117: Representative RMMV Style Design

Maximize Specific Effort Another objective that could be desired is minimum power consumption, or maximum coverage effort per unit of power. This can be a very important factor since operational costs and ultimately life-cycle costs of systems might be directly correlated with energy usage. The cost function for this will be called the *specific effort*.

$$\begin{aligned}
 \text{minimize } \mathbf{f}(\mathbf{x}) &= - \sum_{i=1}^n \frac{ce_i}{P_{Tot_i}} x(i) = - \sum_{i=1}^n \frac{V_{\infty,i} S_i T_i}{P_{Tot_i}} x(i) \\
 \text{subject to: } & \sum_{i=1}^n x(i) = 10 \\
 T_i &= \begin{cases} t_{i,endurance}, & t_{i,endurance} < T_{MissionMax} \\ T_{MissionMax}, & t_{i,endurance} \geq T_{MissionMax} \end{cases}
 \end{aligned} \tag{101}$$

The combination of vehicles for maximum specific effort is ten REMUS style vehicles. Four were with FLS installed, and six were with SSS installed.

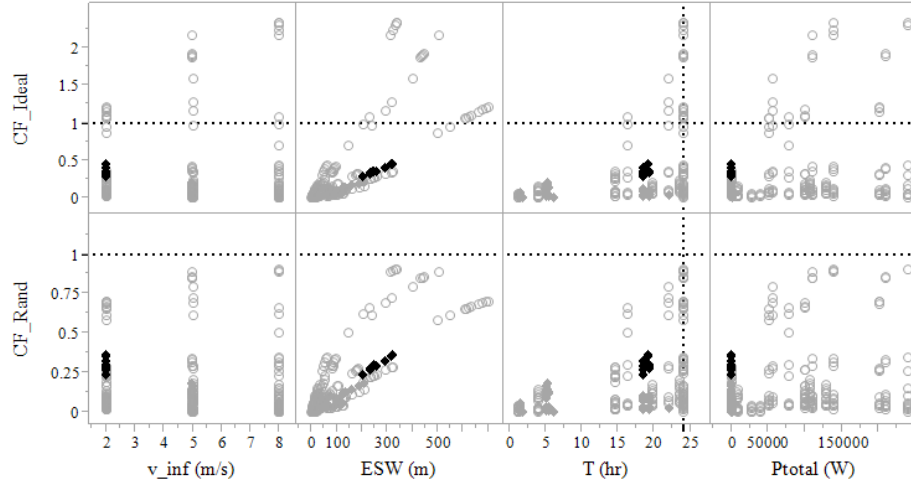


Figure 118: Maximum Specific Coverage Results for Ten Vehicles

Minimize Energy of Full Coverage Another cost function considered was minimum energy expended over the duration of the mission: $\sum T_i P_{Tot_i} x(i)$. However, in considering this cost function, it was evident that the optimization would drive the solutions to those with minimum power and minimum endurance, which would result in a very slow-to-complete mission.

Recapitulation of Optimization It has become clear that constraining the number of vehicles is a poor way to develop an SoS alternative. It would be helpful to use the coverage factor as a constraint, but as was shown earlier, the coverage factor can only be calculated for independent operations. It is inaccurate if search paths overlap. Also, the collaborative schemes implemented up to this point approach coverage times for random motion and are highly inefficient. The next section provides a solution to constrain the problem appropriately and propose a new way to implement the collaborative search scheme.

8.3.4 Path Planning for an Unknown Number of Vehicles

All of the previous simulations have demonstrated collaborative behavior in which the defined vehicle way-points overlap each other. While the vehicles move through the search area, they remove way-points from the queues of other vehicles. However, this has been shown to be inefficient and does not lead to a theoretical estimate of the number of vehicles

that should be utilized. After all, *Brownian* motion and random walks are typically inefficient [41]. However, the ideal coverage factor shows that a structured pattern in which vehicles minimally overlap provides the shortest time for total coverage.

Min and Papanikolopoulos [110] reinforce the observation made in this dissertation that typical area coverage research focuses on maximizing area and minimizing time for a *known* number of systems [1, 136]. However, for an SoS analysis of alternatives design problem, the number of systems is unknown. This was the motivation for implementing mixed-integer linear programming in the previous section. Unfortunately, the cost functions can only be defined relative to Brownian (*i.e.*, random) motion without a predefined operational concept for the vehicles. But, again, the number of vehicles is unknown. This is an underdetermined system.

Min and Papanikolopoulos did put forward a technique for area coverage with an unknown number of robots restricted by a maximum time requirement. However, the technique relied on only having to visit a known set of prioritized points (or key points of interest as they called them). The travel cost associated with the edges of the graph were defined as the Euclidean distances between points. The algorithm determines the minimum number of tours for completing the total area within a specified time, which in turn defines the number of robots. It begins by calculating the path of maximum cost and then finds the minimum tour to return to the starting position. This repeats iteratively until all points have been accounted for. An example of the result of the algorithm versus a k-nearest neighbor (kNN) algorithm for minimum tours is shown in Figure 119.

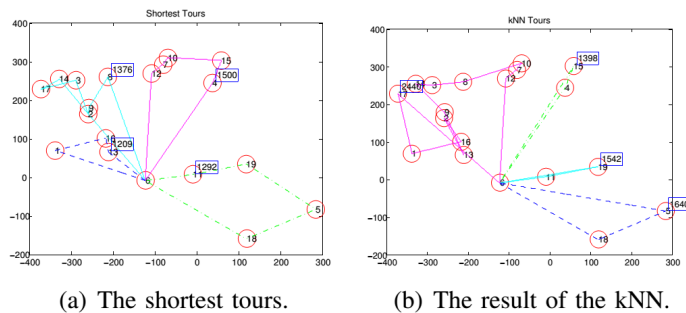


Figure 119: Shortest Tours for Determining Minimum Number of Robots [110]

As can be seen in Figure 119, the algorithm works well for a set of prioritized points. Prioritizing points results in a critical case, so it is no longer under constrained. Unfortunately in an area coverage problem where all points must be covered, there are no prioritized points even if a grid is placed over the area.

In spite of these shortcomings, the algorithm presented by Min and Papanikolopoulos inspired a new heuristic approach developed as part of this dissertation. It is dependent on three factors in order to provide a critical solution to the area coverage problem:

1. The vehicles must all start from the same position. This is reasonable since an underwater search mission will typically be launched from a single mother-ship.
2. The highest cost point in the area is the furthest point diagonally away from the starting position.
3. Sensor widths must be known. They can be homogeneous, heterogeneous, or even fractional if overlap is desired (*i.e.*, they can be defined as less than they actually are by some percentage in order to allow paths to overlap).

The heuristic search coverage algorithm developed here to estimate the total number of vehicles required, assuming the factors listed above, is also a function of vehicle search efforts. Recall that the search effort is an energy-based functional that links the various levels of the SoS hierarchy due to the developments provided in the previous two chapters. The algorithm uses the mixed-integer linear programming approach established earlier in this chapter with two possible cost functions which provide varying SoS alternatives. The two cost functions were delineated in Section 8.3.3. Each of the two cost functions are functions of a required time, $\tau_{i,k}$, for vehicle i and a search path k , to-be-defined.

The two cost functions are given in Equations 102 and 103. Equation 102 is the optimal coverage effort for path k which takes time $\tau_{i,k}$, depending on the velocity and sweep width of vehicle i . Similarly, Equation 103 is the power specific coverage effort for path k which takes time $\tau_{i,k}$, depending on the velocity and sweep width of vehicle i . The optimization problem is a linear programming problem to find the vehicle i out of n vehicles that maximizes (or

minimizes the negative) of f .

$$\underset{i}{\text{maximize}} \quad f = V_{\infty,i} S_i \tau_{i,k} \quad \forall i = 1, \dots, n \quad (102)$$

$$\underset{i}{\text{maximize}} \quad f = V_{\infty,i} S_i \tau_{i,k} / P_{i,\text{total}} \quad \forall i = 1, \dots, n \quad (103)$$

The algorithm begins by calculating an array of size n which contains the required distances of each vehicle to travel path k . The first required distance is to go from the starting point of the area to the furthest diagonal along a path in which the effective sweep width of the vehicle is interior to the path. The initial path, $k = 1$, is shown in Figure 120.

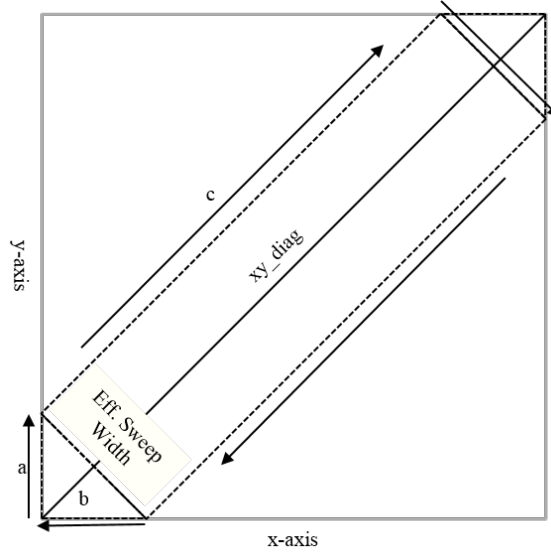


Figure 120: Initial Required Distance for Heuristic Coverage Algorithm

The required distance is dependent on the distances $a_{i,1}$, $b_{i,1}$, and $c_{i,1}$ shown in Figure 120, which are subsequently functions of the ESW of vehicle i and the search area diagonal length, xy_{diag} . The required distance and time to complete the path for each vehicle i is then:

$$\begin{aligned} b_{i,1} &= ESW_i / 2 \\ a_{i,1} &= \sqrt{2} b_{i,1} = \sqrt{2} ESW_i / 2 \\ c_{i,1} &= xy_{diag} - b_{i,1} = xy_{diag} - ESW_i / 2 \\ d_{req,i,1} &= 2a_{i,1} + 2b_{i,1} + 2c_{i,1} = \sqrt{2} ESW_i + 2xy_{diag} \\ \tau_{req,i,1} &= d_{req,i,1} / V_{\infty,i} \end{aligned} \quad (104)$$

Therefore, the algorithm finds a single vehicle to optimize Equation 102 or 103 subject to the following constraints:

$$\begin{aligned}
 \tau_{req,i,k} - t_{avail,i} &\leq 0 \\
 d_{req,i,k} - V_{\infty,i}t_{avail,i} &\leq 0 \\
 \sum_{k=1}^l \tau_{req,i,k} - T_{max} &\leq 0
 \end{aligned} \tag{105}$$

...where l is the total number of paths assigned to vehicle i and T_{max} is the maximum mission time. Also, $t_{avail,i} = E_i/P_i$, which is the total operational time available for vehicle i at the beginning of the mission according to the ratio of the available energy, E_i , and the power consumption, P_i . After the first vehicle is assigned to path $k = 1$, the time for path k is subtracted from the available time: $t_{left,i} = t_{avail,i} - \tau_{req,i,1}$. This is the time left over for vehicle i to potentially be assigned to other subsequent paths. After the first path is assigned a vehicle, subsequent paths on one-half of the search area are assigned vehicles. However, the required distances are slightly different as shown in Figure 121.

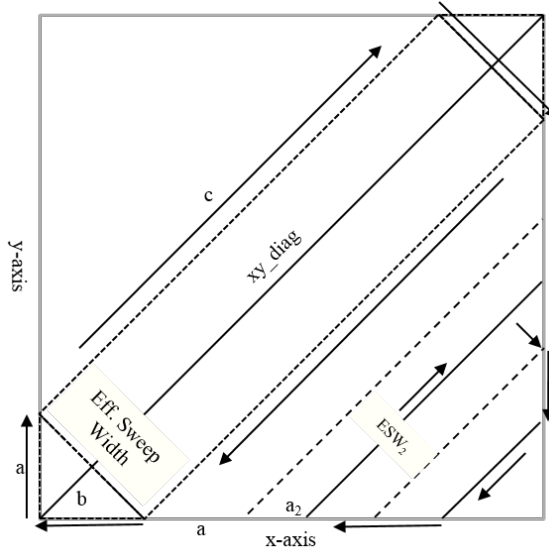


Figure 121: Iterative Required Distance After the Initial Distance

The distances for paths 2 through the total number of paths on one side use the same a and b relationships delineated in Equation 104. After convergence on one side, the algorithm

is repeated for the other side of the search area. The total distance of each path is:

$$d_{req,i,2} = 4a_1 + 2(xy_{diag} - 2ESW_1) + \frac{4\sqrt{2} - 7}{2} ESW_i$$

$$d_{req,i,k} = 4a_1 + 2(xy_{diag} - 2ESW_1) + \frac{4\sqrt{2} - 7}{2} ESW_i + (4\sqrt{2} - 4) \sum_{k=2}^{m-1} ESW_k \quad (106)$$

$$convergence\ when : \quad 2a_1 + 2\sqrt{2} \sum_{k=2}^{m-1} ESW_k + \frac{3}{\sqrt{2}} ESW_m \geq x_{max}\ or\ y_{max}$$

8.4 The Full Method

Experiments 1–6 have led to the development of a full, multi-level trade-off method for analyzing collaborative SoS alternatives which is shown in Figure 122 along with associated comments.

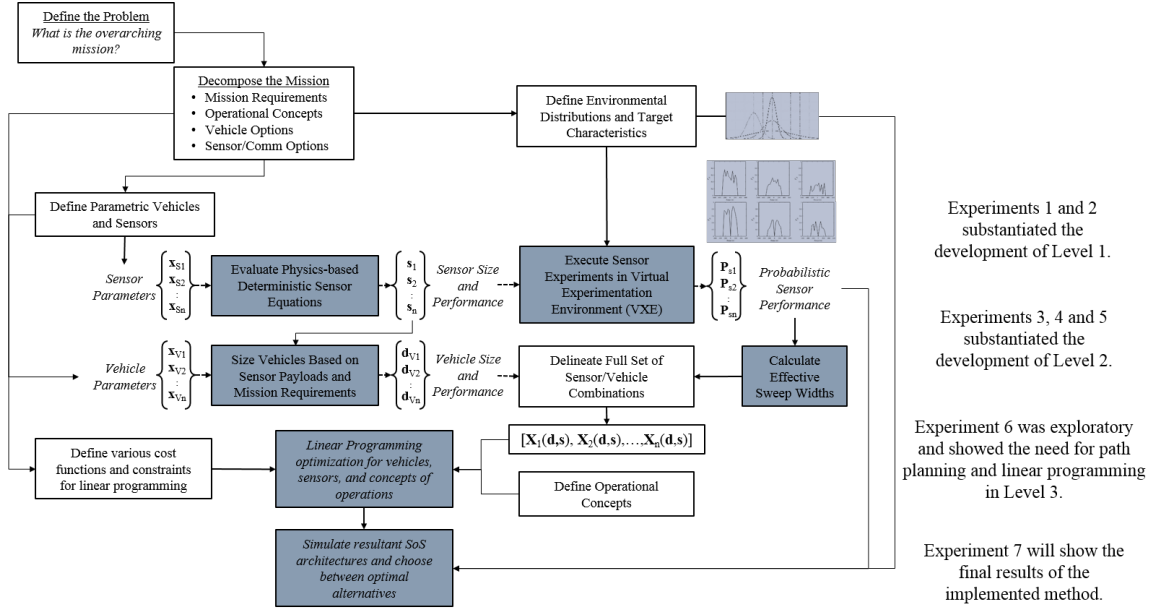


Figure 122: Full Developed Method with Comments

However, the method shown in Figure 122 incorporates specific activities to be performed for the underwater search mission. Consequently, the steps must be generalized to make it applicable to any collaborative system-of-systems problem. The generalized method is given in Figure 123. Experiment 7, provided in the next section, will demonstrate the final results of the method.

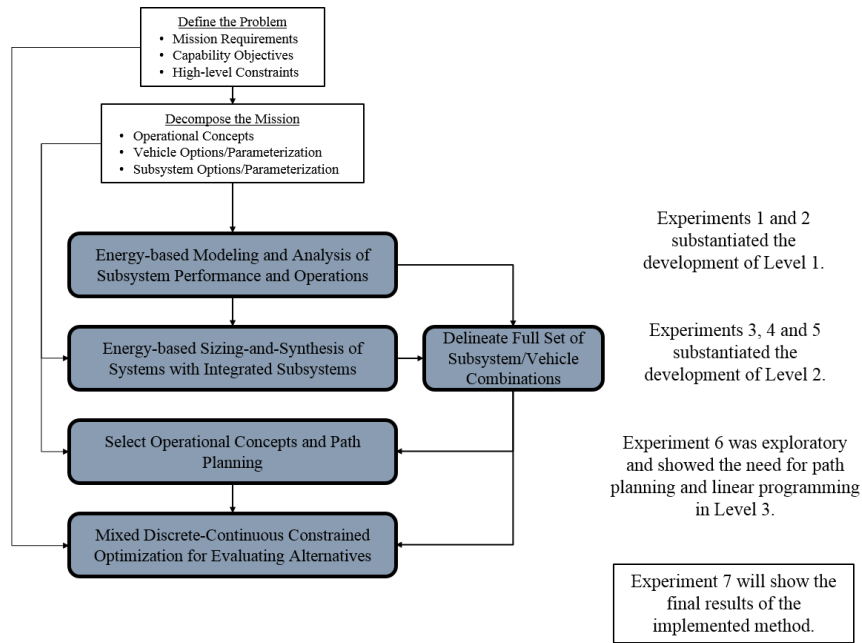


Figure 123: Full Developed Generalized Method with Comments

8.5 *Experiment 7: Application of the Full Method*

Experiment Set 7 takes the next step in the substantiation of the method developed in this dissertation by looking at the trade-offs possible for the collaborative SoS when an energy-based approach is applied. Relevant variables include the number of vehicles (the experiments from the subsystem- and system-level chapters provided hundreds of vehicle possibilities), the sensor ranges and power requirements, and the vehicle dynamics (in particular the drag and energy functionals). The problem is to maximize mission effectiveness for changes in the discrete (number of vehicles, type of operations, etc.) and continuous (thrust, sensor range, etc.) variables.

The first step of the method is defining the problem, including mission requirements and high-level constraints. The full problem definition was provided in Chapter 5 and will not be repeated here. However, it is graphically shown alongside the full method in Figure 124.

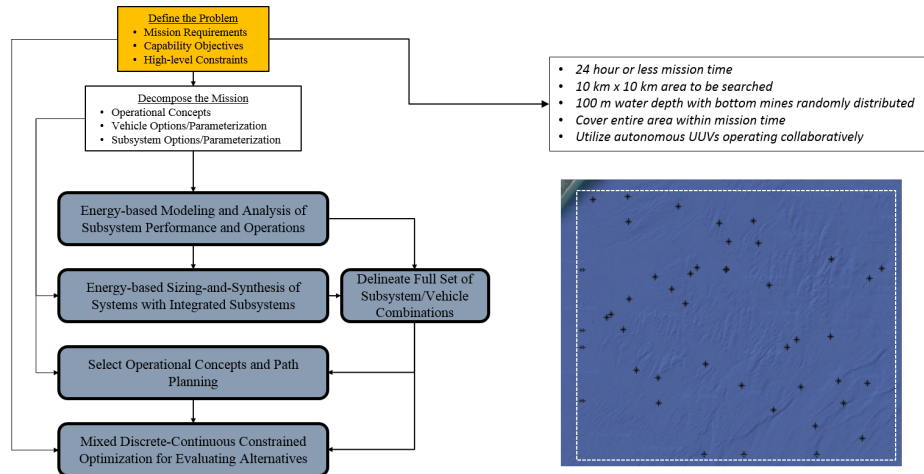


Figure 124: Defining the Problem

The next step of the method is to decompose the problem into desired subsystems, systems, and operational concepts. The decomposition is shown in Figure 125. The highlighted boxes are the options which were chosen for the example problem defined in Chapter 5.

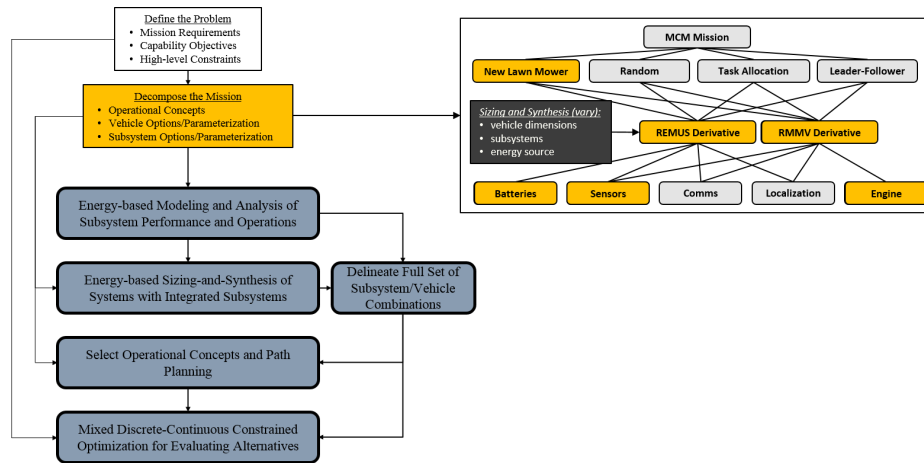


Figure 125: Decomposing the Problem

The next three steps of the method include the subsystem, system and SoS level analyses that have been detailed throughout the last three chapters. For that reason, the results will not be repeated here since they can be easily referred to. However, the relevant step of the method for Experiment 7 is the final step of the method, namely the optimization step for evaluating alternatives. The optimization algorithm is applied to the two cost functions expressed earlier. The results are provided below.

8.5.1 Specific Effort Optimization

The algorithm progressing for the specific effort cost function in Equation 103 is shown in Figure 126. It can be seen that the linear programming optimization along with the area coverage algorithm chose five vehicles to complete the mission. The five vehicles were all REMUS style vehicles, three with SSS sensors and two with FLS sensors. The scatter-plot of the vehicle parameters relative to all of the other possible vehicles is shown in Figure 127. A simulation of the vehicles and the target locations is shown in Figure 128. The mission took 19 hours and detected 80% of the targets.

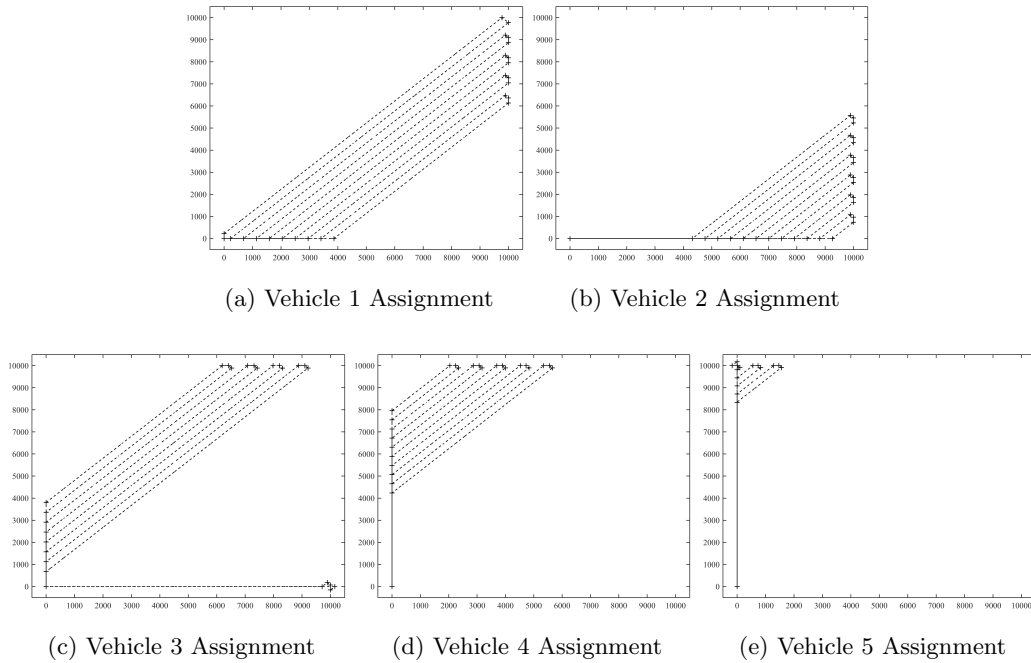


Figure 126: Coverage Algorithm Example Progression for $f = V_{\infty,i} S_i \tau_{i,k} / P_{i,total}$

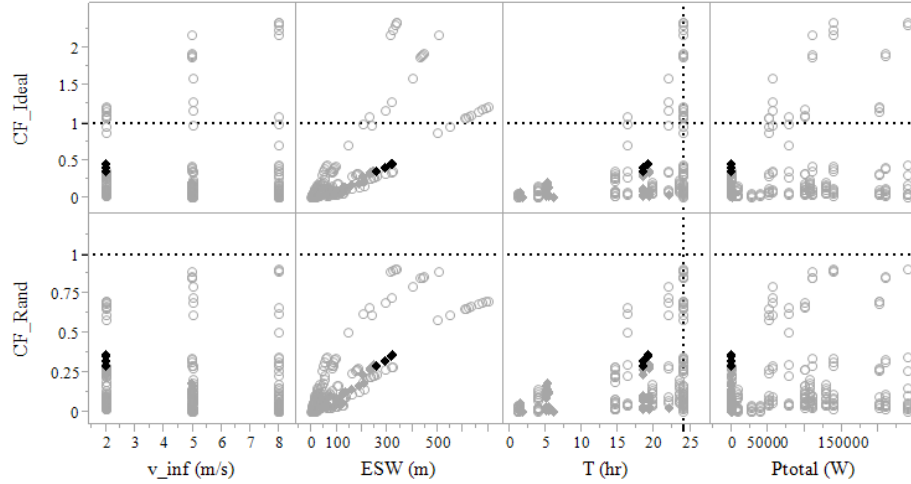


Figure 127: System Parameters for Coverage Algorithm with $f = V_{\infty,i} S_i \tau_{i,k} / P_{i,total}$

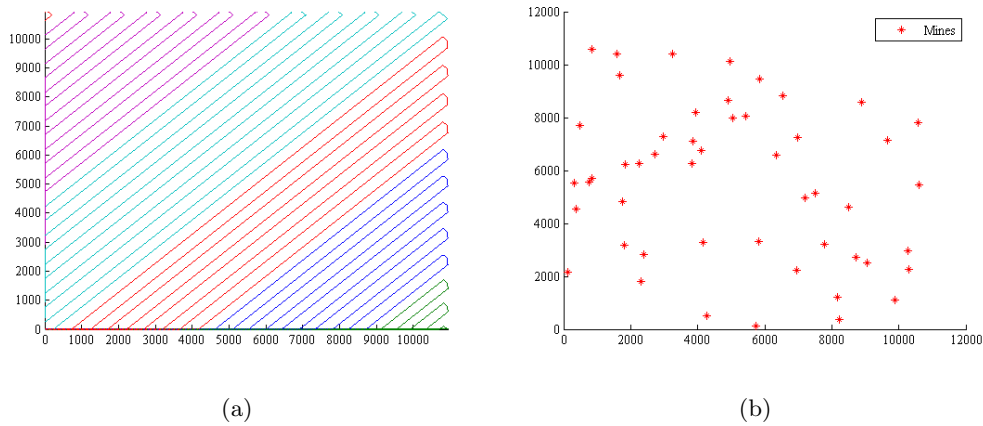


Figure 128: Vehicle Tracks and Target Locations for Virtual Experimentation

8.5.2 Coverage Effort Optimization

In addition, the algorithm progressing for the coverage effort cost function in Equation 102 is shown in Figure 129. It can be seen that the linear programming optimization along with the area coverage algorithm chose two vehicles this time to complete the mission. The two vehicles were both RMMV style vehicles with side-scan-sonars. The scatter-plot of the vehicle parameters relative to all of the other possible vehicles is shown in Figure 130. Finally, a simulation of the vehicles and the target locations is shown in Figure 131. The mission took 24 hours, which was longer than the previous SoS alternative, but it resulted in 90% detection of the targets, which is 10% better in total targets detected.

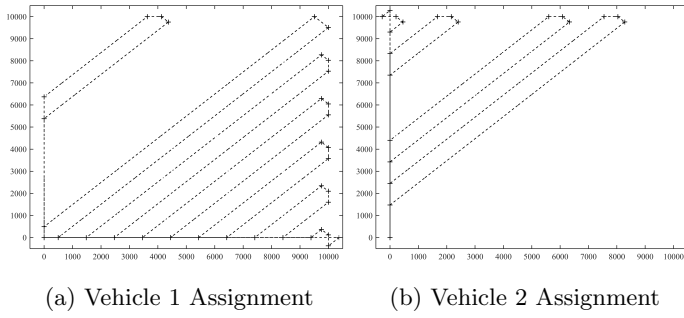


Figure 129: Coverage Algorithm Example Progression for $f = V_{\infty,i} S_i \tau_{i,k}$

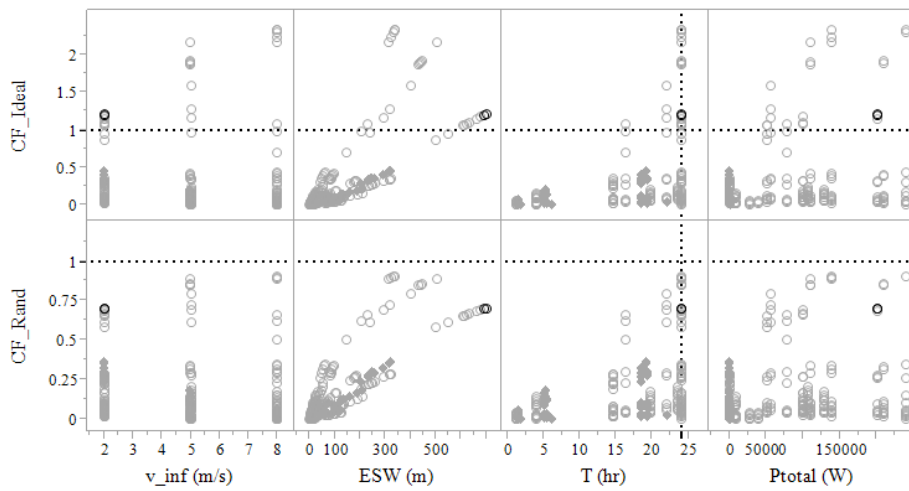


Figure 130: System Parameters for Coverage Algorithm with $f = V_{\infty,i} S_i \tau_{i,k}$

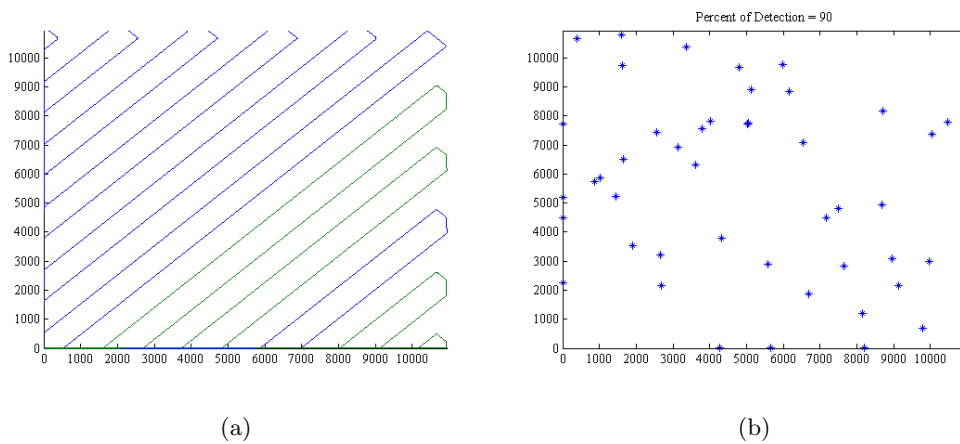


Figure 131: Vehicle Tracks and Target Locations for Virtual Experimentation

8.6 *Experiment Set C Conclusions*

In Section 8.3.3, it was shown that linear programming provided an efficient and transparent way for selecting alternative SoS architectures. In a sense, the linear programming optimization performed the analysis of alternatives. However, the optimization is completely dependent on the cost functions and constraints provided by the design engineer.

In this work, the cost functions and constraints are born out of requirements definition and physics-based analysis. Yet, for a collaborative SoS search problem, the number of vehicles is difficult to determine since the operational scheme is undefined, and therefore the problem is under constrained. With the new heuristic path planning algorithm developed in this work, the SoS alternatives can be determined based on both efficient operations and on system/subsystem performance. This chapter has substantiated **Hypothesis 4**:

Hypothesis 4 *If the coverage effort is defined as a function of linked energy-based parameters from the subsystem level up through the SoS level, then the coverage effort can be formulated as a cost function within a mixed-integer linear programming optimization for the selection of alternative SoS designs.*

CHAPTER IX

SUMMARY AND CONCLUSIONS

This dissertation has provided a new method for analyzing collaborative system-of-system alternatives through an energy-based approach. The starting point of the method was built upon a foundation of accepted generic systems engineering processes. The final generalized method alongside the generic top-down decision support process is shown in Figure 132.

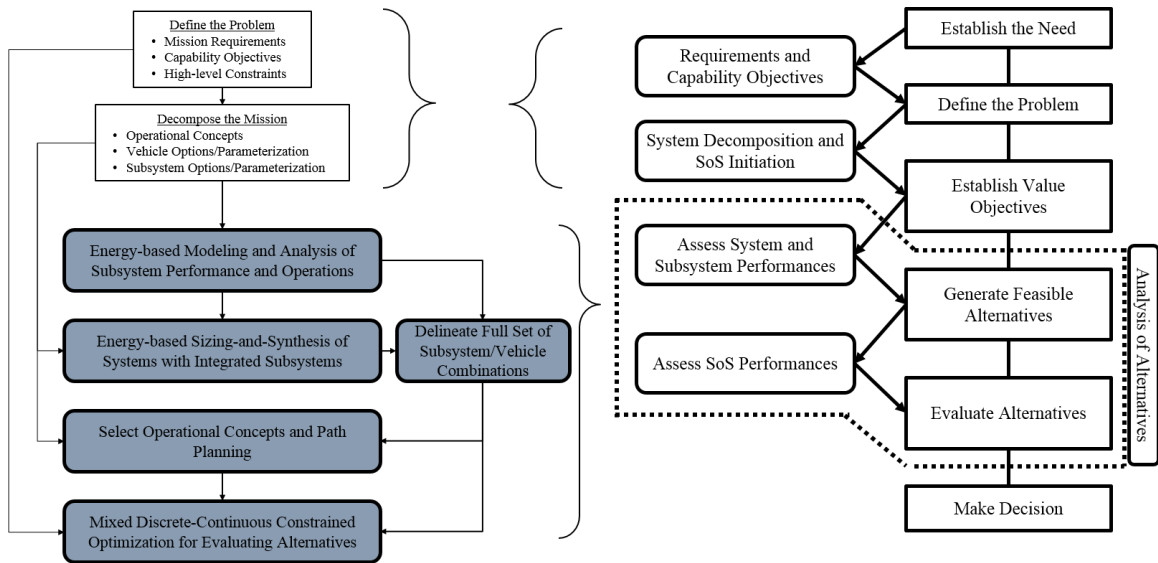


Figure 132: Final Multi-Level Trade-off Methodology Alongside the Top-Down Decision Support Process

The purpose of this research was to ask questions (and offer methodical solutions) about designing systems and groupings of systems that are to work together as effectively as possible. A foundation was built on defining high level mission requirements and subsequently decomposing the problem across multiple levels of the system-of-system hierarchy. Design options at each level of the hierarchy including individual systems, subsystems, and groupings of systems were considered and trade-offs were presented. Various steps of the design process were established and argued for or against, and significant focus was placed on

the analysis of alternatives. The overarching hypothesis of this dissertation was stated as follows:

Hypothesis 1 *An energy-based approach to analyzing system-of-system (SoS) components across multiple levels of the SoS hierarchy will enable more accurate and transparent trade-offs for SoS analysis of alternatives.*

After the literature review, another hypothesis was presented:

Hypothesis 2 *If the performance parameters of the coverage factor metric are defined as energy-based functionals that link the various levels of the SoS hierarchy, then the coverage factor can be used to provide more accurate and transparent analysis of alternatives between disparate SoS subsystem and system components.*

Hypothesis 2 was established due to the investigation of coverage factor as a metric to describe SoS performance. The experimentation in this work leaned on comparisons between the coverage factor calculations when energy-based formulations are used across the levels of the SoS hierarchy versus when energy-limited formulations are not used. This led to two additional hypotheses:

Hypothesis 3 *If a relationship is formed between sensor energy, sensor detection capability, and sensor velocity, then an energy-based link will be established between the effective sweep width parameter at the subsystem level and the vehicle performance at the system level.*

Hypothesis 4 *If the coverage effort is defined as a function of linked energy-based parameters from the subsystem level up through the SoS level, then the coverage effort can be formulated as a cost function within a mixed-integer linear programming optimization for the selection of alternative SoS designs.*

An overview of the experimental approach utilized in substantiating these hypotheses is provided in the next few sections, followed by some final closing comments.

9.1 Experimental Overview

The delineated experimental approach is outlined in Figure 133. The gray boxes represent methods which link the levels of the SoS through energy-based functionals. The white boxes are other approaches typically utilized for analyzing SoS performance and effectiveness at varying levels of the system-of-system hierarchy.

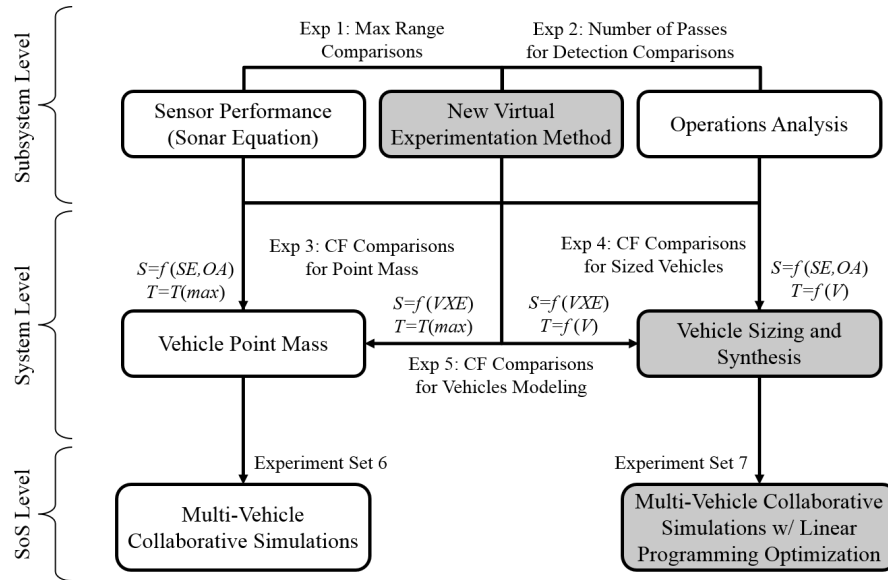


Figure 133: Decomposed Level-by-Level Experimental Approach

The experimental approach utilized in this dissertation was dependent on data acquisition and analysis of various paths to the SoS design problem at each level of the SoS hierarchy.

9.1.1 Experiment Set A: Subsystem Level Review

At the subsystem level, data was acquired to compare the three different approaches through three different analyses. Through a design of experiments and a set of physical constraints, 90 sonar designs were selected to be tested through each analysis path. The specification of the 90 sensor designs was explored in detail in Chapter 6. In context of the *Sensor Performance* path, the 90 sensor designs were analyzed deterministically through the sonar equation (SE) which provided characteristics such as the theoretical maximum sensor range. Along the *Operations Analysis* (OA) path, sensor designs were explored probabilistically,

but the sensor performance was simplified. In particular, the sensors were defined as generic probability distributions which are expected to detect a target within some probability as a function of range away from the sensor.

Finally, through the third subsystem level path, sensor designs were explored through the virtual experimentation method developed in this work, which is one of the major contributions of this dissertation. The approach was to first specify physical constraints for the 90 sensor designs through the sonar equation and then to test each of the sensors in a Virtual Experimentation Environment (VXE). After the inclusion of multiple velocities, target locations, and Monte Carlo runs per sensor, a total of 101,250 simulations were executed. The 101,250 experiments performed within the VXE provided sensor characteristics utilized in comparing the new approach (the energy-based VXE process) against the existing methods (SE and OA).

As was shown, the VXE approach provides an energy-based link between the performance of the subsystem and the operational scheme of the system. This information was not previously available without real-world experiments. Therefore, the development of the new virtual experimentation method can provide highly-desirable information about trade-offs between subsystem capabilities without the expense of real-world experiments. It should be noted that the information acquired is only useful for relative comparisons, not absolute real-world values, in the absence of real-world data for verification.

Experiment Set A partially substantiated Hypothesis 3: *If a relationship is formed between sensor energy, sensor detection capability, and sensor velocity, then an energy-based link will be established between the effective sweep width parameter at the subsystem level and the vehicle performance at the system level.* Full substantiation was developed through the system-level experiments to-be-reviewed next. Additionally, substantiation of Hypothesis 3 is part of substantiating the overall hypothesis of this dissertation.

9.1.2 Experiment Set B: System Level Review

At the system level, data was acquired to compare vehicles modeled as point-masses versus sized-vehicles with energy dependencies. Each system-level approach was tested with the

varying subsystem level techniques described above. The measurement utilized to compare each of the system-level experiments was the coverage factor function which was introduced in Chapter 3, in Section 3.5.3.

In Experiment 3, the coverage factors for point-mass vehicles were compared using subsystems modeled with either: (1) a hybrid Sensor Equation (SE) plus Operations Analysis (OA) approach or (2) the new subsystem Virtual Experimentation (VXE) approach. For Experiment 4, the subsystems were modeled in the same way as Experiment 3, but the comparisons were taken a step further by utilizing energy-dependent sized-vehicles. Finally, Experiment 5 compared the point-mass vehicles against the energy-dependent sized vehicles, but the subsystem-level modeling was only executed through the new VXE approach. The results of Experiments 3, 4 and 5 showed the unquestionable impact of utilizing an energy-based approach which links the subsystem level to the system level in SoS analysis and design.

Experiment Set B provided data and analyses for expressing the importance in modeling systems through an energy-based approach. Often in SoS analysis and design, vehicles and systems are modeled as little more than point-masses as was pointed out throughout this dissertation. In some situations, that level of detail may be fine. However, for analyzing alternative SoS which must collaboratively accomplish a mission under constrained requirements, system capability as a function of energy-limited processes is important.

9.1.3 Experiment Set C: SoS Level Review

At the system-of-systems (SoS) level, the energy-based approaches applied to the subsystem and system levels of the previous experiments were administered to collaborative SoS architectures. In Experiment set 6, experiments were executed for multi-vehicle architectures in which sensor radius, sensor power, vehicle interactions, and vehicle thrust were manipulated. The sensors and vehicles in Experiment set 6 were modeled according to the *old* approach and was exploratory in nature. The purpose of Experiment 6 was to demonstrate the shortcomings in SoS analysis when the subsystem and system level components are not modeled as energy-based functionals. It was apparent that even for a simple set of initial

experiments, variations in performance can be significant, and sometimes counterintuitive. It was shown that multiple factors influence the overall effectiveness of a collaborative SoS mission, which is obvious, but what was not so obvious was how to select the right combination of sensors and vehicles to get the job done in the best way possible. Multiple gaps were identified through Experiment 6, including the need for a way to determine the appropriate combinations of subsystems and systems that should be utilized, along with the need for a path planning scheme for efficient collaboration. Consequently, a new heuristic area coverage algorithm was developed which was applied along with mixed-integer linear programming to perform an analysis of alternative SoS architectures and fill the stated gaps.

Filling the gaps that were identified in Experiment 6 led to the completion of the method developed within this dissertation. Experiment 7 then provided a final demonstration of the applied method. The results of Experiment 7 were based on systematically assessing various performance measures for optimizing the effectiveness of the collaborative mission through combinations of sensors and vehicles. For the mine warfare representative example problem used in this work, the results of the method included two competing options for a decision maker to choose between. One of the SoS solutions had a faster mission time, while the other SoS solution was able to detect more targets within the search area. The full generalized method with the determined solutions alongside the generic top-down decision support process is shown in Figure 134.

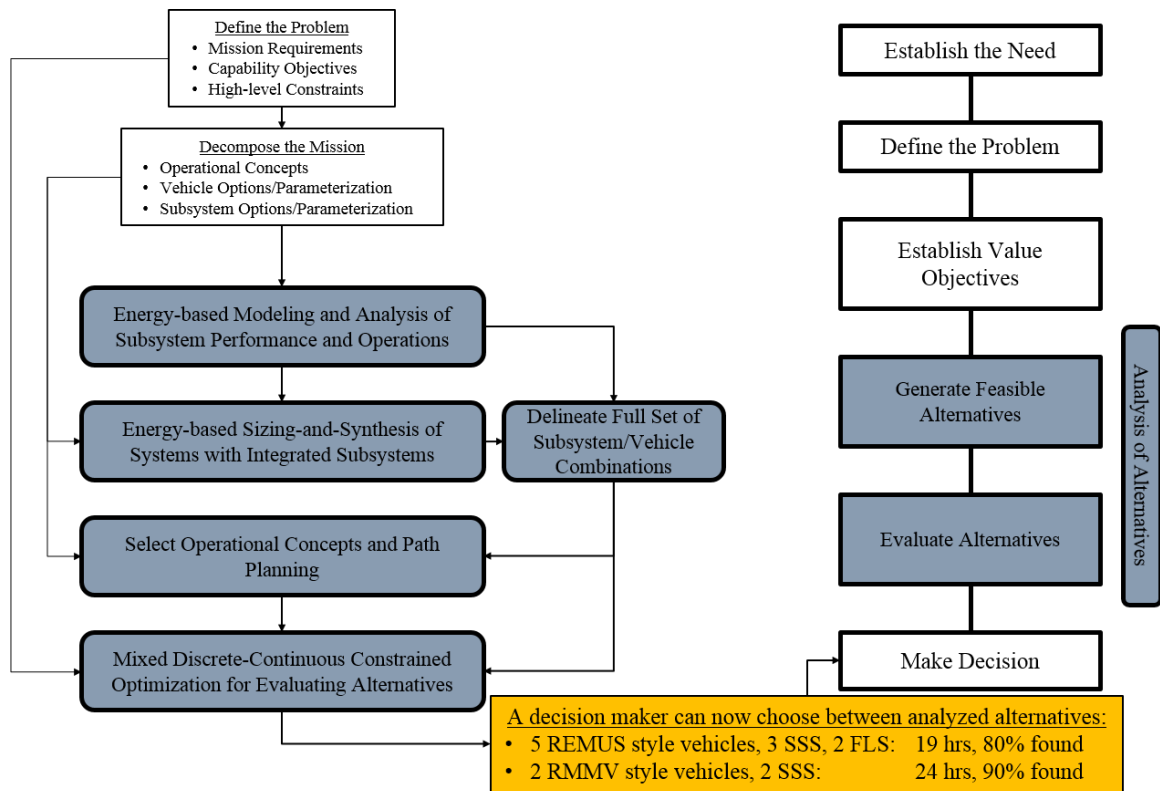


Figure 134: The Applied Method Leads to a Portfolio of Non-Dominated Results for a Decision Maker to Choose Between

9.2 Making a Decision

This dissertation was scoped down to focusing on the analysis of alternatives (as shown by the gray boxes in Figure 134 above). Accordingly, the requirements definition and system decomposition steps at the beginning of the method were not specifically investigated in this work; instead, existing techniques were discussed and utilized. Similarly, the final step of the generic top-down decision support process is to make a decision. Although the decision step is not specifically the concern of this dissertation, it is prudent to provide some insights on how a decision maker can go about the process.

The alternative results of the applied method in this work were typical of multi-attribute design problems. In particular, when there are multiple objectives that a decision maker cares about, there will often be competing solutions. Some of the solutions perform better in a subset of criteria while other solutions are dominant in other dimensions. Mission time

and the percent of objects detected were the objectives considered in this work. Others could include the life cycle cost, the transport volume, reliability, etc. Consequently, a decision maker would likely have a set of preferences, even if the preferences are not explicitly known. The concept of preferring that some dimensions of the problem are met over others has led to entire fields of research, including *Multiple Criteria Decision Making* (MCDM) and *Multi-Attribute Utility Theory* (MAUT) [45].

In MCDM, the theory of conjoint measurement attempts to provide a decision mathematically by constructing a numerical expression of synthesized unique criteria [51]. MCDM methods are often optimization related. For MAUT methods, the unique criterion are often combined in an additive value function (or overall evaluation criteria) to consider the individual effects [45]. The additive value function is the central model of the theory of conjoint measurement for n criteria. Dyer provides an incredibly concise delineation of MCDM and MAUT and how they are often applied [45]:

MCDM assumes that a decision maker is to choose among a set of alternatives whose objective function values or attributes are known with certainty. Many problems in MCDM are formulated as multiple objective linear, integer, or non-linear mathematical programming problems, and many of the procedures proposed for their solution are interactive. MAUT...focuses on the structure of multicriteria or multiattribute alternatives, usually in the presence of risk or uncertainty, and on methodologies for assessing individuals' values and subjective probabilities. MAUT embraces both a large body of mathematical theory for utility models and a wide range of practical assessment techniques that pay attention to limited abilities of assessors. Information obtained from assessment usually feeds into the parent problem to rank alternatives, make a choice, or otherwise clarify a situation for the decision maker. Sensitivity analysis is often involved in the assessment and choice processes.

Accordingly, various methods exist for enabling a quantitative decision making process. Depending on the decision maker preferences, each technique may vary greatly in the final

result. The article written by Dyer et al. [45] can be referred to for seminal sources on a plethora of techniques.

9.3 Where to go Next

This dissertation was scoped down to a reasonable portion of work but still provided a significant degree of complexity. However, there is room to grow in further developments for the method that was produced. In terms of furthering the method, it would be prudent to apply new test problems including collaborative sets of aircraft, cars, and other autonomous systems. Insights can be gleaned from the applications which would help to support the credibility of the multi-level trade-off methodology. Also, a relatively simple next step would be to incorporate communications modeling at the subsystem level of analysis. In addition, various optimization schemes could be applied to the analysis of alternatives, including multi-objective mixed-integer linear programming, evolutionary techniques (genetic algorithms, particle swarm, etc.) and many more. Finally, new and refined path planning algorithms could be implemented.

Another area that could be pushed forward in future research is extending the mine warfare modeling of the representative example problem. This could include more depth in the vehicle models (more subsystems, model motor and engine performance, reliability, etc.). Also, different sensors could be used such as laser-based systems. Other additions would be cost-modeling and additional constraints such as life-cycle costs, operational costs, and transportability. Finally, more of the mine hunting mission could be examined including the identification, localization and neutralization stages.

9.4 Lessons Learned

This dissertation came to fruition because of the important and highly relevant role that system-of-systems analysis and design plays, and will play, in the world today and in the future. As unmanned and autonomous systems become ubiquitous in everyday life, the need and desire for those systems to collaborate will surely increase. From commercial product deliveries to military operations, analyzing alternative systems-of-systems is a rich area for research. While there are multiple disciplinary challenges that must be overcome,

there is also a need for the large-scale perspectives put forward in this dissertation through systems engineering and concurrent engineering. However, the large-scale focus of the problem should be accompanied by highly detailed physics-based analyses. In particular, in this dissertation, the need for physics-based detailed analyses was substantiated through the energy-based approaches presented. The first few chapters of this dissertation detailed relevant literature for developing and supporting the hypotheses introduced in this work. Subsequently, proposed experiments and a representative example problem were outlined. The experimental approach chapters provided analysis, data visualization, and substantiation of the hypotheses.

Chapter 6 presented and analyzed detailed in-depth energy-based relationships for the subsystems applicable to this work, namely the sensors. As was pointed out, the sonar equation (when modeled in depth) provides an energy-based estimation of sonar performance. However, the sensors in a collaborative search mission are not static, and the sonar equation does not capture kinematic effects. Accordingly, it was observed that Operations Analysis and mobile robotics research each take kinematics into consideration, but they tend to negate sensor performance. The method developed in this dissertation bridged the gap. In particular, the approach of modeling the sensor from the sonar equation and simulating its motion in a virtual experimentation environment provided energy-based functionals for both the sensor performance and the sensor kinematics.

In **Chapter 7**, a multi-level design method for generating alternative sensor and vehicle designs that are to be utilized within a collaborative system-of-system mission was delineated. Experiments were performed which compared various approaches for analyzing vehicle-sensor combinations. It became clear that integrating subsystems into their carrier systems often drive the mission capabilities of the individual systems, if the subsystems can even be integrated. In setting up the experiments for subsystem-system integration, it was expected that the energy-based approaches would be more accurate and insightful than the old simplified approaches. However, the gap was much larger than expected, which was surprising.

Finally, in **Chapter 8**, the energy-based approach applied to the subsystem and system levels of the previous two chapters were administered at the system-of-systems level. Through detailed SoS level experiments, substantiation was provided for the overarching hypothesis of this dissertation, namely that *an energy-based approach to analyzing system-of-system (SoS) components across multiple levels of the SoS hierarchy will enable more accurate and transparent trade-offs for SoS analysis of alternatives.*

The experiments performed in this work provided significant insights, some of which were surprising and/or counterintuitive. In particular, it was hypothesized that an energy-based approach would provide more accurate trade-offs of the subsystem and system capabilities. However, it was not expected that the disparity between energy-based analyses and simplified analyses would be as great as were shown in Experiment Sets A and B. A counterintuitive result appeared when it was observed that the energy required to collaborate often made collaboration less efficient than not collaborating. This was shown in Experiment 6. However, as was pointed out, Experiment 6 utilized simple collaboration schemes that could likely be designed to be more efficient. Consequently, a new path-planning algorithm was constructed for collaborative search schemes and was applied in Experiment 7.

This dissertation began by demonstrating that collaborative behavior can be a beneficial and impressive trait of a species and yet, there seem to be some species that have what it takes to cooperate effectively while others do not. Subsequently, this work showed that varying design considerations can prove to be either beneficial or detrimental to the cooperative operations of a grouping of unmanned systems. The method developed in this work provides a road-map for delineating vehicle capabilities at the subsystem, system and SoS levels in order to analyze alternatives and achieve desired increases in mission effectiveness. It is my hope that the work produced here can help to advance the state of collaborative autonomous systems as our world ventures into the future.

APPENDIX A

THE DEFENSE ACQUISITION SYSTEM

A.1 The Joint Capabilities Integration Development System (JCIDS)

Figure 135 presents one rendition of the flow of DoD processes used to identify needs and acquire solutions initiated by a CBA [83, 160]. The white boxes indicate JCIDS produced documents while the gray boxes represent activities under the control of the DoD acquisition process.

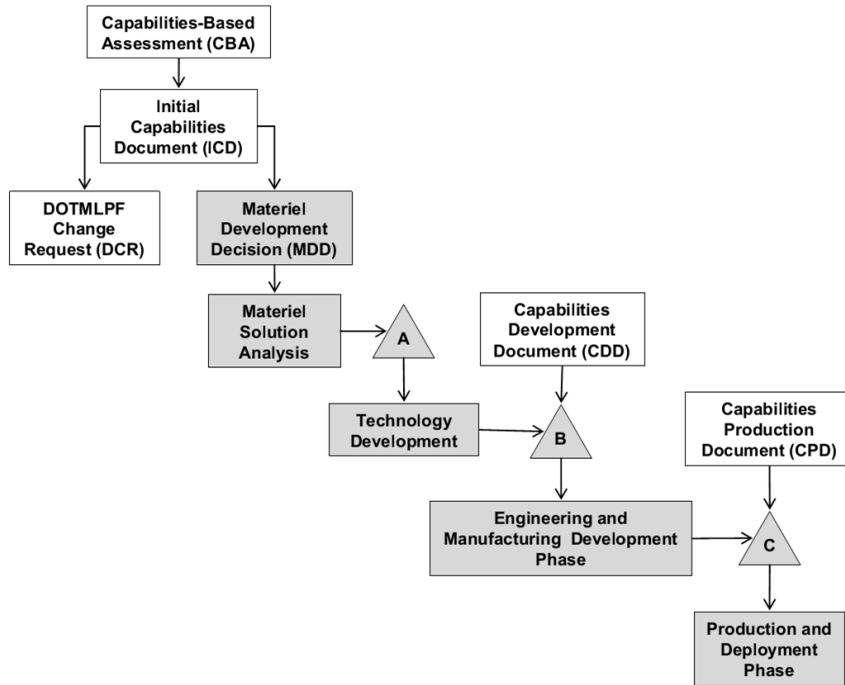


Figure 135: DoD Needs Identification and Solution Process [83]

Figure 135 shows the CBA as the starting point of the process for identifying and acquiring a solution, whether it is materiel or non-materiel. If the CBA is compelling, then the organization that has identified the capability gap will prepare an Initial Capabilities Document (ICD). The ICD conveys the results of the CBA and serves as a decision making document. As part of the JCIDS process, the ICD must then be approved or rejected. Approval of the ICD means the DoD has determined that [83]:

1. The CBA appropriately describes the capabilities needed to perform a particular mission.
2. The CBA has identified the gaps in capabilities and the operational risks associated with those gaps.
3. There is a need to address the stated gaps.

After approval of the ICD, a decision is made as to whether there can be a DOTMLPF change that will close the stated capability gap, or if a materiel development program will be necessary. If a materiel development decision is deemed necessary, then the process moves into the acquisition stages.

Other aspects of the CBA and JCIDS process which are relevant to this research and worth noting include [31]:

- The CBA produces a set of tasks and measures used to assess the programmed capabilities of the force. These measures should be based on the following lists of capability attributes:
 1. Battlespace Awareness Attributes: Comprehensive, persistent, survivable, integrated, timely, credible, adaptable, innovative, interoperable
 2. Command and Control Attributes: Interoperability, understanding, timeliness, accessibility, simplicity, completeness, agility, accuracy, relevance, robustness, operational trust, security
 3. Logistics Attributes: Visibility, reliability, velocity, precision, survivability, economy, capacity, responsiveness, sustainability, flexibility, attainability, simplicity, effective, expeditionary, agile/tailorable, networked, integrated, precise, enduring/persistent
 4. Network-centric Attributes: Accessible, capacity, accurate, timely, throughput, expeditionary, latency, interoperable, survivable, reliable, relevant, scalable, responsive, robust, dynamic, flexible, agile, integrated, maintainable, complete, reconfigurable, security, available, visible, controllable

- The CBA must develop criteria for adequate mission performance. Quantitative criteria for mission success must be established to support the assessment of the materiel reliability characteristics of potential materiel solutions. In most cases, these criteria will not be simple pass-fail standards, but instead will represent a continuum of values.
- A major step in the CBA is to determine the level of analytic rigor needed to estimate operational sufficiency to provide appropriate and timely recommendations to inform decision making.
- Since a validation authority for JCIDS documents will ultimately decide which capability gaps are important enough to develop new capability solutions, the capability gaps must be directly linked to operational situations and consequences of failing to meet objectives. The CBA must explain the methodology for determining the capability gaps, and ensure that the linkage to the capability requirement and strategic guidance is clear.
- A CBA must determine if a non-materiel approach can wholly or partially mitigate any of the capability gaps by recommending changes to existing capabilities in one or more of the DOTmLPF-P areas. The most common non-materiel approaches are:
 1. Alternative Doctrinal Approaches and Alternative CONOPS.
 2. Policy Alternatives.
 3. Organizational and personnel alternatives. A CBA cannot redesign the force, but it can suggest ways in which certain functions can be strengthened to eliminate gaps and point out mismatches between force availability and force needs.
- The CBA must assess general approaches for materiel capability solutions which can wholly or partially mitigate any of the capability gaps after assessing non-materiel solutions. Materiel approaches tend to fall into three broad types (listed in terms of fielding uncertainty from low to high):
 1. Development and fielding of information systems (IS) (or similar technologies with high obsolescence rates) or evolution of the capabilities of existing IS.

2. Evolution of existing systems with significant capability improvement (this may include replacing an existing system with a newer more capable system, or simple recapitalization).
3. Integration of transformational systems that differ significantly in form, function, operation, and capabilities from existing systems and offer significant improvement over current capabilities or transform how the mission is accomplished.

A.2 The Origins of JCIDS and its Role in the Defense Acquisition System

JCIDS was established in 2003 in response to several shortcomings that were present in the existing requirements process. There was a great deal of dissatisfaction with the process throughout the DoD, within the Joint Requirements Oversight Council (JROC), and most notably from the Secretary of Defense, Donald Rumsfeld. In a memo to Vice Chairman of the Joint Chiefs of Staff, General Peter Pace, Rumsfeld stated [83]:

As Chairman of the JROC, please think through what we all need to do, individually or collectively, to get the requirements system fixed. It is pretty clear it is broken, and it is so powerful and inexorable that it invariably continues to require things that ought not to be required, and does not require things that need to be required.

A large amount of activity followed the memo, ultimately resulting in the JCIDS process and three fundamental principles that form it [83]:

- Describing needs in terms of capabilities, instead of systems or force elements.
- Deriving needs from a joint perspective, from a new set of joint concepts.
- Having a single general or flag officer oversee each DoD functional portfolio.

JCIDS, therefore, is the current DoD process which plays the key role in identifying the needs of the DoD and is initiated with a CBA. It assesses existing and proposed capabilities and recommends ways to meet capability gaps. It determines and conveys requirements.

In addition, JCIDS is a major supporting process for the DoD Defense Acquisition System and the Planning, Programming, and Budget Execution (PPBE) processes. “The requirements process [JCIDS] supports the acquisition process by providing validated capability needs and associated performance criteria to be used as a basis for acquiring the right weapon systems. Additionally, JCIDS provides the PPBE process with affordability advice supported by the CBA, and identifies capability gaps and potential materiel and non-materiel solutions” [40]. A very simplified description of this is that the CBA identifies an existing capability gap, the JCIDS process substantiates the gap as a need and defines requirements and performance criteria, the acquisition process uses the requirements and performance criteria to analyze and choose from alternative solutions, and the PPBE process constrains the allocation of resources used to acquire the solution. The concert of interaction between these three processes (JCIDS, PPBE and the Acquisition System—often referred to as ‘the little a’) make up the Defense Acquisition System as a whole, which is often referred to as the ‘Big A’. This is depicted in Figure 136.

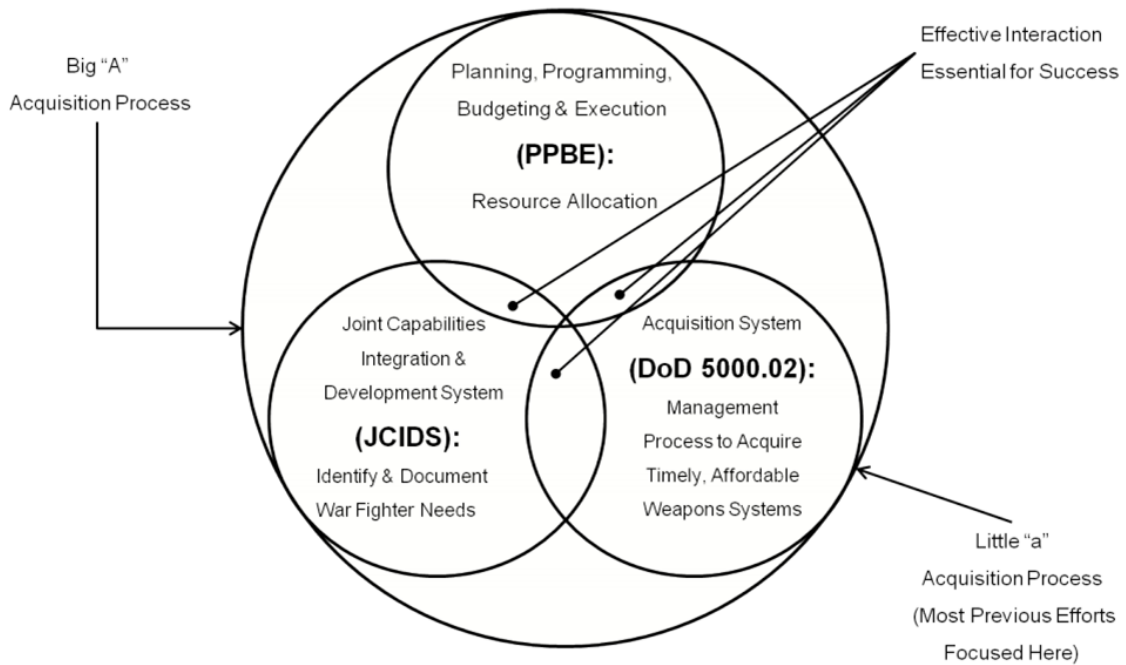


Figure 136: Interaction of the DoD Decision Support Systems [44, 9]

APPENDIX B

SE AND SOSE CHARACTERISTICS

B.1 System-of-System Definitions

While the system and system-of-systems definitions provided in Section 3.2 were helpful, there are still many specifics to defining an SoS in such a way that makes it different than a system that were not addressed. Namely, what does it mean for the elements to be independent? Are there various types of independence for the elements? What types of interactions will still allow it to be classified as an SoS? Various definitions and classifications for an SoS that exist throughout the literature will be helpful.

- A system is termed a system-of-systems when: (1) Its components fulfilled valid purposes in their own right and continued to operate to fulfill those purposes if disassembled from the overall system, and (2) the components systems are managed (at least in part) for their own purposes rather than the purposes of the whole, regardless of the complexity or geographic distribution of the components [98].
 - *The author of the definition above also presents the idea that the term “collaborative systems” may better express the nature of the grouping of systems referred to as a system-of-systems. Nonetheless, the terms “collaborative” and “systems-of-systems” are often used interchangeably throughout the literature.*
- An SoS is a large-scale complex system, involving a combination of technologies, humans, and organizations, and consisting of components which are systems themselves, achieving a unique end-state by providing synergistic capability from its component systems, and exhibiting a majority of the following characteristics: operational and managerial independence, geographic distribution, emergent behavior, evolutionary development, self-organization, and adaptation [127].

- Systems-of-systems are a hierarchical set of systems, associated with different operational levels, where each level consists of interacting collections of component systems that produce results unachievable by the individual subsystems [145].
- Systems-of-systems are large-scale integrated systems which are heterogeneous and independently operable on their own, but are networked together for a common goal. The goal...may be cost, performance, robustness, etc. [81].

Lastly, since the DoD is a major stakeholder in the types of systems-of-systems being researched in this work (groups of autonomous, unmanned, collaborative systems), the DoD definition of an SoS is relevant. The DoD in particular defines an SoS as a “set or arrangement of systems that results when independent and useful systems are integrated into a larger system that delivers unique capabilities” [40]. This definition implies that every individual system within the SoS should be capable of completely independent operations and have its own performance attributes and mission capabilities. However, when these independent systems are integrated into a collection of systems, they jointly provide a capability which is exclusive from the capabilities of any of the systems acting independently. The systems within the SoS may consist of vehicles, satellites, communications relays, static systems, dynamic systems, etc. In general, the systems may be manned or unmanned. Their autonomous characteristics may also fall anywhere within the autonomy scale shown in **Table 1**. It should be stated again that as a consequence of **Observation 3**, this research has down-selected from the general SoS situation and is considering the analysis and design of unmanned, collaborative systems-of-systems. However, since part of this research will consider the implementation of currently available DoD unmanned systems in the SoS architecture, the unmanned systems considered may or may not be fully autonomous.

B.2 System-of-Systems Classifications

Beyond defining a general SoS, it is also possible to develop a classification structure for various types of systems-of-systems. In fact, before a designer would decide to proceed along the process of designing an SoS, it would be appropriate for the designer to wonder if there are different ways in which systems-of-systems may be classified. This is similar

to the situation of designing an individual system, since the design of a system is very dependent on the nature of the system itself. For example, the process of designing a jet engine is very different than the process of designing a computer chip. Though both a jet engine and a computer chip may be considered systems, they are obviously unique in the physical principles and abstract requirements underlying their design, development and operations. Consequently, it makes sense that there may exist various types of systems-of-systems which, if classified appropriately, would have distinct demands in terms of design, development, and operations. Therefore, an appropriate taxonomic distinction is useful.

Dr. Mark Maier¹, a well recognized researcher in the area of Systems Engineering, has provided a detailed description and taxonomic classification for systems-of-systems. In his seminal work on the classification of systems-of-systems he states, “The question addressed by this paper is whether or not there is a useful taxonomic distinction between various complex, large-scale systems that are commonly referred to as ‘systems-of-systems’ ” [98].

Maier’s taxonomic distinction is based on the system components having operational and managerial independence. This coincides with the first definition of an SoS presented in **Section B.1**. The two criteria form a taxonomic node for systems-of-systems, and any systems that do not meet these two criteria, according to Maier, should not be classified as an SoS. The need for a clear taxonomy is due to the concern that design heuristics for an SoS may vary depending on the type of SoS being considered. Expanding upon the two criteria presented for an SoS (managerial and operational independence of components), Maier was able to determine four distinct design principles for systems-of-systems as follows (note that Maier often uses the term ‘collaborative systems’ in place of ‘systems-of-systems’):

- Stable Intermediate Forms: A collaborative designer must pay close attention to the intermediate steps in a planned evolution. The collaborative system will take on intermediate forms dynamically and without direction, as part of its nature. Thus, careful attention must be paid to the existence and stability (in all suitable dimensions) of partial assemblages of components.

¹Dr. Mark Maier was a primary author of IEEE Standard 1471, *Recommended Practice for Architectural Description*

- **Policy Triage:** The collaborative system designer will not have coercive control over the systems configuration and evolution...In communication-centric systems, this means that design leverage will frequently be found in relatively abstract components (like data standards and network protocols).
- **Leverage at the Interfaces:** A collaborative system is defined by its interfaces. The interfaces, whether thought of as the actual physical interconnections or as higher level abstractions, are the primary points at which the designer can exert control.
- **Ensuring Cooperation:** A collaborative system exists because the partially independent elements decide to collaborate. The designer must consider why they will choose to collaborate and foster those reasons in the design.

Maier also argues that it becomes clear that communications are the foundation of an architecture of SoS's based on the design heuristics presented. Another key element from the design heuristics presented above is the idea that the design of an SoS includes "leverage at the interfaces".

B.3 Additional Terminology

The terms itemized below are continued from the discussion on critical terminology given in Section 3.2.1.

- **Requirement:** A statement that identifies a product or process operational, functional, or design characteristic or constraint, which is unambiguous, testable or measurable, and necessary for product or process acceptability. [76]
- **System Effectiveness:** A measurement of the ability of a system to satisfy its intended operational uses as a function of how the system performs under anticipated environmental conditions, and the ability to produce, test, distribute, operate, support, train, and dispose of the system throughout its life cycle [76]. "A measure of the extent to which a system may be expected to achieve a set of specific mission requirements" [65].

- Effectiveness Analysis: An analysis of how well a design solution will perform or operate given anticipated operational scenarios. [76]
- Sensitivity Analysis: An analytical or numerical approach to find which design parameters are most critical to the performance of the design, and what the critical ranges of those parameters are [42]. It studies the effects of parameter variations on the behavior of dynamic systems [147]. “Sensitivity analysis consists of a set of tools that can be utilized in the context of optimization, optimal design, or simply system analysis to assess the influence of parameters on the state of the system. Continuous sensitivity methods construct a sensitivity equation whose solution provides the sensitivity of the state variable with respect to a parameter” [141].

B.4 SoSE Wave Model Artifact Descriptions

The following SoSE wave model artifact descriptions are provided by Lane [94].

- Initiate SoS:
 - Provides foundational information to initiate the SoS. Artifacts created include *capability objectives*, *CONOPS*, *systems information*, and *risks and mitigations*.
 - Capability Objectives: Established to identify critical need(s) that provide justification for an SoS.
 - CONOPS: Created to provide context for critical need(s). Initial SoS CONOPS may be limited and focus only on current capabilities of interest.
 - Systems information: Captures initial system and subsystem level information for analysis.
 - Risks and mitigations: Captures initial risks.
- Conduct SoS Analysis:
 - Provides analysis of the SoS ‘as is’ and sets a basis for SoS evolution. Artifacts created include *SoS baseline*, *performance measures and methods*, *performance*

data, requirements space, the SoS SE planning elements, the SoS-level agreements, and the master plan. The *risks and mitigations* artifact is updated at this point and the other already created artifacts are used as part of the initial analysis.

- SoS baseline: Created as the initial SoS product baseline. The initial SoS should be composed of available systems. Multiple baselines should actually be defined. Each alternative baseline will depend on the selection of systems, the numbers of systems, and the various possible CONOPS.
- Performance measures and methods: Defines the initial set of appropriate measures and methods.
- Capability objectives and CONOPS: Used as part of initial analysis.
- Systems information: Used to guide initial analysis activities.
- Performance data: Captures initial data.
- Requirements space: Established as part of the initial analysis.
- Risks and mitigations: Updated as needed based on initial analyses.

- Develop SoS Architecture:

- Develops/evolves the persistent technical framework for addressing SoS evolution and a migration plan identifying risks and mitigations. The *SoS architecture*, the *SoS technical plans*, and the *Integrated Master Schedule (IMS)* are initiated during this step. The *requirements space* and *risks and mitigations* artifacts are updated at this point.
- SoS architecture: Documents the initial SoS ‘as is’. DoDAF products will likely be used for this. It will update over time and is to be maintained.
- Capability objectives and CONOPS: Used indirectly through performance relationships.
- Performance measures and methods: Used to identify and build in opportunities to measure architecture performance.

- Performance data: Used to assess the architecture and guide its evolution.
 - SoS baseline: Used to guide architecture evolution.
 - Systems information: Used to evaluate architecture evolution options and to identify potential risks.
 - Requirements space: Updated as new architecture needs are identified.
 - Risks and mitigations: Updated as needed with architecture related issues.
- Plan SoS Update:
 - Evaluates SoS backlog, priorities, and options to define plans for the next SoS upgrade cycle. No artifacts are created at this point, but all of the already initiated artifacts are either used or updated.
 - Capability objectives and CONOPS: Used to drive evaluation of alternatives and refine solution requirements.
 - Performance measures and methods: Used to identify and plan mechanisms to measure SoS performance.
 - Performance data: Uses results of analyses to guide planning for the next update cycle.
 - Requirements space: Any issues with alternatives meeting requirements are identified.
 - SoS baseline: Creates requirements for the baseline of the next update cycle.
 - Systems information: Used to evaluate and select capability options for the next update cycle and to identify potential risks.
 - SoS architecture: Used to plan updates.
 - Risks and mitigations: Updates as needed with planning related issues.
 - Implement SoS Update:
 - Oversees system implementations and plans/conducts SoS level testing, resulting in a new SoS product baseline.

- Continue SoS Analysis:
 - Ongoing SoS analysis revisits artifacts for the SoS as the basis for ongoing SoS evolution.

B.5 SoSE Artifact Characteristics

Table 6: SoSE Artifact Characteristics [38]

| SoS Information | Characteristics |
|----------------------------------|---|
| Capability Objectives | Focused on capabilities at the SoS-level. Solution(s) typically require multiple constituent systems, not all of which may be known in advance. Scope typically initially defined in the charter for the SoS. |
| CONOPS | Multiple system focus. Often developed after constituent systems have been fielded; Evolves over time, sometimes substantially. |
| Systems Information | Focus is on system-level information that affects SoS-level capability objectives. Extends beyond technical issues to include operational, fiscal, organizational, and planning issues. |
| Requirements | Requirements space versus set of specific requirements. Defined at a level of detail that enables trades among potential and actual constituent systems and interfacing external systems. |
| Performance Measures and Methods | Focus is on performance of SoS solution. As independent as possible of the specific systems to allow for assessment of alternative implementation approaches. |
| Performance Data | Often collected in operational environment. Used to support continuous improvement of the SoS. |
| SE Planning Elements | Focus is on determining rhythm, organizational structure, technical reviews, and decision processes across SoS evolution. Ability and willingness of constituent systems to support SoS plans is an important consideration. |
| Risks and Mitigations | Focus is on desired capabilities and undesirable emergent behaviors of the SoS. Includes single system risks or dependencies related to SoS capabilities and plans. |
| Master Plan | Focus is on SoS-level view across multiple increments and touch points for constituent systems. Reflects the SoS evolution strategy. Focus is often on continuous improvement versus achievement of a defined end state. |
| Agreements | Focus is on managing relationships among multiple organizations. Agreements support SoS evolution including specific commitments to execute SoS increment development. |
| Architecture | A shared framework primarily aimed at informing analysis and decisions for developing or evolving SoS capabilities. A context for understanding the relationships among constituent systems and developing implementation options for meeting capability requirements. Includes key constituent systems information, connectors and protocols used to communicate and/or synchronize processing across the constituents, key data elements/structures that cross interfaces, and key data conversions to facilitate data sharing and communications between constituents. |
| Technical Baselines | Focus is on SoS-level description plus identification of constituent system baselines that are part of the SoS baseline. |
| Technical Plan(s) | Focus is on planning the implementation and test of changes to constituent systems to execute an SoS increment. |
| Integrated Master Schedule | Set of SoS SE activities and milestones plus key single system activities and milestones that are driving SoS critical path. Focus is on key synchronization points among SoS constituents and pointers to development schedules of constituent systems for the current SoS increment. |

APPENDIX C

SENSOR ORIENTATION

The orientations of the world, vehicles and sensors must be clearly defined. This section will provide nomenclature, variable definitions, transformation matrices and geometrical views of all relevant characteristics. For example, a sensor will maintain a designed orientation relative to its carrier vehicle's body coordinate system. When a target is detected, the bearing and range is known relative to the sensor's frame of reference (*i.e.*, the sensor-centric coordinate system). The position of the target relative to the sensor frame of reference must then be transformed into the vehicle body coordinate system through an appropriate axis rotation (and possibly translation). Finally, the absolute position of the target can be known by transforming the vehicle-centric coordinates into a world-centric coordinate axis. The world-centric axis system is assumed to be an inertial frame fixed to the Earth.

A similar situation exists between the vehicle body axis and the vehicle's stability axis. These two frames of reference share a common origin but the stability axis system points in the direction of the vehicle motion. The angle of rotation between the body axis system and the stability axis results in the vehicle angle of attack (α) and/or the vehicle side-slip angle (β). The stability axis system is therefore useful in defining the forces of drag (*i.e.*, resistance) and lift on the vehicle.

C.1 Coordinate Transformation

The vector \mathbf{A} provides the position of the point A in a given coordinate system \mathbf{x} . Allow another coordinate system \mathbf{x}' to share a common origin with the system \mathbf{x} while rotating the axes of \mathbf{x}' away from \mathbf{x} some amount. Subsequently, the point A' can be described by the vector \mathbf{A}' relative to the \mathbf{x}' coordinate axis. The vector \mathbf{A}' is equivalent to the vector \mathbf{A} , but the components of the vectors differ based on their pose relative to their corresponding frames of reference.

$$\mathbf{A} = A_1\mathbf{i} + A_2\mathbf{j} + A_3\mathbf{k} \equiv A'_1\mathbf{i}' + A'_2\mathbf{j}' + A'_3\mathbf{k}' \quad (107)$$

In this situation it is the coordinate system that is rotating, not the object (the *object* in this example is the vector). The matrix used to describe the rotation of the coordinate system while the object remains fixed is called the *transformation matrix* $[T]$. If the object was being rotated while the coordinate frame remained fixed the *rotation matrix* $[R]$ would be utilized. It turns out that the matrices $[R]$ and $[T]$ are the transpose of each other, which will be useful later. Nonetheless, as for the current scenario the transformation matrix $[T_{x'/x}]$ consists of the nine direction cosine angles between the coordinate directions of each reference frame. The 3-D vector transformation equations are shown in Equation 108.

$$\mathbf{A}' = \begin{pmatrix} A'_1 \\ A'_2 \\ A'_3 \end{pmatrix} = \begin{bmatrix} \cos(\theta_{1'1}) & \cos(\theta_{1'2}) & \cos(\theta_{1'3}) \\ \cos(\theta_{2'1}) & \cos(\theta_{2'2}) & \cos(\theta_{2'3}) \\ \cos(\theta_{3'1}) & \cos(\theta_{3'2}) & \cos(\theta_{3'3}) \end{bmatrix} \begin{pmatrix} A_1 \\ A_2 \\ A_3 \end{pmatrix} = [T_{x'/x}]\mathbf{A} \quad (108)$$

Similarly, the vector \mathbf{A}' can be transformed from the \mathbf{x}' frame into the \mathbf{x} frame by using the transpose of the transformation matrix, $[T_{x'/x}]^T = [T_{x/x'}]$. The transpose turns out to equivalently be the inverse of the transformation matrix, $[T]^T = [T]^{-1}$.

The direction cosines are more easily understood through a 2-D example such as provided in Figure 137. It is shown that the \mathbf{x}' coordinate system has been rotated by an angle of θ away from the \mathbf{x} coordinate system. Therefore the following relationships hold true in defining the direction cosines between the rotated axis and the reference axis:

- $\cos \theta_{1'1} = \cos \theta$ represents the transformation from x_1 to x'_1
- $\cos \theta_{1'2} = \cos 90 - \theta = \sin \theta$ represents the transformation from x_2 to x'_1
- $\cos \theta_{2'1} = \cos 90 + \theta = -\sin \theta$ represents the transformation from x_1 to x'_2
- $\cos \theta_{2'2} = \cos \theta_{1'1}$ represents the transformation from x_2 to x'_2

Therefore, if the position of any point is known in the \mathbf{x} coordinate axis, the position of the point in the \mathbf{x}' axis system can be determined:

$$\begin{aligned} A'_1 &= A_1 \cos(\theta) + A_2 \sin(\theta) \\ A'_2 &= -A_1 \sin(\theta) + A_2 \cos(\theta) \end{aligned} = \begin{bmatrix} \cos(\theta_{1'1}) & \cos(\theta_{1'2}) \\ \cos(\theta_{2'1}) & \cos(\theta_{2'2}) \end{bmatrix} \begin{pmatrix} A_1 \\ A_2 \end{pmatrix} = \begin{pmatrix} A'_1 \\ A'_2 \end{pmatrix} \quad (109)$$

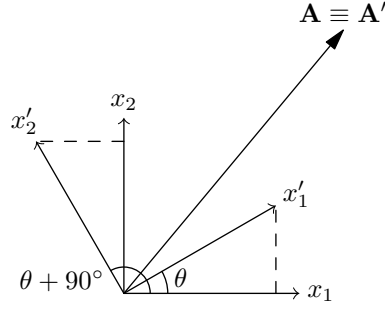


Figure 137: 2D Coordinate Transformation

In addition, successive applications of transformation matrices through matrix multiplication will result in a complete transformation from the initial reference frame to the final coordinate system for some point \mathbf{P} :

$$\mathbf{P}_Z = \begin{pmatrix} P_{Z_1} \\ P_{Z_2} \\ P_{Z_3} \end{pmatrix} = [T_{Z/Y}] \cdot [T_{Y/X}] \cdots [T_{C/B}] \cdot [T_{B/A}] \cdot \begin{pmatrix} P_{A_1} \\ P_{A_2} \\ P_{A_3} \end{pmatrix} = [T_{Z/A}] \cdot \mathbf{P}_A \quad (110)$$

This is particularly useful for rotating around one axis at a time.

C.2 Origin Translation

If the origin of the desired coordinate system is translated some distance away from the reference axes, then the resulting transformation simply includes the translation vector, \mathbf{t} , from one system to the other:

$$\begin{pmatrix} P_{Z_1} \\ P_{Z_2} \\ P_{Z_3} \end{pmatrix} = [T_{Z/A}] \cdot \begin{pmatrix} P_{A_1} - t_{A_1} \\ P_{A_2} - t_{A_2} \\ P_{A_3} - t_{A_3} \end{pmatrix} \quad (111)$$

C.3 Vehicle Body Axis Transformation and Translation

The first desired transformation is the ability to go from the world-axis system into the body-axis system of the vehicle. The world-axis system is defined here as fixed to the Earth with the z -axis pointed down towards the center of the Earth. The x and y axes lie in the horizontal plane and are orthogonal. The axes follow the right-hand rule. The nomenclature for the Earth-axis system will use a subscript e : (x_e, y_e, z_e) . The vehicle-axis system is defined with the x -axis pointing out of the nose of the vehicle, the y -axis facing out of the right side of the vehicle (*i.e.*, the starboard side), and the z -axis pointed down from the vehicle according to the right-hand rule. The nomenclature for the body-axis system will use the subscript b : (x_b, y_b, z_b) .

Euler angles will be used to transform a vector from the Earth-axis system into the body-axis system [182]. The Euler angles represent successive rotations of the axes through yaw (Ψ), pitch (Θ), and roll (Φ). The yaw angle represents a rotation of the xy plane around the z -axis. Pitch is then the rotation of the xz plane about the y axis, and roll is the rotation of the zy plane about the x -axis. These successive rotations produce three transformation matrices. The result for a vector P is:

$$\begin{aligned} \begin{pmatrix} P_{x_b} \\ P_{y_b} \\ P_{z_b} \end{pmatrix} &= [T_{roll}][T_{pitch}][T_{yaw}] \cdot \begin{pmatrix} P_{x_e} - t_{x_e} \\ P_{y_e} - t_{y_e} \\ P_{z_e} - t_{z_e} \end{pmatrix} \\ &= \begin{bmatrix} 1 & 0 & 0 \\ 0 & \cos \Phi & \sin \Phi \\ 0 & -\sin \Phi & \cos \Phi \end{bmatrix} \begin{bmatrix} \cos \Theta & 0 & -\sin \Theta \\ 0 & 1 & 0 \\ \sin \Theta & 0 & \cos \Theta \end{bmatrix} \begin{bmatrix} \cos \Psi & \sin \Psi & 0 \\ -\sin \Psi & \cos \Psi & 0 \\ 0 & 0 & 1 \end{bmatrix} \cdot \begin{pmatrix} P_{x_e} - t_{x_e} \\ P_{y_e} - t_{y_e} \\ P_{z_e} - t_{z_e} \end{pmatrix} \end{aligned} \quad (112)$$

where the yaw, pitch and roll angles maintain the following limits:

$$\begin{aligned} 0 &\leq \Psi \leq 2\pi \\ -\pi/2 &\leq \Theta \leq \pi/2 \\ -\pi &\leq \Phi \leq \pi \end{aligned}$$

In order to perform the reverse transformation, from the body-axis system into the

Earth-axis system, the transformation matrices are transposed and applied in reverse order:

$$\begin{aligned}
\begin{pmatrix} P_{x_e} \\ P_{y_e} \\ P_{z_e} \end{pmatrix} &= [T_{yaw}]^T [T_{pitch}]^T [T_{roll}]^T \cdot \begin{pmatrix} P_{x_b} \\ P_{y_b} \\ P_{z_b} \end{pmatrix} + \begin{pmatrix} t_{x_e} \\ t_{y_e} \\ t_{z_e} \end{pmatrix} \\
&= \begin{bmatrix} \cos \Psi & -\sin \Psi & 0 \\ \sin \Psi & \cos \Psi & 0 \\ 0 & 0 & 1 \end{bmatrix} \begin{bmatrix} \cos \Theta & 0 & \sin \Theta \\ 0 & 1 & 0 \\ -\sin \Theta & 0 & \cos \Theta \end{bmatrix} \begin{bmatrix} 1 & 0 & 0 \\ 0 & \cos \Phi & -\sin \Phi \\ 0 & \sin \Phi & \cos \Phi \end{bmatrix} \cdot \begin{pmatrix} P_{x_b} \\ P_{y_b} \\ P_{z_b} \end{pmatrix} + \begin{pmatrix} t_{x_e} \\ t_{y_e} \\ t_{z_e} \end{pmatrix}
\end{aligned} \tag{113}$$

C.4 Stability Axis Transformation

The transformation from the stability axis into the body axis is initiated through the sideslip (β) transformation followed by the angle of attack (α) transformation.

$$\begin{aligned}
\begin{pmatrix} Q_{x_b} \\ Q_{y_b} \\ Q_{z_b} \end{pmatrix} &= [T_\alpha][T_\beta] \cdot \begin{pmatrix} Q_{x_s} \\ Q_{y_s} \\ Q_{z_s} \end{pmatrix} \\
&= \begin{bmatrix} \cos \alpha & 0 & -\sin \alpha \\ 0 & 1 & 0 \\ \sin \alpha & 0 & \cos \alpha \end{bmatrix} \begin{bmatrix} \cos \beta & \sin \beta & 0 \\ -\sin \beta & \cos \beta & 0 \\ 0 & 0 & 1 \end{bmatrix} \cdot \begin{pmatrix} Q_{x_s} \\ Q_{y_s} \\ Q_{z_s} \end{pmatrix} \\
&= \begin{bmatrix} \cos(\alpha) \cos(\beta) & \cos(\alpha) \sin(\beta) & -\sin(\alpha) \\ -\sin(\beta) & \cos(\beta) & 0 \\ \cos(\beta) \sin(\alpha) & \sin(\alpha) \sin(\beta) & \cos(\alpha) \end{bmatrix} \cdot \begin{pmatrix} Q_{x_s} \\ Q_{y_s} \\ Q_{z_s} \end{pmatrix}
\end{aligned} \tag{114}$$

Then, if the vector is needed in the Earth-axis system, the calculated vector Q_b can be applied to the body-to-Earth transformation given in Equation 113, as shown in Equation 115.

$$\begin{pmatrix} Q_{x_e} \\ Q_{y_e} \\ Q_{z_e} \end{pmatrix} = [T_{yaw}]^T [T_{pitch}]^T [T_{roll}]^T \cdot [T_\alpha][T_\beta] \cdot \begin{pmatrix} Q_{x_s} \\ Q_{y_s} \\ Q_{z_s} \end{pmatrix} + \begin{pmatrix} t_{x_e} \\ t_{y_e} \\ t_{z_e} \end{pmatrix} \tag{115}$$

An important distinction should be raised at this point about the difference between pitch angle (Θ) and angle-of-attack (α). Pitch angle is defined between the horizontal plane of

the body-axis of a vehicle and the horizontal frame of the Earth-axis. In contrast, angle-of-attack is defined between the horizontal plane of the body-axis and the horizontal plane of the *stability-axis*. If the local wind relative to an aircraft (or water current relative to a seacraft), is in the horizontal Earth-axis plane (*i.e.*, if the wind/current vector has no velocity component in the z -direction), then the vehicle pitch angle and the angle-of-attack will be equivalent. But in general this is not true.

Figure 138 presents a scene in which the vehicle is translated away from the Earth-axis with a positive pitch-angle, Θ . The Earth-axis plus the translation vector, t , has also been drawn at the vehicle origin in order to display the rotation of the body-axis away from the translated Earth-axis. The stability axis is not shown since it is coincident with the translated Earth-axis. This results in an angle of attack, α , and pitch angle, Θ , equivalence. The vehicle is placed at a depth $z_v \equiv d$ from the surface of the water.

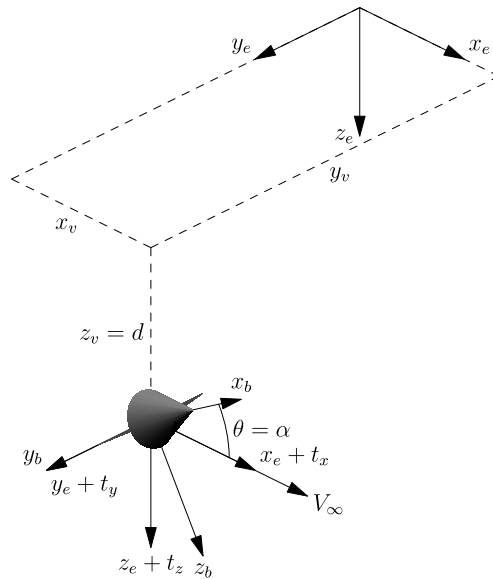


Figure 138: Example of Axis Rotations with $\Theta = \alpha$

C.5 Sensor Axis: Sonar Integration

The installed sensors also require associated coordinate systems. The origin of a sensor-axis system can be located at any point on the vehicle body, but for this work all sensor origins will be coincident with the vehicle body-axis origin. Two sensors are being considered in this work: forward looking sonar and side-scan sonar. Depending on the design, the sonar

can be omnidirectional or directed. For an omnidirectional sonar, orientation of the sensor is arbitrary. However, with directivity included it is possible to maximize the area ensonified by rotating the orientation of the sensor-axis relative to the vehicle body-axis. The sensor-axis system is defined as (x_r, y_r, z_r) and can undergo transformations through pitch (θ) and yaw (ψ) angles.

It is also helpful to define spherical coordinates for the sensor-axis system defined as (r, σ, ρ) . The coordinate r is the magnitude of a vector \mathbf{R} between the sensor-axis origin and a point R . The coordinate σ is the angle between the positive x_r -axis and the projection of the vector \mathbf{R} onto the $x_r y_r$ -plane. Finally, the coordinate ρ is the angle between the positive z_r -axis and the vector \mathbf{R} . The relationship between the sensor-axis Cartesian coordinates and spherical coordinates are given in Equation 116.

$$\begin{aligned}x_r &= r \sin \rho \cos \sigma \\y_r &= r \sin \rho \sin \sigma \\z_r &= r \cos \rho\end{aligned}\tag{116}$$

where r is restricted to $r \geq 0$, $-\pi \leq \sigma \leq \pi$, and $0 \leq \rho \leq \pi$.

Subsequently, to transform a point R from the vehicle body-axis system to the sensor-axis system, the yaw and pitch transformation matrices ($[T_{yaw}]_r$ and $[T_{pitch}]_r$ respectively)

are applied to the body-axis Cartesian coordinates.

$$\begin{aligned}
\begin{pmatrix} R_{x_r} \\ R_{y_r} \\ R_{z_r} \end{pmatrix} &= [T_{pitch}]_r [T_{yaw}]_r \cdot \begin{pmatrix} R_{x_b} \\ R_{y_b} \\ R_{z_b} \end{pmatrix} \\
&= \begin{bmatrix} \cos \theta & 0 & -\sin \theta \\ 0 & 1 & 0 \\ \sin \theta & 0 & \cos \theta \end{bmatrix} \begin{bmatrix} \cos \psi & \sin \psi & 0 \\ -\sin \psi & \cos \psi & 0 \\ 0 & 0 & 1 \end{bmatrix} \cdot \begin{pmatrix} R_{x_b} \\ R_{y_b} \\ R_{z_b} \end{pmatrix} \\
&= \begin{bmatrix} \cos(\theta) \cos(\psi) & \cos(\theta) \sin(\psi) & -\sin(\theta) \\ -\sin(\psi) & \cos(\psi) & 0 \\ \cos(\psi) \sin(\theta) & \sin(\theta) \sin(\psi) & \cos(\theta) \end{bmatrix} \cdot \begin{pmatrix} R_{x_b} \\ R_{y_b} \\ R_{z_b} \end{pmatrix}
\end{aligned} \tag{117}$$

where the yaw and pitch angles can take on the following values:

$$\begin{aligned}
0 &\leq \psi \leq 2\pi \\
-\pi/2 &\leq \theta \leq \pi/2
\end{aligned}$$

Subsequently, to go from the sensor coordinates into the body coordinates:

$$\begin{aligned}
\begin{pmatrix} R_{x_b} \\ R_{y_b} \\ R_{z_b} \end{pmatrix} &= [T_{yaw}]_r^T [T_{pitch}]_r^T \cdot \begin{pmatrix} R_{x_r} \\ R_{y_r} \\ R_{z_r} \end{pmatrix} \\
&= \begin{bmatrix} \cos \psi & -\sin \psi & 0 \\ \sin \psi & \cos \psi & 0 \\ 0 & 0 & 1 \end{bmatrix} \begin{bmatrix} \cos \theta & 0 & \sin \theta \\ 0 & 1 & 0 \\ -\sin \theta & 0 & \cos \theta \end{bmatrix} \cdot \begin{pmatrix} R_{x_r} \\ R_{y_r} \\ R_{z_r} \end{pmatrix} \\
&= \begin{bmatrix} \cos(\theta) \cos(\psi) & -\sin(\psi) & \cos(\psi) \sin(\theta) \\ \sin(\psi) \cos(\theta) & \cos(\psi) & \sin(\psi) \sin(\theta) \\ -\sin(\theta) & 0 & \cos(\theta) \end{bmatrix} \cdot \begin{pmatrix} R_{x_r} \\ R_{y_r} \\ R_{z_r} \end{pmatrix}
\end{aligned} \tag{118}$$

and finally to transform into the Earth-axis:

$$\begin{pmatrix} R_{x_e} \\ R_{y_e} \\ R_{z_e} \end{pmatrix} = [T_{yaw}]_b^T [T_{pitch}]_b^T [T_{roll}]_b^T \cdot [T_{pitch}]_r [T_{yaw}]_r \cdot \begin{pmatrix} R_{x_r} \\ R_{y_r} \\ R_{z_r} \end{pmatrix} \quad (119)$$

Consequently, the orientation of the vehicle and sensor must be clearly defined along with appropriate transformation matrices. Depending on the designed sensor–vehicle interface, a sensor may be constrained to maintain a specific orientation relative to the vehicle’s body coordinate system. When a target is detected, the bearing and range is known relative to the sensor’s frame of reference (*i.e.*, the sensor-centric coordinate system). The position of the target relative to the sensor frame of reference must then be transformed into the vehicle body coordinate system through an appropriate axis rotation (and possibly translation). Similarly, the vehicle motion (which is defined within a stability-axis) may not be in line with the vehicle body-axis, resulting in some angle of attack. These effects should be clearly delineated through the transformations and translations defined above.

APPENDIX D

LATERAL RANGE CURVES FROM VXE

This Appendix provides the full set of lateral range curves that resulted from the Virtual Experimentation Environment (VXE) experiments. Each row of curves in this Appendix corresponds to a specific sensor design depending on parameters such as beam width, frequency, and power level. Each column corresponds to the low, medium and high velocities from left to right, respectively. The velocities are $2m/s$, $5m/s$ and $8m/s$.

D.1 Forward Looking Sonar

There were 36 forward-looking sonar designs established by varying the parameterized power, frequency, and beam width. The setup of those parameters resulted in specific sensor Source Levels (SL), pulse lengths, sizes (diameters), and maximum deterministic ranges based on the sonar equation analysis. Also, the sensor depths were calculated based on the requirement that the sonar beam must intercept the seabed. The required depth was calculated geometrically based on a 45° grazing angle and the maximum range of the specific sensor. The minimum depth allowed was 10 meters.

Table 7 corresponds with the lateral range curve results in Figure 139. Two trends are clear: increasing beam width and increasing velocity caused a decrease in effective sweep width. Recall that the columns in Figure 139 correspond to increasing velocity for each specific sensor design.

Table 7: FLS Parameter Setup Used for VXE Results in Figure 139

| <i>Power (W)</i> | <i>freq (kHz)</i> | <i>pulse length (μs)</i> | <i>BW (rad)</i> | <i>diameter (cm)</i> | <i>SL (dB)</i> | <i>R_{max} (m)</i> | <i>Veh Depth (m)</i> |
|------------------|-------------------|---|-----------------|----------------------|----------------|----------------------------|----------------------|
| 0.1 | 400 | 12.50 | 0.26 | 1.52 | 179.91 | 279.46 | 10.00 |
| 0.1 | 400 | 12.50 | 0.41 | 0.95 | 175.83 | 252.98 | 10.00 |
| 0.1 | 400 | 12.50 | 0.69 | 0.57 | 171.39 | 224.69 | 10.00 |
| 0.1 | 400 | 12.50 | 1.07 | 0.38 | 167.85 | 202.58 | 10.00 |

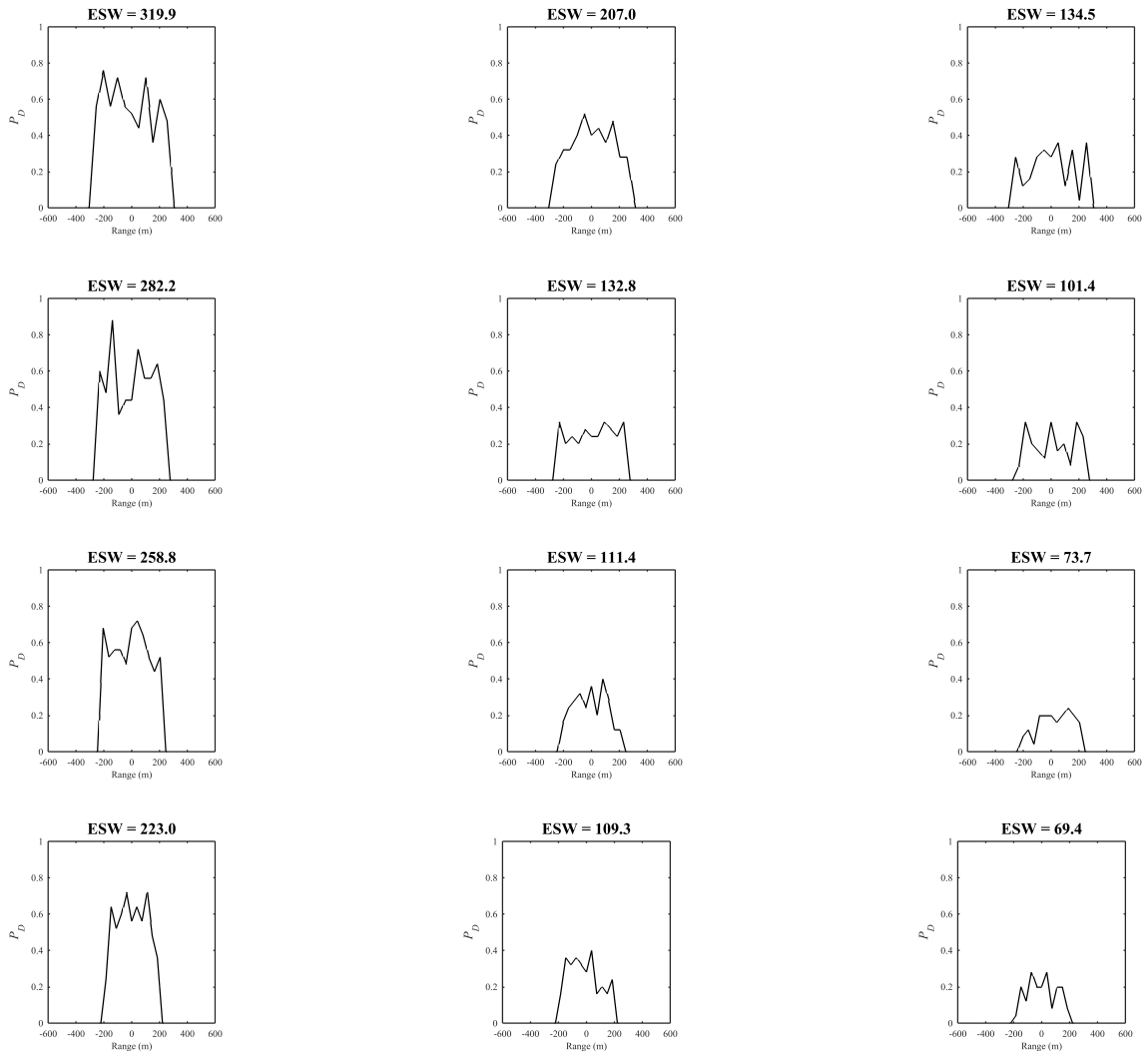


Figure 139: FLS VXE Results for Parameterization in Table 7

Table 8 corresponds with the lateral range curve results in Figure 140. The frequency values are now greater than in the previous plots, and the result was much lower ESW values overall.

Table 8: FLS Parameter Setup Used for VXE Results in Figure 140

| <i>Power (W)</i> | <i>freq (kHz)</i> | <i>pulse length (μs)</i> | <i>BW (rad)</i> | <i>diameter (cm)</i> | <i>SL (dB)</i> | <i>R_{max} (m)</i> | <i>Veh Depth (m)</i> |
|------------------|-------------------|---|-----------------|----------------------|----------------|----------------------------|----------------------|
| 0.1 | 1000 | 5.00 | 0.26 | 0.61 | 179.91 | 113.85 | 19.50 |
| 0.1 | 1000 | 5.00 | 0.41 | 0.38 | 175.83 | 103.50 | 26.81 |
| 0.1 | 1000 | 5.00 | 0.69 | 0.23 | 171.39 | 92.44 | 34.64 |
| 0.1 | 1000 | 5.00 | 1.07 | 0.15 | 167.85 | 83.77 | 40.76 |

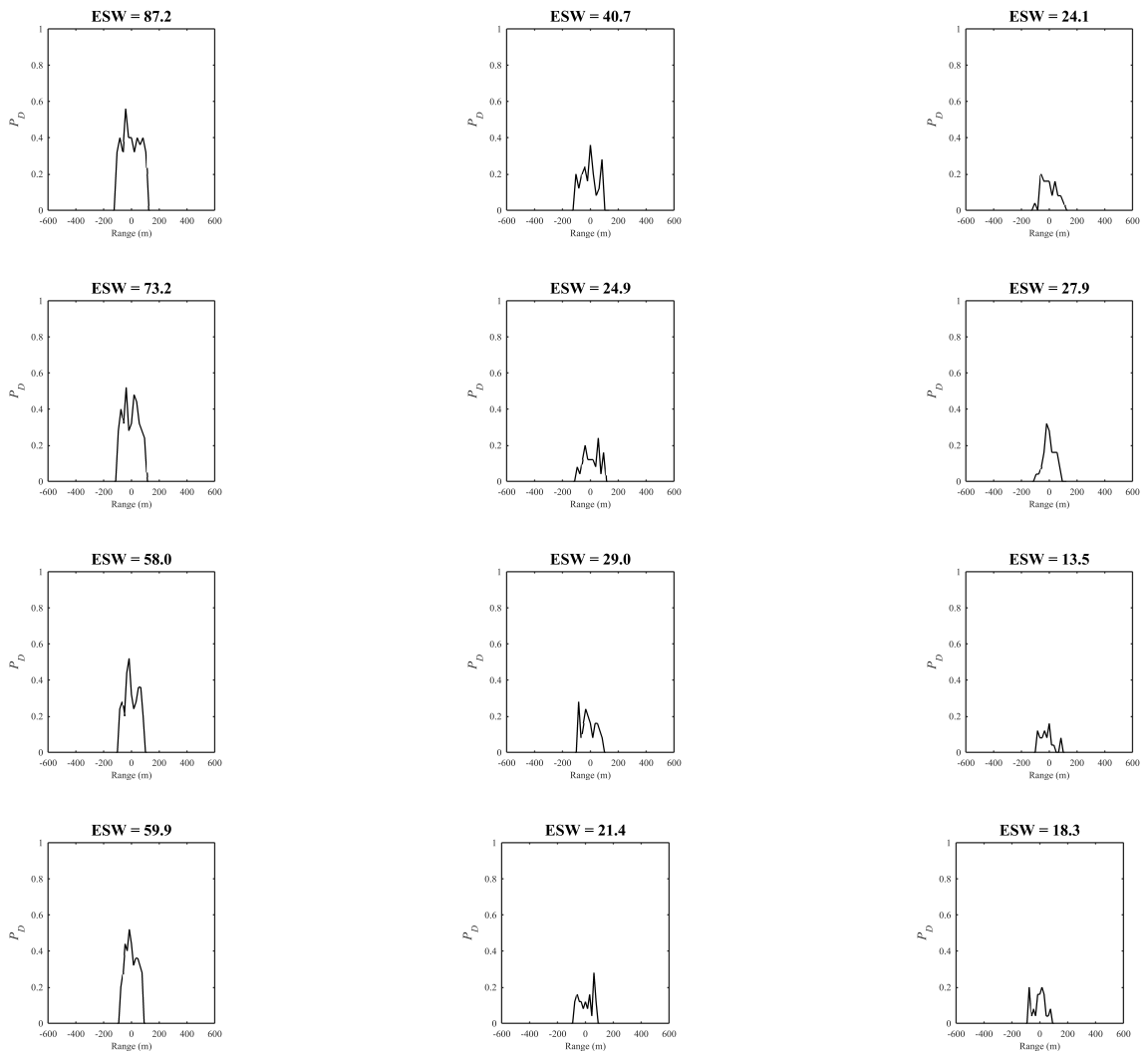


Figure 140: FLS VXE Results for Parameterization in Table 8

Table 9 corresponds with the lateral range curve results in Figure 141. The frequency values are now the highest chosen (1600 kHz).

Table 9: FLS Parameter Setup Used for VXE Results in Figure 141

| <i>Power (W)</i> | <i>freq (kHz)</i> | <i>pulse length (μs)</i> | <i>BW (rad)</i> | <i>diameter (cm)</i> | <i>SL (dB)</i> | <i>R_{max} (m)</i> | <i>Veh Depth (m)</i> |
|------------------|-------------------|---|-----------------|----------------------|----------------|----------------------------|----------------------|
| 0.1 | 1600 | 3.13 | 0.26 | 0.38 | 179.91 | 57.81 | 59.13 |
| 0.1 | 1600 | 3.13 | 0.41 | 0.24 | 175.83 | 52.82 | 62.65 |
| 0.1 | 1600 | 3.13 | 0.69 | 0.14 | 171.39 | 47.47 | 66.44 |
| 0.1 | 1600 | 3.13 | 1.07 | 0.09 | 167.85 | 43.27 | 69.40 |

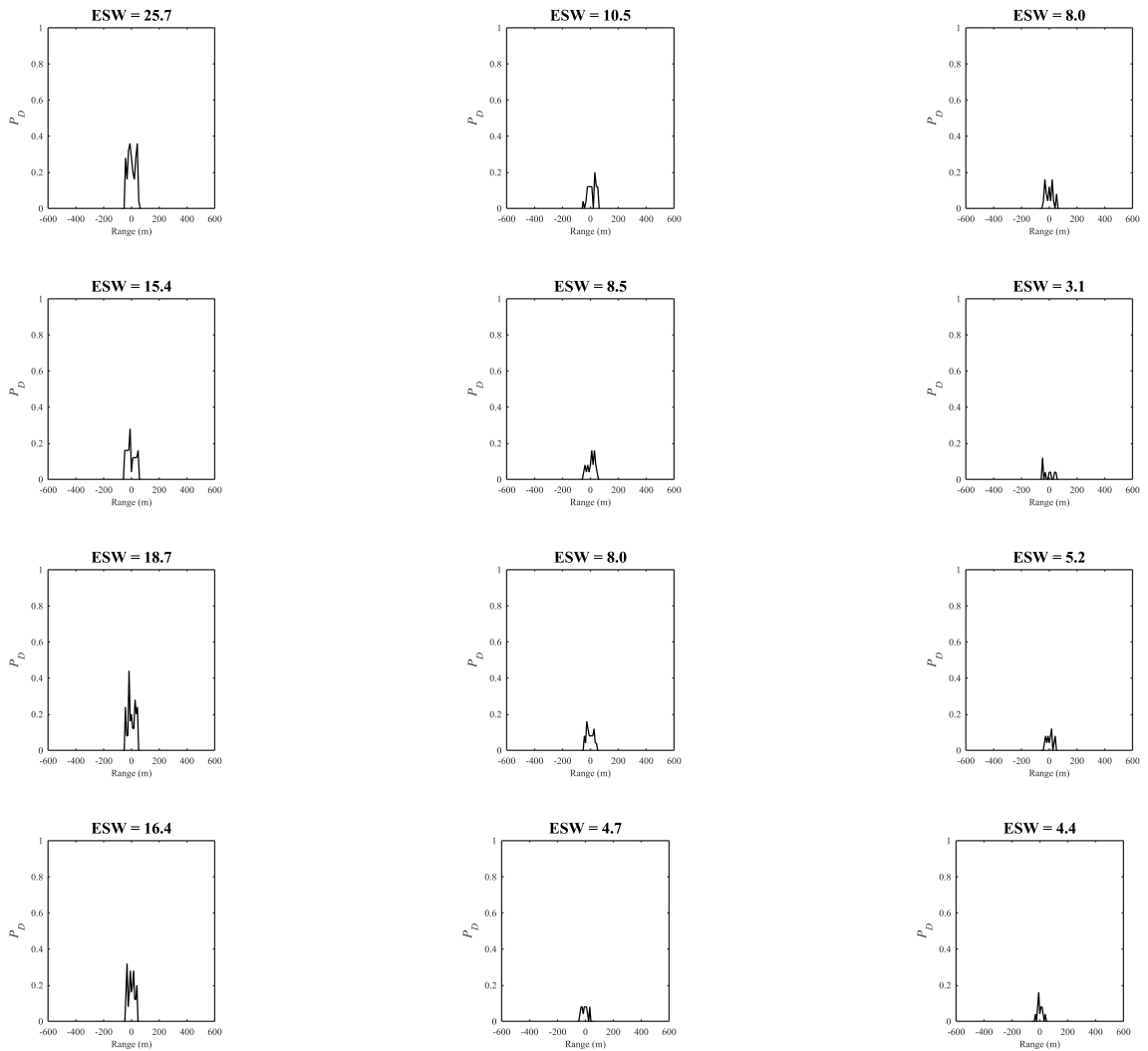


Figure 141: FLS VXE Results for Parameterization in Table 9

Table 10 corresponds with the lateral range curve results in Figure 142.

Table 10: FLS Parameter Setup Used for VXE Results in Figure 142

| <i>Power (W)</i> | <i>freq (kHz)</i> | <i>pulse length (μs)</i> | <i>BW (rad)</i> | <i>diameter (cm)</i> | <i>SL (dB)</i> | <i>R_{max} (m)</i> | <i>Veh Depth (m)</i> |
|------------------|-------------------|---|-----------------|----------------------|----------------|----------------------------|----------------------|
| 50000 | 400 | 12.50 | 0.26 | 1.52 | 236.90 | 472.93 | 10.00 |
| 50000 | 400 | 12.50 | 0.41 | 0.95 | 232.81 | 444.55 | 10.00 |
| 50000 | 400 | 12.50 | 0.69 | 0.57 | 228.38 | 413.90 | 10.00 |
| 50000 | 400 | 12.50 | 1.07 | 0.38 | 224.84 | 389.62 | 10.00 |

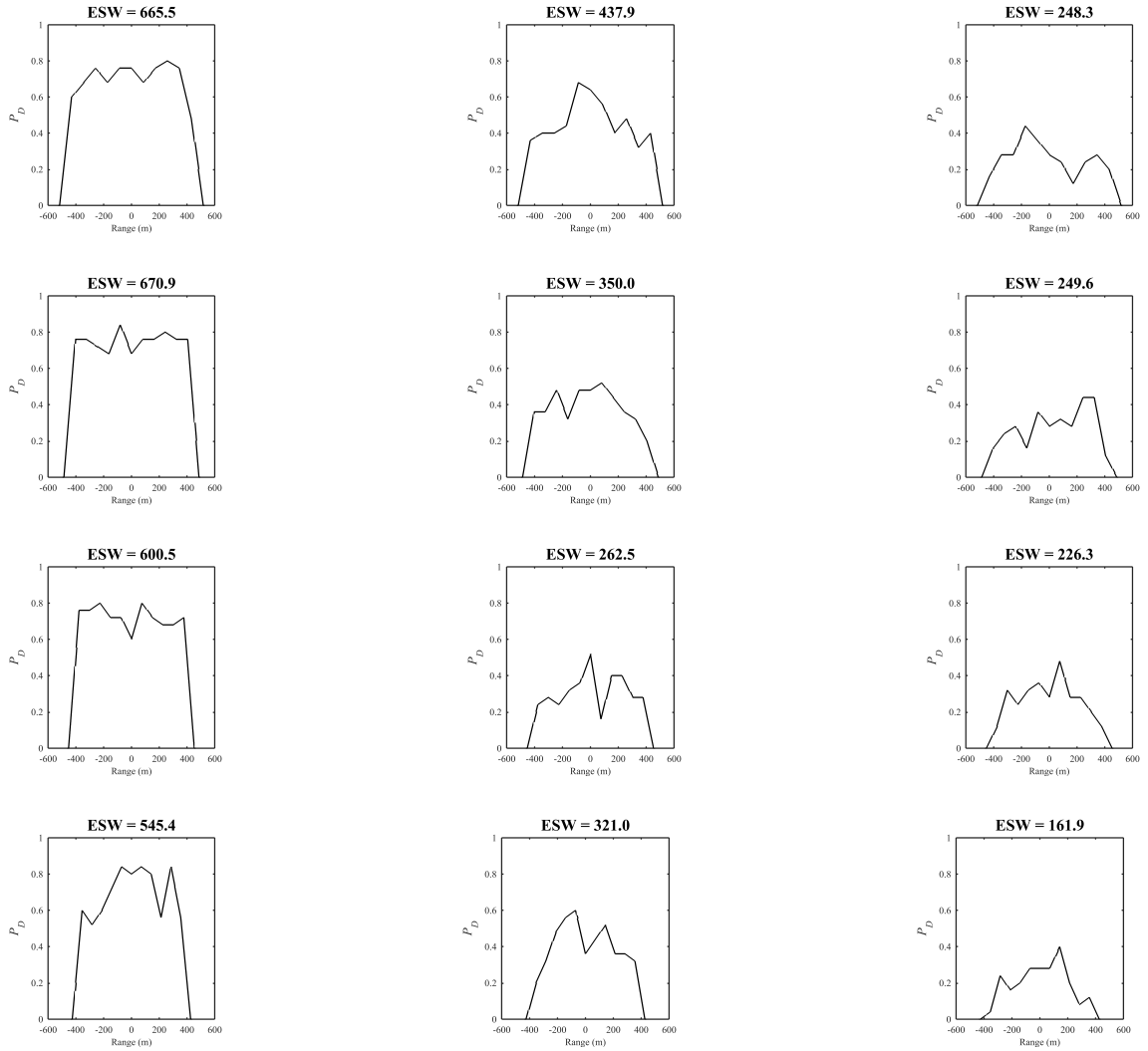


Figure 142: FLS VXE Results for Parameterization in Table 10

Table 11 corresponds with the lateral range curve results in Figure 143.

Table 11: FLS Parameter Setup Used for VXE Results in Figure 143

| <i>Power (W)</i> | <i>freq (kHz)</i> | <i>pulse length (μs)</i> | <i>BW (rad)</i> | <i>diameter (cm)</i> | <i>SL (dB)</i> | <i>R_{max} (m)</i> | <i>Veh Depth (m)</i> |
|------------------|-------------------|---|-----------------|----------------------|----------------|----------------------------|----------------------|
| 50000 | 1000 | 5.00 | 0.26 | 0.61 | 236.90 | 189.15 | 10.00 |
| 50000 | 1000 | 5.00 | 0.41 | 0.38 | 232.81 | 178.12 | 10.00 |
| 50000 | 1000 | 5.00 | 0.69 | 0.23 | 228.38 | 166.20 | 10.00 |
| 50000 | 1000 | 5.00 | 1.07 | 0.15 | 224.84 | 156.76 | 10.00 |

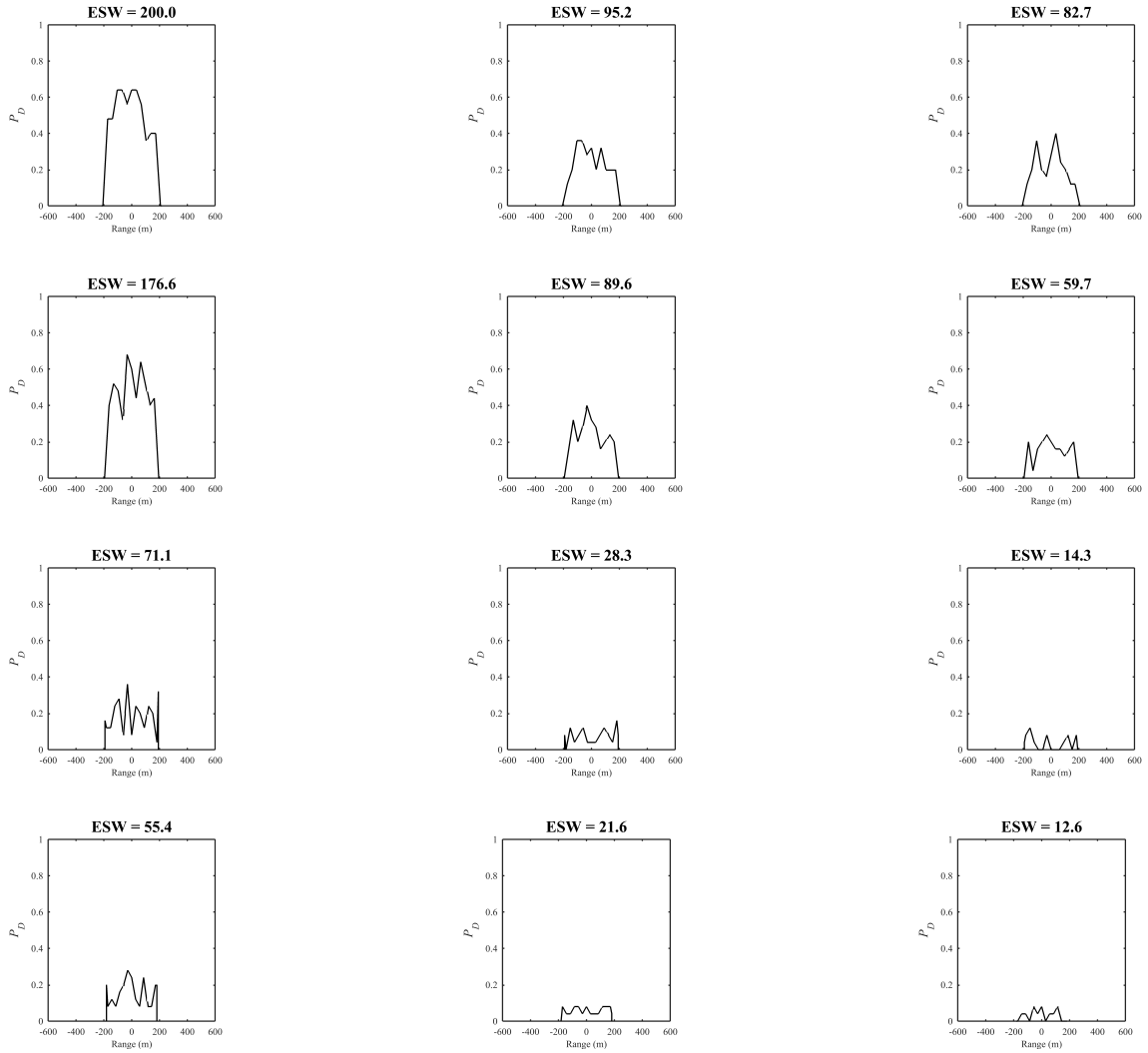


Figure 143: FLS VXE Results for Parameterization in Table 11

Table 12 corresponds with the lateral range curve results in Figure 144.

Table 12: FLS Parameter Setup Used for VXE Results in Figure 144

| <i>Power (W)</i> | <i>freq (kHz)</i> | <i>pulse length (μs)</i> | <i>BW (rad)</i> | <i>diameter (cm)</i> | <i>SL (dB)</i> | <i>R_{max} (m)</i> | <i>Veh Depth (m)</i> |
|------------------|-------------------|---|-----------------|----------------------|----------------|----------------------------|----------------------|
| 50000 | 1600 | 3.13 | 0.26 | 0.38 | 236.90 | 94.00 | 33.53 |
| 50000 | 1600 | 3.13 | 0.41 | 0.24 | 232.81 | 88.70 | 37.28 |
| 50000 | 1600 | 3.13 | 0.69 | 0.14 | 228.38 | 82.98 | 41.32 |
| 50000 | 1600 | 3.13 | 1.07 | 0.09 | 224.84 | 78.45 | 44.53 |

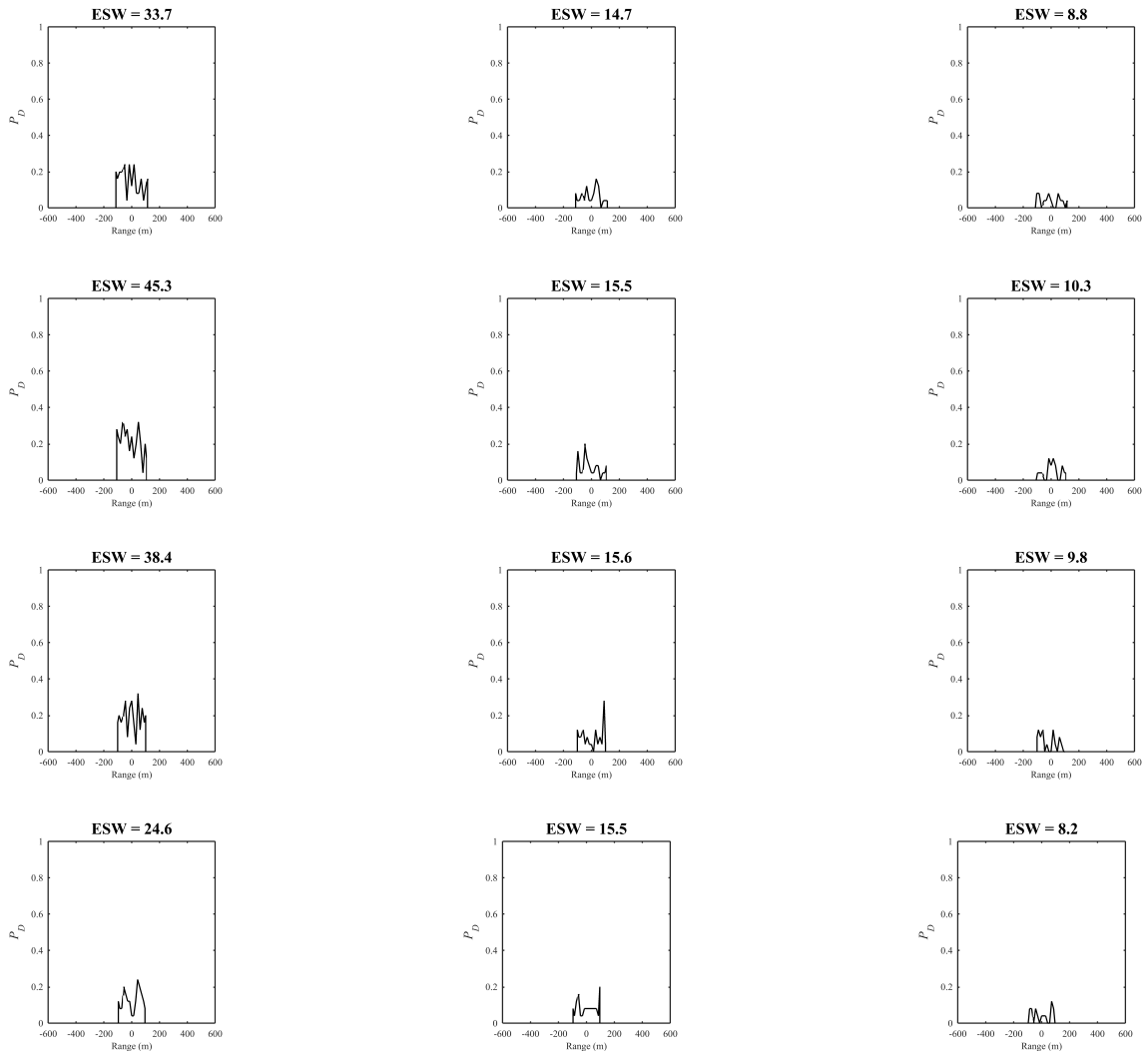


Figure 144: FLS VXE Results for Parameterization in Table 12

Table 13 corresponds with the lateral range curve results in Figure 145.

Table 13: FLS Parameter Setup Used for VXE Results in Figure 145

| <i>Power (W)</i> | <i>freq (kHz)</i> | <i>pulse length (μs)</i> | <i>BW (rad)</i> | <i>diameter (cm)</i> | <i>SL (dB)</i> | <i>R_{max} (m)</i> | <i>Veh Depth (m)</i> |
|------------------|-------------------|---|-----------------|----------------------|----------------|----------------------------|----------------------|
| 100000 | 400 | 12.50 | 0.26 | 1.52 | 239.91 | 483.45 | 10.00 |
| 100000 | 400 | 12.50 | 0.41 | 0.95 | 235.83 | 455.00 | 10.00 |
| 100000 | 400 | 12.50 | 0.69 | 0.57 | 231.39 | 424.27 | 10.00 |
| 100000 | 400 | 12.50 | 1.07 | 0.38 | 227.85 | 399.92 | 10.00 |

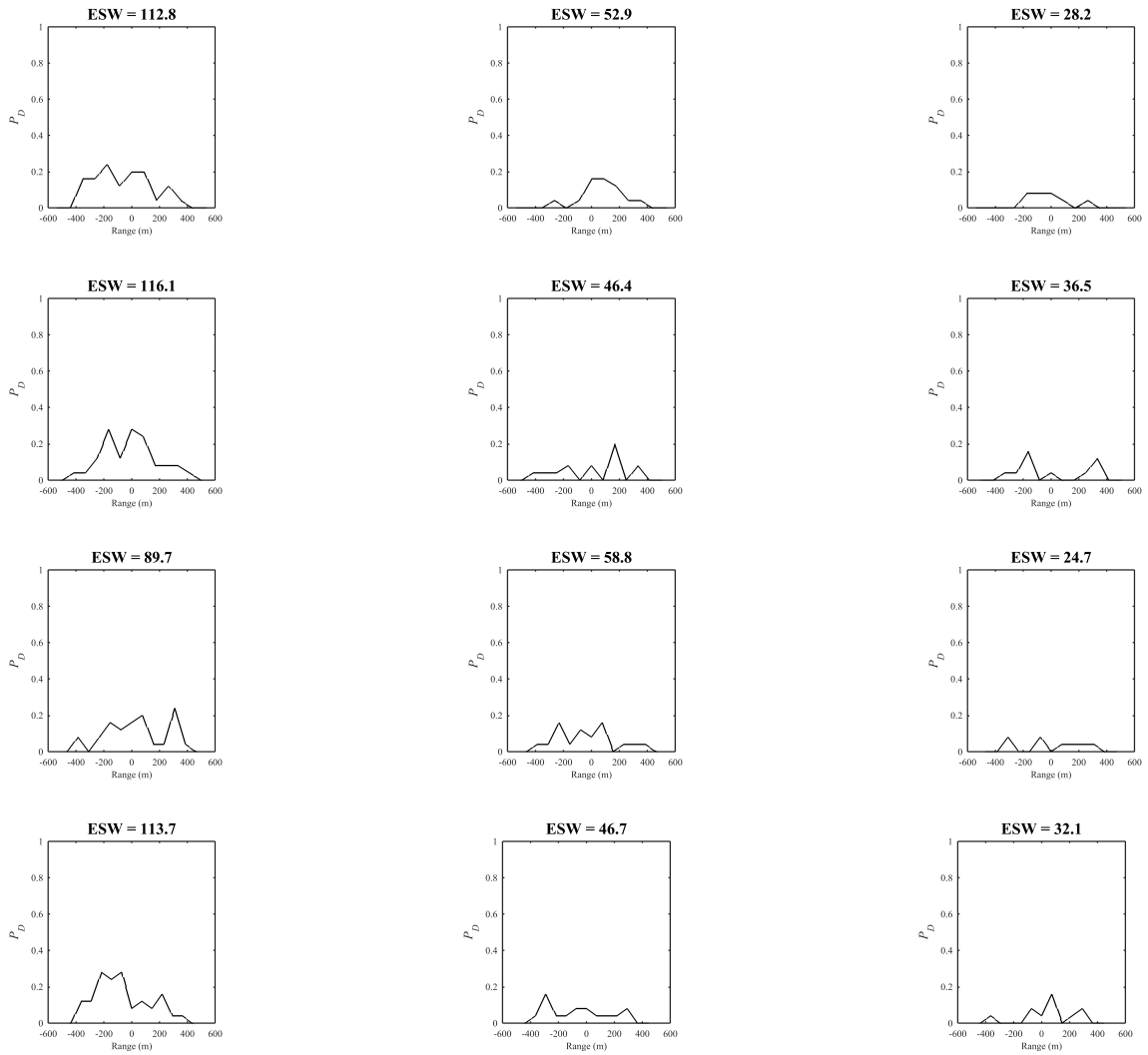


Figure 145: FLS VXE Results for Parameterization in Table 13

Table 14 corresponds with the lateral range curve results in Figure 146.

Table 14: FLS Parameter Setup Used for VXE Results in Figure 146

| <i>Power (W)</i> | <i>freq (kHz)</i> | <i>pulse length (μs)</i> | <i>BW (rad)</i> | <i>diameter (cm)</i> | <i>SL (dB)</i> | <i>R_{max} (m)</i> | <i>Veh Depth (m)</i> |
|------------------|-------------------|---|-----------------|----------------------|----------------|----------------------------|----------------------|
| 100000 | 1000 | 5.00 | 0.26 | 0.61 | 239.91 | 193.23 | 10.00 |
| 100000 | 1000 | 5.00 | 0.41 | 0.38 | 235.83 | 182.18 | 10.00 |
| 100000 | 1000 | 5.00 | 0.69 | 0.23 | 231.39 | 170.23 | 10.00 |
| 100000 | 1000 | 5.00 | 1.07 | 0.15 | 227.85 | 160.77 | 10.00 |

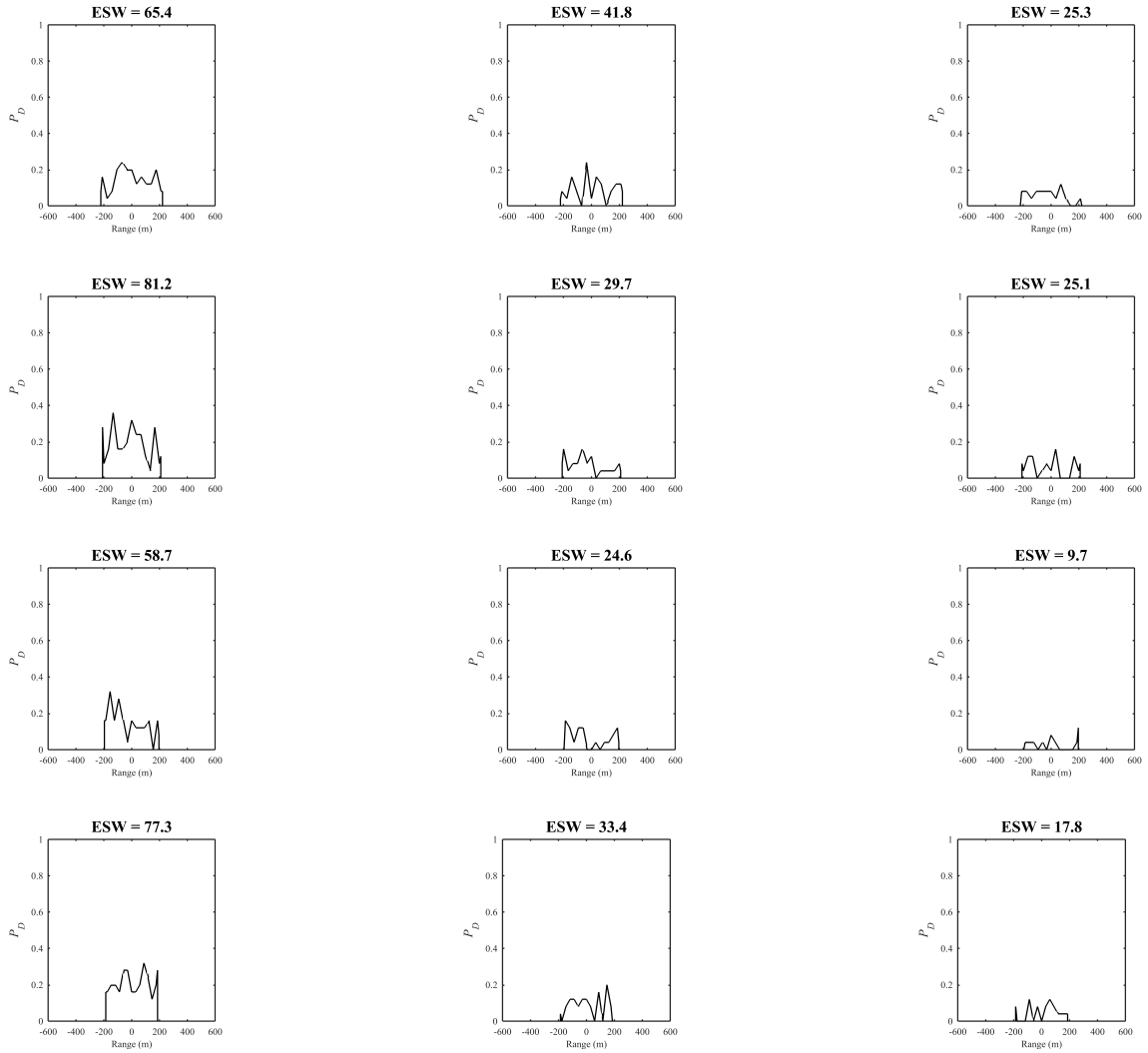


Figure 146: FLS VXE Results for Parameterization in Table 14

Table 15 corresponds with the lateral range curve results in Figure 147.

Table 15: FLS Parameter Setup Used for VXE Results in Figure 147

| Power (W) | freq (kHz) | pulse length (μ s) | BW (rad) | diameter (cm) | SL (dB) | R_{max} (m) | Veh Depth (m) |
|-----------|------------|-------------------------|----------|---------------|---------|---------------|---------------|
| 100000 | 1600 | 3.13 | 0.26 | 0.38 | 239.91 | 95.95 | 32.15 |
| 100000 | 1600 | 3.13 | 0.41 | 0.24 | 235.83 | 90.65 | 35.90 |
| 100000 | 1600 | 3.13 | 0.69 | 0.14 | 231.39 | 84.92 | 39.95 |
| 100000 | 1600 | 3.13 | 1.07 | 0.09 | 227.85 | 80.38 | 43.17 |

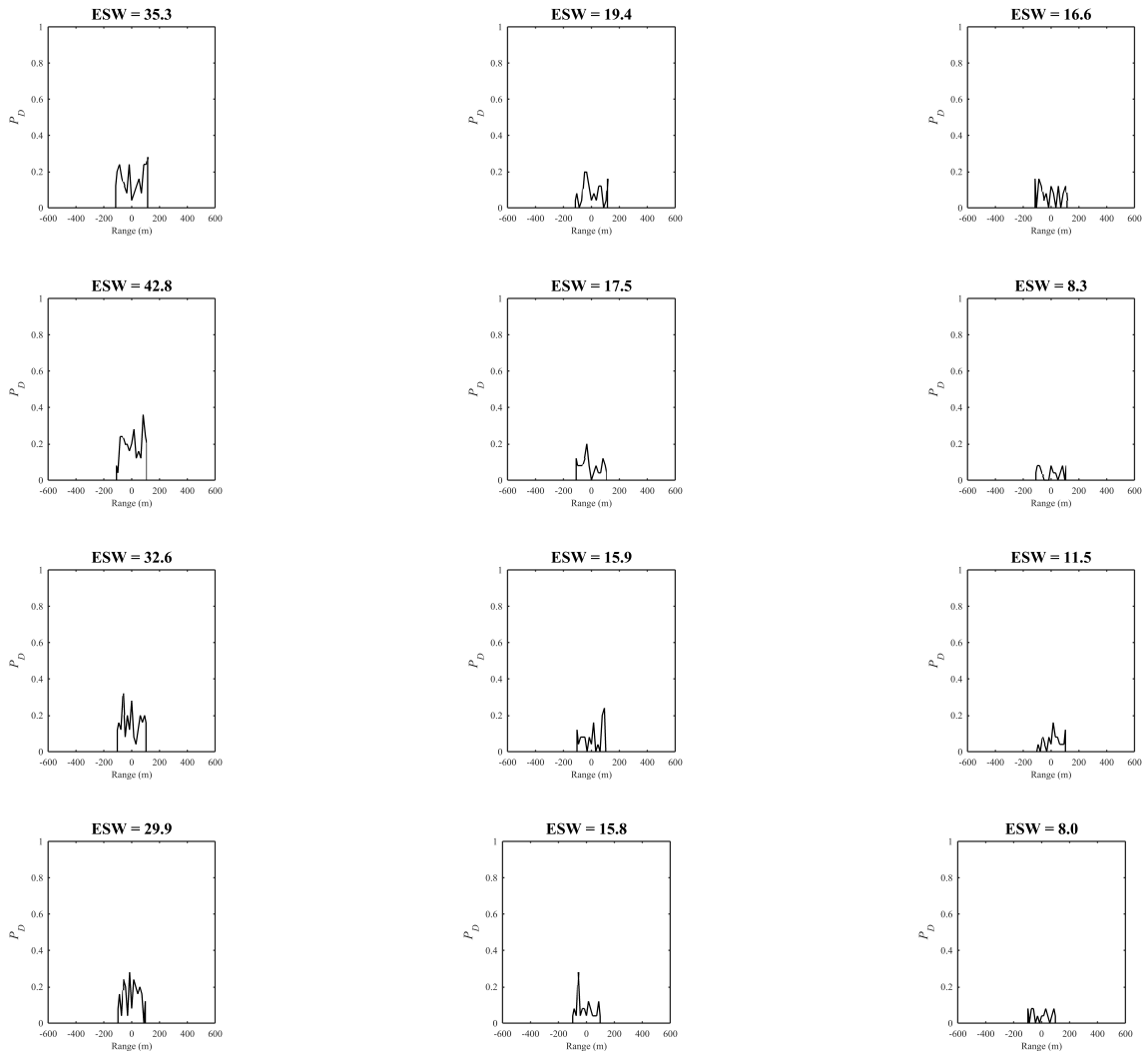


Figure 147: FLS VXE Results for Parameterization in Table 15

D.2 Side Scan Sonar

There were 54 side scan sonar designs established by varying the parameterized power, frequency, and horizontal and vertical beam widths. The setup of those parameters resulted

in specific sensor Source Levels (SL), pulse lengths, sizes (lengths and heights of the arrays), and maximum deterministic ranges based on the sonar equation analysis. Also, the sensor depths were calculated as described in the FLS section. Again, the grazing angles were 45° and the minimum depths allowed were 10 meters.

Table 16 corresponds with the lateral range curve results in Figures 148–150. Increasing frequency and velocity decreased the ESW capabilities. However, within each frequency subset, variations in ESW are affected mostly by beam width, but the relationships aren't always completely linear, suggesting there are other effects causing variations.

Table 16: SSS Parameter Setup Used for VXE Results in Figures 148–150

| Power, W | freq (kHz) | pulse length (μs) | VBW (rad) | HBW (rad) | length (cm) | height (cm) | SL (dB) | R_{max} (m) | VehDepth (m) |
|----------|------------|--------------------------|-----------|-----------|-------------|-------------|---------|---------------|--------------|
| 0.1 | 400 | 12.50 | 0.36 | 0.02 | 17.87 | 0.95 | 177.65 | 264.77 | 10.00 |
| 0.1 | 400 | 12.50 | 0.60 | 0.02 | 17.87 | 0.57 | 177.65 | 264.77 | 10.00 |
| 0.1 | 400 | 12.50 | 0.92 | 0.02 | 17.87 | 0.38 | 177.65 | 264.77 | 10.00 |
| 0.1 | 1000 | 5.00 | 0.36 | 0.02 | 7.15 | 0.38 | 177.65 | 108.11 | 23.56 |
| 0.1 | 1000 | 5.00 | 0.60 | 0.02 | 7.15 | 0.23 | 177.65 | 108.11 | 23.56 |
| 0.1 | 1000 | 5.00 | 0.92 | 0.02 | 7.15 | 0.15 | 177.65 | 108.11 | 23.56 |
| 0.1 | 1600 | 3.13 | 0.36 | 0.02 | 4.47 | 0.24 | 177.65 | 55.04 | 61.08 |
| 0.1 | 1600 | 3.13 | 0.60 | 0.02 | 4.47 | 0.14 | 177.65 | 55.04 | 61.08 |
| 0.1 | 1600 | 3.13 | 0.92 | 0.02 | 4.47 | 0.10 | 177.65 | 55.04 | 61.08 |

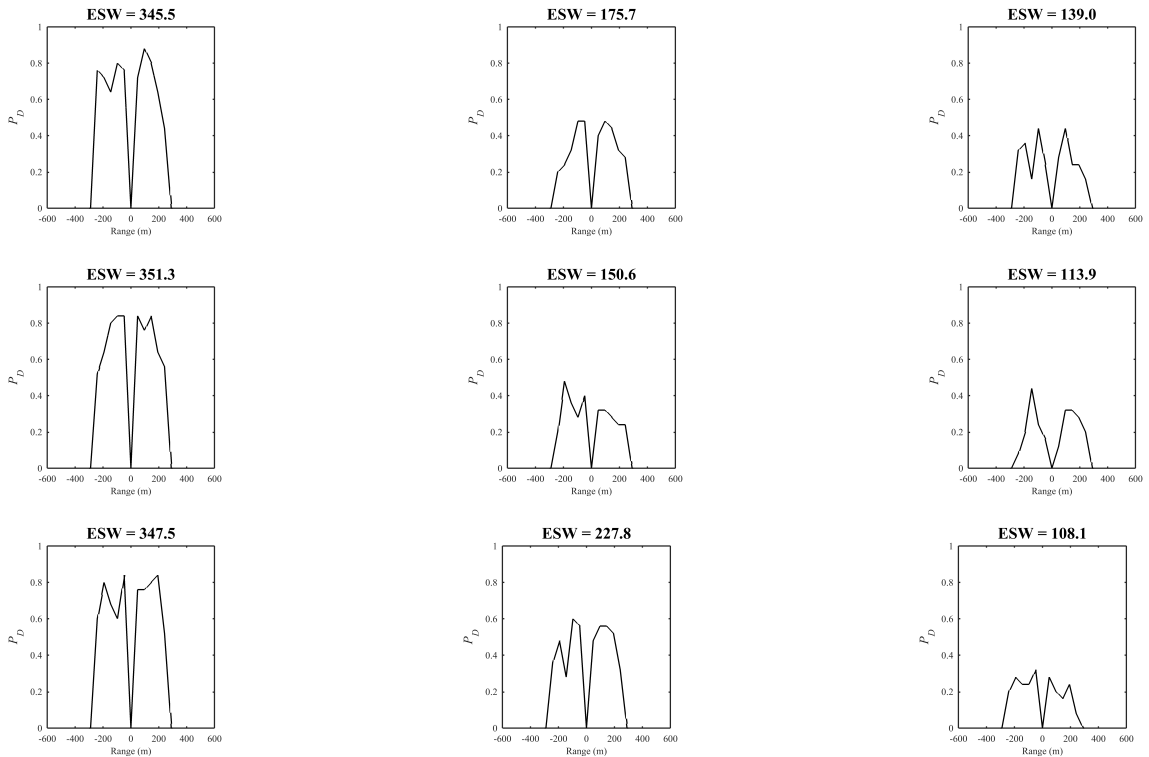


Figure 148: SSS VXE Results for Parameterization in Table 16 with $freq = 400kHz$

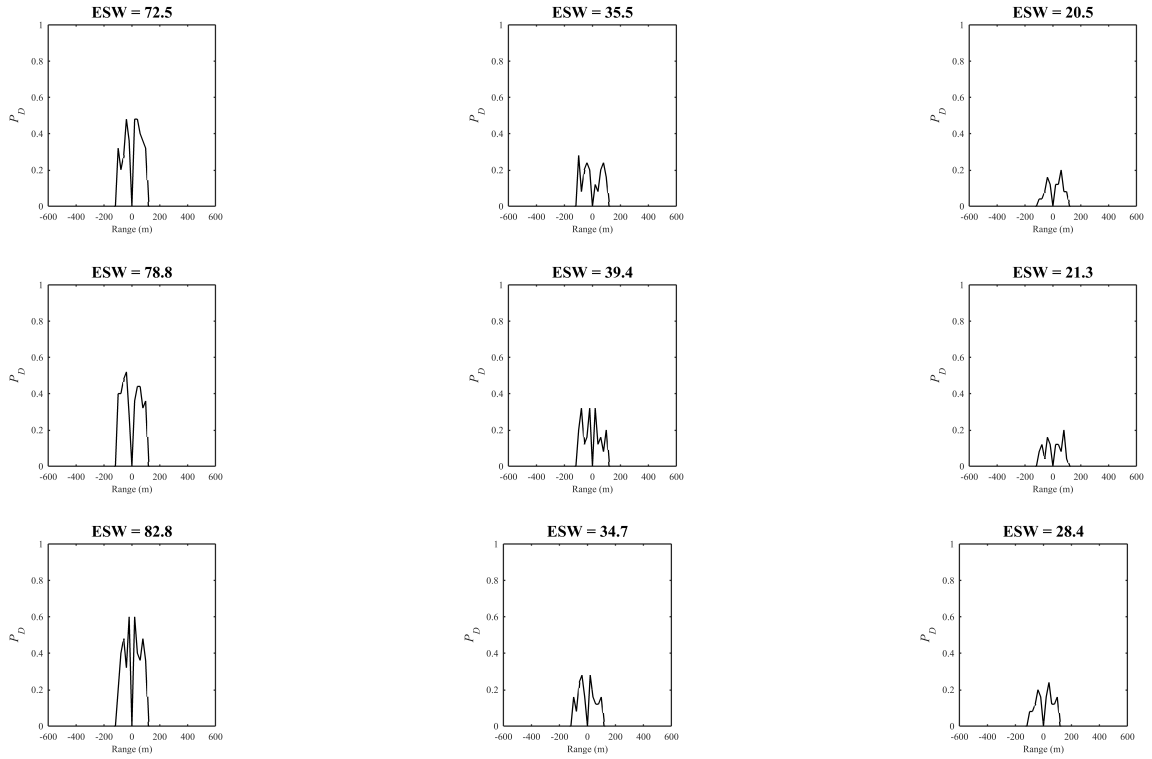


Figure 149: SSS VXE Results for Parameterization in Table 16 with $freq = 1000kHz$

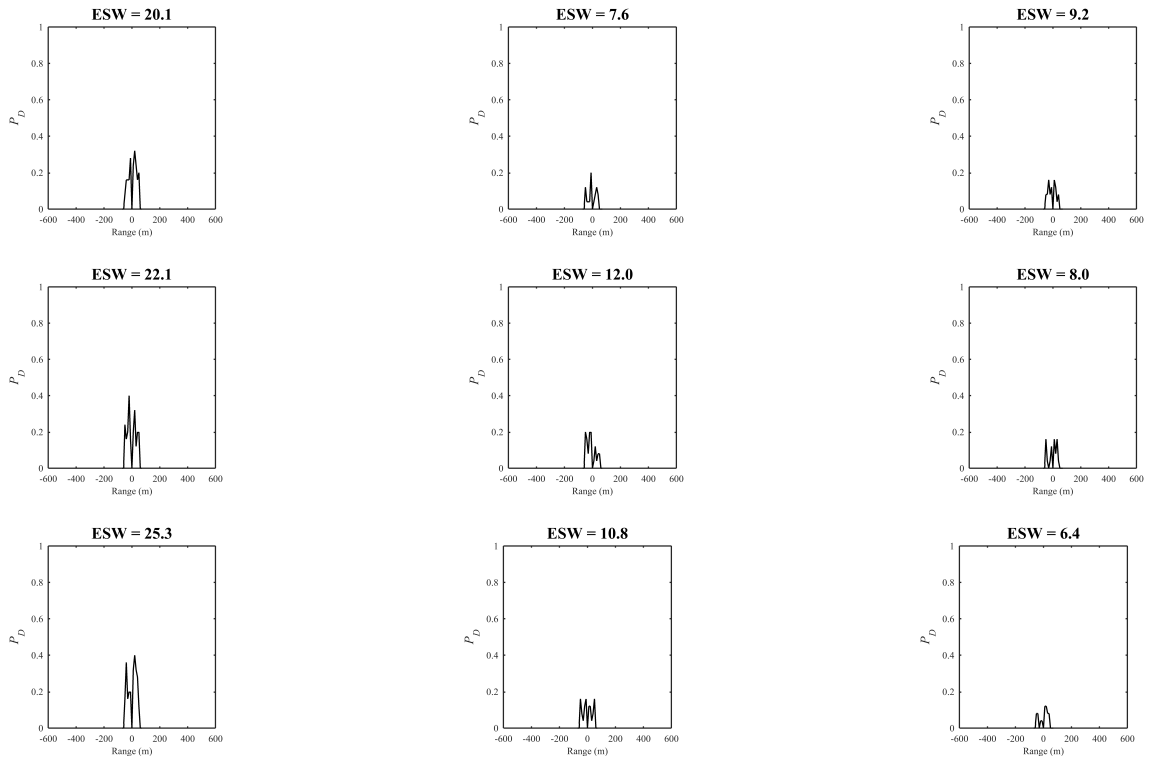


Figure 150: SSS VXE Results for Parameterization in Table 16 with $freq = 1600kHz$

Table 17 corresponds with the lateral range curve results in Figures 151–153. The power is now greater than in the previous charts, and the ESW results are accordingly better.

Table 17: SSS Parameter Setup Used for VXE Results in Figures 151–153

| <i>Power, W</i> | <i>freq (kHz)</i> | <i>pulse length (μs)</i> | <i>VBW (rad)</i> | <i>HBW (rad)</i> | <i>length (cm)</i> | <i>height (cm)</i> | <i>SL (dB)</i> | <i>R_{max} (m)</i> | <i>VehDepth (m)</i> |
|-----------------|-------------------|---|------------------|------------------|--------------------|--------------------|----------------|----------------------------|---------------------|
| 50000 | 400 | 12.50 | 0.36 | 0.02 | 17.87 | 0.95 | 234.64 | 457.22 | 10.00 |
| 50000 | 400 | 12.50 | 0.60 | 0.02 | 17.87 | 0.57 | 234.64 | 457.22 | 10.00 |
| 50000 | 400 | 12.50 | 0.92 | 0.02 | 17.87 | 0.38 | 234.64 | 457.22 | 10.00 |
| 50000 | 1000 | 5.00 | 0.36 | 0.02 | 7.15 | 0.38 | 234.64 | 183.04 | 10.00 |
| 50000 | 1000 | 5.00 | 0.60 | 0.02 | 7.15 | 0.23 | 234.64 | 183.04 | 10.00 |
| 50000 | 1000 | 5.00 | 0.92 | 0.02 | 7.15 | 0.15 | 234.64 | 183.04 | 10.00 |
| 50000 | 1600 | 3.13 | 0.36 | 0.02 | 4.47 | 0.24 | 234.64 | 91.07 | 35.61 |
| 50000 | 1600 | 3.13 | 0.60 | 0.02 | 4.47 | 0.14 | 234.64 | 91.07 | 35.61 |
| 50000 | 1600 | 3.13 | 0.92 | 0.02 | 4.47 | 0.10 | 234.64 | 91.07 | 35.61 |

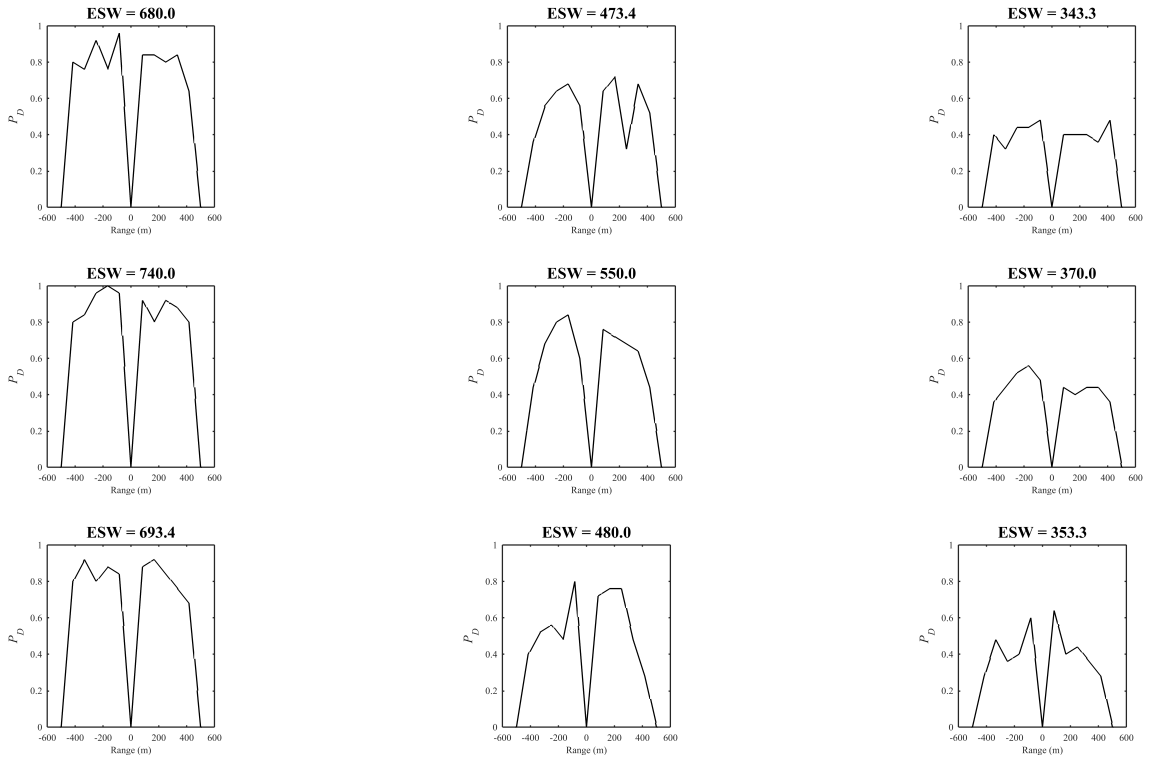


Figure 151: SSS VXE Results for Parameterization in Table 17 with $freq = 400kHz$

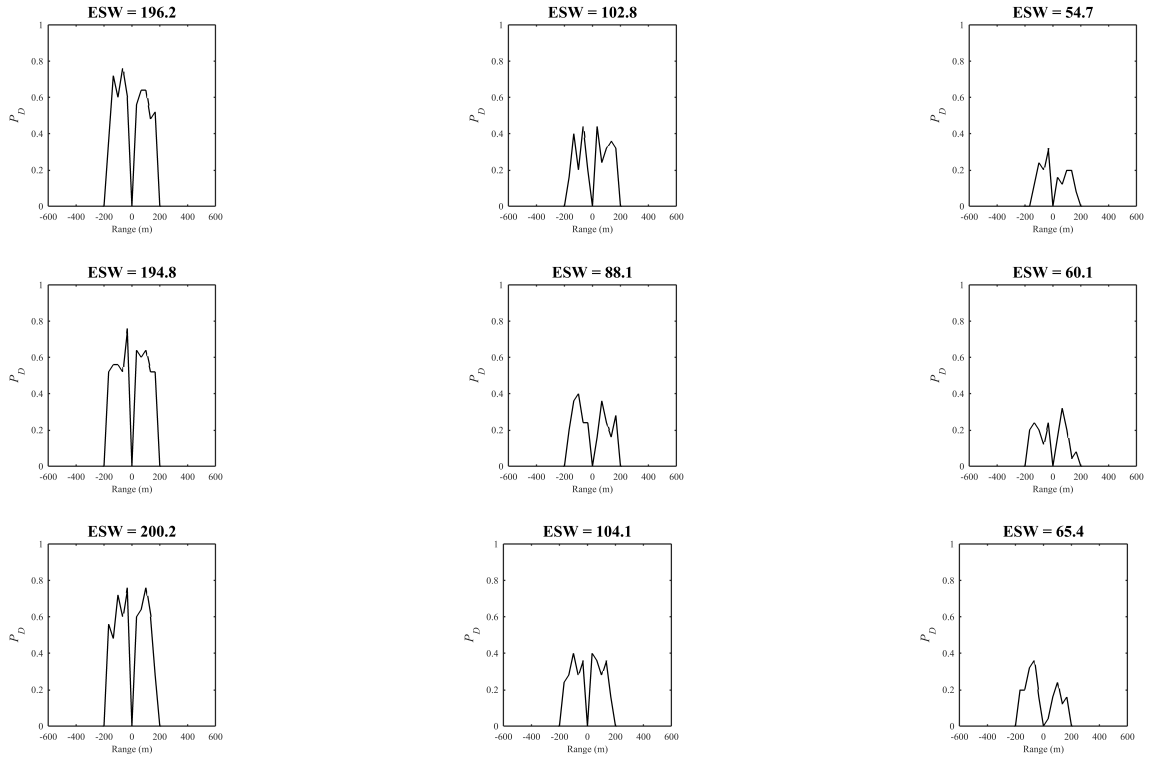


Figure 152: SSS VXE Results for Parameterization in Table 17 with $freq = 1000kHz$

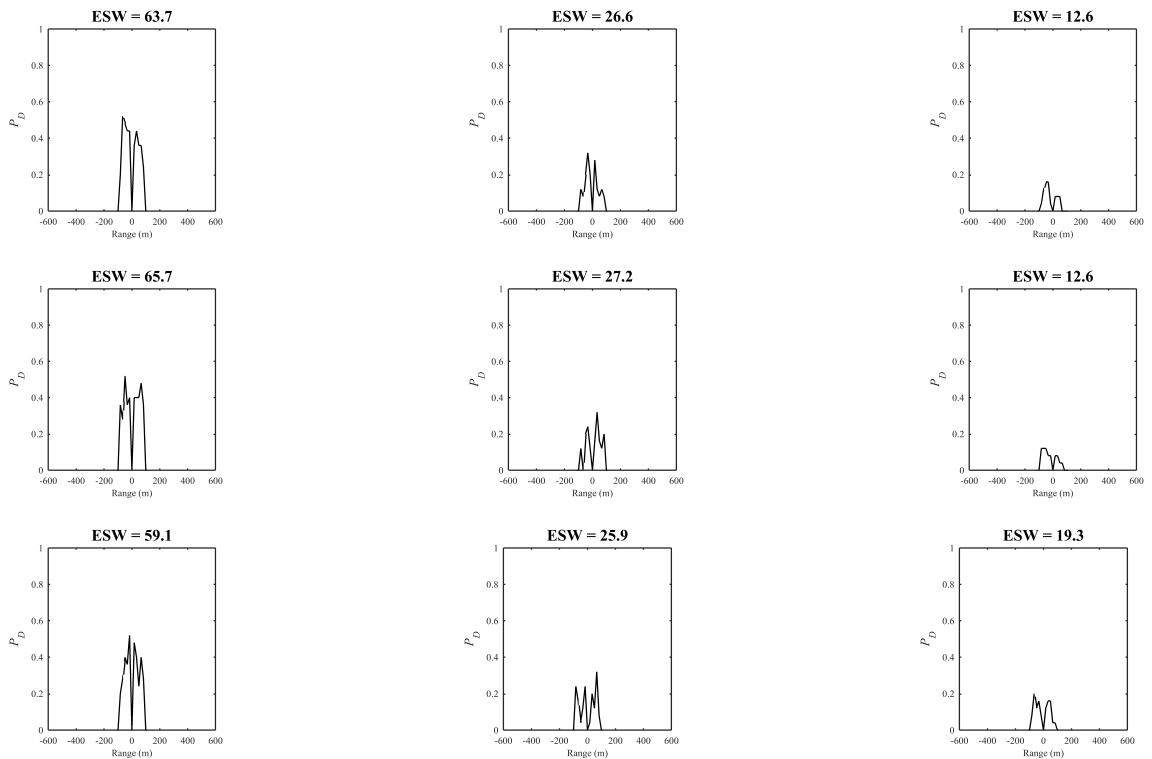


Figure 153: SSS VXE Results for Parameterization in Table 17 with $freq = 1600kHz$

Table 18 corresponds with the lateral range curve results in Figures 154–156. With the greatest power so far, these charts have the best ESW values up to this point. The frequency and beam width effects are similar to the trends pointed out previously.

Table 18: SSS Parameter Setup Used for VXE Results in Figures 154–156

| Power, W | freq (kHz) | pulse length (μ s) | VBW (rad) | HBW (rad) | length (cm) | height (cm) | SL (dB) | R_{max} (m) | VehDepth (m) |
|----------|------------|-------------------------|-----------|-----------|-------------|-------------|---------|---------------|--------------|
| 100000 | 400 | 12.50 | 0.36 | 0.02 | 17.87 | 0.95 | 237.65 | 467.70 | 10.00 |
| 100000 | 400 | 12.50 | 0.60 | 0.02 | 17.87 | 0.57 | 237.65 | 467.70 | 10.00 |
| 100000 | 400 | 12.50 | 0.92 | 0.02 | 17.87 | 0.38 | 237.65 | 467.70 | 10.00 |
| 100000 | 1000 | 5.00 | 0.36 | 0.02 | 7.15 | 0.38 | 237.65 | 187.11 | 10.00 |
| 100000 | 1000 | 5.00 | 0.60 | 0.02 | 7.15 | 0.23 | 237.65 | 187.11 | 10.00 |
| 100000 | 1000 | 5.00 | 0.92 | 0.02 | 7.15 | 0.15 | 237.65 | 187.11 | 10.00 |
| 100000 | 1600 | 3.13 | 0.36 | 0.02 | 4.47 | 0.24 | 237.65 | 93.02 | 34.22 |
| 100000 | 1600 | 3.13 | 0.60 | 0.02 | 4.47 | 0.14 | 237.65 | 93.02 | 34.22 |
| 100000 | 1600 | 3.13 | 0.92 | 0.02 | 4.47 | 0.10 | 237.65 | 93.02 | 34.22 |

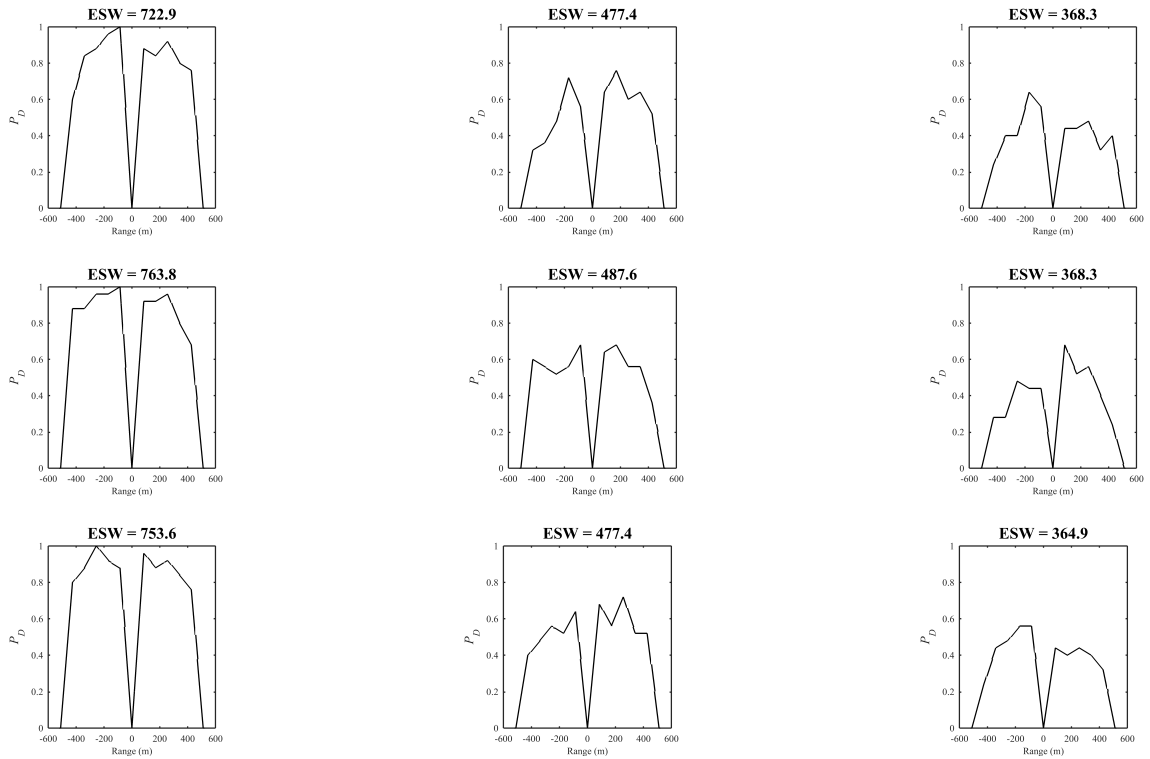


Figure 154: SSS VXE Results for Parameterization in Table 18 with $freq = 400kHz$

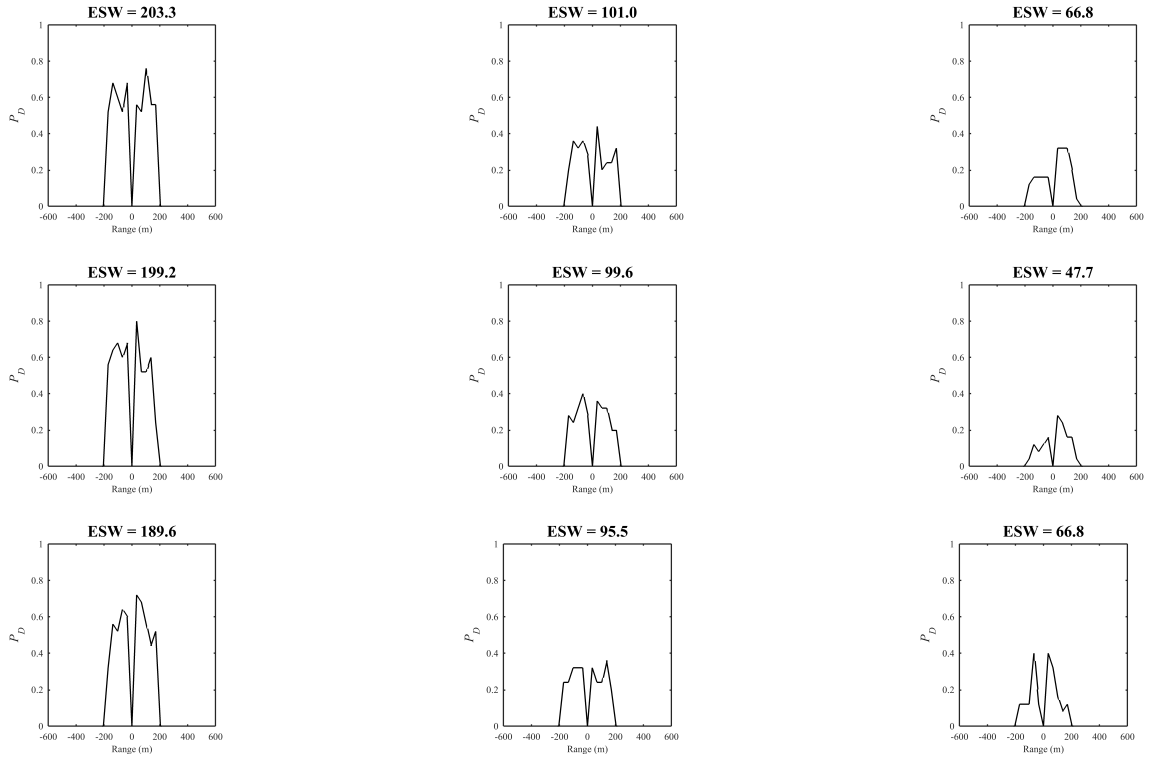


Figure 155: SSS VXE Results for Parameterization in Table 18 with $freq = 1000kHz$

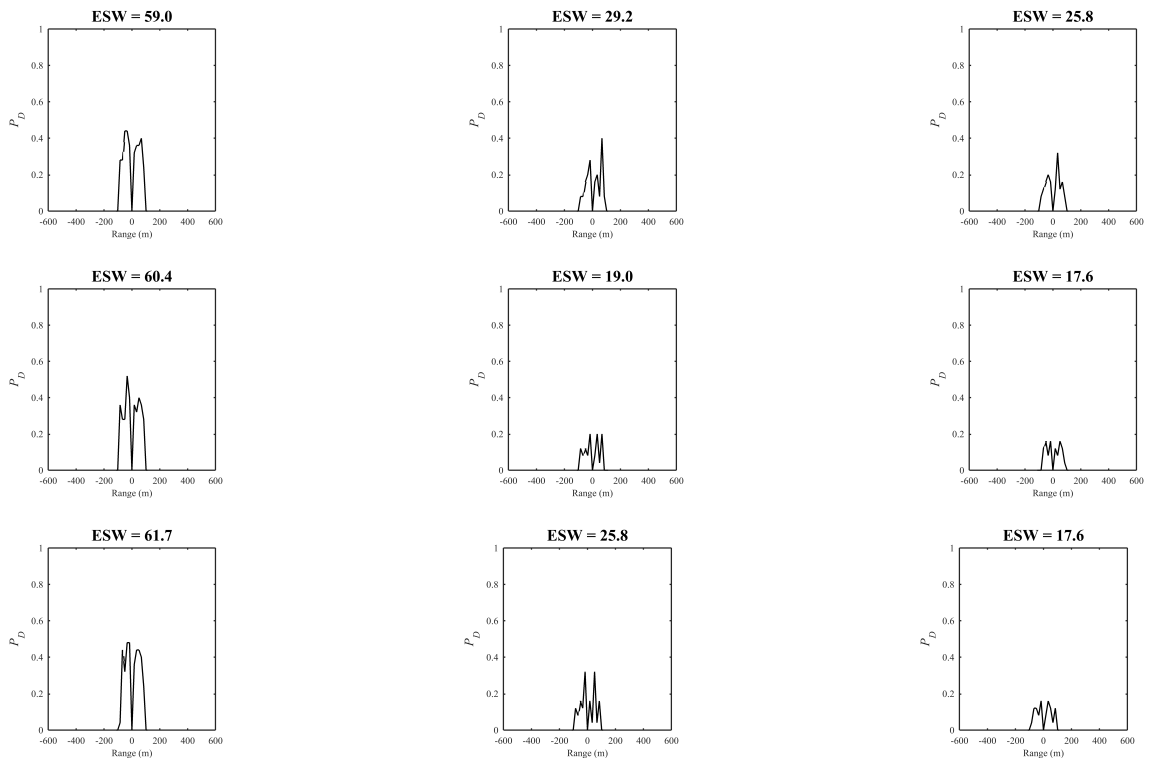


Figure 156: SSS VXE Results for Parameterization in Table 18 with $freq = 1600kHz$

Table 19 corresponds with the lateral range curve results in Figures 157–159. From this point forward, the parameter settings are all the same as the settings in Tables 16–18, except the horizontal beam width is now larger (from 0.02 radian to 0.09 radian). As was expected, the wider beam width has a detrimental effect on the overall effective sweep widths (ESW).

Table 19: SSS Parameter Setup Used for VXE Results in Figures 157–159

| Power, W | freq (kHz) | pulse length (μ s) | VBW (rad) | HBW (rad) | length (cm) | height (cm) | SL (dB) | R_{max} (m) | VehDepth (m) |
|----------|------------|-------------------------|-----------|-----------|-------------|-------------|---------|---------------|--------------|
| 0.1 | 400 | 12.50 | 0.36 | 0.09 | 3.82 | 0.95 | 170.95 | 221.94 | 10.00 |
| 0.1 | 400 | 12.50 | 0.60 | 0.09 | 3.82 | 0.57 | 170.95 | 221.94 | 10.00 |
| 0.1 | 400 | 12.50 | 0.92 | 0.09 | 3.82 | 0.38 | 170.95 | 221.94 | 10.00 |
| 0.1 | 1000 | 5.00 | 0.36 | 0.09 | 1.53 | 0.38 | 170.95 | 91.36 | 35.40 |
| 0.1 | 1000 | 5.00 | 0.60 | 0.09 | 1.53 | 0.23 | 170.95 | 91.36 | 35.40 |
| 0.1 | 1000 | 5.00 | 0.92 | 0.09 | 1.53 | 0.15 | 170.95 | 91.36 | 35.40 |
| 0.1 | 1600 | 3.13 | 0.36 | 0.09 | 0.96 | 0.24 | 170.95 | 46.95 | 66.80 |
| 0.1 | 1600 | 3.13 | 0.60 | 0.09 | 0.96 | 0.14 | 170.95 | 46.95 | 66.80 |
| 0.1 | 1600 | 3.13 | 0.92 | 0.09 | 0.96 | 0.10 | 170.95 | 46.95 | 66.80 |

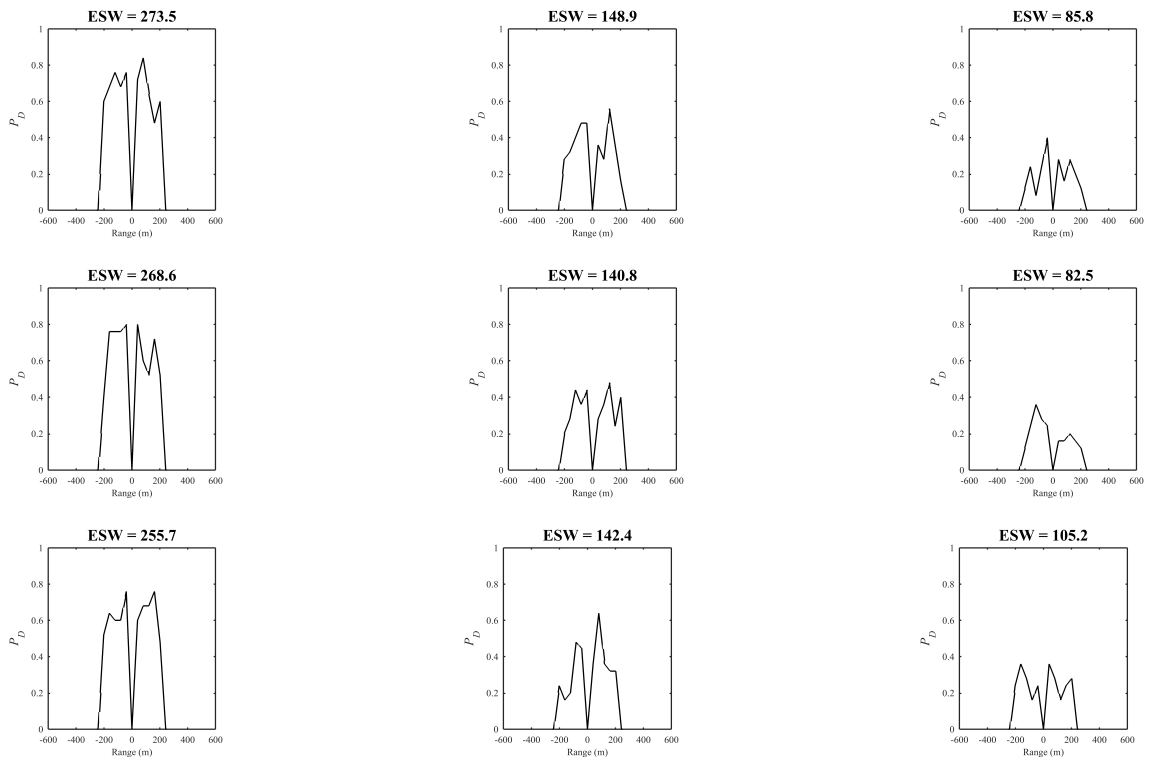


Figure 157: SSS VXE Results for Parameterization in Table 19 with $freq = 400kHz$

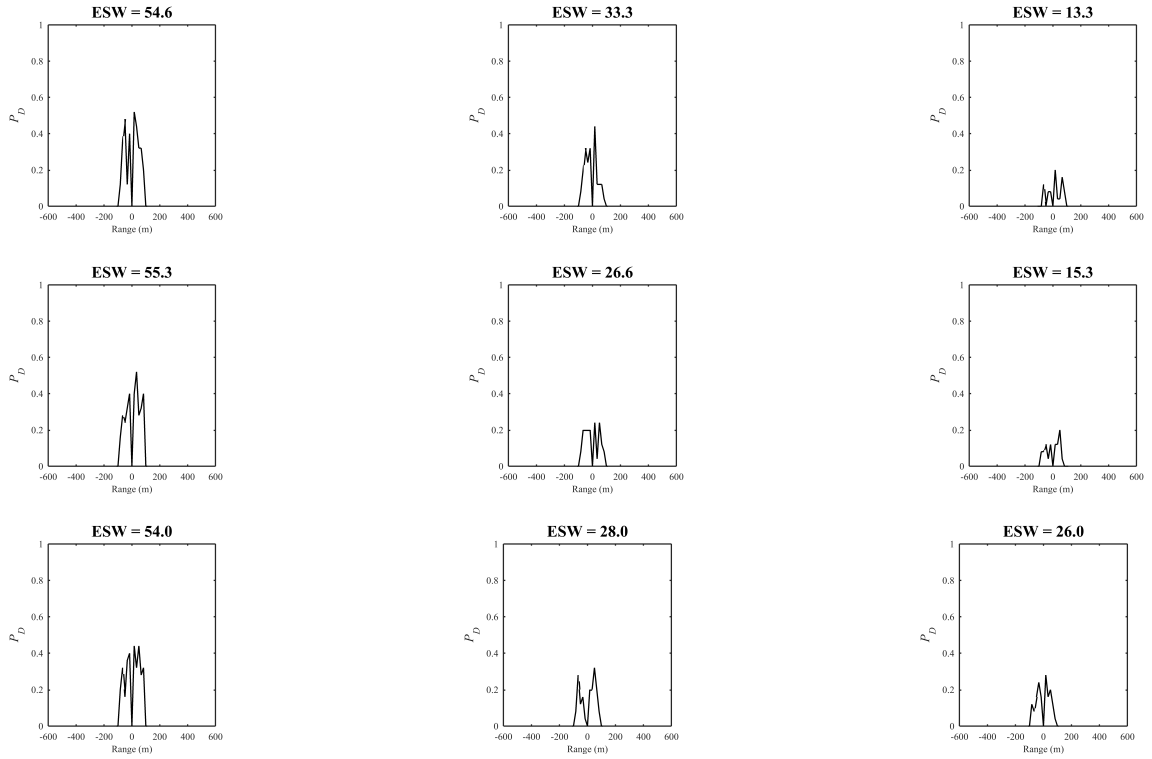


Figure 158: SSS VXE Results for Parameterization in Table 19 with $freq = 1000kHz$

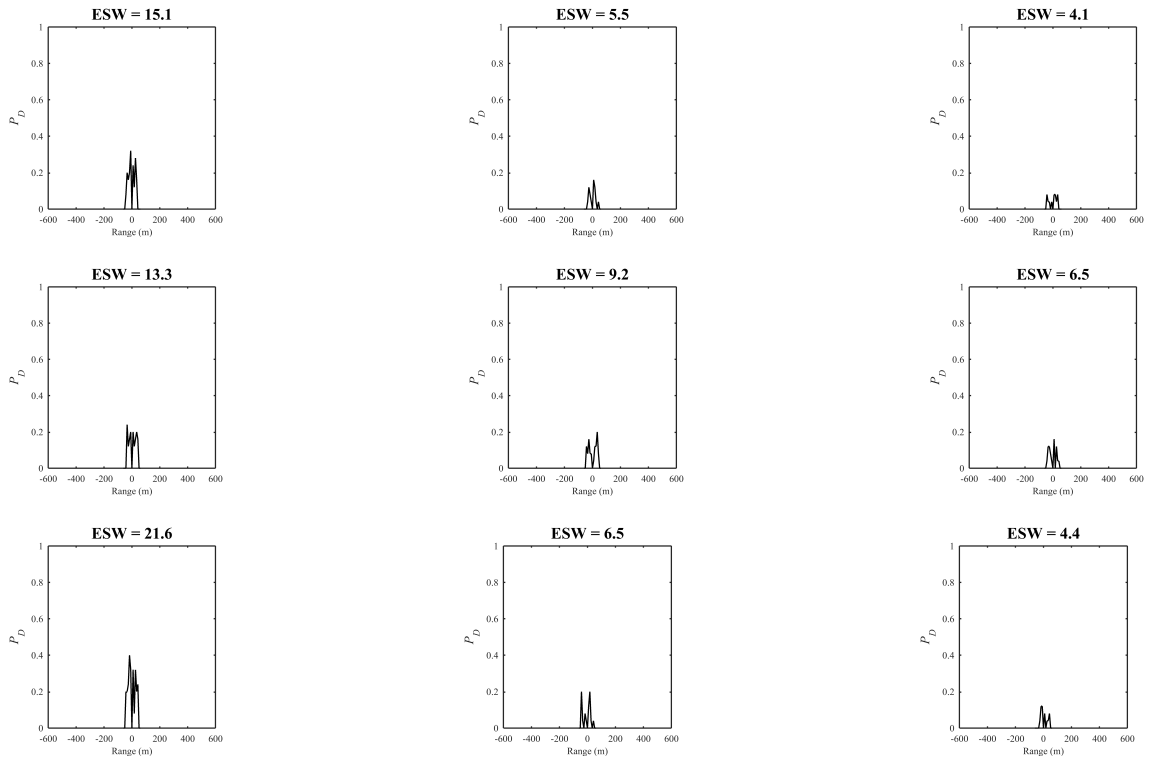


Figure 159: SSS VXE Results for Parameterization in Table 19 with $freq = 1600kHz$

Table 20 corresponds with the lateral range curve results in Figures 160–162. The power settings for these charts are greater than in the previous set. However, the greater power in this case did not lead to better ESW, which is an artifact of the other parameter setting changes that were made (such as a wider beam width).

Table 20: SSS Parameter Setup Used for VXE Results in Figures 160–162

| Power, W | freq (kHz) | pulse length (μ s) | VBW (rad) | HBW (rad) | length (cm) | height (cm) | SL (dB) | R_{max} (m) | VehDepth (m) |
|----------|------------|-------------------------|-----------|-----------|-------------|-------------|---------|---------------|--------------|
| 50000 | 400 | 12.50 | 0.36 | 0.09 | 3.82 | 0.95 | 227.94 | 410.89 | 10.00 |
| 50000 | 400 | 12.50 | 0.60 | 0.09 | 3.82 | 0.57 | 227.94 | 410.89 | 10.00 |
| 50000 | 400 | 12.50 | 0.92 | 0.09 | 3.82 | 0.38 | 227.94 | 410.89 | 10.00 |
| 50000 | 1000 | 5.00 | 0.36 | 0.09 | 1.53 | 0.38 | 227.94 | 165.03 | 10.00 |
| 50000 | 1000 | 5.00 | 0.60 | 0.09 | 1.53 | 0.23 | 227.94 | 165.03 | 10.00 |
| 50000 | 1000 | 5.00 | 0.92 | 0.09 | 1.53 | 0.15 | 227.94 | 165.03 | 10.00 |
| 50000 | 1600 | 3.13 | 0.36 | 0.09 | 0.96 | 0.24 | 227.94 | 82.42 | 41.72 |
| 50000 | 1600 | 3.13 | 0.60 | 0.09 | 0.96 | 0.14 | 227.94 | 82.42 | 41.72 |
| 50000 | 1600 | 3.13 | 0.92 | 0.09 | 0.96 | 0.10 | 227.94 | 82.42 | 41.72 |

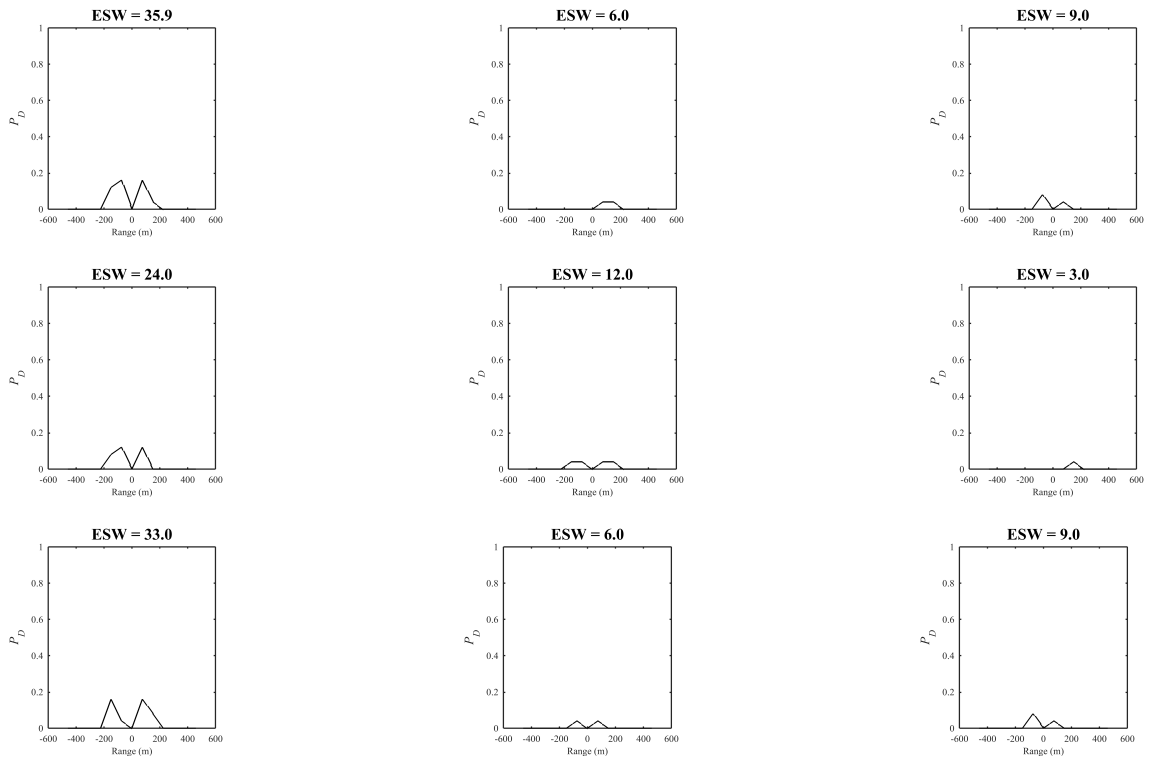


Figure 160: SSS VXE Results for Parameterization in Table 20 with $freq = 400kHz$

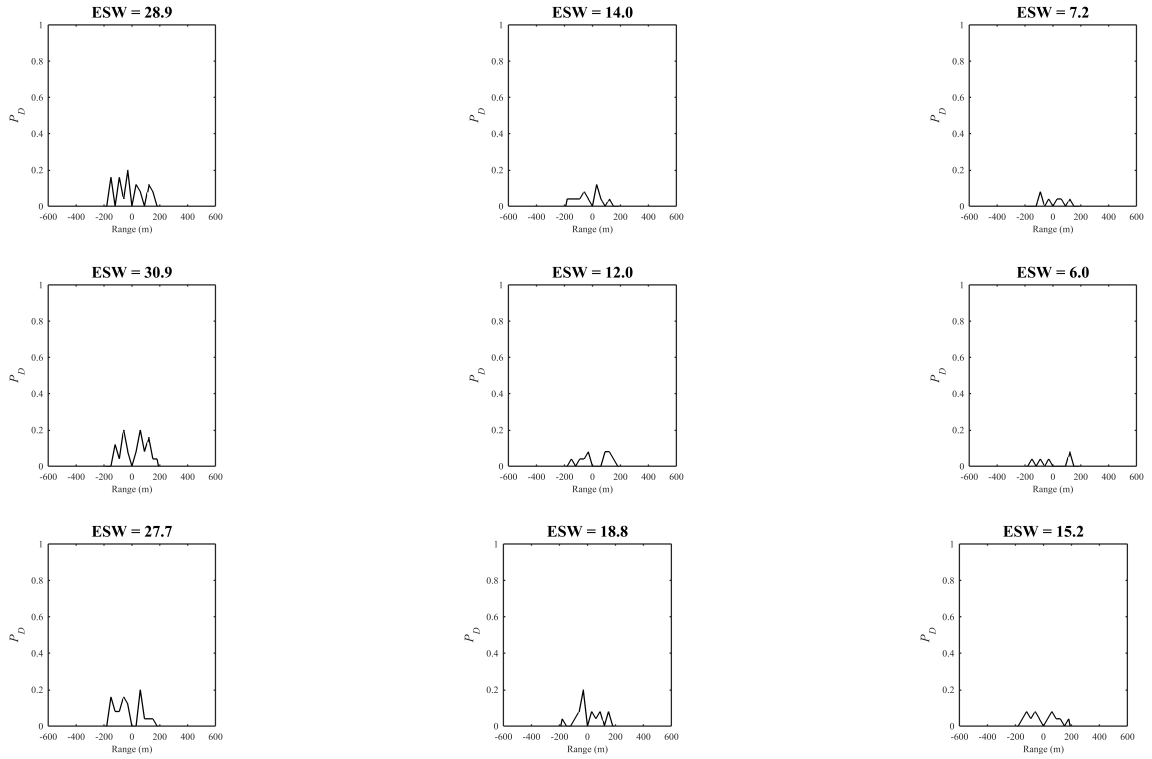


Figure 161: SSS VXE Results for Parameterization in Table 20 with $freq = 1000kHz$

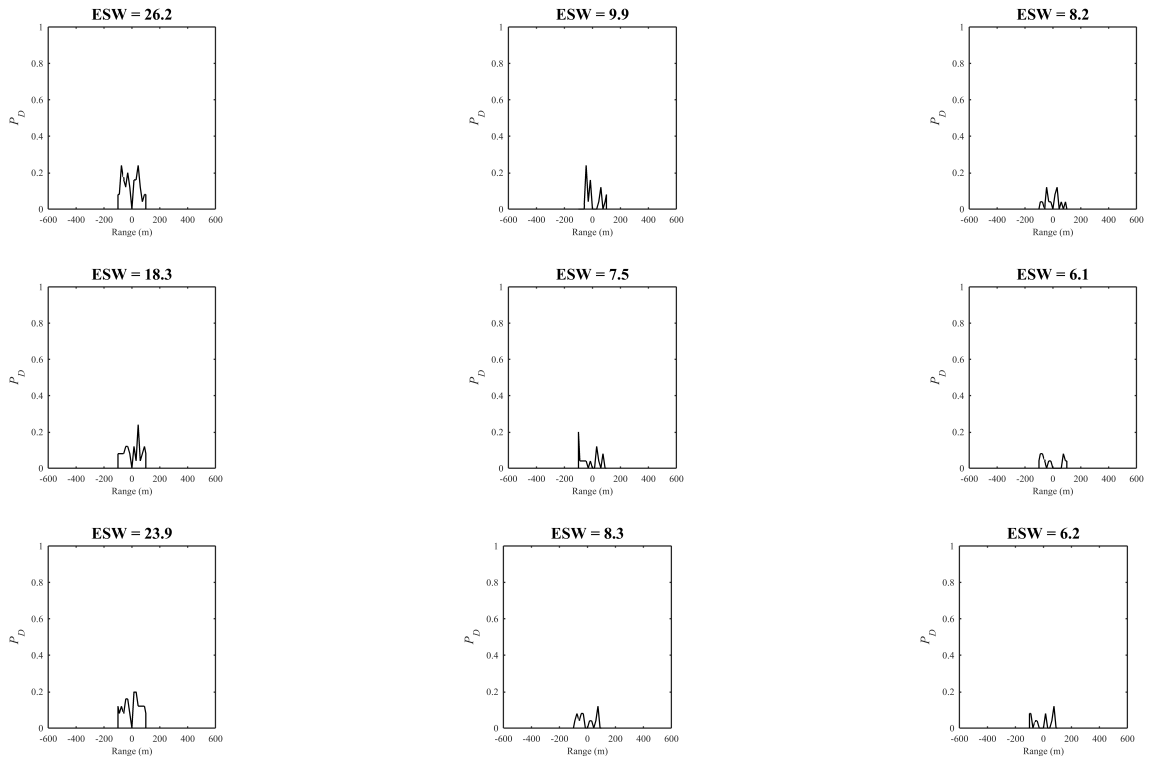


Figure 162: SSS VXE Results for Parameterization in Table 20 with $freq = 1600kHz$

Table 21 corresponds with the lateral range curve results in Figures 163–165.

Table 21: SSS Parameter Setup Used for VXE Results in Figures 163–165

| Power, W | freq (kHz) | pulse length (μs) | VBW (rad) | HBW (rad) | length (cm) | height (cm) | SL (dB) | R_{max} (m) | VehDepth (m) |
|------------|------------|--------------------------|-----------|-----------|-------------|-------------|---------|---------------|--------------|
| 100000 | 400 | 12.50 | 0.36 | 0.09 | 3.82 | 0.95 | 230.95 | 421.25 | 10.00 |
| 100000 | 400 | 12.50 | 0.60 | 0.09 | 3.82 | 0.57 | 230.95 | 421.25 | 10.00 |
| 100000 | 400 | 12.50 | 0.92 | 0.09 | 3.82 | 0.38 | 230.95 | 421.25 | 10.00 |
| 100000 | 1000 | 5.00 | 0.36 | 0.09 | 1.53 | 0.38 | 230.95 | 169.06 | 10.00 |
| 100000 | 1000 | 5.00 | 0.60 | 0.09 | 1.53 | 0.23 | 230.95 | 169.06 | 10.00 |
| 100000 | 1000 | 5.00 | 0.92 | 0.09 | 1.53 | 0.15 | 230.95 | 169.06 | 10.00 |
| 100000 | 1600 | 3.13 | 0.36 | 0.09 | 0.96 | 0.24 | 230.95 | 84.36 | 40.35 |
| 100000 | 1600 | 3.13 | 0.60 | 0.09 | 0.96 | 0.14 | 230.95 | 84.36 | 40.35 |
| 100000 | 1600 | 3.13 | 0.92 | 0.09 | 0.96 | 0.10 | 230.95 | 84.36 | 40.35 |

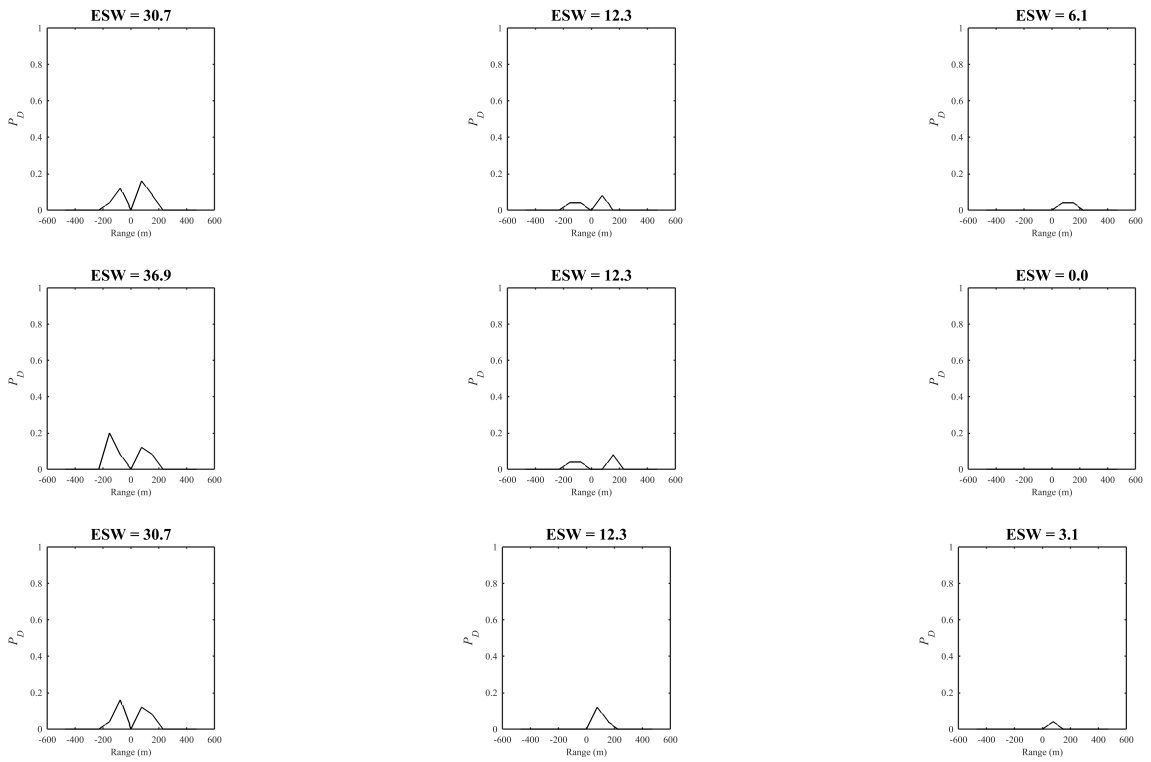


Figure 163: SSS VXE Results for Parameterization in Table 21 with $freq = 400kHz$

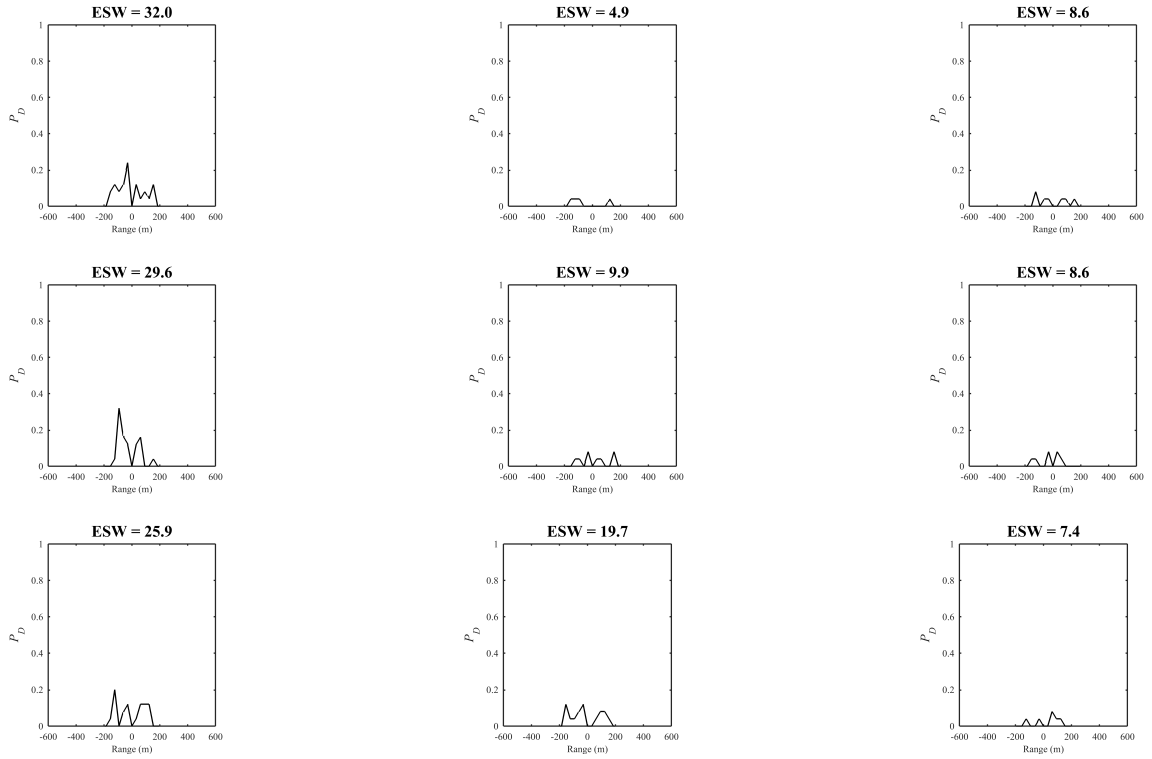


Figure 164: SSS VXE Results for Parameterization in Table 21 with $freq = 1000kHz$

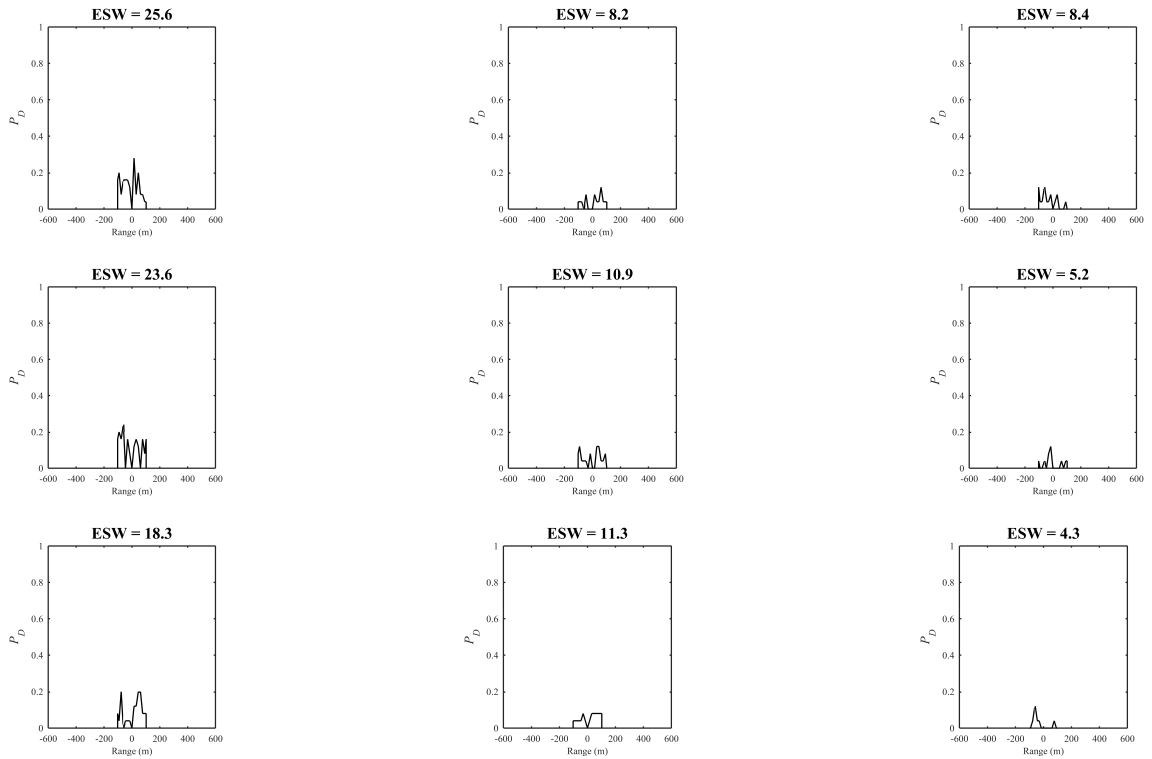


Figure 165: SSS VXE Results for Parameterization in Table 21 with $freq = 1600kHz$

D.3 Final Comments on Virtual Experimentation for Sensor Modeling

Developing the types of results that were provided in this appendix has been a novel endeavor. It was recognized by the author and his advisors that sensor models rarely have a connection to the operations that they must perform. The reason was that the only connections that existed were based on real-world experimental data. However, it is not reasonable or economically viable to acquire the amount of required experimental data that is needed to make trade-offs between multitudes of subsystems early in the conceptual design stages of an SoS development. Therefore, the virtual experimentation method presented in this dissertation provides a physics-based link to make the necessary trade-offs between subsystem options.

APPENDIX E

SIZING AND SYNTHESIS REVIEW

E.1 Aircraft Sizing Approaches

The vehicle sizing process can be characterized as an attempt to vary competing disciplines until convergence is met. For an aircraft, Nam states: “If the aircraft size needs to be changed, the aircraft weight changes, and thus, the required thrust must change because drag and weight increase, which in turn increases aircraft weight due to bigger engines. The chain of this impact propagation will keep moving on until the quantities converge toward a solution, which is the objective of the aircraft sizing process” [113]. Nam also provides what he calls an *architecture independent*, generalized vehicle sizing and synthesis method. It is novel in its ability to size aircraft with revolutionary, alternative energy-propulsion architectures. Other’s such as Mattingly and Raymer provide more traditional vehicle sizing processes [102, 122]. Nam’s interpretation of the Mattingly process is shown in Figure 166, and Nam’s generalized process is displayed in Figure 167.

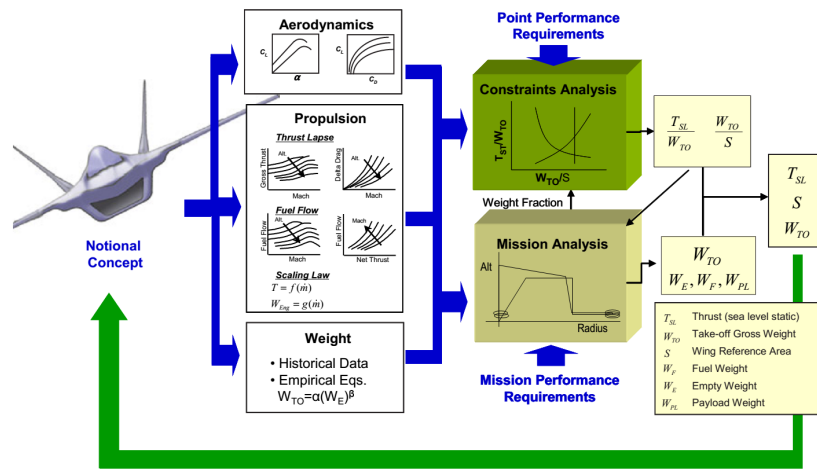


Figure 166: Mattingly’s Aircraft Sizing Process, Adapted by Nam [102, 113]

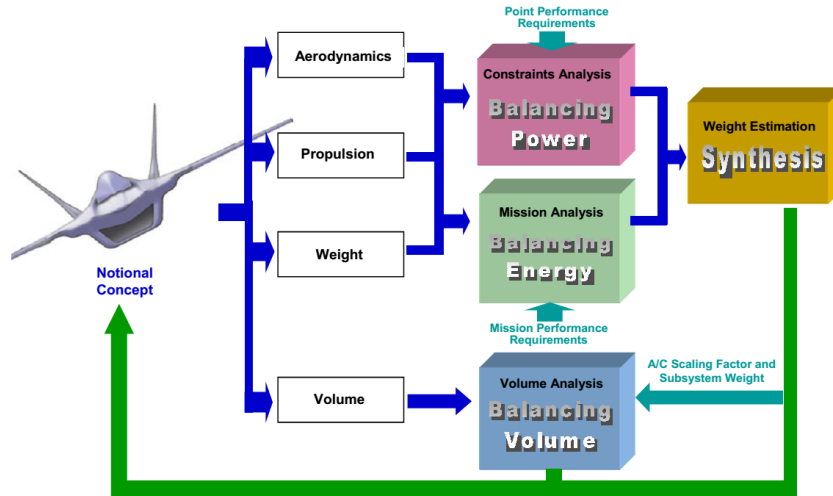


Figure 167: Nam’s Comprehensive, Generalized Sizing Process [113]

One of the main features of Nam’s generalized process is that it can balance the volume of the vehicle for power sources other than liquid fuel. In typical aircraft design, fuel burn over time causes weight to decrease during the mission, which has significant effects on the initial volume, weight and power required as well as the range or endurance over the length of the mission. However, Nam’s process balances the power required, the energy available, and the required vehicle volume and weight for a vehicle that may lose no weight over the mission (battery or solar panel powered), or that may actually gain weight over time (fuel cells with by-product stored on board).

E.2 The Ship Design Process

Ship design is also an incredibly interdisciplinary process. In order to increase the probability of success of both performance and economics, naval architects have increasingly incorporated concurrent engineering (CE), integrated product and process development (IPPD), integrated product teams (IPTs), and Systems Engineering (SE) “to ensure that the isolated specialist solutions are integrated” [92]. Multiple design approaches have been offered over the years, including the design spiral [49], the design bounding approach [91], and the set-based approach [150]. The design spiral, first presented by Evans, is shown in Figure 168.

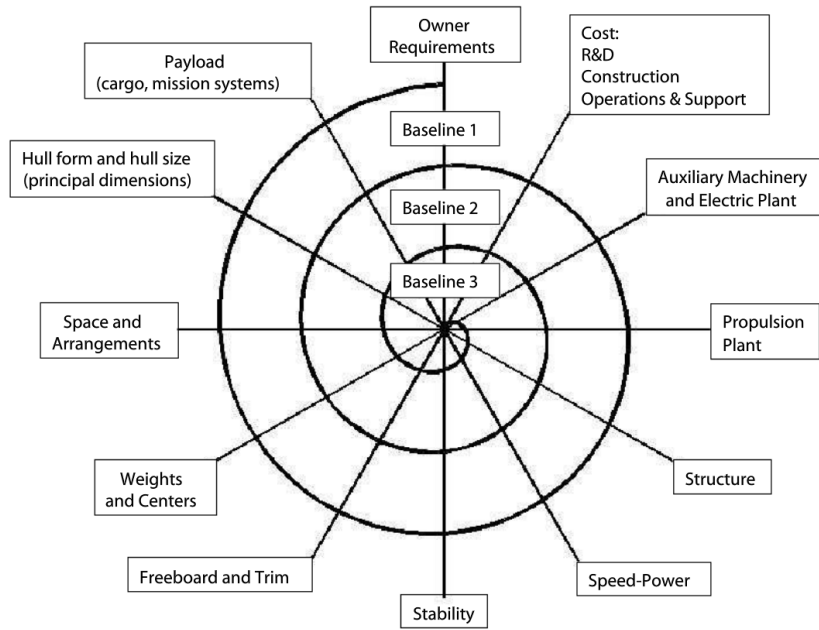


Figure 168: Evan's Design Spiral, Adapted by Lamb [49, 92]

Lamb provides a detailed ship design process which includes the initial generic design steps along with subsequent design feasibility criteria. This process is shown in Figure 169. If a design is acceptable in terms of volume, weight, stability and power required, then the design is feasible. If not, then the process must iterate until convergence is obtained.

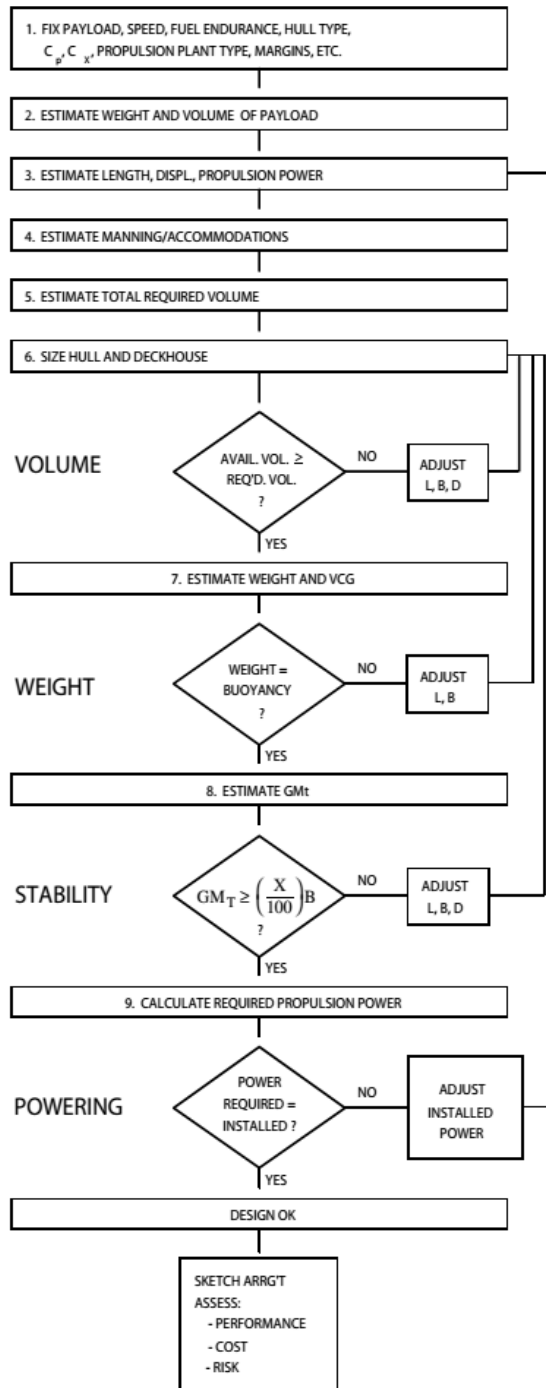


Figure 169: Lamb's Ship Design and Feasibility Process [92]

There are a few commonalities in vehicle design that are becoming apparent, whether the vehicles are aircraft or seacraft. One is that initial estimates are often needed in order to begin the design process, and these estimates usually come from historical data (although physics-based analyses can also provide estimates). Secondly, the process is iterative in

nature. In other words, there is a balance between disciplines that must be achieved.

APPENDIX F

HYDRODYNAMIC ANALYSIS

The motion of a vehicle through its environment is highly constrained by the medium through which it must travel. It is obvious that air will resist a vehicle's motion to a different degree than water. At a fundamental level the properties of the medium, such as density and viscosity, contribute to constraining the dynamics of the vehicle. Properties of the vehicle itself will also contribute to the dynamics of the system. Such properties of the vehicle include geometric shape, skin friction, propulsion capabilities, and static and dynamic control surfaces. Creating relationships between the properties of the medium and the properties of the vehicle in motion is related to the fields of aerodynamics, hydrodynamics, and gas dynamics. Formal definitions of each from Hoerner [70] are as follows:

- Aerodynamics – describing fluid motion characteristics of air and other gaseous fluids from incompressible through hypersonic conditions.
- Gas Dynamics – dealing with the fluid motion of compressible gases from subsonic to supersonic speeds.
- Hydrodynamics – the fluid dynamics of water flow and incompressible fluid flow.

For the example problem used throughout this dissertation, hydrodynamics will be the appropriate field of analysis.

The dynamics of motion can be conceptualized through analyzing the forces acting on the body due to the fluid through which it travels. Newton's laws of motion take this perspective. Newton states, in accordance with the First Law of Motion, that a projectile maintains its current state of motion unless it is retarded by the influence of air or is impelled downward by the force of gravity [115]. The sum of the forces due to the fluid are often conceptualized through two force vectors (drag and lift) and a moment about any point on

the body.¹ Other forces will be present, such as gravity, thrust, and buoyancy, but these forces will not be considered within this hydrodynamics section. Instead, these additional forces will be brought into the fold as other disciplines of the design process are synthesized.

Two important parameters for determining the drag on a vehicle are the reference area, S_{ref} and the coefficient of drag, C_D . The reference area is usually taken as the frontal area of the body for a torpedo shaped underwater vehicle. In other words, it is the area that is seen by the flow as the flow approaches the body [28]. This calculation is shown in Equation 120.

$$S_{Ref} = \pi \frac{d^2}{4} \quad (120)$$

Determining the coefficient of drag is much more involved. The C_D can be determined experimentally or analytically (ideally any analytic development should be validated against experimental data). Allen et. al. [4] performed tow tank experiments to acquire the axial drag force coefficient of the REMUS vehicle. They were able to produce drag coefficients for five velocities between $V_{inf} = 0 \rightarrow 1.5 \frac{m}{s}$. They also outlined a component drag analysis for estimating the total vehicle drag and an overall effective C_D for 3 configurations at an operating velocity of $1.54 \frac{m}{s}$ (3 kts). Additionally, Huggins [73] performed wind tunnel experiments to find drag polars of an underwater vehicle with interesting results. However, experimental data can only be associated with configurations that have a reference area similar to the reference area of the test vehicle. In this work, the desire is to size varying configurations, some of which will have a much larger diameter than the REMUS vehicle. However, there is a lack of empirical data available in the literature for underwater vehicles ranging the full scope of diameters and velocities that this work is interested in. Therefore, application of accepted theories will be used to bracket an appropriate range of hydrodynamic coefficient values.

Multiple authors have developed analytical models for the hydrodynamic coefficients of underwater vehicles, including Jones et. al. [84], Milgram [109], Nahon [112], Granville [63], Evans [50], Bottaccini [24], and seminal work by Hoerner [70]. Many of these authors'

¹In aviation, the term “drag” is typically used, while in marine engineering “resistance” is the common notation [70]. However, throughout this work, “drag” will be the notation utilized.

contributions are included in the theories reviewed below. From an engineering design perspective, functions are desired which relate the forces and moments on a vehicle to the vehicle parameters (e.g., geometry, velocity, attitude of the body, etc.) and the properties of the medium in which it moves. The force of drag on the body can be decomposed into forces due to pressure and forces due to skin friction.

Two types of pressure must be considered: static and dynamic pressure. The static pressure, p_{static} , is a fundamental property of the condition of the fluid (units of p : $N/m^2 \equiv lb\text{-}f/ft^2$). On the other hand, the dynamic pressure is a fundamental property of the fluid *flow* and is therefore a function of the fluid density and the velocity of the vehicle in motion: $q = 0.5\rho V^2$, (units: $N/m^2 \equiv lb\text{-}f/ft^2$). For incompressible flow applications the total pressure at any point in the fluid flow is stated as: $p_{total} = p_{static} + p_{dynamic} = p_{static} + 0.5\rho V^2$, which is recognized as *Bernoulli's* equation. Another important pressure concept is the differential of static pressure along the surface of the body, $\Delta p = p_{local} - p_{ambient}$. If the static pressure increases along the body in the direction of flow then a positive pressure gradient is present. This gradient is also known as an *adverse* pressure gradient since it will increase the likelihood of flow separating from the body. As a result, when the flow separates the static pressure behind the body decreases significantly compared to the pressure in front of the body. This effect results in a large pressure force against the vehicle in the direction of motion. In other words, an adverse pressure gradient can result in a significant amount of drag. The orientation of the vehicle moving through the flow, otherwise known as angle of attack, will also affect the potential for flow separation from the body of the vehicle and therefore the drag force on the vehicle.

The force on the body due to skin friction results from the distribution of shear stress acting over the exposed surface of the body. The shear stress acting across the body is related to the surface texture of the vehicle as well as the *viscosity*, μ , of the fluid (units of μ : $kg/(s \cdot m)$). The skin friction across the body actually contributes to the build up of the boundary layer along the body which then can slow down the flow along the body and increase the adverse pressure gradient. Therefore, the forces due to pressure and skin friction are coupled to an extent. Nonetheless, even without the flow separating from the body skin

friction can be a major contributor to the drag force on the vehicle. Coincidentally, without viscous drag acting on the body the force of lift would not be generated.

Some of the drag on the body also results from the lift produced by the body and so these two forces are highly coupled. The relationship describing the vehicle drag as lift varies (or vice versa) is often called the drag polar for the specific vehicle configuration.

F.0.1 Hydrodynamic Parameters of Interest

The previous discussion regarding the forces of lift and drag emphasizes the fact that the resultant forces and moments stem from detailed and complex pressure and shear stress distributions around a vehicle in motion. However, as was pointed out earlier, the effects of pressure and shear stress are dependent on the properties of the fluid, the shape of the vehicle, the velocity of the vehicle and the attitude of the vehicle in relation to the freestream fluid flow. Therefore, the science of fluid dynamics elucidates a relationship between the magnitudes of the lift (L), drag (D), and moment (M) and the following parameters: freestream velocity (V_∞), freestream density (ρ_∞), a reference area for the vehicle (S_{Ref}), the angle of attack (α), the viscosity of the fluid (μ_∞), and the compressibility of the fluid described through the speed of sound (a_∞) [8]. Consequently, for a given vehicle at a given angle of attack the following expressions can be written:

$$D = f(V_\infty, \rho_\infty, S_{Ref}, \alpha, \mu_\infty, a_\infty) \quad (121)$$

$$L = f(V_\infty, \rho_\infty, S_{Ref}, \alpha, \mu_\infty, a_\infty) \quad (122)$$

$$M = f(V_\infty, \rho_\infty, S_{Ref}, \alpha, \mu_\infty, a_\infty) \quad (123)$$

Through the use of *dimensional analysis*, the functions above can be written in terms of the non-dimensional Reynolds number (Re) and Mach number (M_∞) [7],

$$D = f(V_\infty, \rho_\infty, S_{Ref}, M_\infty, Re) \quad (124)$$

$$L = f(V_\infty, \rho_\infty, S_{Ref}, M_\infty, Re) \quad (125)$$

$$M = f(V_\infty, \rho_\infty, S_{Ref}, M_\infty, Re) \quad (126)$$

where $M = V_\infty/a_\infty$ and $Re = \rho_\infty V_\infty l/\mu_\infty$ in which l is some characteristic length of the vehicle. New quantities are then defined to capture “the physical complexity of the flow field around an aerodynamic body” [7]. These non-dimensional “coefficients” are called the drag coefficient, C_D , the lift coefficient, C_L , and the moment coefficient, C_M . Hence, for a given vehicle shape and noting that the dynamic pressure of the flow field is $q \equiv \frac{1}{2}\rho V^2$, dimensional analysis results in the expressions for the lift, drag and moment equations,

$$D = qS_{ref}C_D \quad (127)$$

$$L = qS_{ref}C_L \quad (128)$$

$$M = qS_{ref}lC_M \quad (129)$$

where the coefficients are functions of Reynolds number (Re), Mach number (M), and angle of attack (α) for a given vehicle shape:

$$C_D = f(\alpha, M_\infty, Re) \quad (130)$$

$$C_L = f(\alpha, M_\infty, Re) \quad (131)$$

$$C_M = f(\alpha, M_\infty, Re) \quad (132)$$

Equations 127 – 129 are powerful expressions for applied aerodynamics and hydrodynamics. They show that the resultant hydrodynamic forces and moments of motion are proportional to dynamic pressure (or to the square of velocity), an appropriate reference area of the vehicle (plus a reference length for the moment equation), and a coefficient which captures the properties of the flow field (density, viscosity, velocity, and the speed of sound). In addition, since the coefficients are functions of Reynolds number (Re), Mach number (M), and angle of attack (α) for a given vehicle shape, derivative functions in terms of these flow field parameters can also be expressed. A primary example is the relationship between the lift coefficient and the vehicle angle of attack. This relationship is called the lift-curve slope ($dC_L/d\alpha$). The drag coefficient can also be related to the angle of attack of the vehicle in motion (although the “drag polar” is often used which represents the change in drag against the change in lift).

This all leads to a very practical question: how does one determine the values of these coefficients for a given vehicle at various flow conditions with varying angles of attack? This can be done experimentally or estimated theoretically, but neither is trivial. Fortunately, for many vehicle body shapes, experimental data has been produced for various fluid flow conditions in wind or water tunnels. Additionally, the power of the non-dimensional parameters lies in the fact that even if a vehicle is tested in two different flow fields, as long as the Reynolds numbers and Mach numbers of the flows are the same, then the lift, drag and moment coefficients will be exactly the same in both. Therefore, coefficients can be estimated for vehicles at various conditions as long as the flows are *dynamically similar*, even if the vehicles are of different scales (e.g., a commercial aircraft versus a small-scale model of the aircraft in a wind tunnel). Furthermore, even underwater vehicle coefficients can be estimated using wind tunnel data since the wind tunnel flow conditions can be tuned to have Reynolds numbers and Mach numbers similar to what the underwater vehicle will experience.

The end goal for the rest of this section is to provide estimates of the hydrodynamic coefficients for a vehicle at various flow conditions. This will be accomplished through theories relative to the flow-field around the body of interest. These estimates will give a good feel for the ranges to expect in order to compare against the Missile DATCOM analysis that will be used for the actual sizing and synthesis process proposed.

F.0.2 Hydrodynamic Coefficients

As was mentioned previously, the Reynolds number can be defined as

$$Re = V_\infty l \rho_\infty / \mu_\infty = V_\infty l / \nu_\infty \quad (133)$$

in which l is some specified length along the vehicle surface in the direction of flow and ν_∞ is the kinematic viscosity, $\nu_\infty \equiv \rho_\infty / \mu_\infty$ (units: m^2/s). In effect, Reynolds number provides a ratio of the amount of dynamic force in a flow (characterized by the velocity, V_∞) to the amount of friction force present (characterized by the kinematic viscosity, ν_∞). The dynamic forces in large part result in the pressure drag on the vehicle, whereas the frictional forces result in viscous drag. Therefore, the Reynolds number is representative of the magnitude of

pressure drag versus viscous drag. This can be demonstrated by considering the differences between a flow field in air versus a flow field in water. Since the kinematic viscosity of air can be an order of magnitude greater than the kinematic viscosity of water, the Reynolds number in air tends to be much smaller than that of water (for flows with similar velocities and characteristic lengths). Consequently, in these two similar flows, the vehicle in water will be dominated by pressure drag much more than the vehicle in air. For comparison, typical values of the kinematic viscosity for air at standard sea level and salt water from the surface of the water to 100 meters depth are as follows:

$$\nu_{SL,air} \approx 1.46 \times 10^{-5} \gg \nu_{SaltWater} \approx 1.05 \times 10^{-6} (m^2/s) \quad (134)$$

Since Reynolds number is inversely proportional to viscosity, low viscosity flows are analogous to high Reynolds number flows. Viscous effects are a major contributor to the friction drag of a vehicle. Therefore, high Reynolds number flows, or even locations along a body at high Reynolds number flows, will result in low friction drag, or even negligible friction drag. Also, as flow proceeds across the surface of a body in a flow, certain Reynolds numbers called the critical Reynolds number (Re_{cr}) may be reached at which point the flow will transition from laminar to turbulent. Reasonable approximations for critical Reynolds numbers are $1 \times 10^5 \leq Re_{cr} \leq 1 \times 10^6$ [70]. All of these effects will have significant consequences in terms of the drag coefficient on the vehicle. Consequently, it is helpful to ascertain the range of Reynolds numbers for flows as a function of velocity and characteristic length of the vehicle (keeping in mind that the viscosity of sea water is constant for all intensive purposes). This can be seen in Figure 170 below. The gray band represents typical ranges for critical Reynolds numbers.

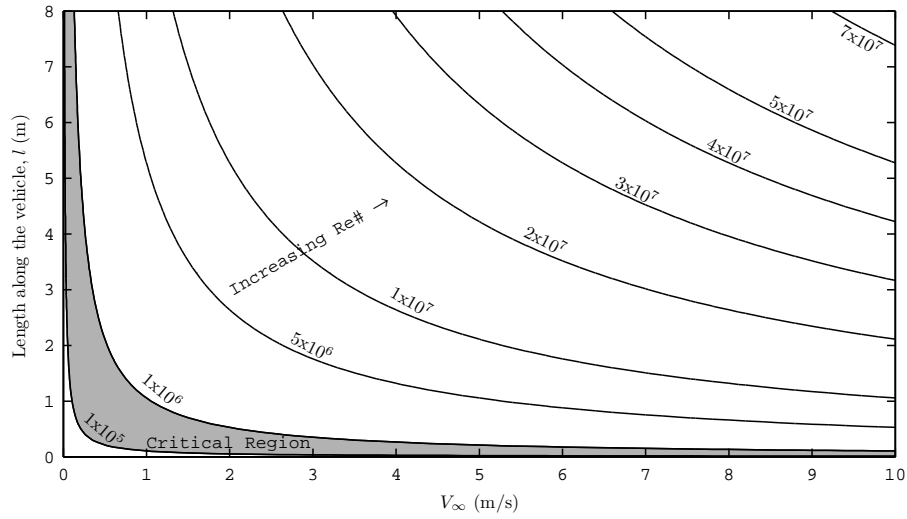


Figure 170: Reynolds Number at a depth of 10 meters, $Re = V_\infty l / \nu_\infty$

As can be seen from Figure 170 above, the Reynolds number of the flow encountered by the vehicle in water is mostly above the critical Reynolds number region. This results in mostly turbulent flow except for very low vehicle velocities and at small regions of characteristic length at the nose of the body.

F.0.2.1 The Coefficient of Friction

In order to account for drag due to friction, the coefficient of friction, C_f , needs to be determined. The coefficient of friction is a function of the boundary layer along the body which may be laminar or turbulent, but as was mentioned most of the flow encountered under this work will be turbulent. When calculating C_f through experimentation, the appropriate expression is:

$$C_f = \frac{D_{friction}}{q_\infty S_{wet}} \quad (135)$$

Numerous experiments have been performed for calculating C_f . Therefore, any theoretical solutions for C_f can be compared against the appropriate data. For ranges of low Reynolds numbers in which the boundary layer is laminar, Blasius was able to numerically solve the boundary layer equations and obtain a theoretical solution for skin friction drag [22, 29]. The Blasius coefficient of friction is presented in Eq. 136 and is valid for laminar

flows before transition to turbulence. Transition may occur between $10^5 \leq Re \leq 10^6$ [70].

$$C_{f,lam} = 1.328/\sqrt{Re} \quad (136)$$

However, a theoretical solution of C_f in turbulent flow is much more complex than that of laminar flow. This has led to solutions that are more often than not just “generalizations of experimentally determined velocity distributions across the boundary layer” [70]. The following approximations collected by Hoerner [70] are some of the most appropriate for the problem at hand.

- a) Prandtl [121] and vonKármán [166] measured velocity distributions along the inside of smooth plane pipes for estimates of C_f in turbulent flow applicable for $Re < 10^6$ (Eq. 137) and also between $Re = 10^6$ and 10^9 (Eq. 138). Their solutions, along with the laminar Blasius solution, are each shown in Figure 171 below.

$$C_f = 0.074/Re^{1/5} \quad (137)$$

$$C_f = 0.455/(\log Re)^{2.58} \quad (138)$$

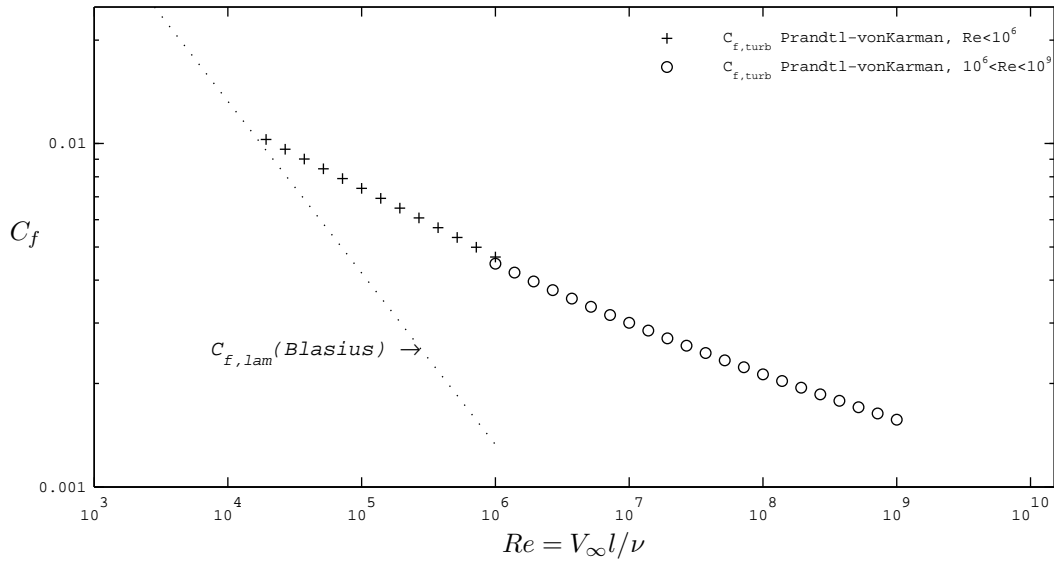


Figure 171: Coefficient of Friction – Prandtl–vonKármán Theoretical Turbulent Solutions

- b) vonKármán [167] also derived a similarity rule, $C_f^{-1/2} \propto \log(ReC_f)$, which Schoenherr [130] applied along with all available empirical data at the time to establish the function

known as the “Schoenherr Line” presented in Eq. 139. Schoenherr was attempting to provide a function to calculate the frictional resistance of ships. The Schoenherr Line is expected to be valid up to a Reynolds number of 10^{10} . It has been superimposed over the Prandtl–vonKármán solutions in Figure 172 below. The Schoenherr Line provides the advantage of a single solution over most of the range of turbulent Reynolds numbers encompassed by the Prandtl–vonKármán solutions. However, the Schoenherr Line requires a numerical solver which makes it difficult to utilize in analysis. Nonetheless, according to Hoerner, the Schoenherr Line is more often than not the approximation applied in practice.

$$\log(ReC_f) = 0.242/\sqrt{C_f} \quad (139)$$

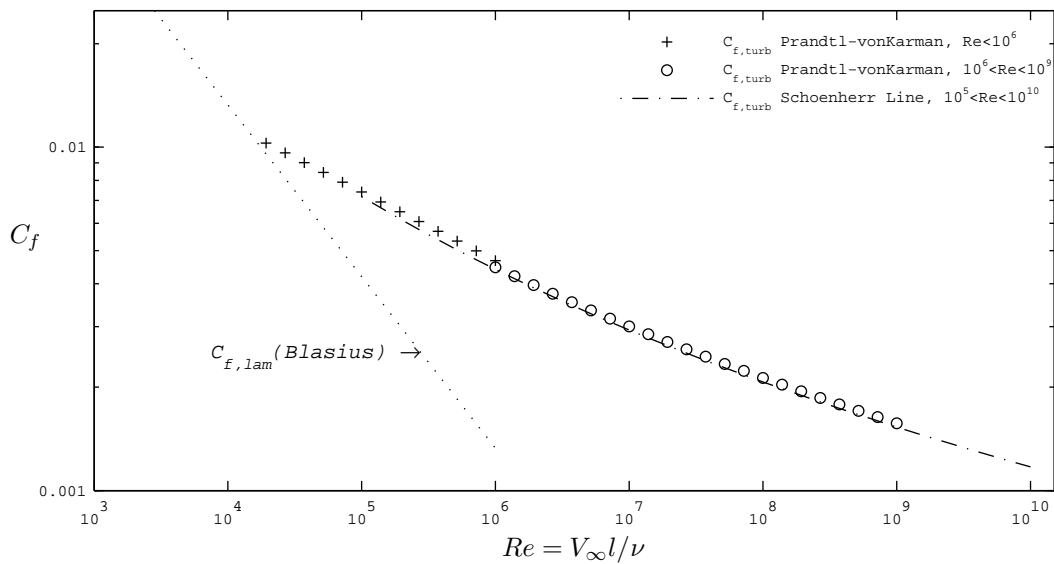


Figure 172: Coefficient of Friction – Including the Schoenherr Line

c) Hama [67] developed a simpler approximation of Schoenherr’s function which is expected to be accurate within $\pm 2\%$. The function is provided in Eq. 140 and is shown alongside the Schoenherr Line in Figure 173. Hama’s approximation is easily solved analytically, spans the entire range of expected turbulent Reynold’s numbers, and closely estimates the Schoenherr Line.

$$1/\sqrt{C_f} = 3.46\log Re - 5.6 \quad (140)$$

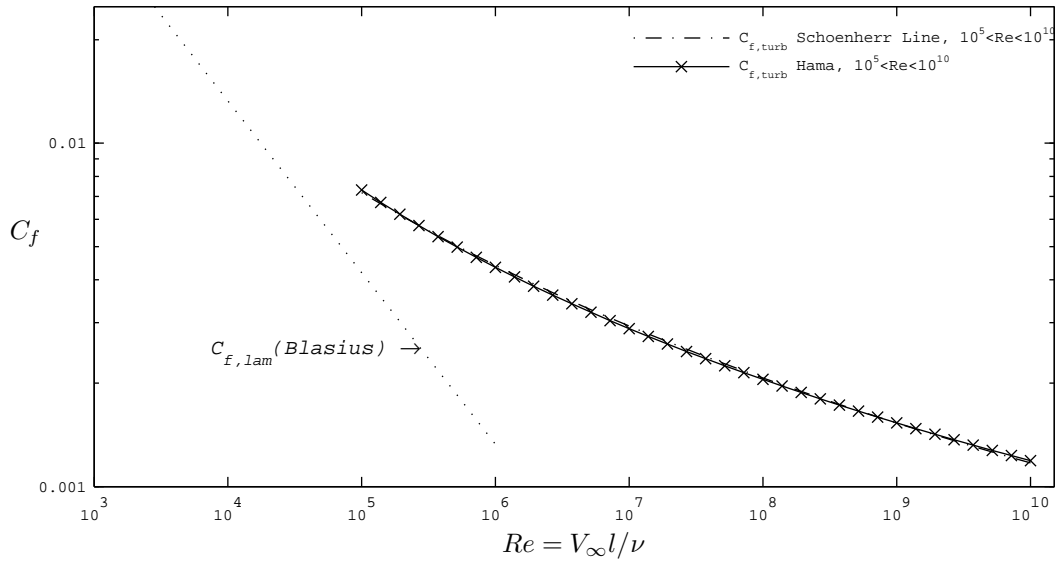


Figure 173: Coefficient of Friction – Schoenherr Line and Hama’s Approximation

d) Schultz-Grunow [133] provides an expression which trends close to the Schoenherr Line as well but was developed through experiments conducted on plane walls rather than in pipes. The function is given in Eq. 141 and is shown alongside the Schoenherr Line in Figure 174. Although the Schults-Grunow approximation is analytically solved and spans the desired range of turbulent Reynold’s numbers, it is not as good of an estimate of the Schoenherr Line as the Hama approximation is.

$$C_f = 0.427 / (\log Re - 0.407)^{2.64} \quad (141)$$

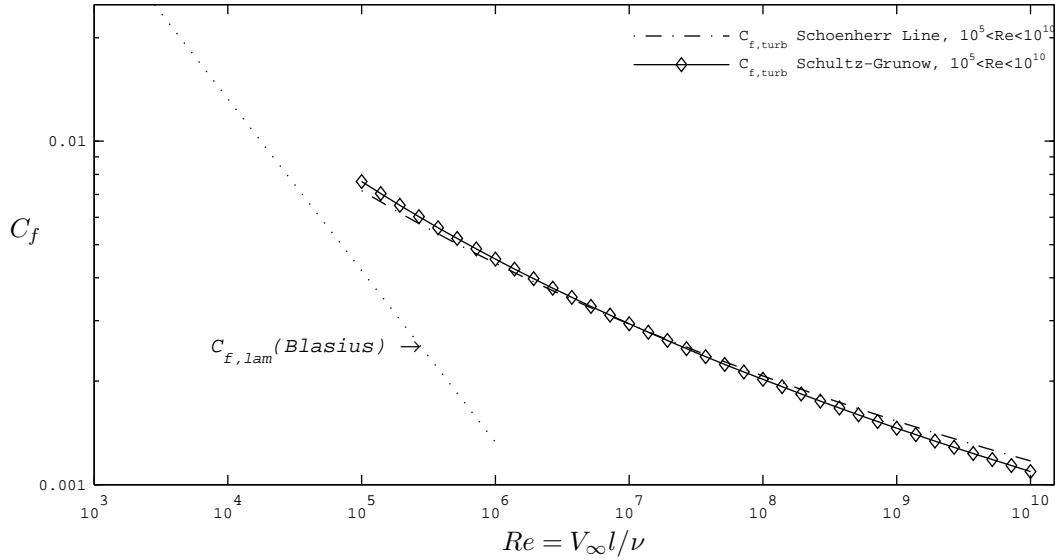


Figure 174: Coefficient of Friction – Schoenherr Line and Schultz-Grunow’s Approximation

e) Hoerner [70] interpolated the Schoenherr Line, the Shults-Grunow approximation, and additional experimental data to produce the function provided in Eq. 142. The function is shown alongside the Schoenherr Line in Figure 175. In Hoerner’s work it appears that he mistakenly stated K for the range $10^6 \leq Re \leq 10^8$ as $K = 0.44$. However, that would produce a wildly inaccurate estimate of the Schoenherr Line. Consequently, I report K for $10^6 \leq Re \leq 10^8$ as $K = 0.044$. That value is just a guess of what Hoerner may have meant, but it seems to be an accurate assumption. Although Hoerner’s functions are easy to calculate analytically and are good estimates of the Schoenherr Line and empirical data, they are not as convenient as the Hama approximation. This is due to the multiple functions necessary depending on the Reynolds number desired and the lack of Reynolds number range in which the solutions are applicable.

$$C_f = K/(Re^{1/m})$$

$$\text{For } 10^6 \leq Re \leq 10^8, m=6 \text{ and } K=0.044 \quad (142)$$

$$\text{For } 10^7 \leq Re \leq 10^9, m=7 \text{ and } K=0.03$$

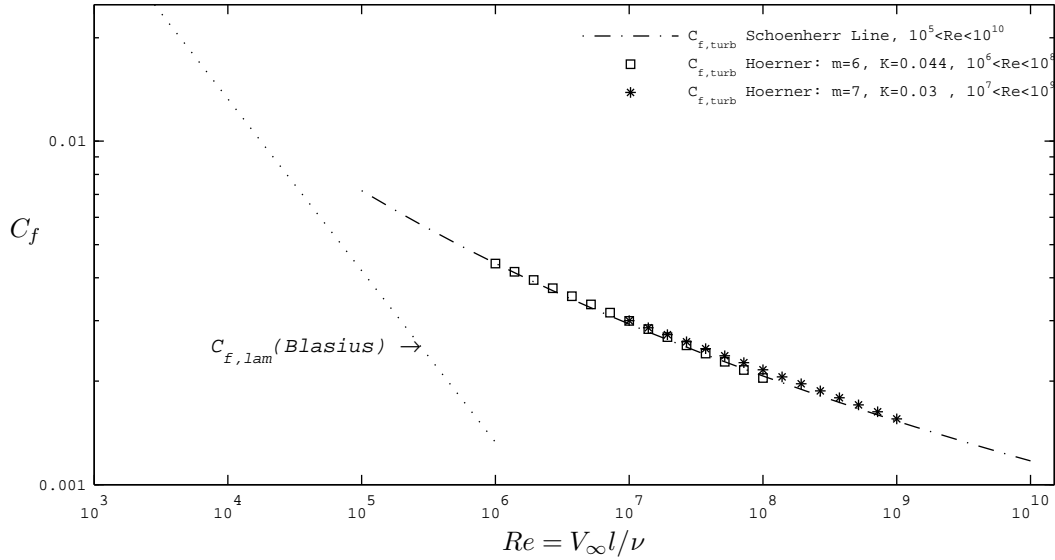


Figure 175: Coefficient of Friction – Schoenherr Line and Hoerner’s Interpolation

In summary, the Hama approximation given in Eq. 140 is the most applicable in this work for $C_{f,turb}$ estimations. The Hama approximation has been chosen since it is easily calculated analytically, it spans a large range of turbulent Reynolds numbers ($10^5 \leq Re \leq 10^{10}$), and it closely approximates the Schoenherr Line and empirical data. The Hama approximation is presented again in Eq. 143 below, but this time C_f has been solved for.

$$C_{f,turb} = \left(\frac{1}{3.46 \log Re - 5.6} \right)^2 \quad (143)$$

In some cases, the ability to calculate the coefficient of friction during transition from laminar to turbulent flow may be desirable, although it is not expected to be of great importance in this work (revisit Figure 170 above). Nonetheless, Hoerner provides a function that should be subtracted from the fully turbulent C_f approximations in order to determine the transitional C_f value [70]. The decrement is given in Eq. 144 below, and Prandtl [121] recommended a k value of $k = 1700$ based on experimental data. Figure 176 presents the chosen Hama approximation along with the transitional relationship and the laminar Blasius solution.

$$\Delta C_{f,trans} = k/Re \quad (144)$$

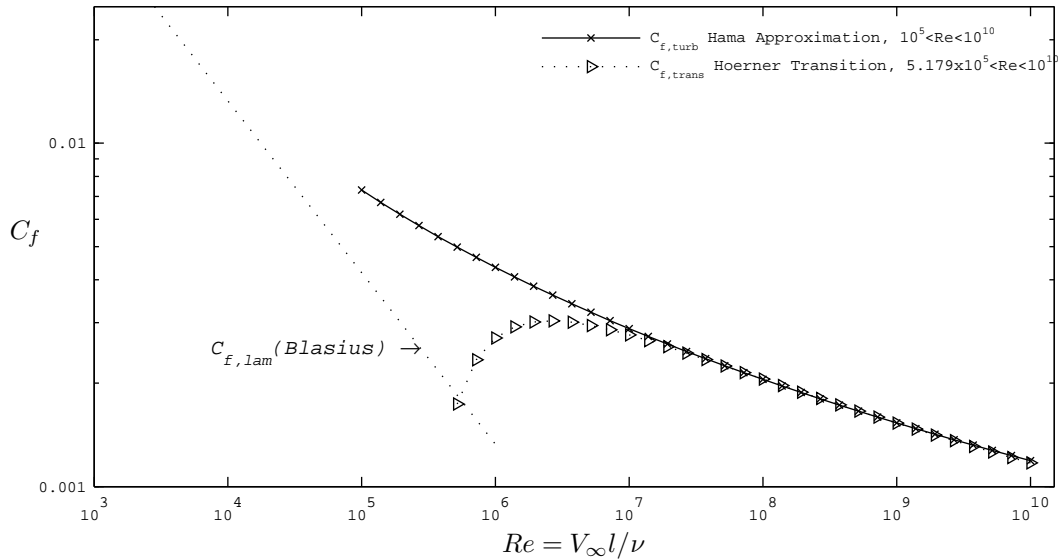


Figure 176: Coefficient of Friction – Hama Turbulence Approximation and the Transitional Estimate

For completeness, a plot generated by Hoerner [70] which shows some of the theoretical approximations discussed along with empirical results from various experiments in wind tunnels and/or tow tanks on smooth plates and other surfaces is given in Figure 177 below.

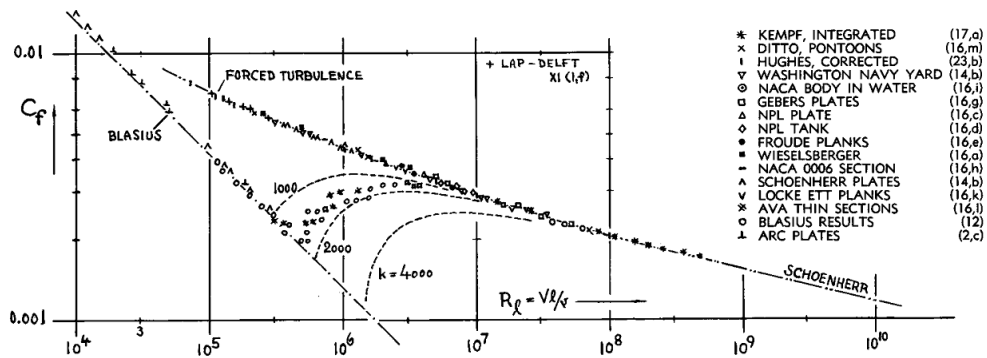


Figure 177: Hoerner Skin Friction Drag Coefficient Plot

Up to this point the only hydrodynamic coefficient considered has been the drag coefficient due to friction across the body. However, as was mentioned earlier, there are many more contributors to the total drag that will resist the vehicle's motion. C_{D_o} is the coefficient representing the total drag on the body at zero angle-of-attack (C_{D_o} will be discussed more in Section F.0.2.3) and it results from the combination of shear and pressure forces

against the body. Therefore, estimates of the total drag coefficient should show an increase of drag as compared to the friction only estimates provided so far. Empirical relationships produced from elliptical sections between walls (providing a 2-dimensional flow effect) are given for laminar and turbulent C_{Do} in Equations 145 and 146 respectively [70]. The expressions are functions of the appropriate friction coefficients ($C_{f,lam}$ or $C_{f,turb}$), the elliptical chord length (c), and the elliptical thickness (t). Figure 178 presents each of the functions along with the coefficient of friction trends. It is observed that C_{Do} in both the laminar and turbulent cases are orders of magnitude greater than the C_f contributions alone. This reinforces that a much more significant amount of drag is induced by the pressure drag as compared to the friction drag for the given flows and body shapes.

$$C_{Do,lam} = 2C_{f,lam}(1 + c/t) + 1.1(t/c) \quad (145)$$

$$C_{Do,turb} = C_{f,turb} (4 + 2(c/t) + 120(t/c)^2) \quad (146)$$

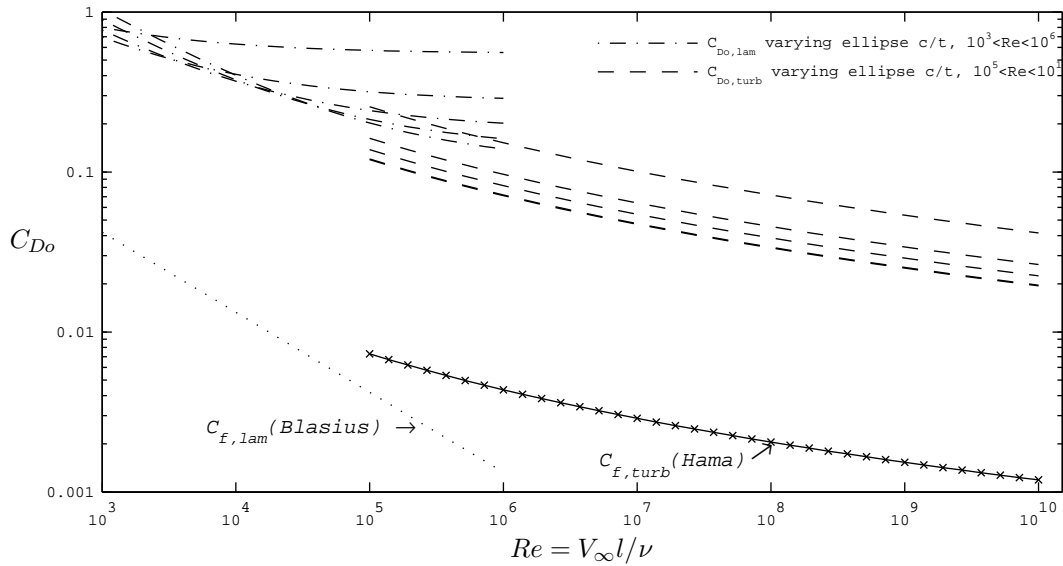


Figure 178: Zero-Lift Drag Coefficient for Elliptical Sections, $c/t = \{2,4,6,8,10\}$

Optimum thickness-to-chord ratios can be found by minimizing the C_{Do} relationships as a function of thickness-to-chord (or chord-to-thickness) ratio. Interestingly, for the elliptical shapes in laminar flow the chord-to-thickness ratio for minimum drag is a function of C_f (or

similarly of Reynolds number; see Equation 147) whereas for turbulent flow the optimum chord-to-thickness ratio is a constant (see Equation 148). This is clearly shown in Figure 178 above. In the low Reynolds number laminar region, the C_{D_o} trends cross over each other such that a different c/t ratio may be optimal depending on the Reynolds number. In the turbulent region, however, there is a distinct singular value of c/t that is optimal.

$$(c/t)_{min,C_{D_o},lam} = \sqrt{\frac{1.1}{2C_{f,lam}}} = \sqrt{\frac{(1.1)(1.328)}{2\sqrt{Re}}} \quad (147)$$

$$(c/t)_{min,C_{D_o},turb} = \sqrt[3]{120} = 4.93 \quad (148)$$

Again, up to this point 3-dimensional effects have not been considered. Therefore, more in depth details about the hydrodynamic coefficients including 3-D effects will be given in the next section.

F.0.2.2 3-Dimensional Effects on the Hydrodynamic Coefficients

Reference Areas Appropriate reference areas become exceedingly important when moving into the realm of 3-dimensional effects. For the body shapes considered in this work, the understanding of two main reference areas, and how to convert between them, will be crucial. These are the frontal area, S_{FA} (sometimes in the literature, the frontal area is S_o), and the wetted area, S_{wet} . The frontal area is the area of the 2-D projection of the body shape when viewing it straight on in the direction of flow. The wetted area is an estimate of the total area of the body contacted by the flow. For streamlined bodies, estimates of the wetted area, the frontal area, and the ratio between them are given in Equations 149, 150, and 151. Note that d is considered the maximum cross-sectional diameter of the body in the equations below. An example of the streamlined body shape is shown in Figure 179. The ratio of reference areas leads to the ratio for converting between a coefficient based on frontal area versus the wetted area. This ratio is also shown in Equation 151 (the subscript X is meant to represent any of the coefficients: drag, lift or moment). Again, Equations 149 – 151 will be extremely important for working with the 3-dimensional force and moment coefficients and for working with empirical data in which the frontal area or the wetted area

are used as the reference area.

$$S_{wet} = 0.75(\pi d)l \quad (149)$$

$$S_{FA} = d^2\pi/4 \quad (150)$$

$$\frac{S_{wet}}{S_{FA}} = 3\frac{l}{d} = \frac{C_{X,ref=FA}}{C_{X,ref=wet}} \quad (151)$$

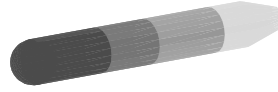


Figure 179: Streamlined Vehicle Body Example

Coefficient of Friction for Streamlined Bodies The C_f approximations given in Section F.0.2.1 can all be considered 2-dimensional estimates. For a rotationally symmetric 3-dimensional streamlined body with a small diameter-to-length (d/l) ratio (Hoerner makes the specification of small d/l but does not define how small is small enough), the shape of the body will stipulate an additional effect on the friction drag. As Hoerner states, “The average drag of streamline bodies and sections is somewhat higher...than that of an equivalent flat plate [*i.e.*, a 2-dimensional plane surface of equal wetted area, equal length, and equivalent Reynolds number]” [70]. As the diameter of the forebody increases along the direction of the flow, the boundary layer is more spread out resulting in an increase in local skin friction. In contrast, as the circumference decreases along the afterbody, the boundary layer thickness increases again, resulting in a decrease in local skin friction. On average, however, spreading out of the boundary layer tends to dominate which results in less of a boundary layer displacement and ultimately a greater average velocity of flow near the surface of the body. Therefore, there is an increase in the average dynamic pressure along the sides approximated as $\Delta q_{av} = 1.5q_{2D}(d/l)^{3/2}$ for turbulent flow and $\Delta q_{av} = q_{2D}(d/l)^{3/2}$ for laminar flow [70]. The increment in the 3-D frictional drag coefficient of the body in turbulent and laminar flow respectively are then: $\Delta C_{Df,SL,turb} = 1.5C_f(d/l)^{3/2}$ and $\Delta C_{Df,SL,lam} = C_f(d/l)^{3/2}$. The C_{Df} coefficients are appropriately based on the wetted body reference area, S_{wet} .

The frictional drag coefficients of rotationally symmetric streamlined bodies in laminar or turbulent flow are consequently given in Equations 152 and 153 below.

$$C_{Df,SL,lam} = C_f + C_f(d/l)^{3/2} \quad (152)$$

$$C_{Df,SL,turb} = C_f + 1.5C_f(d/l)^{3/2} \quad (153)$$

It should be clear that a relatively large length-to-diameter (l/d) ratio (or small d/l) will result in frictional coefficients similar to that of a flat plate. However, as the diameter of the body becomes larger and l/d decreases, the frictional drag coefficient increases more and more due to the spreading out of the boundary layer. Therefore, as the diameter-to-length (d/l) ratio grows, the 3-dimensional effects have a greater impact on the drag due to friction (as can be determined from Equations 152 and 153). This is shown in Figure 180 where the 3-D frictional drag coefficients are plotted with decreasing (l/d) values alongside the laminar Blasius solution and the turbulent Hama approximation. For the range of laminar Reynolds numbers shown, an l/d of 2 results in a frictional drag increase of 35% whereas an l/d of 10 produces only a 3% increase. In the turbulent regime there is a frictional drag increase of 53% for an l/d of 2 but only an increase of about 5% for an l/d of 10.

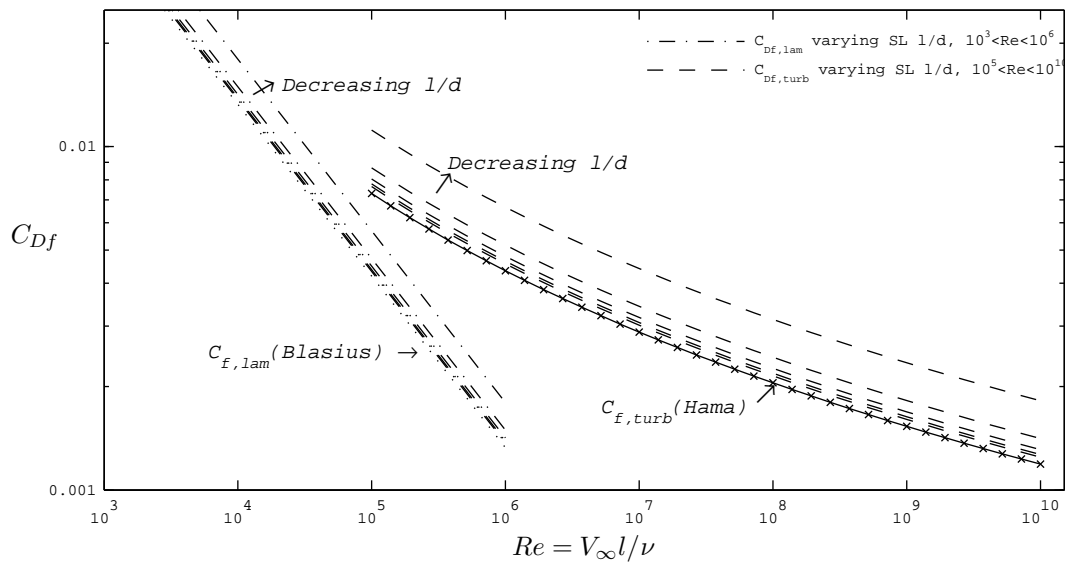


Figure 180: Streamline Body Shape Corrections, $l/d=\{2,4,6,8,10\}$

Coefficient of Friction for Cylindrical Bodies Some vehicle designs under consideration will have more of a cylindrical geometry than that of the streamlined body. Since the nose of the vehicle is comparatively flat in relation to that of the streamlined body, the boundary layer growth is relatively instantaneous. Relationships have been determined for the increase in the coefficient of friction for both laminar and turbulent flow as a function of cylinder length-to-diameter ratio, l/d . The incremental change for laminar flow and turbulent flow are given in Equations 154 and 155 respectively [70, 35, 93]. The resulting C_{Df} coefficients are appropriately based on the wetted body reference area, S_{wet} , and are given in Equations 156 and 157. It should be noted that the l/d effect on the coefficient of friction for the cylindrical body is *opposite* of the streamline body effect. Whereas the streamline body C_{Df} increased with decreasing l/d , the cylindrical body C_{Df} increases with increased l/d . However, the total effect of the cylindrical geometry on the frictional drag is so small that even for an $l/d = 10$ and $Re = 10^6$, the increment is negligible at about 1.5%. This is shown in Figure 182 where the Blasius-laminar and Hama-turbulent solutions are plotted along with the cylindrical body corrections for l/d values of {2,4,6,8,10}. For low laminar Reynolds numbers, the effect is more pronounced. But at the Reynolds numbers in the ranges more applicable to this research, the effects are small and almost indistinguishable from the 2-D solutions.

$$\Delta C_{Df,Cyl,lam} = \frac{2(l/d)}{Re} \quad (154)$$

$$\Delta C_{Df,Cyl,turb} \approx (0.023)C_f \frac{(l/d)}{Re^{2/5}} \quad (155)$$

$$C_{Df,Cyl,lam} = C_f + \frac{2(l/d)}{Re} \quad (156)$$

$$C_{Df,Cyl,turb} = C_f + (0.023)C_f \frac{(l/d)}{Re^{2/5}} \quad (157)$$

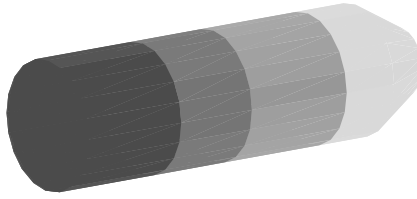


Figure 181: Cylindrical Vehicle Body Example

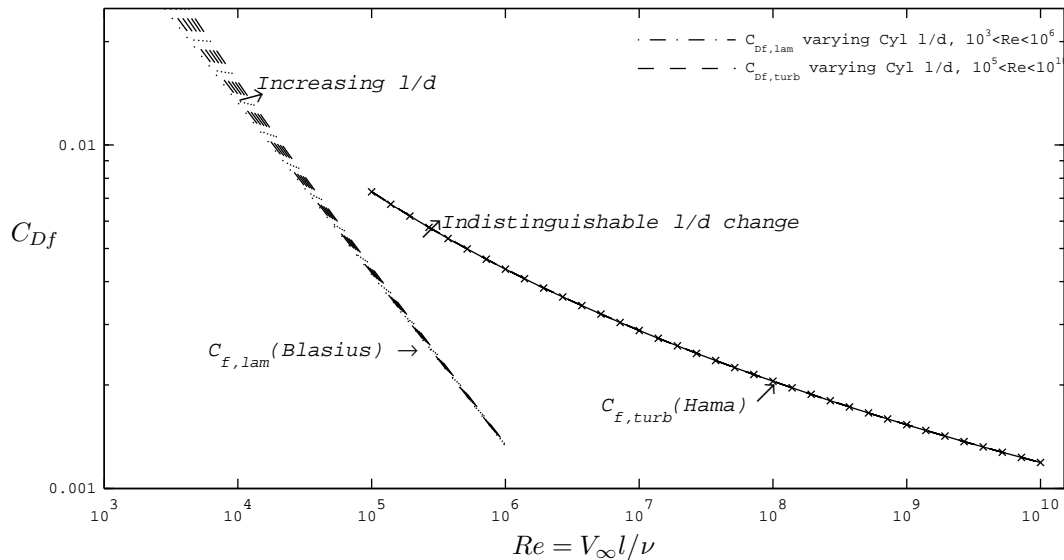


Figure 182: Cylindrical Shape Corrections, $l/d=\{2,4,6,8,10\}$

Friction Drag as a Catalyst for Pressure Drag Ultimately, whether 2 or 3-dimensional effects are considered, the friction drag across the body due to the boundary layer will be a major contributor to another type of drag introduced near the beginning of Section F.0.2.1: pressure drag. As was discussed earlier, the boundary layer along the body slows down the flow causing the static pressure along the body to increase. As a result, a positive pressure gradient is present along the body. This gradient is also known as an *adverse* pressure gradient since it will increase the likelihood of flow separating from the body. When the flow separates the static pressure behind the body decreases significantly compared to the pressure in front of the body. This results in a large pressure force against the vehicle in the direction of motion. In other words, an adverse pressure gradient can result in a significant

amount of drag. This pressure drag due to flow separation is often categorized as *viscous pressure drag*.

Additional Drag Force Considerations In addition to the effects of viscous forces on flow separation, the angle of attack of the vehicle in relation to the flow will affect the potential for flow separation from the vehicle. Furthermore, other factors such as the drag due to lift, the induced drag, and the drag due to hull protrusions will promote further total drag buildup. All of these factors contribute to the total shear and pressure forces against the body (i.e, the total drag of the body). Therefore, with appropriate estimates of the drag due to shear forces (in which the drag due to friction was the subject of this section) and the drag due to pressure forces, the total drag force on the vehicle can be calculated. The total force of drag for a body without camber at zero angle-of-attack is the subject of the next section.

F.0.2.3 Zero-Lift Drag Coefficient

For a vehicle shape without camber (symmetric about the axis perpendicular to the flow), the zero-lift drag coefficient (C_{Do}) is the total drag coefficient for the vehicle at zero angle of attack. C_{Do} results from the combination of shear and pressure forces against the body, equating it to a function of the coefficient of friction and the coefficient of pressure drag, $C_{Do} = f(C_{Df}, C_{Dp})$. Note that C_{Do} uses the reference area based on the frontal area of the body, S_{FA} . Alternatively, C_{Dwet} is the total drag coefficient of the vehicle based on the total wetted area of the body, S_{wet} . Relationships were given for the theoretical treatment of the coefficient of friction for various flow conditions in Equations 136 (2-D laminar), 143 (2-D turbulent), 152 (3-D streamlined laminar), 153 (3-D streamlined turbulent), 156 (3-D cylindrical laminar), and 157 (3-D cylindrical turbulent). However, the theoretical treatment of the coefficient of pressure drag is much more elusive due to the difficulties in calculating flow separation. Often, the pressure drag must be determined by subtracting the theoretical friction drag from the total drag estimated from empirical data.

The Impact of Flow Separation Laminar versus turbulent flow across the vehicle body will have a significant impact on the amount of drag produced. Figures 171 – 176 showed that the drag tangential to the body surface due to friction is greater in turbulent flow than in laminar flow for most flow regimes except at very low Reynolds numbers. However, as was shown in Figure 170, the majority of the flow across the vehicle types considered within this work will be turbulent. Although this results in a detrimental effect on the skin friction drag, it actually produces a much greater positive effect on pressure drag. This is due to the difference in separation effects in laminar versus turbulent flow. Due to imperfections along the body as well as adverse pressure gradients, flow separation will most likely occur in any practical flow. When the flow separates, the pressure drag increases significantly due to the difference between high positive pressures on the front side of the vehicle versus very low to negligible negative pressures on the rear of the vehicle. The resultant pressure differential is large in the direction of vehicle motion, creating significant resistance. However, turbulent flow will actually help the flow stay attached, or reattach, to the body resulting in a less severe pressure differential. Hoerner explains the phenomenon as it occurs around a sphere in a flow field in the following manner [70]:

*Within every turbulent boundary layer, an exchange of mass and momentum takes place...This exchange thus represents a continuous momentum transport from the outer flow toward the surface of the body...near the surface of the body, the turbulent b'layer carries much more momentum than the laminar layer. Approaching the critical Reynolds number, the b'layer begins to turn turbulent around the equator of the sphere. The sheets nearest to the surface are accordingly boosted in velocity and momentum; **and they are therefore better enabled to flow against the positive pressure opposed to their movement along the rear of the body. Subsequently the flow attached itself to the surface...The drag decreases correspondingly.***

The effect is shown in Figure 183 below. In the chart, for low Reynolds numbers (up to about 10), the solid-dotted line represents the theoretical *viscous pressure drag* solution

for a sphere in laminar flow according to viscous theory, ($C_{Do} = 24/Re$). The theoretical solution attempts to capture both the drag due to friction and the drag due to separation and other pressure forces. The difference between the viscous theory line and the plotted data points shows that it is difficult to provide an exact theoretical solution for pressure drag due to flow separation. Nonetheless, the drag coefficient eventually levels out for a range of Reynolds numbers in laminar flow. However, at the critical transition point from laminar to turbulent flow between $10^5 \leq Re \leq 10^6$, the drag coefficient drops significantly. This is due to the initiation of turbulent flow which has increased the exchange of momentum into the boundary layer and has assisted in keeping the flow better attached to the body, resulting in a beneficial decrease in pressure drag.

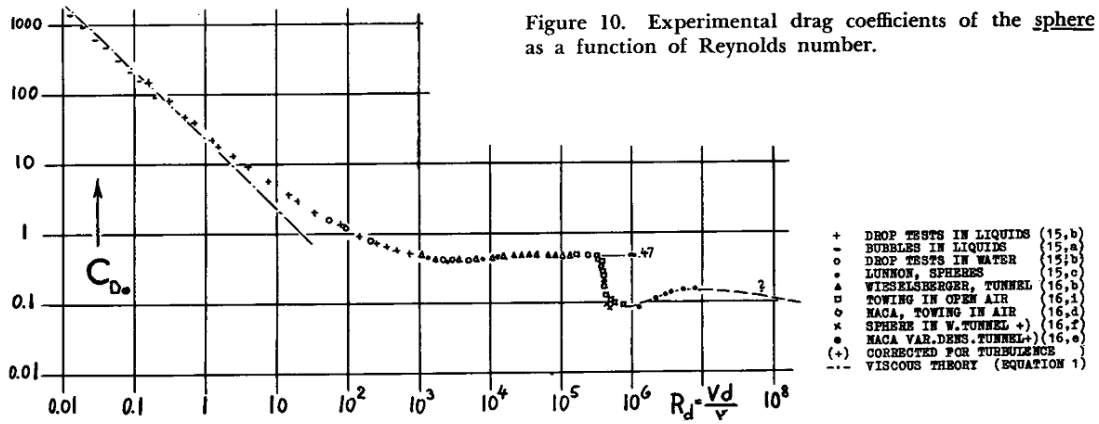


Figure 183: Coefficient of Drag for a Sphere from Hoerner[70]

Zero-Lift Drag on Streamlined Bodies For streamlined bodies in laminar flow, Hoerner estimates that the pressure drag coefficient is $C_{Dp} = 0.33(d/l)$, which is based on the frontal reference area, S_{FA} . Converting to the wetted reference area results in $C_{Dp,wet} = C_{Dp}[\frac{C_{Dp,wet}}{C_{Dp}}] = C_{Dp}[\frac{S_{FA}}{S_{wet}}] = 0.33(d/l)[\frac{d}{3l}] = 0.11(d/l)^2$. The total drag estimate can then be calculated based on $C_{Dwet} = C_{Df} + C_{Dp,wet}$, where C_{Df} is taken from Equation 152 and C_f is the Blasius solution from Equation 136: $C_{f,lam} = 1.328/\sqrt{Re}$. The total drag estimates for the streamlined body in laminar flow based on wetted area and frontal area are then given in Equations 158 and 159 respectively.

$$C_{Dwet,SL,lam} = C_{f,lam} + C_{f,lam}(d/l)^{3/2} + 0.11(d/l)^2 \quad (158)$$

$$C_{D_o,SL,lam} = 3C_{f,lam}(l/d) + 3C_{f,lam}(d/l)^{1/2} + 0.33(d/l) \quad (159)$$

Similarly, Hoerner estimates the pressure drag coefficient in turbulent flow as $C_{Dp} = 21C_{f,turb}(d/l)^2$ based on the frontal area of the streamlined body. Utilizing the same conversion procedures as above, $C_{Dp,wet} = 7C_{f,turb}(d/l)^3$ in turbulent flow. C_{Df} is then taken from Equation 153 and C_f is the Hama approximation from Equation 143: $C_{f,turb} = \left(\frac{1}{3.46 \log Re - 5.6}\right)^2$. The total drag estimates for the streamlined body in turbulent flow based on wetted area and frontal area are then given in Equations 160 and 161 respectively.

$$C_{Dwet,SL,turb} = C_{f,turb} + 1.5C_{f,turb}(d/l)^{3/2} + 7C_{f,turb}(d/l)^3 \quad (160)$$

$$C_{D_o,SL,turb} = 3C_{f,turb}(l/d) + 4.5C_{f,turb}(d/l)^{1/2} + 21C_{f,turb}(d/l)^2 \quad (161)$$

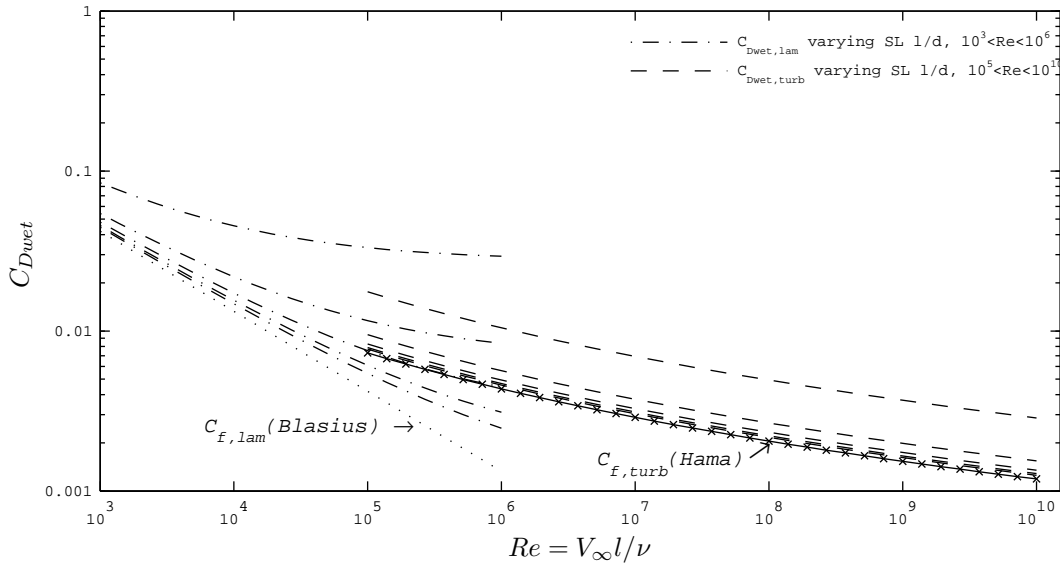


Figure 184: Total Wetted Drag Coefficient, Streamlined Body Shape, $l/d = \{2, 4, 6, 8, 10\}$

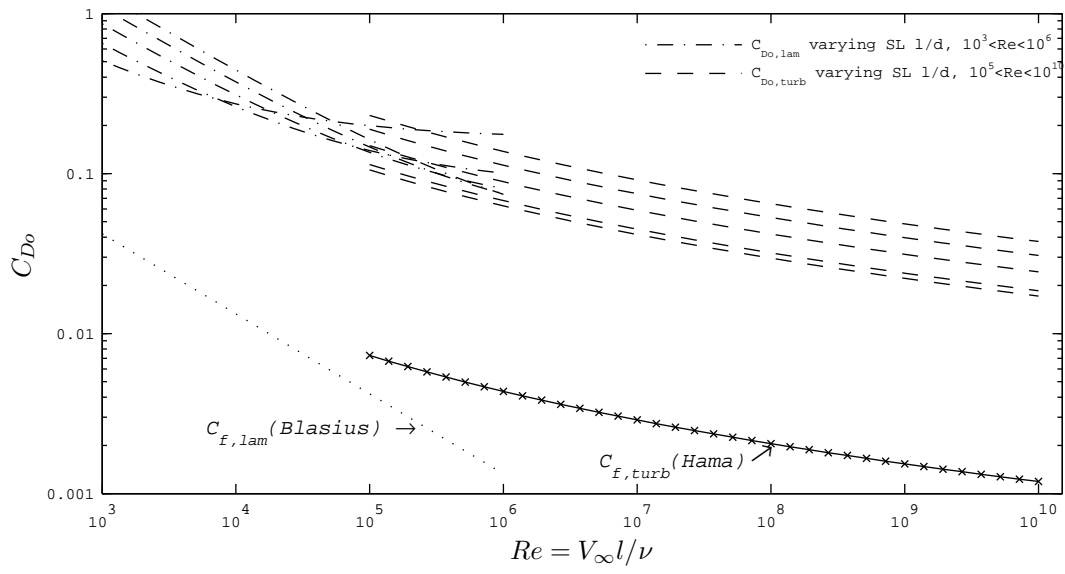


Figure 185: Total Drag Coefficient, Streamlined Body Shape, $l/d = \{2, 4, 6, 8, 10\}$

REFERENCES

- [1] AGMON, N., HAZON, N., and KAMINKA, G. A., “The giving tree: Constructing trees for efficient offline and online multi-robot coverage,” *Annals of Mathematics and Artificial Intelligence*, vol. 52, pp. 143–168, April 2008.
- [2] AHERN, T.M., “Mine warfare: A core navy competency,” November 1999.
- [3] AINSLIE, M., *Principles of Sonar Performance Modelling*. Springer Berlin Heidelberg, 2010.
- [4] ALLEN, B., VORUS, W., and PRESTERO, T., “Propulsion system performance enhancements on remus auvs,” in *OCEANS 2000 MTS/IEEE Conference and Exhibition*, vol. 3, pp. 1869–1873, 2000.
- [5] ALLMENDINGER, E. E., *Submersible Vehicle Systems Design*. Society of Naval Architects and Marine Engineers (SNAME), 1990.
- [6] ANDERSON, R. E., “HRD’s Role in Concurrent Engineering,” *Training & Development*, vol. 47, no. 6, p. 49, 1993.
- [7] ANDERSON JR., J. D., *Introduction to Flight*. McGraw-Hill, 3 ed., 1989.
- [8] ANDERSON JR., J. D., *Aircraft Performance and Design*. McGraw-Hill, 1999.
- [9] ASSESSMENT PANEL OF THE DEFENSE ACQUISITION PERFORMANCE ASSESSMENT PROJECT, “Defense acquisition performance assessment report,” tech. rep., United States Department of Defense, January 2006.
- [10] AXELROD, R. M., *The complexity of cooperation: Agent-based models of competition and collaboration*. Princeton University Press, 1997.
- [11] BAKER, A. P., *The Role Of Mission Requirements, Vehicle Attributes, Technologies And Uncertainty In Rotorcraft System Design*. Dissertation, Georgia Institute of Technology, 2002.
- [12] BALESTRINI-ROBINSON, S., *A Modeling Process to Understand Complex System Architectures*. Dissertation, Georgia Institute of Technology, 2009.
- [13] BEACHKOFKI, B., “Product-based engine health management planning,” in *Aerospace Conference, 2005 IEEE*, pp. 1–6, 2005.
- [14] BEJAN, A., *Shape and Structure, from Engineering to Nature*. Cambridge, UK: Cambridge University Press, 2000.
- [15] BEJAN, A., “Fundamentals of exergy analysis, entropy generation minimization, and the generation of flow architecture,” *International Journal Of Energy Research*, vol. 26, pp. 545–565, 2002.

- [16] BEJAN, A. and MAMUT, E., *Thermodynamic Optimization of Complex Energy Systems*. Kluwer Academic Publishers, 1999.
- [17] BENES, T. A. and SANDEL, E. A., “21st Century U.S. Navy Mine Warfare: Ensuring Global Access and Commerce,” tech. rep., Program Executive Office Littoral and Mine Warfare, Expeditionary Warfare Directorate, U.S. Navy, 2009.
- [18] BERMAN, S., LINDSEY, Q., SAKAR, M. S., KUMAR, V., and PRATT, S., “Experimental study and modeling of group retrieval in ants as an approach to collective transport in swarm robotic systems,” *Proceedings of the IEEE*, vol. 99, pp. 1470–1481, Sept 2011.
- [19] BILTGEN, P. T., *Systems of Systems Engineering: Principles and Applications*, ch. Technology Evaluation for System of Systems. Taylor and Francis Group, 2009.
- [20] BILTGEN, P. T., *A Methodology for Capability-Based Technology Evaluation for Systems-of-Systems*. Dissertation, Georgia Institute of Technology, 2007.
- [21] BILTGEN, P. T., ENDER, T. R., and MAVRIS, D. N., “Development of a collaborative capability-based tradeoff environment for complex system architectures,” in *44th AIAA Aerospace Sciences Meeting and Exhibit*, Georgia Institute of Technology, AIAA, 2006.
- [22] BLASIUS, H., “Boundary layers in fluids with little friction (grenzschichten in flüssigkeiten mit kleiner reibung),” *Zeitschrift für Mathematik und Physik*, vol. 56, 1908.
- [23] BLUMRICH, J. F., “Design,” *Science*, vol. 168, pp. 1551–1554, June 1970.
- [24] BOTTACCINI, M. R., “The stability coefficients of standard torpedoes,” tech. rep., U.S. Naval Ordnance Test Station, China Lake, CA, June 1954.
- [25] BOURGAULT, F., “Coordinated decentralized search for a lost target in a bayesian world,” in *IEEE/RSJ international conference on intelligent robots and systems*, pp. 48–53, 2003.
- [26] BURDIC, W. S., *Underwater Acoustic System Analysis*. Englewood Cliffs, NJ: Prentice-Hall, 1984.
- [27] CAO, Y., FUKUNAGA, A., and KAHNG, A., “Cooperative mobile robotics: Antecedents and directions,” *Autonomous Robots*, vol. 4, no. 1, pp. 7–27, 1997.
- [28] CENGAL, Y. and CIMBALA, J., *Fluid Mechanics: Fundamentals and Applications*. NY: McGraw-Hill, 2006.
- [29] CENGAL, Y. and CIMBALA, J., *Fluid Mechanics: Fundamentals and Applications*, ch. 10, pp. 520–524. NY: McGraw-Hill, 2006.
- [30] CHAIRMAN OF THE JOINT CHIEFS OF STAFF, *Chairman of the Joint Chiefs of Staff Instruction CJCSI 5123.01 F*. U.S. Department of Defense, January 2012.
- [31] CHAIRMAN OF THE JOINT CHIEFS OF STAFF, *Manual for the Operation of the Joint Capabilities Integration and Development System*. U.S. Department of Defense, January 2012.

- [32] CHARNES, A. and COOPER, W. W., “The theory of search: Optimum distribution of search effort,” *Management Science*, vol. 5, p. 4450, 1953.
- [33] CLAPPER, J., YOUNG, J., CARTWRIGHT, J., and GRIMES, J., “Unmanned Systems Roadmap 2007-2032,” *Office of the Secretary of Defense*, p. 188, 2007.
- [34] COMMITTEE ON NETWORK-CENTRIC NAVAL FORCES, NAVAL STUDIES BOARD, N. R. C., *Network-Centric Naval Forces: A Transition Strategy for Enhancing Operational Capabilities*. Washington, DC: The National Academies Press, 2000.
- [35] COOPER, R. and TULIN, M., “The laminar flow about very slender cylinders in axial motion, including the effect of pressure gradients and unsteady motions,” Report 838, David W. Taylor Model Basin, Washington, D.C., April 1953.
- [36] CZACZKES, T. J. and RATNIEKS, F. L., “Cooperative transport in ants (Hymenoptera: Formicidae) and elsewhere,” *Myrmecological News*, vol. 18, pp. 1–11, 2013.
- [37] DAHMANN, J., REBOVICH, G., LANE, J., and LOWRY, R., “System engineering artifacts for SoS,” in *Systems Conference, 2010 4th Annual IEEE*, pp. 13–17, 2010.
- [38] DAHMANN, J., REBOVICH, G., LOWRY, R., LANE, J., and BALDWIN, K., “An implementers’ view of systems engineering for systems of systems,” in *Systems Conference (SysCon), 2011 IEEE International*, pp. 212–217, IEEE, 2011.
- [39] DAWE, R. L., “Detection threshold modelling explained,” tech. rep., DTIC Document, 1997.
- [40] DEFENSE ACQUISITION UNIVERSITY, *Defense Acquisition Guidebook*, November 2012.
- [41] DEMBO, A., PERES, Y., ROSEN, J., and ZEITOUNI, O., “Cover times for brownian motion and random walks in two dimensions,” *Annals of Mathematics*, vol. 160, no. 2, pp. 433–464, 2004.
- [42] DIETER, G. E., *Engineering Design: A Materials and Processing Approach*. Thomas Casson, 3 ed., 2000.
- [43] DIRECTOR, SYSTEMS AND SOFTWARE ENGINEERING, DEPUTY UNDER SECRETARY OF DEFENSE (ACQUISITION AND TECHNOLOGY), AND OFFICE OF THE UNDER SECRETARY OF DEFENSE (ACQUISITION, TECHNOLOGY AND LOGISTICS), *Systems Engineering Guide for Systems of Systems*, 1.0 ed., August 2008.
- [44] DOMERCANT, J. C., *ARC-VM: An Architecture Real Options Complexity-based Valuation Methodology For Military Systems-of-Systems Acquisitions*. Dissertation, Georgia Institute of Technology, 2011.
- [45] DYER, J. S., FISHBURN, P. C., STEUER, R. E., WALLENIUS, J., and ZIONTS, S., “Multiple criteria decision making, multiattribute utility theory: The next ten years,” *Management Science*, vol. 38, no. 5, pp. 645 – 654, 1992.
- [46] EAGLE, J., “Search and detection theory lecture notes: Chapter 2.” <http://or.nps.edu/faculty/JimEagle/searchclass.htm>, Accessed November 2014, March 2008.

- [47] ENDER, T., *A Top-Down, Hierarchical, System-of-Systems Approach to the Design of an Air Defense Weapon*. Dissertation, Georgia Institute of Technology, July 2006.
- [48] EPSTEIN, J. M., *Growing Artificial Societies: Social Science from the Bottom Up*. Brookings Institution Press, 1996.
- [49] EVANS, J. H., “Basic design concepts,” *Journal of the American Society for Naval Engineers*, vol. 71, no. 4, pp. 671–678, 1959.
- [50] EVANS, J. and NAHON, M., “Dynamics modeling and performance evaluation of an autonomous underwater vehicle,” *Ocean Engineering*, vol. 31, no. 1415, pp. 1835 – 1858, 2004.
- [51] FIGUEIRA, J., GRECO, S., and EHROGOTT, M., eds., *Multiple Criteria Decision Analysis: State of the Art Surveys (International Series in Operations Research & Management Science)*. Springer, 1 ed., 2005.
- [52] FRIEDLAND, B., *Control System Design - An Introduction to State-Space Methods*, ch. 2.1 Mathematical Models. Dover Publications, 1986.
- [53] FRIEDLAND, B., *Control System Design - An Introduction to State-Space Methods*. Dover Publications, 1986.
- [54] FRITS, A. P., *Formulation of an Integrated Robust Design and Tactics Optimization Process for Undersea Weapon Systems*. Dissertation, Georgia Institute of Technology, January 2005.
- [55] FUNNEL, C., ed., *Janes Underwater Warfare Systems*. Jane’s Information Group, 2008-2009.
- [56] GABRIELE, S. and DI GIAMBERARDINO, P., “Mobile sensor networks under communication constraints,” *WSEAS Transactions on Systems*, vol. 7, pp. 165–174, Mar. 2008.
- [57] GAGE, D. W., “Randomized search strategies with imperfect sensors,” in *Proceedings of SPIE, Mobile Robots VIII* (WOLFE, W. J. and CHUN, W. H., eds.), vol. 2058, 1994.
- [58] GODDARD, R., “The Sonar Simulation Toolset,” in *Proceedings of OCEANS 1989*, vol. 4, pp. 1217–1222, Sep 1989.
- [59] GONZALEZ, E., ALARCON, M., ARISTIZABAL, P., and PARRA, C., “BSA: A coverage algorithm,” in *IEEE/RSJ International Conference on Intelligent Robots and Systems (IROS)*, vol. 2, pp. 1679–1684, October 2003.
- [60] GONZALEZ, E., ALVAREZ, O., DIAZ, Y., PARRA, C., and BUSTACARA, C., “Bsa: A complete coverage algorithm,” in *Robotics and Automation, 2005. ICRA 2005. Proceedings of the 2005 IEEE International Conference on*, pp. 2040–2044, April 2005.
- [61] GONZALEZ-ZUGASTI, J. P., OTTO, K. N., and BAKER, J. D., “A method for architecting product platforms,” *Research in Engineering Design*, vol. 12, no. 2, pp. 61–72, 2000.

- [62] GOODING, T. R., “A framework for evaluating advanced search concepts for multiple autonomous underwater vehicle (auv) mine countermeasures (mcm),” Master’s thesis, MIT, February 2001.
- [63] GRANVILLE, P. S., “Elements of the drag of underwater bodies,” tech. rep., Naval Ship Research and Development Center, Bethesda, MD, Ship Performance Department, June 1976.
- [64] GREEN, J., “Establishing system measures of effectiveness,” tech. rep., DTIC Document, 2001.
- [65] GREEN, J. and JOHNSON, B., “Towards a theory of measures of effectiveness,” tech. rep., DTIC Document, 2002.
- [66] GRIENDLING, K., *Architect: The Architecture-based Technology Evaluation And Capability Tradeoff Method*. Dissertation, Georgia Institute of Technology, 2011.
- [67] HAMA, F., “Boundary-layer characteristics for smooth and rough surfaces,” *Transactions of the Society of Naval and Marine Engineering (SNAME)*, vol. 62, p. 333, 1954.
- [68] HARRIS, F., “On the use of windows for harmonic analysis with the discrete fourier transform,” *Proceedings of the IEEE*, vol. 66, pp. 51–83, Jan 1978.
- [69] HEXMOOR, H., “Essential principles for autonomous robotics,” *Synthesis Lectures on Artificial Intelligence and Machine Learning*, vol. 7, no. 2, pp. 1–155, 2013.
- [70] HOERNER, S. F., *Fluid Dynamic Drag*. Published by Author, 1965.
- [71] HOFFMANN, G., WASLANDER, S., and TOMLIN, C., “Distributed cooperative search using information–theoretic costs for particle filters, with quadrotor applications,” in *Guidance, Navigation, and Control and Co-located Conferences*, American Institute of Aeronautics and Astronautics, 2006.
- [72] HORA, S. C., “Aleatory and epistemic uncertainty in probability elicitation with an example from hazardous waste management,” *Reliability Engineering & System Safety*, vol. 54, no. 23, pp. 217 – 223, 1996.
- [73] HUGGINS, A. and PACKWOOD, A., “Wind tunnel experiments on a fully appended laminar flow submersible for oceanographic survey,” *Ocean Engineering*, vol. 22, pp. 207–221, 1995.
- [74] HYMAN, M. and SCHNOOR, R., “Influence sweeping of pressure mines,” tech. rep., Navy STTR, 2007.
- [75] IACOBUCCI, J. V., *Rapid Architecture Alternative Modeling (RAAM): A Framework For Capability-based Analysis Of System Of Systems Architectures*. Dissertation, Georgia Institute of Technology, 2012.
- [76] IEEE, *IEEE Standard for Application and Management of the Systems Engineering Process (1220-2005)*. IEEE Computer Society/Software & Systems Engineering Standards Committee, International Standard ISO/IEC 26702:2007(E) ed., 2007.

- [77] INCOSE, *Systems Engineering Handbook: A Guide for System Life Cycle Processes and Activities*, 3.2.1 ed., January 2011.
- [78] ISO/IEC/IEEE, *Systems and Software Engineering – Vocabulary*, 2010.
- [79] IZENMAN, A., *Modern Multivariate Statistical Techniques*. Springer Texts in Statistics, Springer New York, 2008.
- [80] JACKSON, D., “APL-UW High-Frequency Ocean Environmental Acoustic Models Handbook,” *Applied Physics Laboratory, University of Washington, Technical Report*, vol. 9407, 1994.
- [81] JAMSHIDI, M., *Systems of Systems Engineering: Principles and Applications*, ch. Introduction to Systems of Systems, pp. 1–36. Taylor and Francis Group, 2009.
- [82] JOHNSON, D., “Framing.” <http://www.hometime.com/Howto/projects/framing>, Accessed February 8, 2015.
- [83] JOINT CHIEFS OF STAFF, *Capabilities-Based Assessment (CBA) User’s Guide*. United States Department of Defense, 3 ed., March 2009.
- [84] JONES, D., CLARKE, D., BRAYSHAW, I., BARILLON, J., and ANDERSON, B., “The calculation of hydrodynamic coefficients for underwater vehicles,” tech. rep., Maritime Platforms Division, DSTO Platforms Sciences Laboratory, Commonwealth of Australia, 2002.
- [85] KAY, S. M., *Fundamentals of Statistical Signal Processing, Volume III: Practical Algorithm Development*, vol. 3. Pearson Education, 2013.
- [86] KENNEDY, J., EBERHART, R. C., and SHI, Y., *Swarm Intelligence*. Morgan Kaufmann Publishers, 2001.
- [87] KITTS, C. and EGERSTEDT, M., “Design, control, and applications of real-world multirobot systems [from the guest editors],” *IEEE Robotics Automation Magazine*, vol. 15, no. 1, p. 8, 2008.
- [88] KOESTER, R. J., COOPER, D. C., FROST, J., and ROBE, R., “Sweep width estimation for ground search and rescue,” tech. rep., DTIC Document, 2004.
- [89] KOOPMAN, B. O., *Search and Screening*. Elmsford, NY: Pergamon Oress, 2 ed., 1980.
- [90] LAIRD, R. T., “Evolving US Department of Defense (DOD) Unmanned Systems Research, Development, Test, Acquisition, And Evaluation (RDTA&E),” in *SPIE Defense, Security, and Sensing*, pp. 73321J–73321J, International Society for Optics and Photonics, 2009.
- [91] LAMB, T., “A ship design procedure,” *Marine Technology*, vol. 6, no. 4, pp. 362–405, 1969.
- [92] LAMB, T., ed., *Ship Design and Construction*, vol. 1–2. Society of Naval Architects and Marine Engineers (SNAME), 2003.
- [93] LANDWEBER, L., “Effect of transverse curvature on frictional resistance,” Report 689, David W. Taylor Model Basin, Washington, D.C., March 1949.

- [94] LANE, J. A., DAHMANN, J., REBOVICH, G., and LOWRY, R., “Key system of systems engineering artifacts to guide engineering activities,” in *NDIA SE Conference*, October 2010.
- [95] LINKLATER, A., *Design and simulation of a towed underwater vehicle*. Dissertation, Virginia Polytechnic Institute and State University, 2005.
- [96] LOCKHEED MARTIN CORPORATION, “Remote Minehunting System,” Washington, D.C, March 2014.
- [97] LOUREIRO, G. and CURRAN, R., *Complex Systems Concurrent Engineering*. Springer, 2007.
- [98] MAIER, M. W., “Architecting principles for systems-of-systems,” *Systems Engineering*, vol. 1, no. 4, pp. 267–284, 1998.
- [99] MARITIME, K., “REMUS 100 Autonomous Underwater Vehicle.” Accessed May 2012, <http://www.km.kongsberg.com/>, Kongsberg, Norway, 2011.
- [100] MARK, G., “Extreme collaboration,” *Communications of the ACM*, vol. 45, pp. 89–93, June 2002.
- [101] MARTINOLI, A., EASTON, K., and AGASSOUNON, W., “Modeling swarm robotic systems: A case study in collaborative distributed manipulation,” *The International Journal of Robotics Research*, vol. 23, pp. 415–436, April-May 2004.
- [102] MATTINGLY, J. D., HEISER, W. H., and PRATT, D. T., *Aircraft Engine Design*. Reston, VA: American Institute of Aeronautics and Astronautics, 2 ed., 2002.
- [103] MAVRIS, D. N., BILTGEN, P. T., and WESTON, N. R., “Advanced design of complex systems using the Collaborative Visualization Environment (CoVE),” in *AIAA Aerospace Sciences Meeting and Exhibit*, vol. 43, p. 126, AIAA, 2005.
- [104] MCALLISTER, C. D., SIMPSON, T., KURTZ, P., and YUKISH, M., “Multidisciplinary design optimization testbed based on autonomous underwater vehicle design,” in *9th AIAA/ISSMO Symposium on Multidisciplinary Analysis and Optimization*, (Atlanta, GA), Multidisciplinary Analysis Optimization Conferences, American Institute of Aeronautics and Astronautics, September 2002.
- [105] MCCREERY, H. and BREED, M., “Cooperative transport in ants: a review of proximate mechanisms,” *Insectes Sociaux*, vol. 61, no. 2, pp. 99–110, 2014.
- [106] MERRIAM-WEBSTER DICTIONARY, “Collaborate.” <http://www.merriam-webster.com/dictionary/collaborate>, Accessed April 2013.
- [107] MERRIAM-WEBSTER DICTIONARY, “Materiel.” <http://www.merriam-webster.com/dictionary/materiel>, Accessed April 2013.
- [108] MESBAHI, M. and EGERSTEDT, M., *Graph Theoretic Methods in Multiagent Networks*, ch. 1. Princeton University Press, 2010.
- [109] MILGRAM, J., “Strip theory for underwater vehicles in water of finite depth,” *Journal of Engineering Mathematics*, vol. 58, no. 1, pp. 31–50, 2007.

- [110] MIN, H. J. and PAPANIKOLOPOULOS, N., “The multi-robot coverage problem for optimal coordinated search with an unknown number of robots,” in *2011 IEEE International Conference on Robotics and Automation (ICRA)*, pp. 2866–2871, May 2011.
- [111] MYERS, R., MONTGOMERY, D., and ANDERSON-COOK, C., *Response Surface Methodology: Process And Product Optimization Using Designed Experiments*. John Wiley & Sons, 2009.
- [112] NAHON, M., “A simplified dynamics model for autonomous underwater vehicles,” in *Proceedings of the 1996 Symposium on Autonomous Underwater Vehicle Technology*, pp. 373–379, 1996.
- [113] NAM, T., *A Generalized Sizing Method for Revolutionary Concepts Under Probabilistic Design Constraints*. Dissertation, Georgia Institute of Technology, 2007.
- [114] NATIONAL ACADEMY OF SCIENCES AND INSTITUTE OF MEDICINE, *Science, Evolution, and Creationism*. Washington, DC: The National Academies Press, 2008.
- [115] NEWTON, I., *Sir Isaac Newton’s Mathematical Principles of Natural Philosophy and His System of the World*. University of California Press, 1934.
- [116] NOVAK, M. A., “Evolution; why we help,” *Scientific American*, pp. 34–39, July 2012.
- [117] OFFICE OF NAVAL RESEARCH, *Naval Science and Technology Strategic Plan*, 2009.
- [118] OLIVER, D. W., KELLIHER, T. P., and KEEGAN JR., J. G., *Engineering Complex Systems with Models and Objects*. McGraw Hill, 1997.
- [119] OPERATIONS ANALYSIS STUDY GROUP, *Naval Operations Analysis*. Naval Institute Press, 1977.
- [120] POOLE, B. H., *A Methodology for the Robustness-based Evaluation of Systems-of-Systems Alternatives Using Regret Analysis*. Dissertation, Georgia Institute of Technology, 2008.
- [121] PRANDTL, L., “Über den reibungswiderstand strömender luft,” *Ergebnisse der Aerodynamischen Versuchsanstalt zu Göttingen*, pp. 620–626, 1927.
- [122] RAYMER, D. P., *Aircraft Design: A Conceptual Approach*. Reston, Va.: American Institute of Aeronautics and Astronautics, 4 ed., 2006.
- [123] RIGGINS, D. W., MOORHOUSE, D. J., and CAMBEROS, J. A., *Exergy Analysis and Design Optimization for Aerospace Vehicles and Subsystems*, ch. 6, Entropy Generation and Aerospace Vehicle Performance. AIAA, 2011.
- [124] RIGGINS, D. W. and TAYLOR, T., “Methodology for performance analysis of aerospace vehicles using the laws of thermodynamics,” *Journal of Aircraft*, vol. 43, no. 4, 2006.
- [125] ROTH, B. A., *A Theoretical Treatment of Technical Risk in Modern Propulsion System Design*. Dissertation, Georgia Institute of Technology, March 2000.

- [126] ROY, N. and EARNEST, C., “Dynamic action spaces for information gain maximization in search and exploration,” in *American Control Conference*, p. 6, June 2006.
- [127] SAGE, A. P. and BIEMER, S. M., “Processes for system family architecting, design, and integration,” *EEE Systems Journal*, vol. 1, no. 1, pp. 5–16, 2007.
- [128] SAHIN, F., *System of Systems Engineering*, ch. Robotic Swarms as System of Systems, pp. 482–519. John Wiley & Sons, Inc., 2008.
- [129] SAMUELSON, D. A. and MACAL, C. M., “Agent-based simulation comes of age,” *OR/MS Today*, vol. 33, no. 4, 2006.
- [130] SCHOENHERR, K. E., “Resistance of flat plates moving through a fluid,” *Society of Naval Architects and Marine Engineering*, vol. 40, 1932.
- [131] SCHRAGE, D. P. and MAVRIS, D. N., “Integrated design and manufacturing for the high speed civil transport,” in *AIAA Aircraft Design, Systems and Operations Meeting*, (Washington, D.C.), AIAA, August 1993.
- [132] SCHRAGE, D. and MAVRIS, D., “Technology for affordability – how to define, measure, evaluate and implement it?,” in *American Helicopter Society 50th Annual Forum*, (Washington D.C.), May 1994.
- [133] SCHULTZ-GRUNOW, F., “New frictional resistance law for smooth plates,” tech. rep., NACA TM 986, Washington, DC, 1941.
- [134] SCIUBBA, E. and WALL, G., “A brief commented history of exergy from the beginnings to 2004,” *International Journal of Thermodynamics*, vol. 10, no. 1, 2007.
- [135] SCOTT, W. B., “Vision takes form,” *Aviation Week and Space Technology*, p. 22, August 2005.
- [136] SEDGEWICK, R., *Algorithms*. Boston, MA: Addison-Wesley Longman Publishing Co., Inc., 1988.
- [137] SHANNON, C., “A mathematical theory of communication,” *Bell System Technical Journal*, vol. 27, pp. 379–423, July 1948.
- [138] SHUKUYA, M. and HAMMACHE, A., “Introduction to the concept of exergy,” *Low Exergy Systems For Heating And Cooling Of Buildings, Iea Annex 37*, pp. 41–44, 2002.
- [139] SKOGLAR, P., “UAV path and sensor planning methods for multiple ground target search and tracking - a literature survey,” Report no.: LiTH-ISY-R-2835, Technical report from Automatic Control at Linkopings Universitet, Linkoping, Sweden, December 2007.
- [140] SOBAN, D., *A Methodology for the Probabilistic Assessment of System Effectiveness as Applied to Aircraft Survivability and Susceptibility*. Dissertation, Georgia Institute of Technology, 2001.
- [141] STANLEY, L. G. and STEWART, D. L., *Design Sensitivity Analysis - Computational Issues of Sensitivity Equation Methods*, ch. Front Matter, pp. i–xxi. Philadelphia: Society for Industrial and Applied Mathematics, 2002.

- [142] STEWART, T. J., “Search for a moving target when search motion is restricted,” *Computers and Operations Research*, vol. 6, pp. 129–140, 1979.
- [143] SUNG, W. J., *A Neural Network Construction Method for Surrogate Modeling Of Physics-Based Analysis*. Dissertation, Georgia Institute of Technology, 2012.
- [144] TADJDEH, Y., “As technology matures, new roles emerge for underwater drones,” *National Defense*, vol. 99, no. 730, pp. 24 – 26, 2014.
- [145] TALLEY, D. N., *Methodology for the Conceptual Design of A Robust And Opportunistic System-of-Systems*. Dissertation, Georgia Institute of Technology, December 2008.
- [146] TAYLOR, J. S. and HULGAN, M. C., “Electro-optic identification research program,” in *Fifth International Symposium on Technology and Mine Problem*, (Monterey, CA), Naval Coastal Systems Station, Code R22, Panama City, FL, April 2002.
- [147] TOMOCIV, R. and VUKOBRATOVIC, M., *General Sensitivity Theory*. American Elsevier, 1972.
- [148] TRUVER, S. C., “Mines and Underwater IEDs in US Ports and Waterways: Context, Threats, Challenges, and Solutions,” *Naval War College Review*, vol. 61, pp. 106–127, Winter 2008.
- [149] TUNDRON, T., “Target Reacquisition for Identification in the AN/WLD-1(V)1 System,” in *Fifth International Symposium on Technology and the Mine Problem*, (Monterey, CA), April 2002.
- [150] ULRICH, K. T., *Product Design And Development*. McGraw-Hill Education, 2003.
- [151] UNITED STATES AIR FORCE CHIEF SCIENTIST, “Report on Technology Horizons; A Vision for Air Force Science and Technology During 2010–2030,” *United States Air Force*, 2010.
- [152] UNITED STATES NAVAL ACADEMY OPERATIONS ANALYSIS STUDY GROUP, *Naval Operations Analysis*. Annapolis, MD: Naval Institute Press, 2 ed., 1997.
- [153] UNITED STATES NAVY, “Naval Expeditionary Warfare Vision 2010,” 2010.
- [154] URICK, R. J., “Ambient noise in the sea,” tech. rep., Undersea Warfare Technology Office, Naval Sea Systems Command, Department of the Navy, Washington, D.C., 1984.
- [155] U.S. COAST GUARD, “The theory of search: A simplified explanation,” Tech. Rep. 96-F-HNG040, Soza & Company and the Office of Search and Rescue, October 1996.
- [156] U.S. DEPARTMENT OF DEFENSE, “Joint Defense Capabilities Studies (Improving DOD Strategic Planning, Resourcing and Execution to Satisfy Joint Capabilities),” *Joint Defense Capabilities Study Team*, 2004.
- [157] U.S. DEPARTMENT OF DEFENSE, “The Navy Unmanned Undersea Vehicle (UUV) Master Plan,” *Washington DC: Department of the Navy*, 2004.

- [158] U.S. DEPARTMENT OF DEFENSE, “The US Air Force Remotely Piloted Aircraft and Unmanned Aerial Vehicle Strategic Vision,” *The United States Air Force*, 2005.
- [159] U.S. DEPARTMENT OF DEFENSE, “The Navy Unmanned Surface Vehicle (USV) Master Plan,” *Washington DC: Department of the Navy*, 2007. Thomsen, James E and Guillory, Victor G and Benes, Thomas A.
- [160] U.S. DEPARTMENT OF DEFENSE, *Department of Defense Instruction Number 5000.02, Operation of the Defense Acquisition System*, December 2008.
- [161] U.S. DEPARTMENT OF DEFENSE, “US Army Unmanned Aircraft Systems Roadmap 2010–2035,” *The United States Army*, vol. 27, 2010.
- [162] U.S. DEPARTMENT OF DEFENSE, “Unmanned Ground Systems Roadmap,” *Robotic Systems Joint Project Office*, 2011.
- [163] U.S. DEPARTMENT OF DEFENSE, “Unmanned Systems Integrated Roadmap FY2011–2036,” 2011.
- [164] U.S. DEPARTMENT OF DEFENSE, “Unmanned Systems Integrated Roadmap FY2013–2038,” 2013.
- [165] U.S. NAVY, *Universal Naval Task List (UNTL)*, January 2007.
- [166] VON KÁRMÁN, T., “Über laminare und turbulente reibung,” *ZAMM*, pp. 70–97, 1921.
- [167] VON KÁRMÁN, T., “Turbulence and skin friction,” *Journal of the Aeronautical Sciences*, pp. 20–48, 1934.
- [168] WANG, Y. and HUSSEIN, I., “Bayesian-based decision making for object search and characterization,” in *American Control Conference*, pp. 1964–1969, 2009.
- [169] WANG, Y., *Decision-Making for Search and Classification using Multiple Autonomous Vehicles over Large-Scale Domains*. Dissertation, Worcester Polytechnic Institute, March 2011.
- [170] WANG, Y. and HUSSEIN, I., “Bayesian-based decision-making for object search and classification,” *IEEE Transactions on Control Systems Technology*, vol. 19, no. 6, pp. 1639–1647, 2010.
- [171] WASHBURN, A., *Search and Detection*. Operations Research Society of America, 1981.
- [172] WASHINGTON SECRETARIAT, “Policies, Organisation and Procedures in The Technical Cooperation Program (TTCP 210),” tech. rep., The Technical Cooperation Program: Australia - Canada - New Zealand - United Kingdom - United States of America, September 2009.
- [173] WEATHERINGTON, D., “Unmanned aircraft systems roadmap, 2005-2030,” *Deputy, UAV Planning Task Force, OUSD (AT&L)*, 2005.
- [174] WEAVER, B. L., “A methodology for ballistic missile defense systems analysis using nested neural networks,” Master’s thesis, Georgia Institute of Technology, Atlanta, Ga., August 2008.

- [175] WEINBERG, H., “Generic Sonar Model,” in *OCEANS 82*, pp. 201–205, 1982.
- [176] WEISSTEIN, E. W., “Nearest integer function.” From *MathWorld* – A Wolfram Web Resource. <http://mathworld.wolfram.com/NearestIntegerFunction.html>, Accessed September 2014.
- [177] WILDLIFE CONSERVATION SOCIETY, “Mongolian gazelle.” <http://www.wcs.org/saving-wildlife/hoofed-mammals/mongolian-gazelle.aspx>, Accessed April 2013.
- [178] WILLAERT, S. S., DE GRAAF, R., and MINDERHOUD, S., “Collaborative engineering: A case study of concurrent engineering in a wider context,” *Journal of Engineering and Technology Management*, vol. 15, no. 1, pp. 87 – 109, 1998.
- [179] WOJTUSIAK, J., GODZINSKA, E. J., and DEJEAN, A., “Capture and retrieval of very large prey by workers of the african weaver ant, *oecophylla longinoda* (latreille 1802),” *Tropical Zoology*, vol. 8, no. 2, pp. 309–318, 1995.
- [180] WONG, E., BOURGAULT, F., and FURUKAWA, T., “Multi-vehicle bayesian search for multiple lost targets,” in *Proceedings of the 2005 IEEE International Conference on Robotics and Automation (ICRA)*, pp. 3169–3174, April 2005.
- [181] XU, J. and HO, D. W., “A new training and pruning algorithm based on node dependence and jacobian rank deficiency,” *Neurocomputing*, vol. 70, no. 13, pp. 544 – 558, 2006.
- [182] YECHOUT, T. R., *Introduction to Aircraft Flight Mechanics*. American Institute of Aeronautics and Astronautics, Inc., 2003.
- [183] YEUNG, R. W., *Information Theory and Network Coding*. Springer Publishing Company, 1 ed., 2008.